Robust Model Predictive Control of an Electric Arc Furnace Refining Process

by

Lodewicus Charl Coetzee

Submitted in partial fulfilment of the requirements for the degree

Master of Engineering (Electronic Engineering)

in the

Faculty of Engineering, the Built Environment and

Information Technology

UNIVERSITY OF PRETORIA

June 28, 2006

Summary

Title:	Robust Model Predictive Control of an Electric Arc Furnace Refining Process
By:	Lodewicus Charl Coetzee
Supervisor:	Professor I.K. Craig
Department:	Department of Electrical, Electronic and Computer Engineering
Degree:	Master of Engineering (Electronic Engineering)

This dissertation forms part of the ongoing process at UP to model and control the electric arc furnace process. Previous work focused on modelling the furnace process from empirical thermodynamic principles as well as fitting the model to actual plant data. Automation of the process mainly focused on subsystems of the process, for example the electric subsystem and the off-gas subsystem.

The modelling effort, especially the model fitting, resulted in parameter values that are described with confidence intervals, which gives rise to uncertainty in the model, because the parameters can potentially lie anywhere in the confidence interval space.

Robust model predictive control is used in this dissertation, because it can explicitly take the model uncertainty into account as part of the synthesis process. Nominal model predictive control - not taking model uncertainty into account - is also applied in order to determine if robust model predictive control provides any advantages over the nominal model predictive control.

This dissertation uses the process model from previous work together with robust model predictive control to determine the feasibility of automating the process with regards to the primary process variables. Possible hurdles that prevent practical implementation are identified and studied.

Keywords: Electric Arc Furnace, Robust Model Predictive Control, EAF, RMPC.

Opsomming

Titel:	Robuuste Model Voorspellende Beheer van 'n Elektriese Boogoond Verfyningsproses
Deur:	Lodewicus Charl Coetzee
Studieleier:	Professor I.K. Craig
Departement:	Departement van Elektries, Elektronies and Rekenaar Ingenieurswese
Graad:	Meester van Ingenieurswese (Elektroniese Ingenieurswese)

Die verhandeling vorm deel van die voortgaande studie deur UP om 'n elektriese boogoondproses te modelleer en te beheer. Vorige modellering het gefokus op die gebruik van empiriese termodinamiese beginsels waarna die empiriese model gepas is op gemete aanlegdata. Outomatisasie word hoofsaaklik gemik op substelsels van die proses, byvoorbeeld die elektriese substelsel.

Die modelleringsproses, veral die passing van die model op aanlegdata, het daartoe gelei dat daar onsekerhede in die model vervat word. Die onsekerhede word beskryf deur parameters wat binne vasgestelde grense lê.

In die verhandeling word robuuste model voorspellende beheer gebruik, omdat dit die onsekerhede van die aanleg eksplisiet in ag kan neem gedurende die sinteseproses. Die robuuste beheerder word vergelyk met 'n nominale beheerder - wat nie die onsekerhede in ag neem nie - om te bepaal watter voordeel die robuuste beheerder oor die nominale beheerder bied.

Die aanlegmodel, wat in 'n vorige studie verkry is, tesame met robuuste model voorspellende beheerteorie word gebruik om te bepaal hoe haalbaar dit is om die elektriese boogoondverfyningsproses te outomatiseer. Die studie het moontlike struikelblokke geïdentifiseer wat praktiese implementering kan belemmer.

Sleutelwoorde: Elektriese Boogoond, Robuuste Model Voorspellende Beheer.

Acknowledgement

I thank God for blessing me with the opportunity to study. I owe my parents a debt of gratitude for their support and understanding throughout my studies. I thank my supervisor Prof. Craig for his guidance and help with this research and Mr. Bellingan from Cape Gate for his insight in the practical operation of an electric arc furnace.

Contents

List of abbreviations

ANN	Artificial Neural Network
BOF	Basic Oxygen Furnace
DMC	Dynamic Matrix Control
DRI	Direct Reduced Iron
DRMPC	Dual-mode Robust Model Predictive Control
EAF	Electric Arc Furnace
FRMPC	Feedback Robust Model Predictive Control
GPC	Generalized Predictive Control
IDCOM	Identification and Command
LMI	Linear Matrix Inequalities
MPC	Model Predictive Control
ODE	Ordinary Differential Equation
QP	Quadratic Programming
RHC	Receding Horizon Control
RMPC	Robust Model Predictive Control
SCADA	Supervisory Control And Data Acquisition
SDP	Semidefinite Programming
SMOC	Shell Multi-variable Optimizing Control
UP	University of Pretoria

List of symbols

List of Chemical Symbols

C	Carbon
CaO	Calcium Oxide
CO	Carbon monoxide
FeO	Iron Oxide
MgO	Magnesium Oxide
MnO	Manganese Oxide
P_2O_5	Phosphorus Oxide
Si	Silicon
SiO_2	Silicon Dioxide

Nonlinear model symbols

Nonlinear model states

x_3	Carbon content in bath [kg]
x_4	Silicon content in bath [kg]
x_7	FeO content in slag [kg]
x_8	SiO_2 content in slag [kg]
x_{12}	Bath and molten slag temperature $[^0C]$

Nonlinear model inputs

d_1 Rate of oxygen injection [kg/s]

d_2 Rate of DRI addition [kg/s]

d_3 Rate of slag forming additions [kg/s]

d_4 Electric power [kW]

d_5 Rate of graphite injection [kg/s]

Nonlinear model outputs

y_1 Bath and molten slag temperature [^0C]

y_2 Percentage carbon in bath [%]

y_3 FeO content in slag [kg]

Nonlinear model parameters

$C_p(k)$ Heat capacity of element / compound k [kJ/(mol.K)]

M_k Molar mass of element / compound k [kg/mol]

X_k Mole fraction of element / compound k

X_k^{eq} Equilibrium mole fraction of element / compound k

ΔH_k Enthalpy of formation of compound k [kJ/mol]

T_k Initial temperature of element / compound k [K]

k_{XC} Equilibrium concentration constant for carbon

k_{XSi} Equilibrium concentration constant for silicon

k_{dC} Decarburization rate constant [kg/s]

k_{dSi} Desiliconization rate constant [kg/s]

k_{gr} Graphite reactivity constant

k_{VT} EAF heat loss coefficient

η_{FeO} Efficiency of bath oxidation

η_{ARC} Efficiency of arc power input

Chapter 1

Introduction

This chapter provides a motivation for the the study undertaken in this dissertation. A short overview of the electric arc furnace process is given, followed by an explanation of the contribution of this dissertation as well as the organization of the rest of the dissertation.

1.1 Motivation

With the growth of the world economies, the demand on natural resources is growing. Iron ore is no different, and like most natural resources, it is not renewable. The solution is to reuse old materials through recycling in order to reduce the demand for natural resources. The use of electric arc furnaces (EAFs) is an important part of the recycling effort in the steel industry. EAFs are capable of melting down solid scrap metal and refining it to the required steel grade by manipulating the chemical properties of the steel. The electric arc furnace is slowly replacing the basic oxygen furnace (BOF) (IISI, 2003), because it uses chemical as well as electrical energy to melt the scrap metal. The electrical energy is introduced by three carbon electrodes that form an electric arc between them that radiates heat to the metal. Chemical energy is primarily provided by natural gas and oxygen.

The electric arc furnace process is still heavily dependent on operator control. The operator uses a recipe based on initial measurements of the chemical composition to determine how long electrical power should be applied, as well as how much oxygen,

carbon and other additives should be added. The melting time is often based on a feel for the process and the sound emanating from the furnace. Measurements are taken intermittently to gauge the progress and to make adjustments as needed. This leads to varying success in obtaining the desired steel grade.

The process could benefit hugely from the use of better automation to increase energy efficiency as well as to improve the consistency of the quality of the final product by employing good set-point following. Automation could also improve the safety of the process. Most of the current automation only focuses on the parts of the process that ultimately do not have a direct influence on the grade of the steel produced.

The mathematical model of the electric arc furnace refining process includes uncertainty. Control of the process requires that the controller needs to remain stable over all possible realizations of the model while providing acceptable performance. Robust model predictive control is well suited for uncertain multi-variable systems with constraints, because it takes the model uncertainty explicitly into account as part of the synthesis process. The closed-loop system is guaranteed stable over all modelled realizations of the uncertain system. This makes robust model predictive control well suited as a control method for the electric arc furnace refining process.

1.2 Operation of the Electric Arc Furnace

The electric arc furnace process is concerned with melting scrap metal and producing steel. Each iteration of the process is called a tap. The time it takes to finish one iteration of the process is called the tap-to-tap time. One tap consists of a few stages; charging the furnace, melting down the scrap metal, refining the steel, removing the slag layer, tapping the finished steel, and furnace turnaround. The electric arc furnace refining process is well described by Taylor (1985); Fruehan (1998)

Charging: Figure 1.1 shows a schematic representation of an electric arc furnace that is being charged. Charging consists of composing a bucket made up of scrap, other metallic elements and slag formers. The composition of the scrap metal is dependent on the desired grade of steel to be produced. The layering of the scrap is important: softer scrap

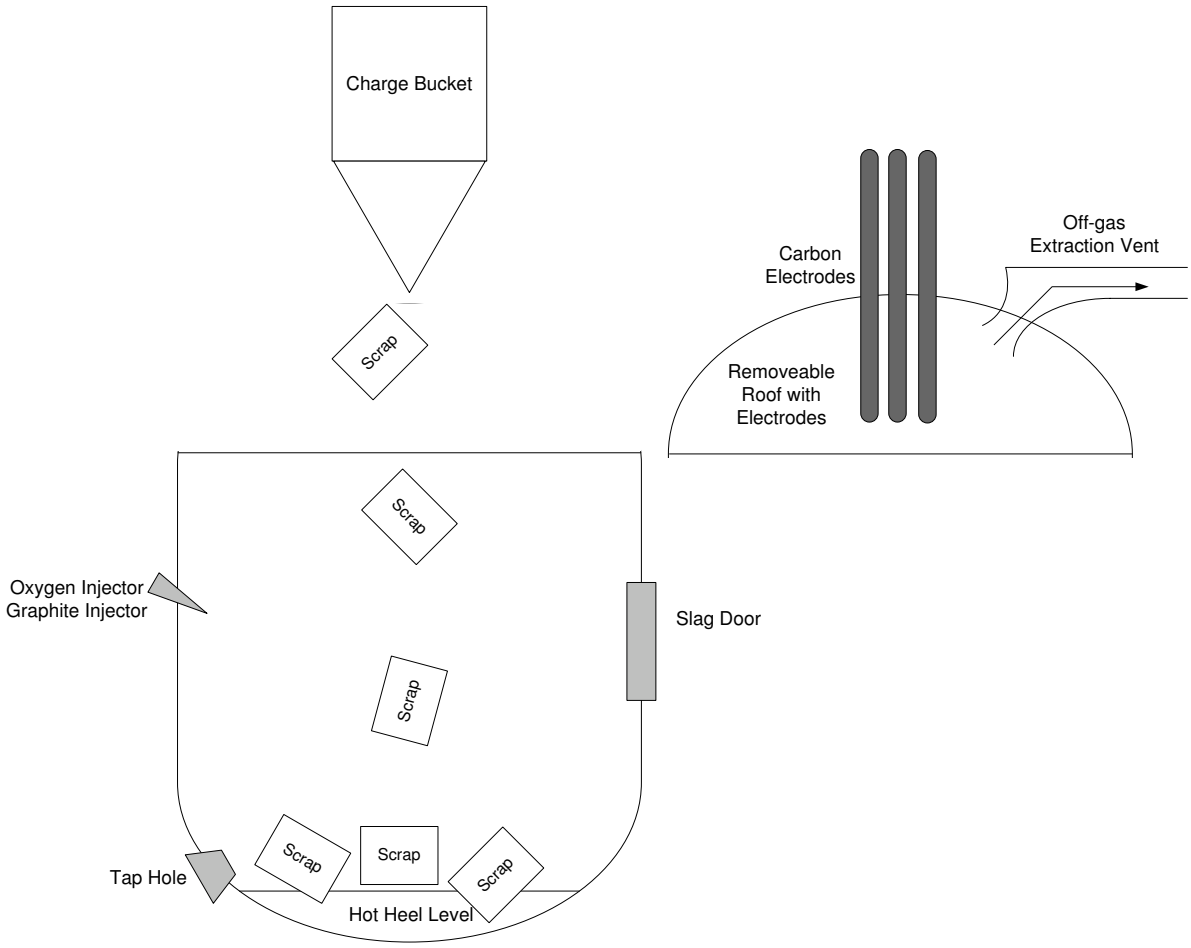

Figure 1.1: Electric arc furnace schematic - Charging.

is placed at the bottom of the bucket, while harder scrap is loaded on top. The softer scrap protects the furnace during charging and also melts down quickly. The melted scrap forms a pool of molten metal that aids in melting the larger pieces. This physical layering should prevent cave-ins from occurring, which could damage the carbon electrodes and cause a catastrophic breakdown. To charge the bucket into the furnace, the roof of the furnace swings away to expose the inside of the furnace. A crane positions the bucket on top of the furnace and the floor of the bucket is opened to allow the scrap to fall into the furnace. Some melt-shops only charge one bucket and then add direct reduced iron (DRI) through chutes in the roof of the furnace. This requires extra infrastructure such as a conveyor belt to transport the DRI to the chutes.

The type of scrap used in charging will have an influence on the time of the meltdown stage. Light scrap melts down easily but does not contain as much metal as denser, heavier scrap. More buckets of light scrap will thus be necessary to reach the required molten weight. With heavier scrap the melting process takes longer, but less charging needs to be done. The danger with denser scrap is the potential for late cave-ins that can damage the electrodes.

Melting: Figure 1.2 shows a schematic representation of an electric arc furnace in the process of melting down the solid scrap. The roof of the furnace is swung back on top of the furnace. The roof contains the three carbon electrodes that are used to create an electrical arc. Melting is initiated by applying electrical power to the furnace's electrodes as well as firing up the oxyfuel burners. The heat from the arc radiates towards the scrap to melt it down. A long arc between the electrodes and scrap is selected during meltdown, because it radiates more heat over a greater area than a short arc. The electric arc bores a hole into the middle of the scrap heap, and as the hole is forming, the electrodes are lowered into the hole. The surrounding scrap protects the furnace walls from the heat radiating from the arc. As the electrodes bore into the scrap, a molten pool of metal forms, which protects the bottom of the furnace from the arc. The burners proceed to melt the metal at the edges of the furnace that are not reached by the arc.

The use of oxyfuel burners and oxygen lances do not guarantee that there will be no

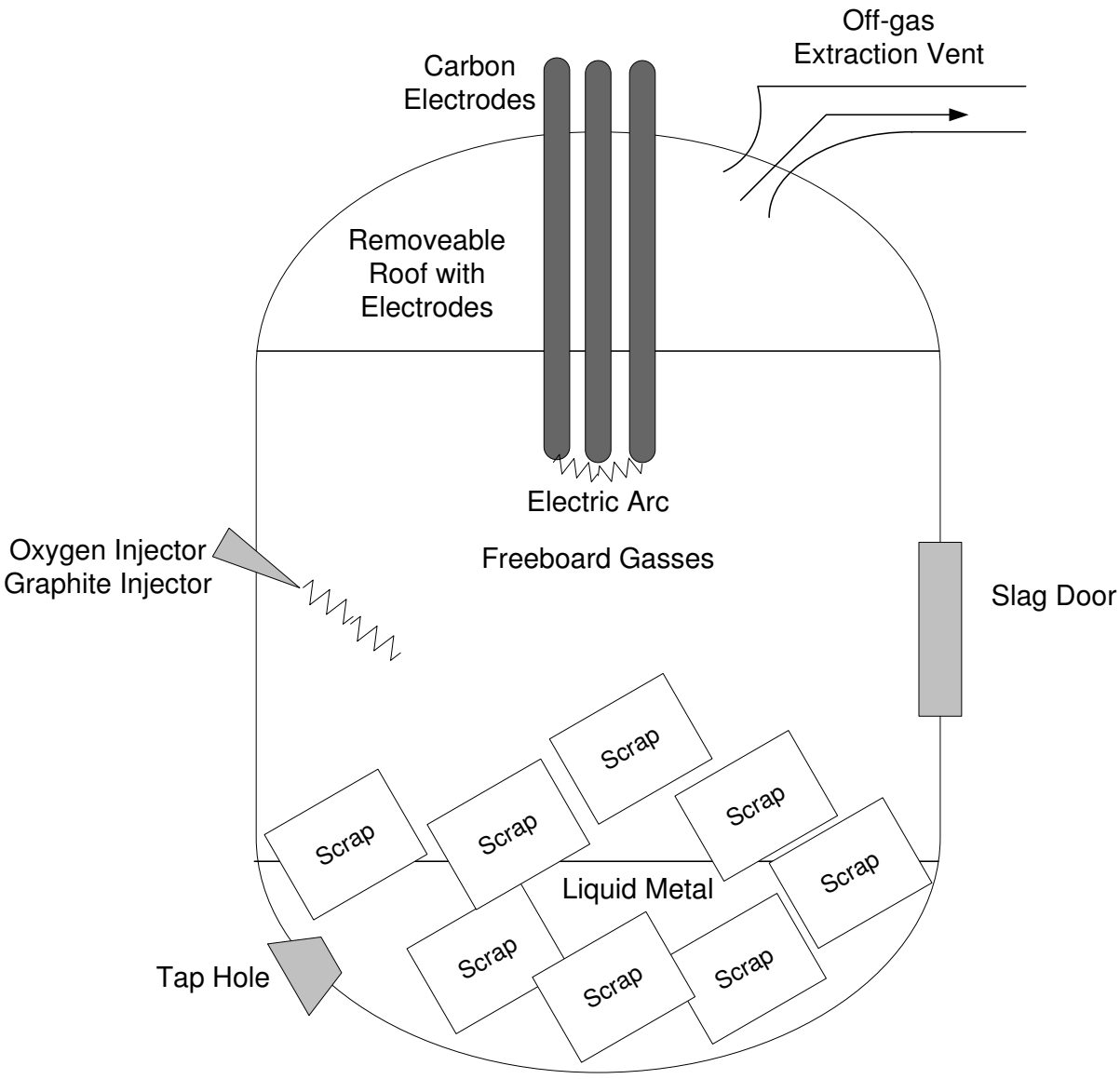

Figure 1.2: Electric arc furnace schematic - Melting.

cold spots in the furnace. When heavy pieces of scrap are caught in the cold spots, it can lead to late cave-ins during flat bath conditions (this is when all the scrap has melted). These heavy pieces can fall onto the electrodes and damage them (Taylor, 1985). The damaged electrodes will partially dissolve in the bath, leading to higher carbon content, which in turn leads to long delays in order to remove it.

The oxyfuel system is the most efficient during the early meltdown stage. The solid scrap usually has a large surface area exposed to the burner flame, which yields good heat transfer to the scrap. As the scrap melts, it moves away from the flame and makes way for other scrap to come into contact with the flame. A high temperature difference between the scrap and flame leads to good heat transfer, but the burner's effectiveness decreases as the temperature difference shrinks (Fruehan, 1998). The effectiveness of the oxyfuel burners are monitored by measuring the off-gas temperature. The less heat that is transferred to the scrap, the higher the off-gas temperature will become.

Refining: Figure 1.3 shows a schematic representation of an electric arc furnace in the refining stage, where all the solid scrap is melted down and flat bath conditions are obtained. Refining commences as soon as all the scrap is melted down and only a molten pool of metal remains. There is no longer any solid scrap left to protect the furnace walls and roof from the electric arc. A short arc is selected during refining, because it focuses the heat more locally. To protect the walls and roof further as well as improve heat transfer to the molten metal, a foamy slag layer is formed that covers the arc. The slag layer is controlled by injecting C and O_2 into the bath. The CO gas bubbles rise up and form a foamy slag layer on top of the molten metal. The impurities are removed from the molten metal primarily through oxidation. The oxidized impurities are trapped in the slag layer. Common impurities found in the bath are phosphorus, sulphur, aluminium, silicon, manganese and carbon. During the refining process the oxyfuel system is used in lancing mode. Large amounts of oxygen are forced into the bath. The carbon reacts with the oxygen and is an efficient source of heat for the bath, while the remaining oxygen reacts with the iron to form FeO that is transferred to the slag. The oxidation of carbon is the primary mechanism for decarburization when bath carbon is high. As the bath

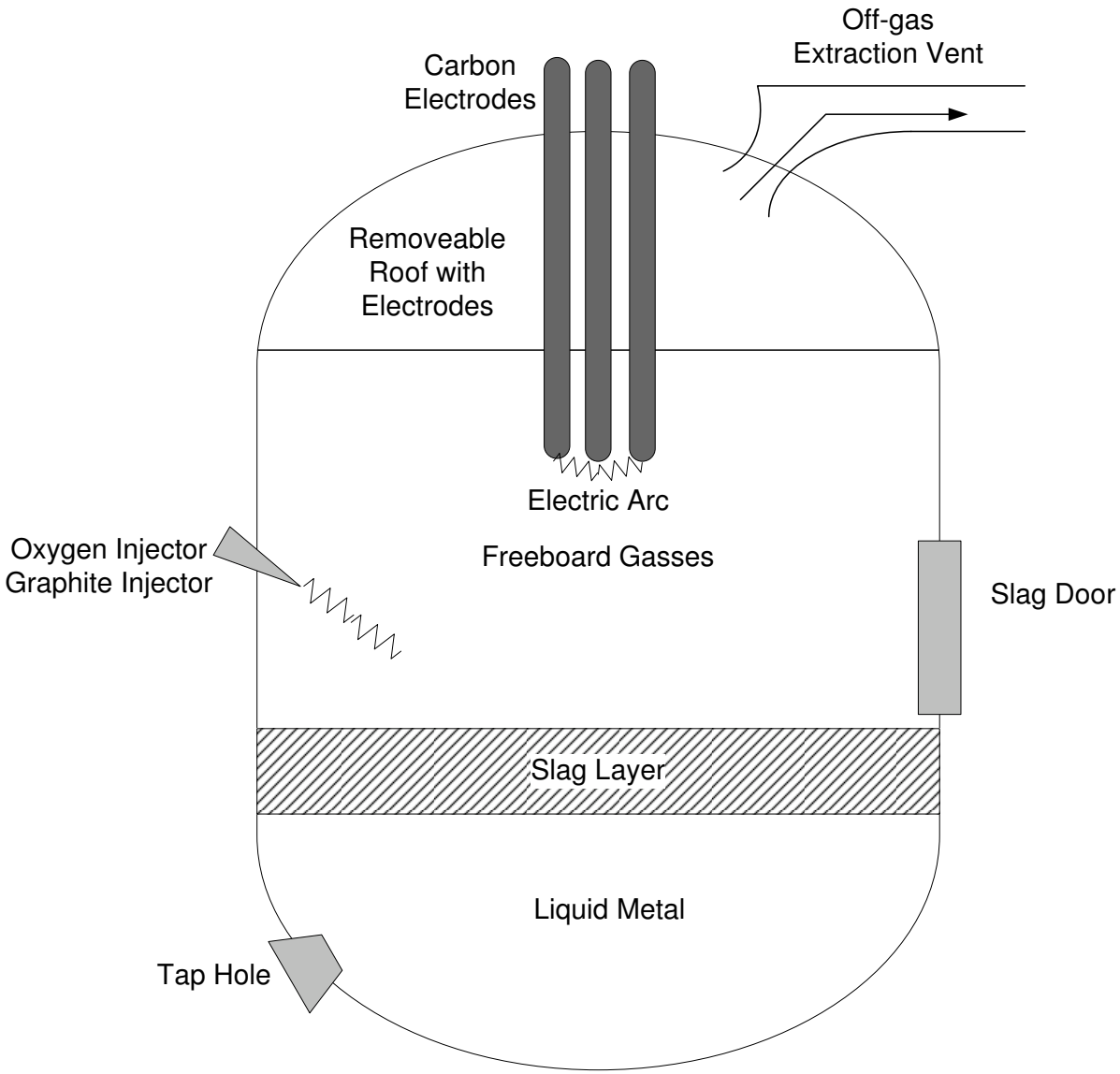

Figure 1.3: Electric arc furnace schematic - Refining.

carbon decreases, the reduction of FeO from the slag becomes the main mechanism of decarburization.

Phosphorus is removed from the bath through oxidation. The phosphorus is oxidized to P_2O_5 and transferred to the slag. The capacity of the slag to retain P_2O_5 is controlled by MgO and CaO components of the slag as well as a relatively lower temperature, high FeO content in the slag and the acidity of the slag (Fruehan, 1998). The slag should be basic, which requires a CaO/SiO_2 of greater than 2.2. Most of the phosphorus is removed during the early part of refining when the temperature is lower. Deslagging should occur early in the refining stage to prevent phosphorus from returning to the bath when the temperature rises (Taylor, 1985).

Manganese is oxidized as MnO and transferred to the slag. It has most of the same requirements as phosphorus, except that CaO/SiO_2 should be less than 2.2. To compensate for the suboptimal conditions, more oxygen can be injected into the bath to aid in the removal of manganese.

Sulphur is one of the more difficult impurities to remove from the bath, because it requires the opposite conditions to most of the other impurities. It requires high basicity, low bath oxygen and thus low FeO in the slag as well as high slag fluidity (Taylor, 1985). The other impurities such as SiO_2 and P_2O_5 cause the slag to become more acidic and reduce the ability of the slag to retain sulphur. The process is also primarily based on oxidation, while sulphur needs to be reduced from the bath. If the steel producer has a ladle furnace, it is used for desulphurization, because additions can be made to lower the bath oxygen and improve the conditions for desulphurization.

Silicon is the easiest impurity to remove from the bath. It is oxidized during decarburization much faster than carbon and is present as SiO_2 in the slag. The silicon level is usually lower than specified and ferrosilicon is added to bring it back up to specification.

Deslagging: To prevent the impurities caught in the slag layer from re-entering the bath, the slag is removed from time to time in a process called deslagging. This is accomplished by opening a door above the molten metal level and tipping the furnace slightly toward the opening to drain off the slag. Phosphorus is primarily removed in

the early stages of refining, while sulphur is removed later in the process, because of the changing chemical composition of the environment and bath.

Tapping: At the end of the process when the steel has reached the desired chemical composition and temperature, it is removed from the furnace. The steel is removed by opening the tap hole at the bottom of the furnace and pouring it into a ladle for further processing. This process is called tapping. In the ladle, de-oxidisers and bulk alloy additions are added. The de-oxidizers aid in removing sulphur from the steel, because removing sulphur requires low oxygen levels. The tap hole is just higher than the bottom of the furnace. This is to ensure that a small amount of molten metal remains in the furnace for the next heat. This is called a hot heel practice. The remaining molten metal aids in melting down the new scrap early in the meltdown stage.

Furnace turnaround is where the furnace is inspected for damage and repairs are conducted before the next tap is started.

1.3 Aims and objectives

The main aim of this dissertation is to determine the feasibility of automating the electric arc furnace process with regards to the main variables of steel carbon content, temperature at tapping and impurities in the steel. To this aim:

- a robust model predictive controller needs to be synthesised, which explicitly takes model uncertainty into consideration during controller synthesis.
- The controller should be verified through a simulation study of the closed-loop system in order to evaluate the performance of the controller:
  - in the presence of uncertainty,
  - and under limited feedback conditions inherent in most EAF melt-shops.
- The performance of the robust controller is compared to nominal model predictive control to gauge the advantage of using robust control.

This dissertation contributes the following:

- Linearized models of the reduced nonlinear model in structured uncertainty description.
- Synthesis of a nominal model predictive controller (one that does not take model uncertainty into account) for the electric arc furnace refining process.
- Synthesis of a *feedback* robust model predictive controller for the electric arc furnace refining process.
- Synthesis of a *dual-mode* robust model predictive controller for the electric arc furnace process.
- Simulation study to compare the stability and performance of the above-mentioned controllers under extreme model mismatch situations:
  - using full state feedback in order to evaluate the performance of the controller in the presence of uncertainty,
  - using a five state nonlinear predictor with one correction measurement from the plant for a more realistic closed-loop analysis,
  - and a five state nonlinear predictor with one correction measurement from the plant, and an internal model parameter update which attempts to improve the closed-loop performance.

1.4 Organization

Chapter 2 provides a brief overview of the modelling of the process as well as the linearization approach and model validation.

Chapter 3 provides an overview of the theory of stability of model predictive control and the development of robust model predictive control theory. The chapter continues by taking an in-depth look at the two robust model predictive control methods employed in the simulation study.

Chapter 4 provides an in-depth study of the robust and nominal model predictive control of the reduced nonlinear model of the electric arc furnace process. Practical scenarios are investigated in an attempt to quantify the effects of a lack of feedback from the plant, as well as practical disturbances such as leaving the slag door open and late cave-ins.

Chapter 5 provides a short summary of the dissertation, some conclusions drawn from the simulation studies and recommendations for further work regarding the automation of the electric arc furnace refining process.

Appendix A provides a simulation study on an academic problem in order to show the advantage of robust model predictive control in terms of stability with regards to nominal model predictive control. The academic problem gives further insight into the performance of feedback and dual-mode robust model predictive controllers.

Appendix B provides additional simulation results.

Appendix C provides measured bath and slag data.

Chapter 2

Process modelling

This chapter details the mathematical model of the electric arc furnace. The chapter starts by outlining the models that are available for the electric arc furnace and then focuses on the chosen model. The chosen nonlinear model is then linearized around an operating point with different model parameters to include the total uncertainty region around that operating point.

2.1 Introduction

The electric arc furnace process is a very difficult process to model accurately, because it is difficult to obtain process data. This is due to the extreme environment in which the furnace operates, which makes it difficult to install measurement instruments. Some of the instruments that are in common use do not allow for on-line measurements to be taken, e.g. temperature probes that are manually dipped into the bath and burnt away as part of the measurement process. Before any temperature measurements and samples can be taken, the slag layer must be removed. The electrical power level must be reduced, which in turn will cause the furnace to operate at a reduced efficiency. The sample of molten steel that is taken during the measurement process takes a few minutes to analyse in a lab. All these measurements have associated costs, and these also influence the operation of the furnace.

There are different approaches to modelling the electric arc furnace (EAF) process.

The first approach is to develop static models of the EAF process. This is a popular method of modelling the EAF process (Taylor, 1985; Turkdogan, 1989; Fruehan, 1998; Deo and Boom, 1993). The modelling method is adapted from basic oxygen furnaces where the model calculates offline the bulk mass and energy additions to attain required steel properties with regards to temperature and chemical composition. Corrections are made on-line to account for deviations once measurements have been made. Nyssen *et al.* (1999) created a static model as an operator aid. The operating schedule is calculated before the process is started and updates are made during the process to account for deviations in the predicted and actual progress. The authors extended their work to create a dynamic model as an on-line operator aid. The model gives an estimate of the progress with regards to material melting, slag foam height, bath temperature and composition (Nyssen *et al.*, 2002). De Vos (1993) developed a static model with economic objectives in mind. The model helped optimize the slag additives in order to reduce costs.

The second approach is to use dynamic models to model the process as consisting of equilibrium zones with limited mass transfer between the equilibrium zones governed by concentration gradients.

Cameron *et al.* (1998) (as discussed in MacRosty (2005)) developed the EAF model with simulation in mind. The authors used the model to find improved practices for the EAF through dynamic simulation. The model consists of four equilibrium zones with six interfaces between the zones. The four zones are metal, slag, organic solid and gas. The material is transferred between the zones driven by concentration gradients. Chemical equilibrium is assumed at the interfaces. Off-gas data was used to validate the model. Proprietary reasons may account for the lack of detail disclosed about the model.

Matson and Ramirez (1999) (as discussed in MacRosty (2005)) created a model of the EAF by describing it as two control volumes. One volume contains the bath, slag and a small amount of gas. The other volume contains the freeboard gases. The transfer of mass between the control volumes is modelled as diffusion driven by a concentration gradient.

Modigell and coworkers (Modigell *et al.*, 2001*a*,*b*; Traebert *et al.*, 1999) (as discussed in MacRosty (2005)) created a mathematical model of the EAF that consists of four

reaction zones. The zones are assumed to be in chemical equilibrium and the transport of mass between the zones is driven by concentration gradients. The model was developed for simulation purposes, but details of the model are lacking, probably because of proprietary reasons.

The third approach is to model the process from fundamental thermodynamic and kinetic principles. Bekker *et al.* (1999) created a dynamic model of the EAF that consists of 17 ordinary differential equations (ODEs). This is a generic model that can be fitted with plant data to any electric arc furnace. Rathaba (2004) fitted the generic model of Bekker *et al.* (1999) with plant data from an industry partner. Rathaba (2004) reduced the complexity of the generic model for the refining stage to a nonlinear model consisting of 5 ODEs. The refining stage is of further interest, because during this stage the actual grade of the steel is determined.

There are models that only focus on certain subsystems of the process. The oxyfuel system increases the efficiency of the EAF process by adding an extra source of energy. The oxygen injection by the oxyfuel subsystem has an effect on the decarburization of the process (Fruehan, 1998; Thomson *et al.*, 2001; Pujadas *et al.*, 2003; Khan *et al.*, 2003).

The foamy slag is an important aspect of the electric arc furnace process. It is responsible for trapping the impurities that are oxidized from the bath. The foamy slag covers the electric arc to shield the walls and roof of the furnace from the radiating heat and also increases the heat transfer from the arc to the bath. It is important to control the slag height in order to produce the greatest efficiency in the process (Oosthuizen *et al.*, 2001; Galgali *et al.*, 2001; Morales *et al.*, 2001*b*; Kimihisa and Fruehan, 1987, 1989*a*,*b*; Jiang and Fruehan, 1991; Gou *et al.*, 1996). One of the main contributors to EAF modelling and the study of slag foaming is Morales *et al.* (2001*b*). Extensive slag data was collected and analysed, during which the advantages of extended use of foaming were observed through reduced electrical consumption and increased yield (Morales *et al.*, 2001*b*). This work was extended by creating an EAF simulator with emphasis placed on the behaviour of the slag; especially the effects that FeO and direct reduced iron (DRI) have on the slag and the process (Morales *et al.*, 2001*a*). The EAF modelling and slag foaming

results were combined in a new model. The emphasis was still on slag composition, but the effect of changing conditions in the furnace on slag foaming was added to the model; a concept named dynamic foaming index (Morales *et al.*, 2002). Controlling the foaming in the electric arc furnace has been done successfully by using sonic analysis to measure the acoustics of foaming. The sound emanating from the foaming slag is recorded and analysed and the results used to control graphite injection which has a direct influence on the slag foaming (Holmes and Memoli, 2001; Marique *et al.*, 1999).

Neural networks are a popular modelling tool for stochastic processes, making it well suited for modelling the voltage and current relationships that occur in the electric arc. King and Nyman (1996) used neural networks to predict the future behaviour of the electric arc. Neural networks were used by Raisz *et al.* (2000) to predict the furnace state in terms of meltdown and flat bath foaming. Billings and Nicholson (1977) and Billings *et al.* (1979) made an important contribution to the modelling and control of the electric arc by studying impedance and current control and the need for a strategy that includes both methods, which will help improve efficiency of heat transfer to the bath. Chen-Wen *et al.* (2000) modelled the dramatic current variations called flicker that occur during the early meltdown stage in order to design compensation circuits. Other contributions to the modelling of the electrical subsystem of the electric arc furnace were made by Collantes-Bellido and Gomez (1997); Meng and Irons (2000) and Guo and Irons (2003), who created a detailed three-dimensional model of the furnace in order to investigate the radiative heat transfer.

Post combustion in the furnace free board gases was studied and modelled by Kleimt and Kohle (1997); Tang *et al.* (2003).

2.2 Reduced Nonlinear Model

The following criteria were used in selecting the mathematical model:

1. The model should be able to predict the nonlinear dynamic behaviour during the refining stage of the electric arc furnace process. The key reason is that the model is

intended to be used to control the grade of the steel, which is primarily determined during the refining stage, given that the correct charging is performed.

2. The model should be simple enough to be used on-line. The reason is that the model will be used as a predictor for the on-line controller.

The reduced nonlinear model of Rathaba (2004) was chosen. The model specifically models the refining stage of the process. Rathaba (2004) reduces the generic electric arc furnace model of Bekker *et al.* (1999) from 17 to 5 ordinary differential equations. Rathaba (2004) identifies the parameters of the reduced Bekker *et al.* (1999) model and used process data from an industry partner to fit the parameters. The resulting parameters are uncertain and have confidence intervals describing the uncertainty.

Over an entire tap, the process is very unpredictable due to delays and breakdowns that invalidate the assumption of process continuity. The advantage of the refining stage is that after the initial measurement, except for deslagging, the process is mostly uninterrupted until the final measurement is made. At the start of the refining stage, all the solid scarp is usually melted; the modelling assumption of homogeneity is also valid. Process variables that undergo significant change during refining are bath temperature, carbon and silicon concentrations (masses), masses of SiO_2 and FeO in slag and all free-board gases. The masses of the bath and composite slag are approximately at steady state - they can be treated as constants.

The reduced Bekker *et al.* (1999) model is given as

$$\dot{x_3} = -k_{dC}\left(X_C - X_C^{eq}\right), \tag{2.1}$$

$$\dot{x_4} = -k_{dSi}\left(X_{Si} - X_{Si}^{eq}\right), \tag{2.2}$$

$$\dot{x_7} = \frac{2M_{FeO}d_1}{M_{O_2}} - \frac{x_7 k_{gr} M_{Fe} d_5}{\left(m_{T(slag)} + x_7 + x_8\right) M_C} + 0.13d_2, \tag{2.3}$$

$$\dot{x_8} = \frac{M_{SiO_2}}{M_{Si}} k_{dSi}\left(X_{Si} - X_{Si}^{eq}\right) + 0.045d_2, \tag{2.4}$$

$$\dot{x_{12}} = \left(p_t + \eta_{ARC} d_4 - k_{VT}\left(x_{12} - T_{air}\right)\right)/ \tag{2.5}$$

$$\left[\frac{m_{T(Fe)}C_{p(FeL)}}{M_{Fe}} + \frac{2m_{T(slag)} + 2x_7 + 3x_8}{M_{slag}} C_{p(slag_{(L)})}\right],$$

where the molar concentrations are given as

$$X_c = \frac{x_3/M_C}{m_{T(Fe)}/M_{Fe} + x_3/M_C + x_4/M_{Si}}, \tag{2.6}$$

$$X_{FeO} = \frac{x_7/M_{FeO}}{m_{T(slag)}/M_{slag} + x_7/M_{FeO} + x_8/M_{SiO_2}}, \tag{2.7}$$

$$X_C^{eq} = k_{XC}\left(\frac{m_{T(slag)}M_{FeO}}{x_7 M_{slag}} + \frac{x_8 M_{FeO}}{x_7 M_{SiO_2}} + 1\right), \tag{2.8}$$

$$X_{Si} = \frac{x_4/M_{Si}}{m_{T(Fe)}/M_{Fe} + x_3/M_{Si} + x_4/M_{Si}}, \tag{2.9}$$

$$X_{Si}^{eq} = k_{XSi}\left(\frac{m_{T(slag)}M_{FeO}}{x_7 M_{slag}} + \frac{x_8 M_{FeO}}{x_7 M_{SiO_2}} + 1\right)^2. \tag{2.10}$$

The reduced equations for the heat balance are:

$$p_2 = \left(-2\Delta H_{FeO} d_1/M_{O_2}\right)\eta_{FeO}, \tag{2.11}$$

$$p_5 = \frac{d_1}{M_{O_2}}\left(x_{12} - T_{O_2}\right)C_{P(O_2)}, \tag{2.12}$$

$$p_{11} = \frac{x_7 k_{gr} d_5 \left(\Delta H_{FeO} - \Delta H_{CO}\right)}{\left(m_{T(slag)} + x_7 + x_8\right) M_C}, \tag{2.13}$$

$$p_t = p_2 + p_5 + p_{11}, \tag{2.14}$$

with the parameters that are relevant to the reduced model

State	State Description	Input	Input Description
x_3	Dissolved Carbon [kg]	d_1	Oxygen injection rate [kg/s]
x_4	Dissolved Silicon [kg]	d_2	DRI addition rate [kg/s]
x_7	FeO in bath [kg]	d_3	Slag addition rate [kg/s]
x_8	SiO_2 in bath [kg]	d_4	Arc power [Kilowatt]
x_{12}	Bath temperature [Celsius]	d_5	Graphite injection rate [kg/s]

Table 2.1: Reduced model states and inputs.

$$\Theta = \begin{bmatrix} k_{dC} \\ k_{dSi} \\ k_{gr} \\ k_{VT} \\ \eta_{ARC} \\ \eta_{FeO} \end{bmatrix}, \tag{2.15}$$

where k_{dC} and k_{dSi} are the rate constants for removal of carbon and silicon from the bath; k_{gr} is the graphite reactivity constant; k_{VT} is the EAF heat loss coefficient; η_{ARC} and η_{FeO} are the efficiencies of arc energy input and bath oxidation; $m_{T(Fe)}$ and $m_{T(slag)}$ are the total masses of the slag formers and bath - both are assumed constant; M_C, M_{Fe}, M_{FeO}, M_{Si}, M_{SiO_2} and M_{slag} are the molar masses of the different elements. The states and inputs are described in table 2.1. A schematic of the electric arc furnace is shown in figure 2.1, which shows the physical location of the states.

2.3 Predictor design

The simulation of the closed-loop system where only limited feedback is available, requires a predictor to estimate the plant states between measurements. The predictor is the reduced nonlinear model of the previous section. The parameters of the predictor need to be updated in some of the simulation scenarios of chapter 4, where a simple ad-hoc method is used as outlined in (2.16-2.17). Only one variable, temperature, is measured and only one measurement is available, therefore the number of parameters that are updated needs

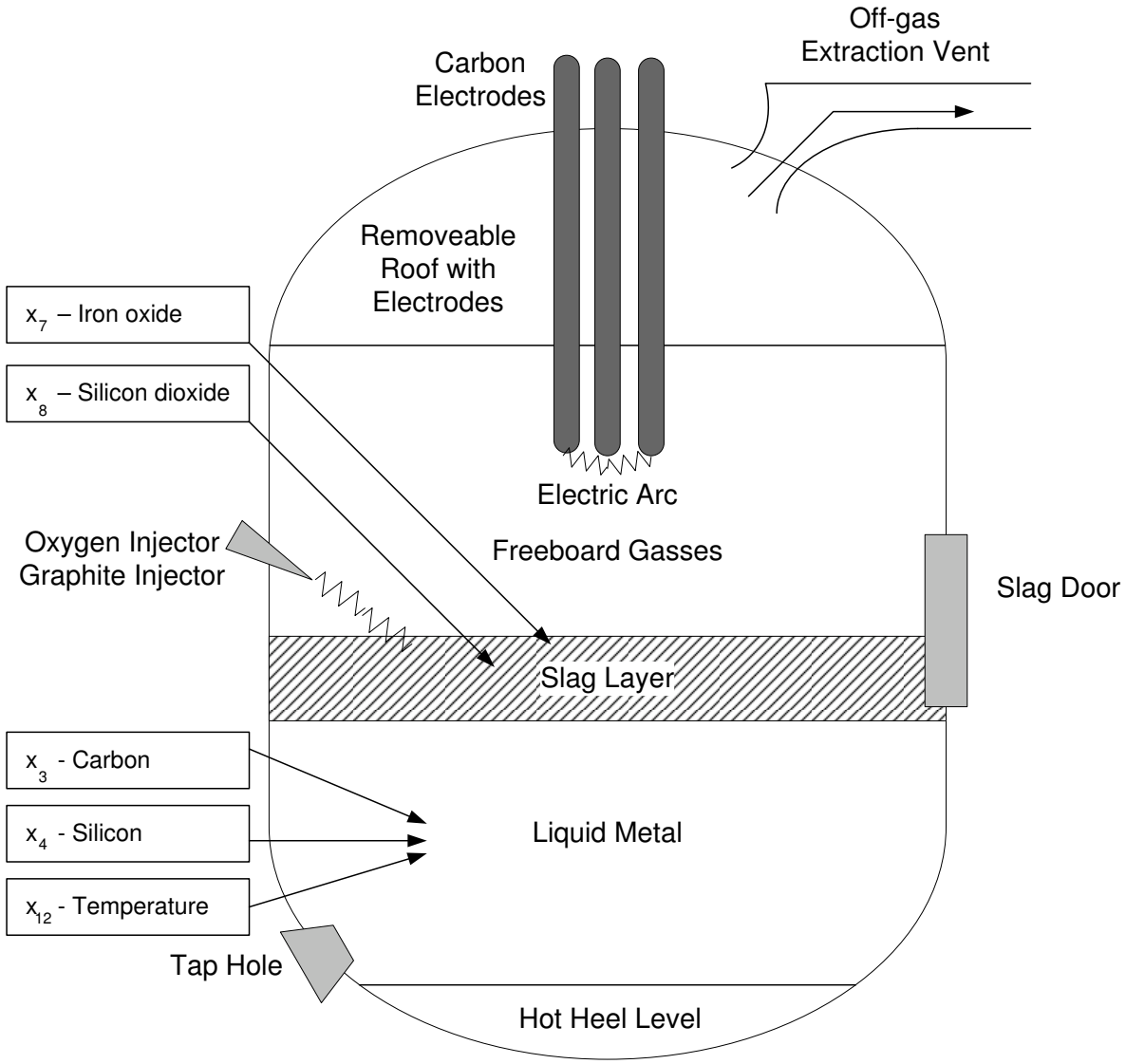

Figure 2.1: Electric arc furnace schematic showing states.

to be limited. The parameters are updated by taking the difference between the estimated temperature and the measured temperature value and multiplying it with a scale factor before applying it to the efficiencies η_{FeO} and η_{ARC}.

$$\eta_{FeO-New} = \eta_{FeO-Old} + C_{FeO}(T_{actual} - T_{estimated}), \quad (2.16)$$

$$\eta_{ARC-New} = \eta_{ARC-Old} + C_{ARC}(T_{actual} - T_{estimated}), \quad (2.17)$$

where C_{FeO} and C_{ARC} are constants that affect the rate of change for $\eta_{FeO-New}$ and $\eta_{ARC-New}$. The constants C_{FeO} and C_{ARC} are tuned until the error between the predictor and plant is minimized. The temperature is most significantly influenced by the parameter variations. The top row of figure 2.2 (a to c) shows the scenario where the efficiencies (η_{FeO} and η_{ARC}) are at their maximum versus the scenario where all parameters are set to produce the fastest temperature response. The bottom results of figure 2.2 (d to f) show the scenario where the efficiencies are at their minimum versus the scenario where all parameters are set to produce the slowest temperature response. In both scenarios the predictor remains sufficiently accurate just by manipulating the efficiencies η_{FeO} and η_{ARC}.

2.4 Linearized model

The robust model predictive control theory used in this study is dependent on a linear internal model to predict the future response of the system. Therefore the model of section 2.2 should be linearized for use in the model predictive controllers.

The linearization procedure for the nonlinear model of section 2.2 consists of the following steps (Goodwin *et al.*, 2001):

1. Calculate the operating point of the process.

2. Calculate the derivative of the nonlinear model.

3. Substitute the operating point into the derivatives.

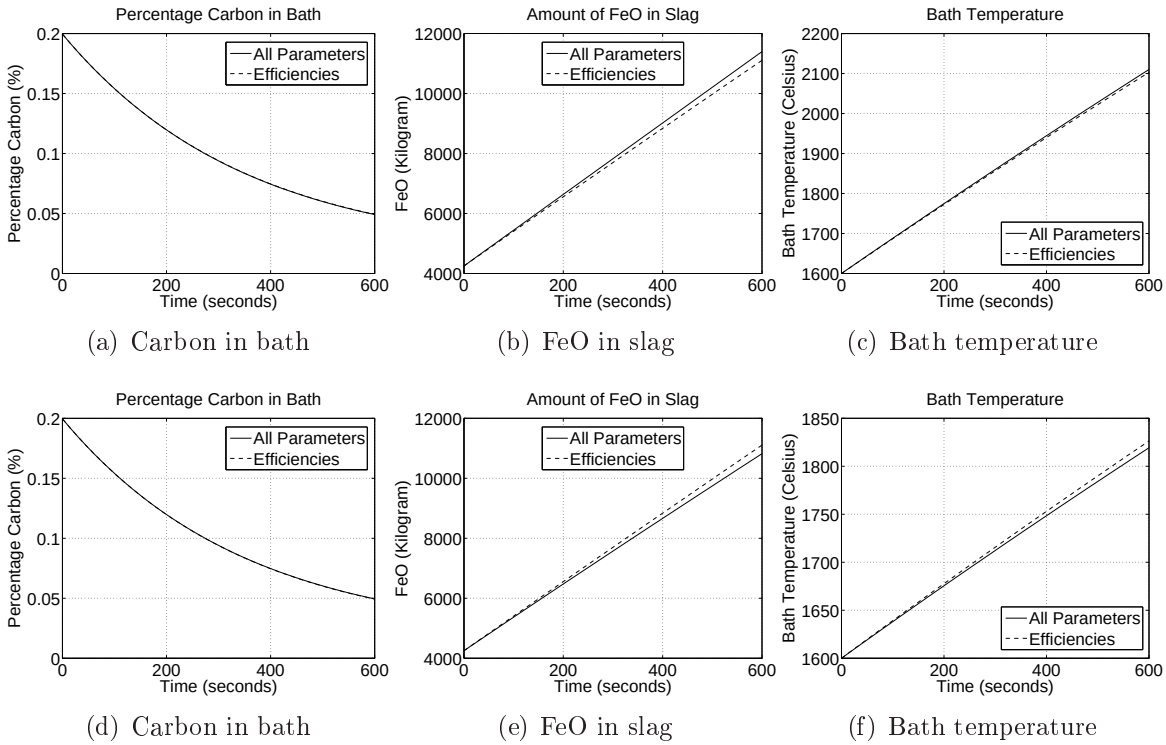

(a) Carbon in bath (b) FeO in slag (c) Bath temperature

(d) Carbon in bath (e) FeO in slag (f) Bath temperature

Figure 2.2: Influence of η_{FeO} and η_{ARC} versus all the parameters.

4. Repeat for all the different sets of parameters.

2.4.1 Operating point

The operating point of a system is the area of the state space where the process is in operation most of the time. The process dynamics can be approximated by linear dynamics in the region around the operating point. The procedure for finding the operating point would be to simulate the process over the time interval of operation and average the values for each state. Initial conditions and the time interval are required to commence the simulation. The initial conditions are obtained by averaging the process data at the start of refining over all the measured taps. The time interval is the average time it takes from the start of refining until tapping, as obtained from process data. The initial conditions are summarized in table 2.2 and the average time for the refining stage is 10 minutes or 600 seconds.

Table 2.2: Operating point of reduced model.

State		Initial Condition	Operating Point
x_3	Dissolved Carbon	160 kg	76 kg
x_4	Dissolved Silicon	24 kg	24 kg
x_7	FeO in bath	4250.6 kg	7692.3 kg
x_8	SiO_2 in bath	1405 kg	1405 kg
x_{12}	Bath temperature	1600 ^0C	1785 ^0C

2.4.2 Derivative of nonlinear model

The next step in the linearization procedure is to calculate the partial derivative of each state or output equation with regards to one of the state or input variables, depending on which matrix is calculated. The nonlinear system is defined as

$$\dot{x}(t) = f(x(t), d(t)), \tag{2.18}$$

$$y(t) = g(x(t), d(t)), \tag{2.19}$$

where $x \in \mathbb{R}^n$ is the state vector, $d \in \mathbb{R}^m$ is the input vector, $y \in \mathbb{R}^p$ is the output vector of the system and f and g are nonlinear functions of the vectors x and d. The number of states is n, the number of inputs is m and the number of outputs is p. The nonlinear system can be linearized to the form

$$\dot{x}(t) = Ax(t) + Bd(t), \tag{2.20}$$

$$y(t) = Cx(t) + Dd(t), \tag{2.21}$$

where $A \in \mathbb{R}^{n \times n}$, $B \in \mathbb{R}^{n \times m}$, $C \in \mathbb{R}^{p \times n}$ and $D \in \mathbb{R}^{p \times m}$ are matrices of the appropriate dimensions. The procedure (Goodwin *et al.*, 2001) for the reduced Bekker *et al.* (1999) model of (2.1) to (2.5) can be summarized as follows:

$$A = \left[\begin{array}{ccccc} \frac{\partial f_1}{\partial x_3} & \frac{\partial f_1}{\partial x_4} & \frac{\partial f_1}{\partial x_7} & \frac{\partial f_1}{\partial x_8} & \frac{\partial f_1}{\partial x_{12}} \\ \frac{\partial f_2}{\partial x_3} & \frac{\partial f_2}{\partial x_4} & \frac{\partial f_2}{\partial x_7} & \frac{\partial f_2}{\partial x_8} & \frac{\partial f_2}{\partial x_{12}} \\ \frac{\partial f_3}{\partial x_3} & \frac{\partial f_3}{\partial x_4} & \frac{\partial f_3}{\partial x_7} & \frac{\partial f_3}{\partial x_8} & \frac{\partial f_3}{\partial x_{12}} \\ \frac{\partial f_4}{\partial x_3} & \frac{\partial f_4}{\partial x_4} & \frac{\partial f_4}{\partial x_7} & \frac{\partial f_4}{\partial x_8} & \frac{\partial f_4}{\partial x_{12}} \\ \frac{\partial f_5}{\partial x_3} & \frac{\partial f_5}{\partial x_4} & \frac{\partial f_5}{\partial x_7} & \frac{\partial f_5}{\partial x_8} & \frac{\partial f_5}{\partial x_{12}} \end{array}\right]\Bigg|_{\substack{x=x_Q \\ d=d_Q}}, \tag{2.22}$$

$$B = \left[\begin{array}{ccccc} \frac{\partial f_1}{\partial d_1} & \frac{\partial f_1}{\partial d_2} & \frac{\partial f_1}{\partial d_3} & \frac{\partial f_1}{\partial d_4} & \frac{\partial f_1}{\partial d_5} \\ \frac{\partial f_2}{\partial d_1} & \frac{\partial f_2}{\partial d_2} & \frac{\partial f_2}{\partial d_3} & \frac{\partial f_2}{\partial d_4} & \frac{\partial f_2}{\partial d_5} \\ \frac{\partial f_3}{\partial d_1} & \frac{\partial f_3}{\partial d_2} & \frac{\partial f_3}{\partial d_3} & \frac{\partial f_3}{\partial d_4} & \frac{\partial f_3}{\partial d_5} \\ \frac{\partial f_4}{\partial d_1} & \frac{\partial f_4}{\partial d_2} & \frac{\partial f_4}{\partial d_3} & \frac{\partial f_4}{\partial d_4} & \frac{\partial f_4}{\partial d_5} \\ \frac{\partial f_5}{\partial d_1} & \frac{\partial f_5}{\partial d_2} & \frac{\partial f_5}{\partial d_3} & \frac{\partial f_5}{\partial d_4} & \frac{\partial f_5}{\partial d_5} \end{array}\right]\Bigg|_{\substack{x=x_Q \\ d=d_Q}}, \tag{2.23}$$

$$C = \left[\begin{array}{ccccc} \frac{\partial g_1}{\partial x_3} & \frac{\partial g_1}{\partial x_4} & \frac{\partial g_1}{\partial x_7} & \frac{\partial g_1}{\partial x_8} & \frac{\partial g_1}{\partial x_{12}} \\ \frac{\partial g_2}{\partial x_3} & \frac{\partial g_2}{\partial x_4} & \frac{\partial g_2}{\partial x_7} & \frac{\partial g_2}{\partial x_8} & \frac{\partial g_2}{\partial x_{12}} \\ \frac{\partial g_3}{\partial x_3} & \frac{\partial g_3}{\partial x_4} & \frac{\partial g_3}{\partial x_7} & \frac{\partial g_3}{\partial x_8} & \frac{\partial g_3}{\partial x_{12}} \end{array}\right]\Bigg|_{\substack{x=x_Q \\ d=d_Q}}, \tag{2.24}$$

$$D = \left[\begin{array}{ccccc} \frac{\partial g_1}{\partial d_1} & \frac{\partial g_1}{\partial d_2} & \frac{\partial g_1}{\partial d_3} & \frac{\partial g_1}{\partial d_4} & \frac{\partial g_1}{\partial d_5} \\ \frac{\partial g_2}{\partial d_1} & \frac{\partial g_2}{\partial d_2} & \frac{\partial g_2}{\partial d_3} & \frac{\partial g_2}{\partial d_4} & \frac{\partial g_2}{\partial d_5} \\ \frac{\partial g_3}{\partial d_1} & \frac{\partial g_3}{\partial d_2} & \frac{\partial g_3}{\partial d_3} & \frac{\partial g_3}{\partial d_4} & \frac{\partial g_3}{\partial d_5} \end{array}\right]\Bigg|_{\substack{x=x_Q \\ d=d_Q}}, \tag{2.25}$$

where x_Q is the operating point and d_Q the input vector that keeps the system at the operating point.

The output functions for the system are as follows: the first equation (2.26) gives the temperature, the second equation (2.27) gives percentage carbon in the bath and the third equation (2.28) gives the amount of FeO in the slag:

$$y_1 = x_{12}, \tag{2.26}$$

$$y_2 = 100\frac{x_3}{M_{T(Fe)} + x_3 + x_4}, \tag{2.27}$$

$$y_3 = x_7. \tag{2.28}$$

The partial derivatives are too large to put in matrix form, thus the matrices (2.22-2.25) show which derivative fits where and the actual derivatives are shown below. The derivatives that form the A matrix:

$$\begin{aligned}
\frac{\partial f_1}{\partial x_3} &= -k_{dC}\left(\frac{1/M_C}{m_{T(Fe)}/M_{Fe} + x_3/M_C + x_4/M_{Si}} - \right. \\
&\qquad \left. \frac{x_3/M_C^2}{\left(m_{T(Fe)}/M_{Fe} + x_3/M_C + x_4/M_{Si}\right)^2}\right), \\
\frac{\partial f_1}{\partial x_4} &= -k_{dC}\left(-\frac{x_3/\left(M_C M_{Si}\right)}{\left(m_{T(Fe)}/M_{Fe} + x_3/M_C + x_4/M_{Si}\right)^2}\right), \\
\frac{\partial f_1}{\partial x_7} &= -k_{dC}\left(\frac{m_{T(slag)} M_{FeO} M_{slag}}{\left(x_7 M_{slag}\right)^2} + \frac{x_8 M_{FeO} M_{SiO_2}}{\left(x_7 M_{SiO_2}\right)^2}\right), \\
\frac{\partial f_1}{\partial x_8} &= k_{dC}\left(\frac{M_{FeO}}{x_7 M_{SiO_2}}\right), \\
\frac{\partial f_1}{\partial x_{12}} &= 0, \\
\frac{\partial f_2}{\partial x_3}, \frac{\partial f_2}{\partial x_4}, \frac{\partial f_2}{\partial x_7}, \frac{\partial f_2}{\partial x_8}, \frac{\partial f_2}{\partial x_{12}} &= 0, \\
\frac{\partial f_3}{\partial x_3}, \frac{\partial f_3}{\partial x_4}, \frac{\partial f_3}{\partial x_{12}} &= 0, \\
\frac{\partial f_3}{\partial x_7} &= -\frac{k_{gr} M_{Fe} d_5}{\left(m_{T(slag)} + x_7 + x_8\right) M_C} + \frac{x_7 k_{gr} M_{Fe} d_5 M_C}{\left(\left(m_{T(slag)} + x_7 + x_8\right) M_C\right)^2}, \\
\frac{\partial f_3}{\partial x_8} &= \frac{x_7 k_{gr} M_{Fe} d_5 M_C}{\left(\left(m_{T(slag)} + x_7 + x_8\right) M_C\right)^2}, \\
\frac{\partial f_4}{\partial x_3}, \frac{\partial f_4}{\partial x_4}, \frac{\partial f_4}{\partial x_7}, \frac{\partial f_4}{\partial x_8}, \frac{\partial f_4}{\partial x_{12}} &= 0, \\
\frac{\partial f_5}{\partial x_3}, \frac{\partial f_5}{\partial x_4} &= 0, \\
\frac{\partial f_5}{\partial x_7} &= \left[\frac{k_{gr} d_5 \left(\Delta H_{FeO} - \Delta H_{CO}\right)}{\left(m_{T(slag)} + x_7 + x_8\right) M_C} - \frac{x_7 k_{gr} d_5 \left(\Delta H_{FeO} - \Delta H_{CO}\right) M_C}{\left(\left(m_{T(slag)} + x_7 + x_8\right) M_C\right)^2}\right] /
\end{aligned} \tag{2.29}$$

$$\left[\frac{m_{T(Fe)}C_{p(FeL)}}{M_{Fe}}+\frac{2m_{T(slag)}+2x_7+3x_8}{M_{slag}}C_{p(slag_{(L)})}\right]-$$
$$\left[p_t+\eta_{ARC}d_4-k_{VT}\left(x_{12}-T_{air}\right)\right]2C_{p(slag_{(L)})}/M_{slag}/$$
$$\left[\frac{m_{T(Fe)}C_{p(FeL)}}{M_{Fe}}+\frac{2m_{T(slag)}+2x_7+3x_8}{M_{slag}}C_{p(slag_{(L)})}\right]^2,$$

$$\frac{\partial f_5}{\partial x_8} = \left[-\frac{x_7k_{gr}d_5\left(\Delta H_{FeO}-\Delta H_{CO}\right)M_C}{\left(\left(m_{T(slag)}+x_7+x_8\right)M_C\right)^2}\right]/$$
$$\left[\frac{m_{T(Fe)}C_{p(FeL)}}{M_{Fe}}+\frac{2m_{T(slag)}+2x_7+3x_8}{M_{slag}}C_{p(slag_{(L)})}\right]-$$
$$\left[p_t+\eta_{ARC}d_4-k_{VT}\left(x_{12}-T_{air}\right)\right]3C_{p(slag_{(L)})}/M_{slag}/$$
$$\left[\frac{m_{T(Fe)}C_{p(FeL)}}{M_{Fe}}+\frac{2m_{T(slag)}+2x_7+3x_8}{M_{slag}}C_{p(slag_{(L)})}\right]^2,$$

$$\frac{\partial f_5}{\partial x_{12}} = \left[\frac{d_1}{M_{O_2}}C_{P(O_2)}-k_{VT}\right]/$$
$$\left[\frac{m_{T(Fe)}C_{p(FeL)}}{M_{Fe}}+\frac{2m_{T(slag)}+2x_7+3x_8}{M_{slag}}C_{p(slag_{(L)})}\right].$$

The derivatives that form the B matrix:

$$\begin{aligned}
\frac{\partial f_1}{\partial d_1},\frac{\partial f_1}{\partial d_2},\frac{\partial f_1}{\partial d_3},\frac{\partial f_1}{\partial d_4},\frac{\partial f_1}{\partial d_5} &= 0,\\
\frac{\partial f_2}{\partial d_1},\frac{\partial f_2}{\partial d_2},\frac{\partial f_2}{\partial d_3},\frac{\partial f_2}{\partial d_4},\frac{\partial f_2}{\partial d_5} &= 0,\\
\frac{\partial f_3}{\partial d_1} &= \frac{2M_{FeO}}{N_{O_2}},\\
\frac{\partial f_3}{\partial d_2} &= 0.13,\\
\frac{\partial f_3}{\partial d_3},\frac{\partial f_3}{\partial d_4},\frac{\partial f_3}{\partial d_5} &= 0,\\
\frac{\partial f_4}{\partial d_1},\frac{\partial f_4}{\partial d_3},\frac{\partial f_4}{\partial d_4},\frac{\partial f_4}{\partial d_5} &= 0,\\
\frac{\partial f_4}{\partial d_2} &= 0.045,\\
\frac{\partial f_5}{\partial d_1} &= \left[\left(\frac{-2\Delta H_{FeO}}{M_{O_2}}\right)\eta_{FeO}+\frac{\left(x_{12}-T_{O_2}\right)C_{P(O_2)}}{M_{O_2}}\right]/\\
&\quad \left[\frac{m_{T(Fe)}C_{p(FeL)}}{M_{Fe}}+\frac{2m_{T(slag)}+2x_7+3x_8}{M_{slag}}C_{p(slag_{(L)})}\right],\\
\frac{\partial f_5}{\partial d_2} &= 0,\\
\frac{\partial f_5}{\partial d_3} &= 0,
\end{aligned} \tag{2.30}$$

$$\begin{aligned}
\frac{\partial f_5}{\partial d_4} &= \eta_{ARC} d_4 / \left[\frac{m_{T(Fe)} C_{p(FeL)}}{M_{Fe}} + \frac{2m_{T(slag)} + 2x_7 + 3x_8}{M_{slag}} C_{p(slag_{(L)})} \right], \\
\frac{\partial f_5}{\partial d_5} &= \left[\frac{x_7 k_{gr} \left(\Delta H_{FeO} - \Delta H_{CO} \right)}{\left(m_{T(slag)} + x_7 + x_8 \right) M_C} \right] / \\
&\quad \left[\frac{m_{T(Fe)} C_{p(FeL)}}{M_{Fe}} + \frac{2m_{T(slag)} + 2x_7 + 3x_8}{M_{slag}} C_{p(slag_{(L)})} \right].
\end{aligned}$$

The derivatives that form the C matrix:

$$\begin{aligned}
\frac{\partial g_1}{\partial x_3}, \frac{\partial g_1}{\partial x_4}, \frac{\partial g_1}{\partial x_7}, \frac{\partial g_1}{\partial x_8} &= 0, \\
\frac{\partial g_1}{\partial x_{12}} &= 1, \\
\frac{\partial g_2}{\partial x_3} &= 100 \frac{1}{M_{T(Fe)} + x_3 + x_4} - 100 \frac{x_3}{\left(M_{T(Fe)} + x_3 + x_4 \right)^2}, \\
\frac{\partial g_2}{\partial x_4} &= -100 \frac{x_3}{\left(M_{T(Fe)} + x_3 + x_4 \right)^2}, \\
\frac{\partial g_2}{\partial x_7}, \frac{\partial g_2}{\partial x_8}, \frac{\partial g_2}{\partial x_{12}} &= 0, \\
\frac{\partial g_3}{\partial x_3}, \frac{\partial g_3}{\partial x_4}, \frac{\partial g_3}{\partial x_8}, \frac{\partial g_3}{\partial x_{12}} &= 0, \\
\frac{\partial g_3}{\partial x_7} &= 1.
\end{aligned} \tag{2.31}$$

2.4.3 Linearized models

The nonlinear model has uncertain parameters with the uncertainty described in terms of confidence intervals. The parameter uncertainty is assumed to be uniform and can therefore lie anywhere within the confidence intervals. Each parameter vector produces a model with different dynamics. The linear model can only model a specific parameter vector within a specific region of state-space. In order to model all the possible dynamics, different linear models are constructed. The uncertain space can be represented by a *polytopic uncertainty* (Kothare *et al.*, 1996) with each linear model representing a vertex of the polytope. This representation requires 2^n models, where n is the number of uncertain entries in the linear model. In this case, there are 17 uncertain entries, which would require $2^{17} = 131072$ different models.

Table 2.3: Nonlinear reduced model parameters.

Parameter	Lower bound	Nominal	Upper bound
k_{VT}	1.73	2.08	2.42
η_{ARC}	0.29	0.51	0.73
η_{FeO}	0.54	0.75	0.96
k_{dC}	54.74	54.90	55.05
k_{gr}	0.08	0.42	0.76

Polytopic uncertainty descriptions are very inefficient, thus the *structured uncertainty* (Kothare *et al.*, 1996) representation is preferred. The structured uncertainty representation makes use of a nominal model and a deviation model as follows

$$A = A_{nominal} + B_p \Delta C_q, \tag{2.32}$$

$$B = B_{nominal} + B_p \Delta D_{qu}, \tag{2.33}$$

where

$$\Delta = \begin{bmatrix} \Delta_1 & & & & \\ & \Delta_2 & & & \\ & & \cdot & & \\ & & & \cdot & \\ & & & & \cdot \\ & & & & \Delta_n \end{bmatrix}, \tag{2.34}$$

where $-1 \leq \Delta_i \leq 1,\ i = 1, 2, ..., n$ and $B_P C_q$ is the maximum deviation from $A_{nominal}$ and $B_p D_{qu}$ is the maximum deviation from $B_{nominal}$.

The nonlinear model has five parameters that can vary, but when the model is linearized the uncertainty affects 17 entries in the A and B matrices. Four parameters were varied in small increments, which resulted in over $21^4 \approx 200{,}000$ models being constructed. For each parameter, 21 different values were used and k_{dC} was assumed constant. The parameters of the nonlinear model are shown in table 2.3.

The nominal linear model is given below:

$$A_{nominal} = \begin{bmatrix} 0.996 & 1.78e-5 & -4.47e-6 & 4.18e-6 & 0 \\ 0 & 1 & 0 & 0 & 0 \\ 0 & 0 & 1 & 2.94e-5 & 0 \\ 0 & 0 & 0 & 1 & 0 \\ 0 & 0 & -7.96e-6 & -1.08e-5 & 1 \end{bmatrix}, \tag{2.35}$$

$$B_{nominal} = \begin{bmatrix} -2.68e-5 & -1.97e-7 & 0 & 2.11e-6 \\ 0 & 0 & 0 & 0 \\ 12 & 0.13 & 0 & -0.943 \\ 0 & 0.045 & 0 & 0 \\ 0.42 & -7.61e-7 & 6.20e-6 & -0.014 \end{bmatrix}. \tag{2.36}$$

To construct the structured uncertainty description, the extreme points K_{min} and K_{max} of the uncertain values are used as follows:

$$K_{nom} = \frac{1}{2}(K_{max} + K_{min}), \tag{2.37}$$

$$K_{dev} = \frac{1}{2}(K_{max} - K_{min}), \tag{2.38}$$

which results in the following linear models

$$AK_{nom} = \begin{bmatrix} 0.996 & 1.78e-5 & -4.47e-6 & 4.18e-6 & 0 \\ 0 & 1 & 0 & 0 & 0 \\ 0 & 0 & 1 & 3.64e-5 & 0 \\ 0 & 0 & 0 & 1 & 0 \\ 0 & 0 & -7.96e-6 & -1.04e-5 & 1 \end{bmatrix}, \tag{2.39}$$

$$AK_{dev} = \begin{bmatrix} 0 & 0 & 0 & 0 & 0 \\ 0 & 0 & 0 & 0 & 0 \\ 0 & 0 & 0 & 3.08e-5 & 0 \\ 0 & 0 & 0 & 0 & 0 \\ 0 & 0 & 3.22e-6 & 4.82e-6 & 0 \end{bmatrix}, \tag{2.40}$$

$$BK_{nom} = \begin{bmatrix} -2.68e-5 & -1.97e-7 & 0 & 2.11e-6 \\ 0 & 0 & 0 & 0 \\ 12 & 0.13 & 0 & -1.17 \\ 0 & 0.045 & 0 & 0 \\ 0.41 & -7.46e-7 & 6.08e-6 & -0.017 \end{bmatrix}, \tag{2.41}$$

$$BK_{dev} = \begin{bmatrix} 0 & 0 & 0 & 2.21e6 \\ 0 & 0 & 0 & 0 \\ 0 & 0 & 0 & 0.988 \\ 0 & 0 & 0 & 0 \\ 0.11 & 2.92e-7 & 3.03e-6 & 0.014 \end{bmatrix}, \tag{2.42}$$

where $AK_{dev} \equiv B_p C_q$ and $BK_{dev} \equiv B_p D_{qu}$.

2.4.4 Linear models analysis

The linear models are compared to the nonlinear model in order to ascertain whether they approximate the nonlinear model sufficiently well. Three scenarios are used; the nominal case; parameters that produce the least efficiency, and parameters that produce the best efficiency, i.e. the lower and upper bounds respectively as given in table 2.3. The parameters influence the dynamics of the model and cause deviation from the nominal case. Only the extreme cases are documented here, because they would provide the largest deviation from the nominal case. In all cases, the inputs are first set to their maximum levels, and then to their minimum levels. All these simulations (figures 2.3, 2.4 and 2.5) show that the linear models approximate the nonlinear model very well. The worst approximation is for carbon, which shows the most nonlinear response of all the

variables. In figure 2.6, the decarburization responses of all the different scenarios are shown on top of each other, and it is clear that only the inputs cause a slightly different response, while the parameter values have no significant influence. This result shows that the inputs do have a slight influence on decarburization, but not enough to accelerate the process significantly. The process can only be accelerated if the target temperature and carbon content can be reached in a shorter time.

A modal analysis (How, 2001) is done on the linearized model in order to determine if the carbon content is controllable. Before the modal analysis can be performed, the A matrix is decomposed into its eigenvectors and eigenvalues as follow:

$$A = T\Lambda T^{-1}, \tag{2.43}$$

where

$$T = \begin{bmatrix} | & & | \\ v_1 & \cdots & v_n \\ | & & | \end{bmatrix}, \tag{2.44}$$

$$T^{-1} = \begin{bmatrix} - & w_1^T & - \\ & \vdots & \\ - & w_n^T & - \end{bmatrix}, \tag{2.45}$$

and $v_i,\ i = 1, \ldots, n$ is the right eigenvector of eigenvalue λ_i, $w_i,\ i = 1, \ldots, n$ is the left eigenvector of eigenvalue λ_i and $\Lambda = \text{diag}(\lambda_1, \ldots, \lambda_n)$ is the matrix of eigenvalues. To check the controllability of the carbon content, a modal analysis is performed as follows:

$$\text{Controllability}_\text{C} = w_1^T B, \tag{2.46}$$

$$= \begin{bmatrix} 1.00 & -5.70e-3 & 1.45e-3 & -1.36e-3 & 0 \end{bmatrix} B, \tag{2.47}$$

$$= \begin{bmatrix} 1.74e-2 & 1.28e-4 & 0 & -1.70e-3 \end{bmatrix}, \tag{2.48}$$

where the B matrix used in the analysis is the matrix (2.36). The controllability analysis

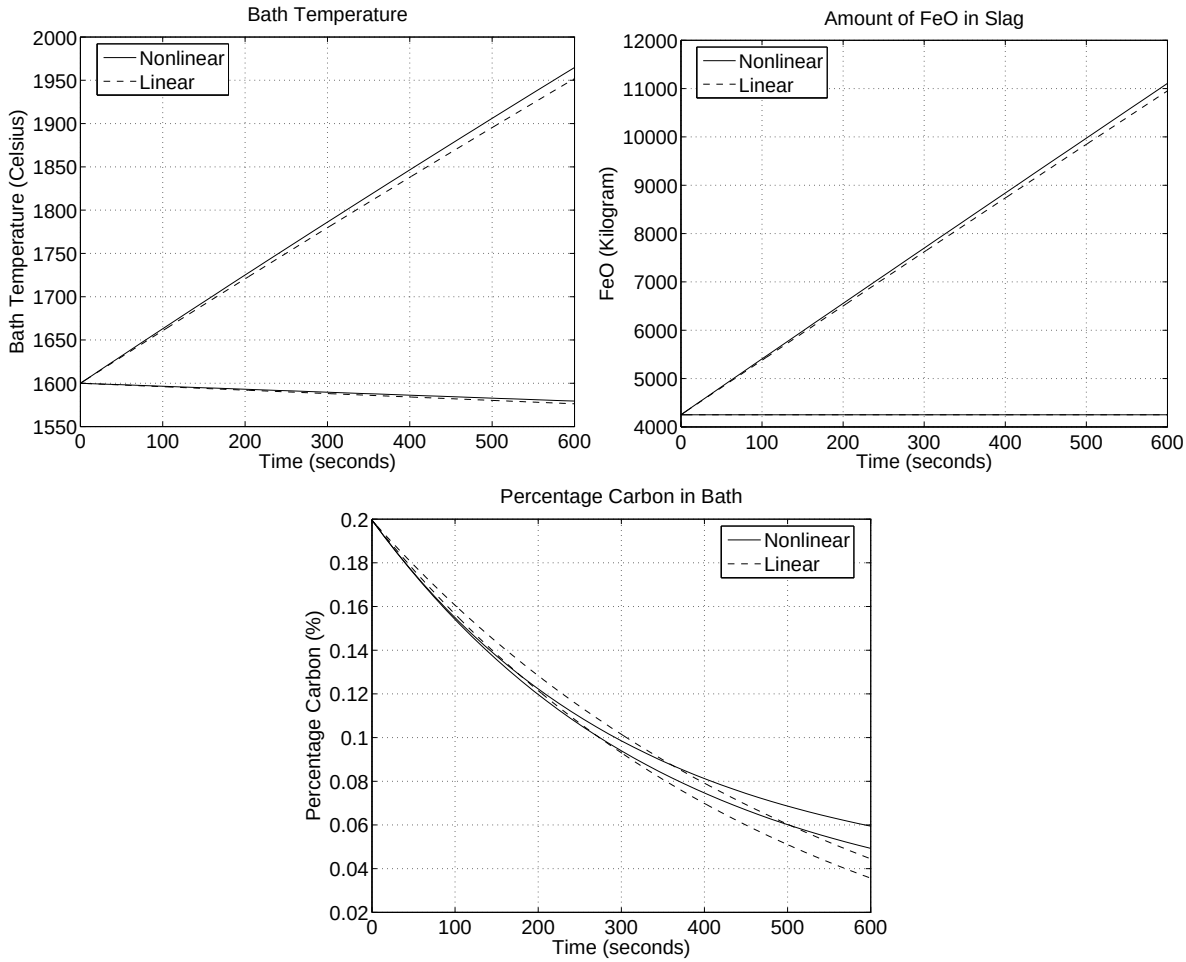

Figure 2.3: Linear and nonlinear model comparison with nominal parameters.

of the carbon content (2.46-2.48) shows that the carbon content is controllable through oxygen injection, slag additives and graphite injection. The modal analysis does not take constraints on the inputs into consideration. The constraints on the inputs limit the effect of the inputs on the decarburization rate. This can be seen from figure 2.3 which shows the reduction in carbon content with the inputs at their maximum and minimum. Decarburization can therefore be described as marginally controllable.

2.4.5 Simplification of linear models

From the previous section, it is clear that carbon is only marginally controllable. Studying the linear models more closely, it is clear that certain states and inputs can be eliminated. The inputs that are controlled during the refining stage are oxygen injection, electric power and graphite injection. DRI and slag are not added during the refining stage and

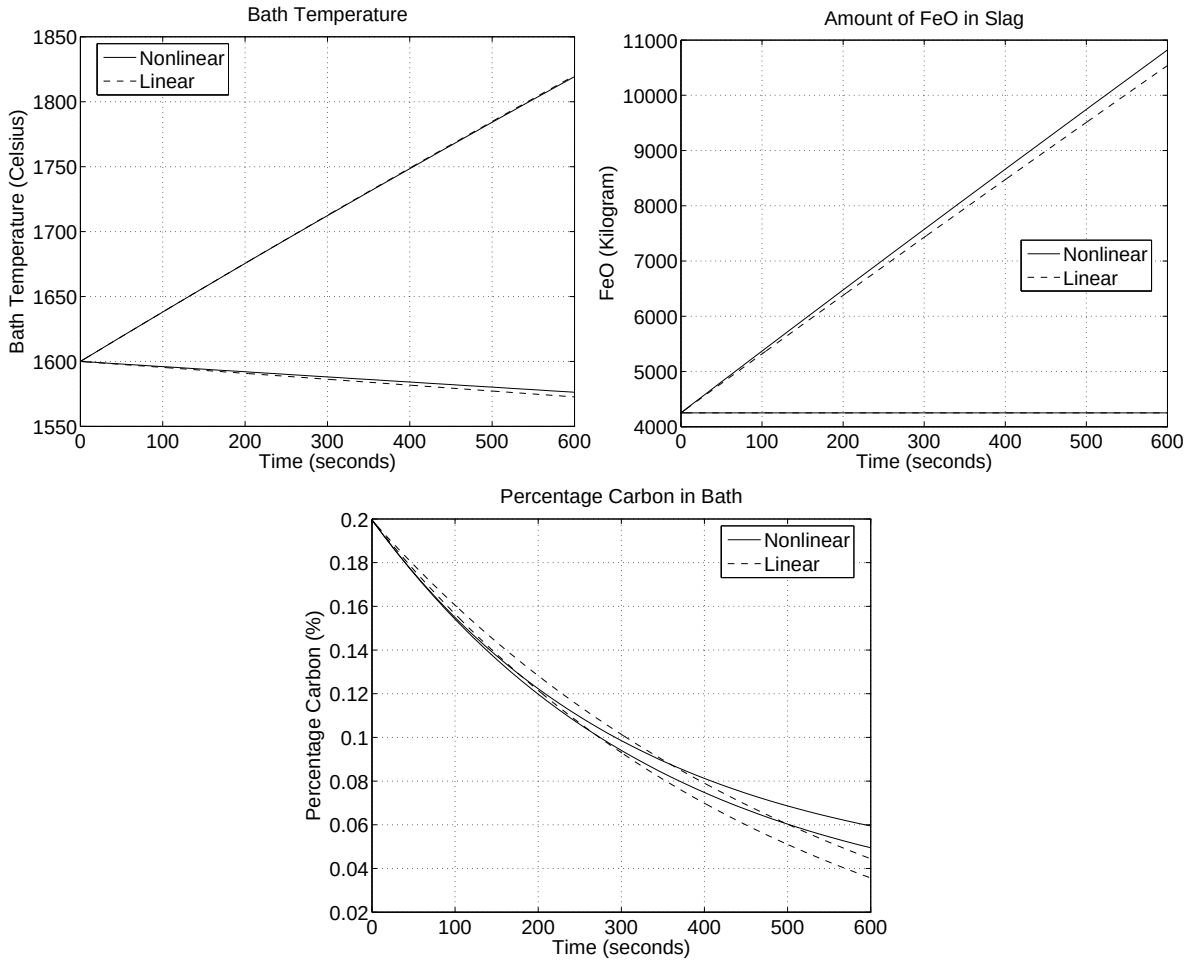

Figure 2.4: Linear and nonlinear model comparison with efficiencies at their minimum.

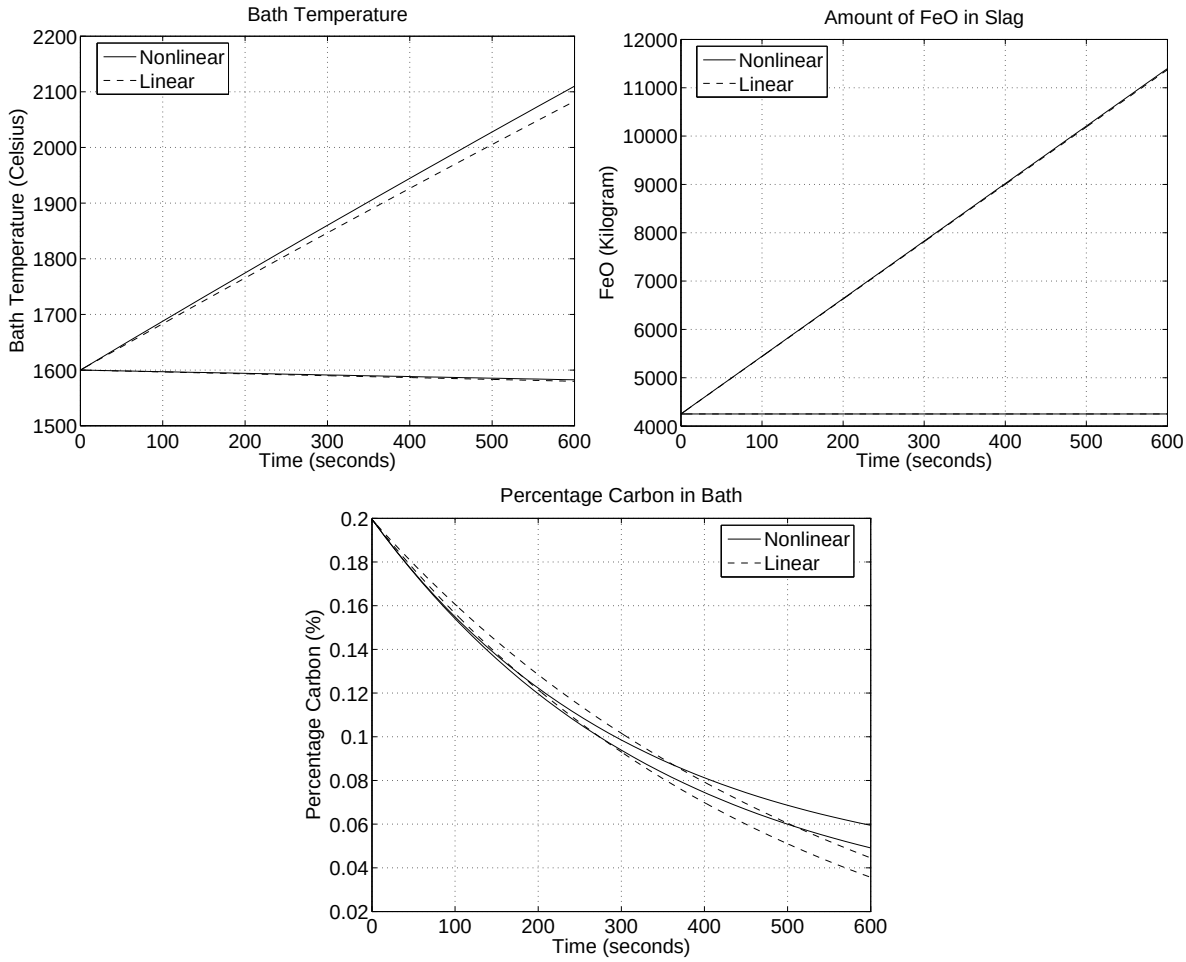

Figure 2.5: Linear and nonlinear model comparison with efficiencies at their maximum.

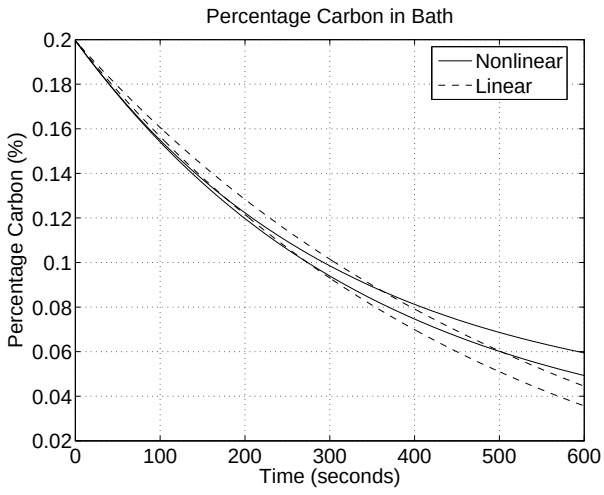

Figure 2.6: Decarburization response with all parameter variations.

can be removed from the linear models. The important states are carbon content, FeO content in the slag as well as temperature. Si and SiO_2 are impurities that need to be minimized, or steered to a desired specification.

From the second row of equation (2.41) , it is clear that there is no input that influences Si. The first column of equation (2.39), shows that carbon has no influence on the other states. The second column shows that only Si has an influence on carbon. The influence of Si on carbon is very insignificant. Carbon will therefore be removed from the model, for control purposes, because it cannot be significantly controlled as shown in the previous section. Si cannot be controlled and has no effect on any relevant term, and can therefore also be removed.

From the fourth row of equation (2.41) , it is clear that only DRI addition influences SiO_2. The fourth column of (2.39) shows that SiO_2 has a very small influence on carbon, FeO and temperature. In each instance, the cross-coupling term of SiO_2 is at least 1000 times smaller than the term for SiO_2 itself. SiO_2 can therefore be removed from the model without significantly affecting the dynamics of the system.

DRI only affects SiO_2 and thus becomes redundant and can be safely removed. The two remaining states in (2.49) have no uncertainty on the diagonal terms. The only remaining term that has significant uncertainty is the term that links FeO to temperature. The cross-couple term between FeO and temperature is a 1000 times smaller than the diagonal term, and the uncertainty entry of this term is therefore left out, because of its insignificant contribution to temperature. The simplified linear model can then be given as follows

$$A_{nominal-simplified} = \begin{bmatrix} 1 & 0 \\ -7.87e-6 & 1 \end{bmatrix}, \tag{2.49}$$

$$B_{nominal-simplified} = \begin{bmatrix} 12 & 0 & -1.17 \\ 0.41 & 6.07e-6 & -0.017 \end{bmatrix}, \tag{2.50}$$

$$B_{dev-simplified} = \begin{bmatrix} 0 & 0 & 0.988 \\ 0.11 & 3.03e-6 & 0.014 \end{bmatrix}, \tag{2.51}$$

where $B_{dev-simplified} \equiv B_p D_{qu}$. B_p and D_{qu} can be realized from $B_{dev-simplified}$ as

$$B_p = \begin{bmatrix} 1 & 0 & 0 & 0 \\ 0 & 1 & 1 & 1 \end{bmatrix}, \tag{2.52}$$

$$D_{qu} = \begin{bmatrix} 0 & 0 & 0.988 \\ 0.11 & 0 & 0 \\ 0 & 3.03e-6 & 0 \\ 0 & 0 & 0.014 \end{bmatrix}, \tag{2.53}$$

and the delta operator that is manipulated to describe the uncertain system is

$$\Delta = \begin{bmatrix} \Delta_1 & 0 & 0 & 0 \\ 0 & \Delta_2 & 0 & 0 \\ 0 & 0 & \Delta_3 & 0 \\ 0 & 0 & 0 & \Delta_4 \end{bmatrix}, \tag{2.54}$$

where $-1 \leq \Delta_i \leq 1,\ i = 1, 2, 3, 4$.

2.4.6 Analysis of simplified linear models

The simplified linear models are compared to the original nonlinear model. Three scenarios are used; the nominal case; parameters that produce the least efficiency, and parameters that produce the best efficiency. In all cases, the inputs are set to their maximum levels.

Figure 2.7 shows that the simplified linear models approximate the nonlinear model reasonably well. The simplified linear models are therefore taken to be suitable as the internal model for the model predictive controllers.

2.5 Conclusion

In this chapter the reduced nonlinear model for the refining stage of the electric arc furnace was linearized. The structured uncertainty description was used to describe the

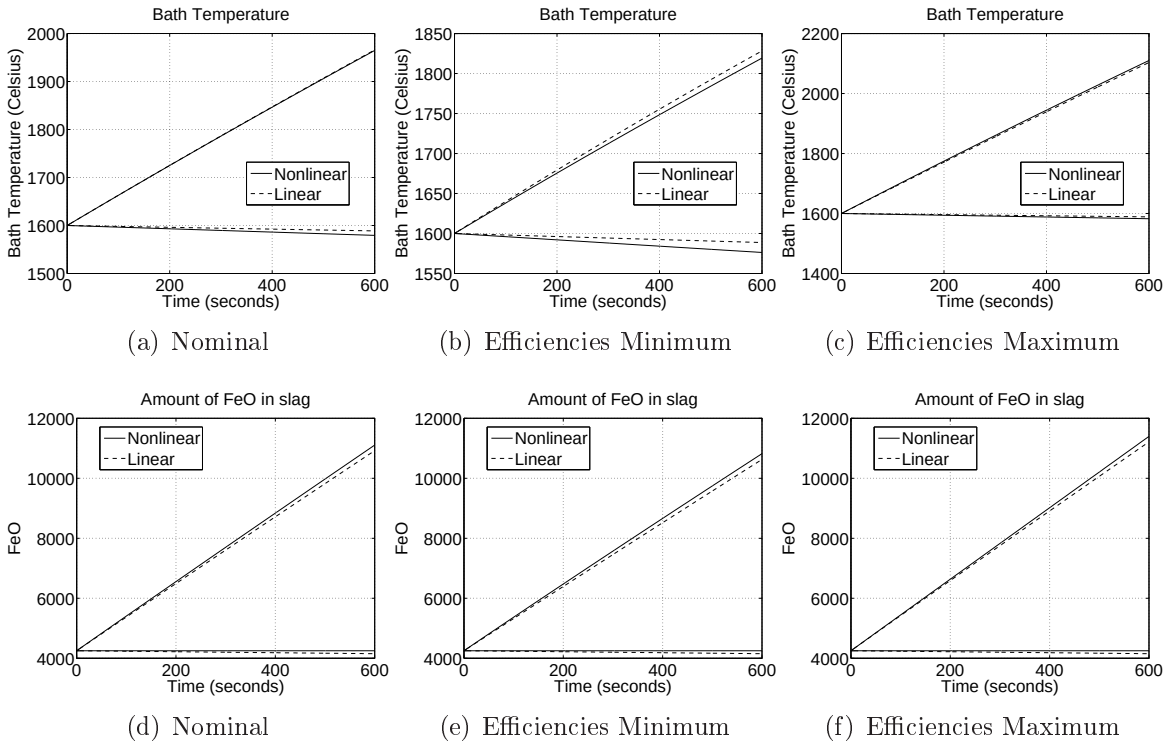

(a) Nominal (b) Efficiencies Minimum (c) Efficiencies Maximum

(d) Nominal (e) Efficiencies Minimum (f) Efficiencies Maximum

Figure 2.7: Simulation to compare simplified linear model to nonlinear model.

uncertainty of the nonlinear model in terms of linear models. A simulation study showed that the linear models approximated the nonlinear models reasonably well. The only variable that showed significant deviation was carbon, because of its highly nonlinear behaviour.

In the simplification of the linear models, it was shown that carbon is not significantly controllable, which implies that control cannot be used to accelerate the refining stage. The best option would be to ensure that the tapping temperature is at the desired value by the time carbon reaches its desired level.

The simplified linear models approximated the nonlinear model reasonably well with regards to FeO and temperature.

The simplified linear models are used in the synthesis of the model predictive controllers in chapter 3.

Chapter 3

Model predictive control

This chapter describes model predictive control and especially robust model predictive control that is applied to the plant outlined in chapter 2. The chapter starts by explaining model predictive control and its history, followed by a description of robust model predictive control and the reason for its development, and finally focuses on the controller theory used for the simulation study in chapter 4. The description of model predictive control and the development of stability theory including robust stability are summarized in the survey done by Mayne *et al.* (2000).

3.1 Introduction

Model predictive control (MPC), also known as receding horizon control (RHC), uses a mathematical model of a system to predict its future behaviour in order to calculate a sequence of control moves (N steps) into the future that will optimize (usually minimize) an objective or penalty function, which describes a measure of performance of the system. The first control move of the calculated sequence is applied to the system and a new measurement is taken. The process is then repeated for the next time step. Model predictive control calculates the control sequence on-line at each time step, compared to conventional control theory where the control law is pre-calculated and valid for all possible states of the system. Model predictive control has the distinct advantage of controlling multi-variable systems well and can explicitly take into consideration constraints on the inputs (such as

actuators, valves, etc.) as well as states or outputs (Camacho and Bordons, 2003). MPC is especially useful in situations where an explicit controller cannot be calculated offline.

The basic ideas present in the model predictive control family according to Camacho and Bordons (2003) are:

- outputs at future time instances are predicted by the explicit use of a *mathematical model*;
- an *objective function* is minimized by calculating the appropriate control sequence; and
- at each time instant, the horizon is displaced towards the future, which involves applying the first control signal calculated at each time instance to the system; called the *receding horizon* strategy.

The MPC theory described in this chapter is in discrete time and the system takes the following form (Mayne *et al.*, 2000):

$$x(k+1) = f(x(k), u(k)), \tag{3.1}$$

$$y(k) = g(x(k)). \tag{3.2}$$

The control and state sequences must satisfy

$$x(k) \in \mathbb{X}, \tag{3.3}$$

$$u(k) \in \mathbb{U}, \tag{3.4}$$

where $\mathbb{X} \subset \mathbb{R}^n$ and $\mathbb{U} \subset \mathbb{R}^m$. The objective function that is used in the optimization process has the following form:

$$V(x, k, \mathbf{u}) = \sum_{i=k}^{k+N-1} l(x(i), u(i)) + F(x(k+N)), \tag{3.5}$$

where $l(x(i), u(i))$ is the cost at each time step into the future with regards to the states and inputs, while $F(x(k+N))$ is the cost at the final state reached after the whole control sequence has been applied. At each time k, the final time is k+N, which increases as k increases and is called a *receding horizon*. In certain model predictive control formulations, a terminal constraint set is defined

$$x(k+N) \quad \in \quad X_f \subset \mathbb{X}. \tag{3.6}$$

The optimization of the objective function is performed subject to the constraints on the control and state sequences and in certain cases the terminal constraint to yield the optimized control sequence

$$\mathbf{u}^o(x,k) \quad = \quad (u^o(k;(x,k)), u^o(k+1;(x,k)), ..., u^o(k+N-1;(x,k))), \tag{3.7}$$

and optimized value for the objective function

$$V^o(x,k) \quad = \quad V(x,k,\mathbf{u}^o), \tag{3.8}$$

where (x,k) denotes that the current state is x at time k. The first control move at time k of the sequence $\mathbf{u}^o(x,k)$ is implemented to form an implicit control law for time k

$$\kappa(x,k) \quad = \quad u^o(k;(x,k)). \tag{3.9}$$

The objective function is time invariant, because neither $l(x(i), u(i))$ nor $F(x(k+N))$ have terms that depend on time. The optimization problem $P_N(x)$ can be defined as starting at time 0. N represents the finite prediction horizon over which the optimization takes place, and the optimization problem can be redefined as

$$P_N(x) : V_N^o(x) \quad = \quad \min_{\mathbf{u}} \{V_N(x,\mathbf{u}) | \mathbf{u} \in \mathbb{U}_N\}, \tag{3.10}$$

where the objective function is now

$$V_N(x, \mathbf{u}) = \sum_{i=0}^{N-1} l(x(i), u(i)) + F(x(N)), \tag{3.11}$$

with $\mathbb{U}_N$ the set of feasible control sequences that satisfy the control, state and terminal constraints. If problem $P_N(x)$ is solved, the optimal control sequences are obtained

$$\mathbf{u}^o(x) = \{u^o(0, x)), u^o(1, x)), ..., u^o(N-1, x)\}, \tag{3.12}$$

and the optimal state trajectory, if the control actions are implemented, is given by

$$\mathbf{x}^o(x) = \{x^o(0, x), x^o(1, x), ..., x^o(N-1, x), x^o(N, x)\}. \tag{3.13}$$

The optimal objective value is

$$V_N^o(x) = V_N(x, \mathbf{u}^o). \tag{3.14}$$

The first control action is implemented, leading to the implicit time invariant control law

$$\kappa_N(x) = u^o(0, x). \tag{3.15}$$

Dynamic programming can be used to determine a sequence of objective functions $V_j(\cdot)$ deterministically in order to calculate the sequence of control laws $\kappa_j(\cdot)$ offline, where j is the time-to-go until the prediction horizon. This is possible because of the deterministic nature of the open-loop optimization. This would be preferable, but is usually not possible. The difference between MPC and dynamic programming is purely a matter of implementation. MPC differs from conventional optimal control theory in that MPC uses a receding horizon control law $\kappa_N(\cdot)$ rather than an infinite horizon control law.

3.2 Historical background

Model predictive control builds on optimal control theory, the theory (necessary and sufficient conditions) of optimality, Lyapunov stability of the optimal controlled system, and algorithms for calculating the optimal feedback controller (if possible) (Mayne *et al.*, 2000). There are a few important ideas in optimal control that underlie MPC. The first links together two principles of the control theory developed in the 1960s: Hamilton-Jacobi-Bellman theory (Dynamic Programming) and the maximum principle, which provides necessary conditions for optimality. Dynamic programming provides sufficient conditions for optimality as well as a procedure to synthesise an optimal feedback controller $u = \kappa(x)$. The maximum principle provides necessary conditions of optimality as well as computational algorithms for determining the optimal open-loop control $u^o(\cdot; x)$ for a given initial state x. These two principles are linked together as

$$\kappa(x) \quad = \quad u^o(0; x), \tag{3.16}$$

in order for the optimal feedback controller to be obtained by calculating the open-loop control problem for each x (Mayne *et al.*, 2000). From the commencement of optimal control theory it is stated by Lee and Markus (1967, p. 423): "One technique for obtaining a feedback controller synthesis from knowledge of open-loop controllers is to measure the current control process state and then compute very rapidly for the open-loop control function. The first portion of this function is then used during a short time interval, after which a new measurement of the process state is made and a new open-loop control function is computed for this new measurement. The procedure is then repeated."

Kalman, as discussed inMayne *et al.* (2000), observed that *optimality* does not guarantee *stability*. There are conditions under which optimality results in stability: *infinite horizon* controllers are stabilizing, if the system is stabilizable and detectable. Calculating infinite horizon optimal solutions is not always practical on-line and an alternate solution was needed to stabilize the receding horizon controller. The first results for stabilizing receding horizon controllers were given by (Kleinman, 1970), who developed a minimum

energy controller for linear systems. He showed that the feedback controller is linear, time invariant and stable if a Lyapunov function $V(x) = x^T Px$ is used as the objective function. Another approach is to define a *stability constraint* as part of the optimal control problem. The stability constraint is defined as an equality constraint $x(T) = 0$ that forces the solution to converge to the origin. Thomas, as discussed in Mayne *et al.* (2000), suggested this technique as part of a linear quadratic control problem and implemented it by using $M := P^{-1}$ in place of P as the Ricatti variable and solving the Ricatti-like differential equation with terminal condition $M(T) = 0$.

MPC was really driven by industry as part of process control theory. Richalet *et al.* (1978) was the first to propose MPC for process control applications, but MPC was proposed earlier by Propoi and Lee and Markus (as discussed in Mayne *et al.* (2000)). The MPC method, called identification and command (IDCOM), was proposed by Richalet *et al.* (1978). It uses a linear model in the form of a finite horizon impulse response, quadratic cost and constraints on the inputs and outputs. The method makes provision for linear estimation using least squares and the algorithm for solving the open-loop optimal control problem is the "dual" of the identification algorithm.

Dynamic matrix control (DMC) is a later method proposed by Cutler and Ramaker (1980) and Prett and Gillette (as discussed in Mayne *et al.* (2000)). DMC uses a step response model, but as in IDCOM, handled constraints in an ad-hoc fashion. This limitation was addressed by García and Morshedi (as discussed in Mayne *et al.* (2000)) by using quadratic programming to solve the constrained open-loop optimization problem. This method also allows certain violations of the constraints in order to enlarge the set of feasible states. This method is called QDMC (Quadratic Dynamic Matrix Control).

The third generation of MPC technology, introduced about a decade ago, "distinguishes between several levels of constraints (hard, soft and ranked). This technology provides some mechanism to recover from an infeasible solution, and addresses the issues resulting from a control structure that changes in real time, and allows for a wider range of process dynamics and controller specifications" (Qin and Badgwell, 2003). The Shell multi-variable optimizing control (SMOC) uses state-space models, incorporates general

disturbance models and allows for state estimation using Kalman filters (as discussed in Mayne *et al.* (2000)).

An independent but similar approach was developed from the adaptive control theory and is called generalized predictive control (GPC). The method uses models in the backward shift operator q^{-1} which is more general than the impulse and step response models of DMC. GPC started as minimum variance control (Mayne *et al.*, 2000) that only allowed for a horizon of length 1. Minimum variance control was extended to allow for longer prediction horizons by Peterka (1984) as well as Clarke *et al.* (1987*a*,*b*). GPC, and early versions of DMC, did not explicitly incorporate stability in the method and had to rely on the tuning of the prediction horizon as well as the weights on the states and inputs to achieve stability.

3.3 Stability of MPC

The inability of both GPC and DMC to guarantee stability caused researchers to focus more on modifying $P_N(x)$ to ensure stability due to increased criticism (Bitmead *et al.*, 1990) of the makeshift approach of using tuning to attain stability.

With *terminal equality constraints*, the system is forced to the origin by the controller that takes the form $F(x) = 0$, as there is no terminal cost and the terminal set is $X_f = \{0\}$. Keerthi and Gilbert, as discussed in Mayne *et al.* (2000), proposed this stabilizing strategy for constrained, nonlinear, discrete systems, and showed a stability analysis of this version (terminal equality constraints) of discrete-time receding horizon control. MPC with a terminal equality constraint can be used to stabilize a system that cannot be stabilized by continuous feedback controllers, according to Meadows *et al.* (as discussed in Mayne *et al.* (2000)).

Using a *terminal cost function* is an alternative approach to ensure stability. Here the terminal cost is $F(\cdot)$, but there is no terminal constraint and the terminal set is thus $X_f = \mathbb{R}^n$. For unconstrained linear systems the terminal cost of $F(x) = \frac{1}{2}x^T P_f x$ is proposed by Bitmead *et al.* (1990).

Terminal constraint sets differ from the terminal equality constraints, in that subsets

of $\mathbb{R}^n$ that include a neighbourhood of the origin are used to stabilize the control, not just the origin. The terminal constraint set, as with the terminal equality constraint, does not employ a terminal cost, thus $F(x) = 0$. The MPC controller should steer the system to X_f within a finite time, after which a local stabilizing controller $\kappa_f(\cdot)$ is employed. This methodology is usually referred to as dual mode control and was proposed by Michalska and Mayne (1993) in the context of constrained, nonlinear, continuous systems by using a variable horizon N.

A *terminal cost and constraint set* is employed in most modern model predictive controllers. If a infinite horizon objective function can be used, on-line optimization is not necessary and stability and robustness can be guaranteed. In practical systems, constraints and other nonlinearities make the use of infinite horizons impossible, but it is possible to approximate an infinite horizon objective function if the system is suitably close to the origin. By choosing the terminal set X_f as a suitable subset of $\mathbb{R}^n$, the terminal cost $F(\cdot)$ can be chosen to approximate an infinite horizon objective function. A terminal cost and constraint set controller therefore needs a terminal constraint set $\mathbb{X}_f$ in which the terminal cost $F(\cdot)$ and infinite horizon feedback controller K_f are employed. To synthesise these, Sznaier and Damborg (as discussed in Mayne *et al.* (2000)) proposed that the terminal cost $F(\cdot)$ and feedback controller K_f of a standard LQ problem be used, which is an unconstrained infinite horizon problem, when the system is linear ($f(x, u) = Ax + Bu$) and the state and input constraint sets, $\mathbb{X}$ and $\mathbb{U}$, are polytopes. The terminal constraint set X_f is chosen to be the *maximal output admissible set* (Gilbert and Tan, 1991) of the system $f(x, u) = (A + BK_f)x$.

3.3.1 Stability conditions for model predictive controllers

From the above discussion, it is clear that the additions of a terminal constraint set X_f, terminal cost $F(\cdot)$ and local feedback controller κ_f in the terminal constraint set, form the basis of stabilizing model predictive control. Some conditions, in the form of axioms, are formulated (Mayne *et al.*, 2000) for the terminal constraint set, terminal cost and local feedback controller, which ensure that the controller is stabilizing.

Two related methods are available for establishing stability. Both methods use a Lyapunov function as the objective function. The first method ensures that the objective function $V_N^o(x)$ evolves with the state from x to $x^+ = f(x, \kappa_N(x))$ so that

$$V_N^o(x^+) - V_N^o(x) + l(x, \kappa_N(x)) \leq 0, \tag{3.17}$$

while the alternative method uses the fact that

$$V_N^o(x^+) - V_N^o(x) + l(x, \kappa_N(x)) = V_N^o(x^+) - V_{N-1}(x^+), \tag{3.18}$$

and shows that the right-hand side is negative, either directly or by showing that $V_1^o(\cdot) \leq V_0^o(\cdot)$ and exploiting monotonicity which implies that if $V_1^o(\cdot) \leq V_0^o(\cdot)$ then $V_{i+1}^o(\cdot) \leq V_i^o(\cdot)$ for all $i \geq 0$.

Assume a model predictive controller that can steer the system state x to the terminal constraint set X_f within the prediction horizon N or fewer steps. The control sequence that accomplishes this is called an admissible or feasible control sequence $\mathbf{u} = \{u(0), u(1), ..., u(N-1)\}$. This control sequence should satisfy the control constraints $u(i) \in \mathbb{U}$ for $i = 0, 1, ..., N-1$ and ensure that the controlled states satisfy the state constraints $x^{\mathbf{u}}(i) \in \mathbb{X}$ for $i = 0, 1, .., N$ and the final state satisfies the terminal constraint set $x^{\mathbf{u}}(N) \in \mathbb{X}_f$. If the control problem $P_N(x)$ is solved, the control sequence $\mathbf{u}^o(x)$ is obtained that will steer the system within the set of states that is possible with a model predictive control of horizon N, $x \in \mathbb{X}_N$. The optimal control sequence $\mathbf{u}^o(x) = \{u(0; x), u(1; x), ..., u(N-1; x)\}$ will result in the optimal state sequence $\mathbf{x}^o(x) = \{x^o(0; x), x^o(1; x), ..., x^o(N-1; x), x^o(N; x)\}$. The first control action of $\mathbf{u}^o(x)$, that is $u = \kappa_N(x) = u^o(0; x)$ is implemented to get to the next state $x^+ = f(x, \kappa_N(x)) = x^o(1; x)$. A feasible control sequence $\tilde{\mathbf{x}}(x^+)$ for the state x^+, will result in an upper bound for the optimal objective function $V_N^o(x^+)$, because a feasible control sequence should give a larger value for the objective function than an optimal control sequence. The abbreviated control sequence $\{u(1; x), u(2; x), ..., u(N-1; x)\}$ derived from $\mathbf{u}^o(x)$ should be a feasible control sequence to steer state x^+ to $x^o(N; x) \in \mathbb{X}_f$. If an extra term is added to the

control sequence $\{u(1;x), u(2;x), ..., u(N-1;x), u\}$, the control sequence will be feasible for $P_N(x^+)$ if $u \in \mathbb{U}$ and u steers $x^o(N;x) \in \mathbb{X}_f$ to $f(x^o(N;x), u) \in \mathbb{X}_f$. This will be true if $u = \kappa_f(x^o(N;x))$, with the terminal state constraint X_f and local controller $\kappa_f(\cdot)$ having the properties:

$$\mathbb{X}_f \subset \mathbb{X},\ \kappa_f(x) \in \mathbb{U} \quad \text{and} \quad f(x, \kappa_f(x)) \in \mathbb{X}_f\ \forall x \in \mathbb{X}_f, \tag{3.19}$$

implying that the terminal set $\mathbb{X}_f$ is invariant when the controller is $\kappa_f(\cdot)$. The feasible control sequence for $P_N(x^+)$ is

$$\tilde{\mathbf{u}}(x) \quad = \quad \{u^o(1;x), u^o(2;x), ..., u^o(N-1;x), \kappa_f(x^o(N;x))\}, \tag{3.20}$$

with the associated cost

$$\begin{aligned} V_N(x^+, \tilde{\mathbf{u}}(x)) \quad = \quad & V_N^o(x) - l(x, \kappa_N(x)) - F(x^o(N;x)) \\ & + l(x^o(N;x), \kappa_f(x^o(N;x)) \\ & + F(f(x^o(N;x), \kappa_f(x^o(N;x))). \end{aligned} \tag{3.21}$$

This cost is the upper bound on $V_N^o(x^+)$ and satisfies

$$V_N(x^+, \tilde{\mathbf{u}}(x)) \quad \leq \quad V_N^o(x) - l(x, \kappa_N(x)), \tag{3.22}$$

if $F(f(x, \kappa_f(x))) - F(x) + l(x, \kappa_f(x)) \leq 0\ \forall x \in \mathbb{X}_f$. This is accomplished if $F(\cdot)$ is a control Lyapunov function in the neighbourhood of the origin and the controller κ_f and the terminal constraint set $\mathbb{X}_f$ are chosen appropriately. If this condition is satisfied, then (3.17) will hold for all $x \in \mathbb{X}_N$ and it is sufficient to say that the closed-loop system $x^+ = f(x, \kappa_N(x))$ will converge to zero as time tends to infinity, provided that the initial state is within $\mathbb{X}_N$. The stability conditions can be summarized in the following axioms (Mayne *et al.*, 2000):

A1: $\mathbb{X}_f \subset \mathbb{X}, \mathbb{X}_f$ is a closed set and $0 \in \mathbb{X}_f$. This condition implies that the state

constraints should be satisfied in the terminal constraint set.

A2: $\kappa_f(x) \in \mathbb{U},\ \forall x \in \mathbb{X}_f$. This condition implies that the constraints on the controls should be satisfied by the local controller in the terminal constraint set $\mathbb{X}_f$.

A3: $f(x, \kappa_f(x)) \in \mathbb{X}_f,\ \forall x \in \mathbb{X}_f$. This implies that the terminal constraint set $\mathbb{X}_f$ is positively invariant under the local controller $\kappa_f(\cdot)$.

A4: $F(f(x, \kappa_f(x))) - F(x) + l(x, \kappa_f(x)) \leq 0\ \forall x \in \mathbb{X}_f$. The terminal cost function $F(\cdot)$ is a local Lyapunov function in the terminal constraint set $\mathbb{X}_f$.

The conditions as summarized in A1 to A4 are merely sufficient conditions to ensure stability in model predictive controllers. These conditions can be shown to hold for the monotonicity approach as well as the continuous case (Mayne *et al.*, 2000). The following few paragraphs will show how the stabilizing methods of section 3.3 satisfy the stability conditions A1 to A4.

3.3.2 Terminal state MPC

The *terminal state* variant of model predictive controllers (Mayne *et al.*, 2000) uses the terminal state $\mathbb{X}_f = \{0\}$ with no terminal cost $F(\cdot) = 0$. The local controller in the terminal constraint set is $\kappa_f(x) = 0$ that will ensure that the state remains at the origin if this controller is applied. The functions $F(\cdot)$ and $\kappa_f(\cdot)$ are only valid in $\mathbb{X}_f$ which is at the origin. The satisfaction of the stability conditions A1 to A4 are as follows:

A1: $\mathbb{X}_f = \{0\} \in \mathbb{X}$ - Satisfied.

A2: $\kappa_f(0) = 0 \in \mathbb{U}$ - Satisfied.

A3: $f(0, \kappa_f(0)) = f(0, 0) = 0 \in \mathbb{X}_f$ - Satisfied.

A4: $F(f(0, \kappa_f(0))) - F(0) + l(0, \kappa_f(0)) = 0$ - Satisfied.

The controller ensures that the closed-loop system is asymptotically (exponentially) stable with region of attraction $\mathbb{X}_N$.

3.3.3 Terminal cost MPC

Terminal cost model predictive controllers are only valid for linear unconstrained (Bitmead *et al.*, 1990) and linear, stable, constrained (Rawlings and Muske, 1993) cases. In order to ensure stability a terminal constraint is necessary if the system is nonlinear or linear, constrained and unstable. *Linear, unconstrained systems* are defined as $f(x,u) = Ax + Bu$, and $l(x,u) = \frac{1}{2}(|x|_Q^2 + |u|_R^2)$ where $Q > 0$ and $R > 0$. The first three conditions A1 to A3 are trivially satisfied in the unconstrained case, because $\mathbb{X} = \mathbb{R}^n$ and $\mathbb{U} = \mathbb{R}^m$. In the case where A and B are stabilizable, the local controller is defined as $\kappa_f := K_f x$, and $P_f > 0$ should satisfy the Lyapunov equation

$$A_f^T P A_f + Q_f = 0, \quad A_f := A + BK_f, \quad Q_f := Q + K_f R K_f, \tag{3.23}$$

then the terminal cost function $F(x) := \frac{1}{2}x^T P_f x$ satisfies A4 and the closed-loop system is asymptotically (exponentially) stable with a region of attraction $\mathbb{R}^n$. *Linear, constrained, stable* systems have control constraints $u \in \mathbb{U}$, but no constraints on the states, thus $\mathbb{X} = \mathbb{X}_f = \mathbb{R}^n$. In order to satisfy A2, the controller function, if linear, should be $\kappa_f(x) = 0$ (Rawlings and Muske, 1993), that leads to the first three conditions (A1 to A3) being satisfied. The final condition A4 is satisfied if the terminal cost function is $F(x) := \frac{1}{2}x^T P_f x$, where P_f satisfy the Lyapunov equation $A^T P A + Q = 0$, that results in a controller with asymptotic (exponential) stability with region of attraction $\mathbb{R}^n$.

3.3.4 Terminal constraint set MPC

Terminal constraint set model predictive controllers employ a terminal constraint set $x(N) \in \mathbb{X}_f$ without a terminal cost $F(x) = 0$ for nonlinear, constrained systems. Michalska and Mayne (1993) introduced the idea of a variable prediction horizon N for continuous-time, constrained, nonlinear systems. Scokaert *et al.* (1999) proposed a fixed horizon version for nonlinear, constrained, discrete-time systems. The controller steers the state of the system x to within the terminal constraint set $\mathbb{X}_f$, after which a local stabilizing controller $\kappa_f(x) = K_f x$ is employed. This type of MPC is sometimes referred to as *dual-mode MPC*.

This method is similar to the terminal equality constraint method, except that the equality $\{0\}$ is replaced by a set $\mathbb{X}_f$. The local controller $\kappa_f(\cdot)$ and the terminal constraint set $\mathbb{X}_f$ are chosen to satisfy the first three conditions A1 to A3. The local controller $\kappa_f(\cdot)$ is chosen to steer the system exponentially fast to the origin for all states in the terminal constraint set ($\forall x \in \mathbb{X}_f$). The stage cost of the objective function $l(x, \kappa_f(x))$ should be 0 when the system state is within the terminal constraint set $\mathbb{X}_f$ in order to satisfy A4. A suitable choice for the stage cost is

$$l(x,u) \quad := \quad \alpha(x)\bar{l}(x,u), \tag{3.24}$$

where $\alpha(x) = 1,\ \forall x \notin \mathbb{X}_f,$ else $\alpha(x) = 0$ and $\bar{l}(x,u) = \frac{1}{2}(x^TQx + u^TRu)$, where $Q > 0$ and $R > 0$. The closed-loop system is exponentially stable with domain of attraction $\mathbb{X}_N$, because the MPC controller steers the system with initial state $x \in \mathbb{X}_N$ within finite time to $\mathbb{X}_f$ with the controller value $\kappa_N(\cdot)$.

3.3.5 Terminal cost and constraint set MPC

Terminal cost and constraint sets are employed by most modern model predictive controllers. In *linear, constrained systems* the terminal cost function can be chosen $F(x) = V^0_{uc}(x) = \frac{1}{2}x^TP_fx$, that is the same as the unconstrained infinite horizon optimal control problem. The local controller $\kappa_f(x) = K_fx$ is the optimal infinite horizon controller and the terminal constraint set $\mathbb{X}_f$ is the maximal admissible set for the system $x^+ = A_fx,\ A_f := A + BK_f$, thus satisfying A1-A4. This results in an exponentially stable controller with domain of attraction $\mathbb{X}_f$. The ideal choice for the terminal cost would be to choose $F(x) = V^o_\infty(x)$, the objective function of an infinite horizon optimal controller, that would result in the objective function for model predictive controller being $V^o_N(x) = V^o_\infty(x)$, and on-line optimization would not be necessary. The resulting MPC controller will have all the advantages of infinite horizon control. This is usually not practical, and the use of the terminal constraint set $\mathbb{X}_f$ and $F(x) = V^0_{uc}(x) = \frac{1}{2}x^TP_fx$ approximates the advantages of using $F(x) = V^o_\infty(x)$. The nonlinear case is also given in

Mayne *et al.* (2000).

From this discussion, it is clear that the use of a terminal constraint set $\mathbb{X}_f$, terminal cost function $F(\cdot)$ and local stabilizing controller $\kappa_f(\cdot)$ is necessary to ensure stability in model predictive control. The first two requirements, terminal constraint set $\mathbb{X}_f$ and terminal cost function $F(\cdot)$, are explicitly incorporated into the controller, while the feedback controller $\kappa_f(\cdot)$ is only implicitly needed to prove stability. If the cost function $F(\cdot)$ is as close to the objective function $V_\infty^o(\cdot)$ as possible, the closed-loop trajectory is exactly the same as that predicted by the solution of the optimal control problem $P_N(x)$.

3.4 Robust MPC - Stability of uncertain systems

Robust model predictive control is concerned with the stability and performance of the closed-loop system in the presence of uncertainty in the plant model. Early studies in robustness of model predictive controllers considered unconstrained systems and found that if the Lyapunov function retains its descent property in the presence of disturbances (uncertainty), it will remain stable. In the constrained case, the problem becomes more complex, because the uncertainty or disturbances should not cause the closed-loop system to violate its state or control constraints.

Richalet *et al.* (1978) performed one the earliest studies in robustness on systems with impulse response models, by investigating the effect of gain mismatches on the closed-loop system. Later work on systems modelled by impulse responses approached the optimal control problem as a min-max problem, that caused the problem to grow exponentially with the size of the prediction horizon.

There are several approaches to robust model predictive control, the first being a study of the robustness of model predictive control designed with a nominal model (that does not take uncertainty into account). The second approach considers all the possible realizations of the uncertain system when calculating the open-loop optimal controller (min-max open-loop MPC). The open-loop nature of model predictive control is a problem when model uncertainty is present and the third approach addresses this by introducing feedback in the optimal control problem that is solved on-line.

For the discussion of robust model predictive control, the uncertain system is described as

$$x^+ = f(x, u, w), \tag{3.25}$$

$$y = g(x), \tag{3.26}$$

where the state x and control u satisfy the same constraints

$$x(k) \in \mathbb{X}, \tag{3.27}$$

$$u(k) \in \mathbb{U}, \tag{3.28}$$

and the disturbance or uncertainty w satisfies $w \in W(x(k), u(k))$ for all k where, for each $(x, u), W(x, u)$ is closed and contains the origin in its interior. The disturbance sequence $\mathbf{w} := \{w(0), w(1), ..., w(N-1)\}$ together with the control sequence $\mathbf{u}$ and initial state x will produce the resulting state trajectory $x^{\mathbf{u},\mathbf{w}}(\cdot; x)$. Let $\mathcal{F}(x, u) := f(x, u, W(x, u))$, which will map values in $\mathbb{X}$ and $\mathbb{U}$ to subsets of $\mathbb{R}^n$, resulting in $x^+ \in \mathcal{F}(x, u)$.

De Nicolao *et al.* (1996) and Magni and Sepulchre (1997) studied the inherent robustness of model predictive controllers that were designed without taking uncertainty into account.

3.4.1 Stability conditions for robust MPC

Most versions of robust model predictive control take all the realizations of the uncertainty or disturbance w into consideration that requires strengthened assumptions to be satisfied, which are summarized as *robust* versions of axioms A1-A4 (Mayne *et al.*, 2000):

A1: $\mathbb{X}_f \subset \mathbb{X}, \mathbb{X}_f$ closed, $0 \in \mathbb{X}_f$.

A2: $\kappa_f(x) \in \mathbb{U}, \ \forall x \in \mathbb{X}_f$.

A3a: $f(x, \kappa_f(x), w) \in \mathbb{X}_f, \ \forall x \in \mathbb{X}_f, \ \forall w \in W(x, \kappa_f(x))$.

A4a: $F(f(x, \kappa_f(x), w)) - F(x) + l(x, \kappa_f(x), w) \leq 0, \ \forall x \in \mathbb{X}_f, \ \forall w \in W(x, \kappa_f(x))$.

If $F(\cdot)$ is a robust Lyapunov function in the neighbourhood of the origin, there exists a triple $(F(\cdot), \mathbb{X}_f, \kappa_f(\cdot))$, which ensures that A4a is satisfied and results in an asymptotically or exponentially stable controller.

3.4.2 Open-loop min-max MPC

Open-loop min-max model predictive control considers all the possible realizations of the uncertain system in order to ensure that the state, control and terminal constraints are met for all the possible realizations (Michalska and Mayne, 1993). The objective function value in this case is determined for each realization

$$J(x, \mathbf{u}, \mathbf{w}) \quad := \quad \sum_{i=0}^{N-1} l(x(i), u(i)) + F(x(N)), \tag{3.29}$$

where $x(i) = x^{\mathbf{u},\mathbf{w}}(i; x; 0)$ and the final objective value is the worst case for all the realizations

$$V_N(x, \mathbf{u}) \quad := \quad \max\{J(x, \mathbf{u}, \mathbf{w}) | \mathbf{w} \in W_N(x, \mathbf{u})\}, \tag{3.30}$$

where $W_N(x, \mathbf{u})$ is the set of admissible disturbance sequences. Other choices are to take the objective value as the nominal objective value by using $\mathbf{w} = \mathbf{0}$. Badgwell (as discussed in Mayne *et al.* (2000)) used an interesting approach, where the controller should reduce the objective function value for every realization, which is assumed finite, for a linear system. This is stronger than only reducing the worst-case objective value.

The set of admissible control sequences $\mathcal{U}_N^{ol}(x)$ is that set which satisfies the control, state and terminal constraints for all possible realization of the disturbance sequence $\mathbf{w}$ when the initial state is x. Suppose the the set $\mathbb{X}_i^{ol}$, for all $i \geq 0$, is the set of states that can be robustly steered to the terminal state constraint $\mathbb{X}_f$ in i steps or less by an admissible control sequence $\mathbf{u} \in \mathcal{U}_N^{ol}(x)$. The open-loop optimal control problem is

$$P_N^{ol}(x) : \; V_N^o(x) \quad = \quad \min\{V_N(x, \mathbf{u}) | \mathbf{u} \in \mathcal{U}_N^{ol}(x)\}. \tag{3.31}$$

The solution to $P_N^{ol}(x)$ yields the optimal control sequence $\mathbf{u}^o(x)$, where the implicit min-max control law is

$$\kappa_N^{ol}(x) \quad := \quad \mathbf{u}^o(0;x), \tag{3.32}$$

as in the nominal case. The control sequence will result in a "bundle" of optimal state sequences $\{\mathbf{x}^o(x,\mathbf{w})\}$ as a result of the disturbance sequences $\mathbf{w}$, so that

$$\mathbf{x}^o(x,\mathbf{u}) \quad = \quad \{x^o(0;x;\mathbf{w}), x^o(1;x;\mathbf{w}), ..., x^o(N-1;x;\mathbf{w}), x^o(N;x;\mathbf{w})\}. \tag{3.33}$$

The triple $(F(\cdot), \mathbb{X}_f, \kappa_f(\cdot))$ is assumed to satisfy the stability conditions A1-A4a. Assume the process is started with an initial state $x \in \mathcal{X}_N^{ol}$ and has an optimal (and by implication a feasible) control sequence $\{u^o(0;x), u^o(1;x), ..., u^o(N-1;x)\}$ for the optimal control problem $P_N^{ol}(x)$ that steers the state to within the terminal constraint set $\mathbb{X}_f$ within N steps or less, so that $x^o(N;x;\mathbf{w}) \in \mathbb{X}_f$, $\forall w \in \mathcal{W}(x,\mathbf{u}^o(x))$. As a result the abbreviated control sequence $\{u^o(1;x), u^o(2;x), ..., u^o(N-1;x)\}$ should steer the state $x^+ \in \mathcal{F}(x,\kappa_N(x))$ to the terminal constraint set $\mathbb{X}_f$ within $N-1$ steps or less, where $x^+ \in \mathcal{X}_{N-1}^{ol}$. A problem arises when a feasible control sequence needs to be generated by adding a term to the abbreviated control sequence

$$\tilde{\mathbf{u}}(x) \quad = \quad \{u^o(1;x), u^o(2;x), ..., u^o(N-1;x), v\}, \tag{3.34}$$

for the optimal control problem $P_N^{ol}(x^+)$, where the control action $v \in \mathbb{U}$ is required to satisfy $f(x^o(N;x;\mathbf{w}), v, w_N) \in \mathbb{X}_N$ for all $\mathbf{w} \in \mathcal{W}(x,\mathbf{u}^o(x))$. The stability condition A3a does not ensure that such a control action v can be obtained, which prevents the upper bound of the objective function $V_N^o(x^+)$ from being calculated. Michalska and Mayne (1993) circumvent this problem by using a variable horizon optimal control problem $P(x)$ with decision variables $(\mathbf{u}, N)$. The optimal solution $(\mathbf{u}^o(x); N^o(x))$ is obtained by solving

the optimal control problem $P(x)$, where

$$\mathbf{u}^o(x) \quad = \quad \{u^o(0;x), u^o(1;x), ..., u^o(N(x)-1;x)\}.$$

For the optimal control problem $P(x^+)$ the solution $(\overline{\mathbf{u}}(x), N^o(x)-1)$ is a feasible solution for any $x^+ \in \mathcal{X}(x, \kappa_N(x))$. The variable horizon objective function $V^o(\cdot)$ and implicit controller $\kappa^{ol}(\cdot)$ will ensure that stability condition A4a holds for all $x \in \mathbb{X}_N^{ol} \subset \mathbb{X}_f$, $\forall w \in W(x, \kappa^{ol}(x))$. Inside the terminal constraint set $\mathbb{X}_f$, a suitable local controller $\kappa_f(\cdot)$ is used subject to stability conditions A1-A4a. This will result in an asymptotic (exponential) stable controller with domain of attraction $\mathbb{X}_N^{ol}$, subject to further modest assumptions (Michalska and Mayne, 1993).

3.4.3 Feedback robust MPC

Feedback robust model predictive control is better suited for uncertain systems than open-loop min-max controllers, because open-loop controllers assume that the trajectories of the system may diverge, which may cause $\mathbb{X}_N^{ol}$ to be very small, or even empty for a modest sized prediction horizon N, which is very conservative. This happens because the open-loop min-max controllers do not take the effect of feedback into consideration, which would prevent the trajectories from diverging too much. To address the shortcomings of open-loop min-max control, feedback MPC was proposed by Lee and Yu (1997), Scokaert and Mayne (1998), Magni *et al.* (2001) and Kothare *et al.* (1996). In feedback model predictive control, the control sequence $\mathbf{u}$ is replaced by a control policy π which is a sequence of control laws:

$$\pi \quad := \quad \{u(o), \kappa_1(\cdot), ..., \kappa_{N-1}(\cdot)\}, \tag{3.35}$$

where $\kappa_i(\cdot) : \mathbb{X} \rightarrow \mathbb{U}$ is a control law for each i, while $u(0)$ is a control action, because there is only one initial state. The objective function for the feedback model predictive

controller is

$$V_N(x,\pi) \quad := \quad max\{J(x,\pi,\mathbf{w})|\mathbf{w} \in \mathcal{W}_N(x,\pi)\} \tag{3.36}$$

and the objective function for each realization

$$J(x,\pi,\mathbf{w}) \quad := \quad \sum_{i=0}^{N-1} l(x(i),u(i)) + F(x(N)), \tag{3.37}$$

where $x(i) = x^{\pi,\mathbf{u}}(i;x)$ is the state at time i resulting from an initial state at time 0, a control policy π and a disturbance sequence $\mathbf{w}$. The admissible set of disturbances, given the control policy π is implemented, is $\mathcal{W}_N(x,\pi)$. The set of admissible control policies that will satisfy the control, state and terminal constraints for all the admissible disturbances with initial state x, is $\Pi_N(x)$. The set of initial states that can be steered to the terminal constraint set $\mathbb{X}_f$ by an admissible control policy π in i steps or less, is $\mathbb{X}_i^{fb}$, $\forall i \geq 0$. The feedback optimal control problem becomes

$$P_N^{fb}(x): \; V_N^o(x) \quad = \quad \min\{V_N(x,\pi)|\pi \in \Pi_N(x)\}. \tag{3.38}$$

If a solution to $P_N^{fb}(x)$ exists, the optimal control policy is

$$\pi^o(x) \quad = \quad \{u^o(0;x), \kappa_1^o(\cdot;x), \kappa_2^o(\cdot;x), ..., \kappa_{N-1}^o(\cdot;x)\}, \tag{3.39}$$

where the implicit feedback model predictive control law is

$$\kappa_N^{fb}(x) \quad := \quad u^o(0;x). \tag{3.40}$$

If the stability conditions A1-A4a are satisfied for $P_N^{fb}(x)$, a feasible control policy for $P_N^{fb}(x^+)$ for all $x^+ \in \mathcal{F}(x,\kappa_N^{fb}(x))$ and $x \in \mathbb{X}_N^{fb}$ is

$$\tilde{\pi}(x,x^+) \quad := \quad \{\kappa_1^o(x^+;x), \kappa_2^o(\cdot;x), ..., \kappa_{N-1}(\cdot;x), \kappa_f(\cdot)\}. \tag{3.41}$$

With this feasible control policy, and with $\mathbb{X}_N^{fb}$ an invariant set for $x^+ \in \mathcal{F}(x, \kappa_N^{fb}(x))$, assumption A4a will be satisfied for all $x \in \mathbb{X}_N^{fb}$ and $w \in W(x, \kappa_N^{fb}(x))$. The resulting robust model predictive controller is asymptotically (exponentially) stable with domain of attraction $\mathbb{X}_N^{fb}$ under further modest assumptions. The results are very similar to open-loop min-max control, except that the domain of attraction $\mathbb{X}_N^{fb}$ includes $\mathbb{X}_N^{ol}$ and could possibly be much larger. Feedback MPC is encouraging, but suffers from much higher complexity than open-loop min-max control.

3.4.4 Robust MPC implementations

Some implementations of robust model predictive controllers that fall into the above-mentioned categories, are linear matrix inequality (LMI) based controllers that produce feedback policies which are implemented at each time interval. The problem with these controllers is that they use an ellipsoid invariant set for their domain of attraction, which makes them conservative. This is because the sets must be symmetric, and in systems where the constraints are non-symmetric, the ellipsoid sets will be a small subset of the maximum admissible set. The feedback robust MPC technique was introduced by Kothare *et al.* (1996). The technique was improved by Cuzzola *et al.* (2002) by describing the uncertain system as a polytope and applying different Lyapunov functions to each vertex of the uncertain polytope to reduce the conservatism of the method. The method uses semidefinite programming (SDP) to solve the minimization problem on-line, which is computationally very expensive compared to quadratic programming (QP) used in nominal MPC. Further improvements made by Wan and Kothare (2003); Casavolaa *et al.* (2004); Ding *et al.* (2004) resulted in an attempt to move as much of the calculation as possible offline. The LMI methods have been used to robustify PID (Proportional, Integral and Derivative) control (Ge *et al.*, 2002) and a few case studies on LMI based control were done by Park and Rhee (2001) and Wu (2001).

An approach to feedback robust model predictive control is proposed by Langson *et al.* (2004) who uses tubes to encapsulate all the possible states that can result from the controller. If the uncertainties can be sufficiently described, the optimization problem

needs only be calculated once, and the control policy will steer the system to the terminal constraint set $\mathbb{X}_f$, where a local stabilizing controller will keep the uncertain system in the terminal constraint set.

There is a movement in robust model predictive control to reduce the on-line computational burden. Lee and Kouvaritakis (2002) propose a method where optimal control sequences are computed offline for certain canonical states. A feasible (suboptimal) control sequence is generated on-line for the state x by using linear combinations of the precomputed optimal control sequences. The on-line computation is reduced to a simple matrix multiplication, and no on-line optimization is performed. De la Pena *et al.* (2004) proposed using multi-parametric methods to describe a suboptimal control strategy that will be less computationally expensive for on-line use. Fukushima and Bitmead (2005) incorporate the uncertainties and bounded disturbances into a comparison model, and the control algorithm can then be set up as a nominal MPC (without uncertainties) with only a QP problem to solve on-line. The comparison model provides an upper bound on the objective function value used in the on-line optimization. Mayne *et al.* (2005) reduced the on-line optimization of robust model predictive control to a QP problem, with the initial state as well as the control sequence as part of the decision variables. As the on-line problem is a nominal control problem, tighter constraints are used to ensure robustness. This is only valid for linear systems, and cannot be easily extended to nonlinear systems.

An interesting robust controller, in a process control environment, was proposed by Tsai *et al.* (2002), which uses neural adaptive control based on artificial neural networks (ANN) in conjunction with normal robust MPC. The outputs of the two controllers are combined and the weightings are calculated from regional knowledge of the ANN, which determines whether the ANN is operating in an area of good prediction characteristics or not.

An alternative approach to robust model predictive control, is to modify the objective function to ensure robust stability in the presence of uncertainties. Wang and Romagnoli (2003) used robust identification theory to construct a generalized objective function, to replace the quadratic objective function usually employed to produce a robust controller.

The on-line optimization uses the nominal model, and robustness is provided by the objective function. A method for robustifying generalized predictive control (GPC) has been proposed by Rodríguez and Dumur (2005).

The robust model predictive controllers do not always provide off-set free tracking, and this problem is addressed by Wang and Rawlings (2004*b*,*a*) who use a robust predictor that updates itself each time measurements are available to ensure that the off-set is eliminated. Pannocchia (2004) approaches the problem by designing a robust linear feedback controller and an appropriate invariant set where the controller will satisfy the constraints. The controller uses the dual-mode approach suggested by Rossiter *et al.* (1998) and later implemented by Kouvaritakis *et al.* (2000); Schuurmans and Rossiter (2000) and Lee and Kouvaritakis (2000), where the feedback law $u_i(\cdot)$ in the policy π is restricted to have the form $u_i(x) = v_i + Kx,\ i = 0, 1, 2, ..., N-1$, that changes the optimization problem to calculating the free control moves $\{v_0, v_1, v_2, ..., v_{N-1}\}$ rather than the policy. The dual-mode controller remains essentially a feedback model predictive control, because Kx limits the diversion of trajectories of the closed-loop system.

3.5 Robust model predictive controllers

In this section two robust model predictive controller methods, used in comparison with nominal MPC in the next chapter, are discussed in more detail. The first method, proposed by Kothare *et al.* (1996) calculates a feedback policy at each time interval for the system. The second method consists of a dual-mode controller first proposed by Rossiter *et al.* (1998), where the feedback policy is a combination of an open-loop feedback control law $\kappa_f \equiv -Kx$ with free control moves v, $u_i(\cdot) = v - Kx$.

3.5.1 Robust MPC using LMIs

Traditional model predictive control solves an open-loop constrained optimization problem. The internal model is a nominal model and the assumption is that feedback will compensate for the model uncertainty and unmeasured disturbances. The structure of

the value function usually does not take the effect of feedback into consideration.

Kothare *et al.* (1996) formulated a new model predictive control strategy with robustness in mind. The robust controller design explicitly incorporates model uncertainty. The value function is also formulated to take feedback into consideration. The whole theory is based on linear matrix inequalities (LMI) (Boyd *et al.*, 1994). With current interior point methods and computer technology, these functions can now be solved fast enough to be applicable in on-line use. Current model predictive control theory can be recast as linear matrix inequalities that incorporate input and output constraints, model uncertainty and robustness measures.

3.5.1.1 System descriptions

The system is defined as a linear time-varying system by Kothare *et al.* (1996).

$$x(k+1) = A(k)x(k) + B(k)u(k), \tag{3.42}$$

$$y(k) = Cx(k), \tag{3.43}$$

$$\begin{bmatrix} A(k) & B(k) \end{bmatrix} \in \Omega, \tag{3.44}$$

where $x(k)$ is the state of the system, $u(k)$ is the control vector, $y(k)$ is the output of the system and Ω is the set of models that describes the system. For polytopic uncertain systems, the set Ω is the polytope

$$\Omega \in Co\left\{\begin{bmatrix} A_1 & B_1 \end{bmatrix}, \begin{bmatrix} A_2 & B_2 \end{bmatrix}, ..., \begin{bmatrix} A_i & B_i \end{bmatrix}\right\},$$

where Co denotes the convex hull.

A second representation of the system is called the *structured feedback uncertainty*. The uncertainty is described as perturbations in the feedback loop. The system description looks as follows:

$$\begin{aligned} x(k+1) &= Ax(k) + Bu(k) + B_p p(k), \\ y(k) &= Cx(k), \\ q(k) &= C_p x(k) + D_{qu} u(k), \\ p(k) &= (\Delta q)(k). \end{aligned} \tag{3.45}$$

The operator Δ is block-diagonal:

$$\Delta = \begin{bmatrix} \Delta_1 & & & & \\ & \Delta_2 & & & \\ & & . & & \\ & & & . & \\ & & & & \Delta_r \end{bmatrix}, \tag{3.46}$$

with $\Delta_i : \mathbb{R}^{n_i} \rightarrow \mathbb{R}^{n_i}$.

For a linear time varying system, it can be shown that (3.45) can be cast in the form of (3.42-3.43) by using

$$\Omega = \left\{ \begin{bmatrix} A + B_p \Delta C_q & B + B_p \Delta D_{qu} \end{bmatrix} : \Delta \text{ satisfies (3.46) with } \overline{\sigma}(\Delta_i) \leq 1 \right\}. \tag{3.47}$$

3.5.1.2 Objective function

The stage cost of the objective function used is a standard quadratic function of the form

$$J_p(k) = \sum_{i=0}^{p} \left[x(k+i|k)^T Q_1 x(k+i|k) + u(k+i|k)^T R u(k+i|k) \right], \tag{3.48}$$

where $Q_1 > 0$ and $R > 0$ are symmetric weighting matrices. The objective function strives to drive the state vector to zero. The Q weighting matrix defines the severity of the state position penalty and the R matrix that of the control action. The ratio of Q and R will determine the priority of state position versus control action objectives.

3.5.1.3 Linear matrix inequalities

Linear matrix inequalities have the following form

$$F(x) \quad = \quad F_0 + \sum_{i=1}^{f} x_i F_i > 0, \tag{3.49}$$

where x_1, x_2, ..., x_f are the variables, $F_i = F_i^T \in \mathbb{R}^{nxn}$ are given, and $F(x) > 0$ means that $F(x)$ is positive-definite. Multiple LMIs $F_1(x) > 0, ..., F_n(x) > 0$ can be expressed as the single LMI

$$diag\left(F_1(x), ..., F_n(x)\right) \quad > \quad 0. \tag{3.50}$$

Convex quadratic inequalities are converted to linear form using Schur's complements. In the case of matrix inequalities of the form

$$R(x) > 0, \quad Q(x) - S(x)R(x)^{-1}S(x)^T \quad > 0, \tag{3.51}$$

or

$$Q(x) > 0, \quad R(x) - S(x)^T Q(x)^{-1}S(x) \quad > 0, \tag{3.52}$$

where $Q(x) = Q(x)^T$, $R(x) = R(x)^T$, and $S(x)$ depends affinely on x, then the matrix inequality can be rewritten as

$$\begin{bmatrix} Q(x) & S(x) \\ S(x)^T & R(x) \end{bmatrix} \quad > \quad 0. \tag{3.53}$$

3.5.1.4 Unconstrained robust model predictive control

For robust model predictive control, the optimization becomes a min-max problem. The objective function is maximized as a function of the uncertain models. The worst case is then minimized as a function of the control sequence.

$$\min_{u(k+i/k),i=0,1,2,..,m} \max \begin{bmatrix} A(k+i) & B(k+i) \end{bmatrix}_{\in\Omega, i\geq 0} J_p(k), \tag{3.54}$$

with

$$J_p(k) = \sum_{i=0}^{p} \left[x(k+i|k)^T Q_1 x(k+i|k) + u(k+i|k)^T R u(k+i|k) \right]. \tag{3.55}$$

This problem can be recast as linear matrix inequalities and in this case the optimized state-feedback gain $x(k+i|k) = Fx(k+i|k)$ is determined that minimizes the objective function as

$$\min_{\gamma,Q,Y} \quad \gamma \tag{3.56}$$

subject to

$$\begin{bmatrix} 1 & x(k|k) \\ x(k|k) & Q \end{bmatrix} \geq 0 \tag{3.57}$$

and

$$\begin{bmatrix} Q & QA_j^T + Y^T B_j^T & QQ_1^{1/2} & Y^T R^{1/2} \\ A_j Q + B_j Y & Q & 0 & 0 \\ Q^{1/2} Q & 0 & \gamma I & 0 \\ R^{1/2} Y & 0 & 0 & \gamma I \end{bmatrix} \geq 0, \; j = 1, 2, .., L, \tag{3.58}$$

where L is the number of linear models in the set Ω and $x(k|k)$ is the measured state. From this optimization the feedback gain is $F = YQ^{-1}$.

In the case of structured feedback uncertainty, the optimization becomes

$$\min_{\gamma,Q,Y,\Lambda} \quad \gamma \tag{3.59}$$

subject to

$$\begin{bmatrix} 1 & x(k|k) \\ x(k|k) & Q \end{bmatrix} \geq 0 \tag{3.60}$$

and

$$\begin{bmatrix} Q & Y^T R^{1/2} & QQ_1^{1/2} & QC_q^T + Y^T D_{qu}^T & QA^T + Y^T B^T \\ R^{1/2}Y & \gamma I & 0 & 0 & 0 \\ Q_1^{1/2}Q & 0 & \gamma I & 0 & 0 \\ C_q Q + D_{qu}Y & 0 & 0 & \Lambda & 0 \\ AQ + BY & 0 & 0 & 0 & Q - B_p \Lambda B_p^T \end{bmatrix} \geq 0, \tag{3.61}$$

where

$$\Lambda = \begin{bmatrix} \lambda_1 I_{n_1} & & & & \\ & \lambda_2 I_{n_2} & & & \\ & & . & & \\ & & & . & \\ & & & & . \\ & & & & \lambda_r I_{n_r} \end{bmatrix} > 0, \tag{3.62}$$

where $x(k|k)$ is the measured state and $I_{n_i},\ i = 1, 2, .., r$ is the identity matrix of the correct dimensions for the diagonal entry i. The optimal feedback gain is $F = YQ^{-1}$.

3.5.1.5 Input constraints

Input constraints can be incorporated into the robust model predictive formulation as additional linear matrix inequalities. The input constraints of the form

$$\|u(k+i|k)\|_2 \leq u_{max}, \tag{3.63}$$

can be written as linear matrix inequalities of the form

$$\begin{bmatrix} u_{max}^2 I & Y \\ Y^T & Q \end{bmatrix} \geq 0. \tag{3.64}$$

For constraints on the individual components of the input vector of the form

$$|u_j(k+i|k)| \leq u_{j,max},\ i \geq 0,\ j = 1, 2, ..., n_u, \tag{3.65}$$

the linear matrix inequalities are

$$\begin{bmatrix} X & Y \\ Y^T & Q \end{bmatrix} \geq 0, \text{ with } X_{jj} \leq u_{j,max}^2,\ j = 1, 2, ..., n_u, \tag{3.66}$$

with X a symmetric matrix.

3.5.1.6 Output constraints

Output constraints can be added to the robust model predictive control formulation as additional linear matrix inequalities. Here the output has to be maximized over the uncertain models. This ensures that the constraints will not be violated even in the worst case scenario. The output constraints of the form

$$\max_{[\ A(k+i) \quad B(k+i)]\ \in\Omega, i\geq 0} \|y(k+i|k)\|_2 \leq y_{max}, \quad i \geq 1, \tag{3.67}$$

can be written in the following linear matrix inequality form for a polytopic uncertainty description

$$\begin{bmatrix} Q & (A_jQ + B_jY)^T C^T \\ C(A_jQ + B_jY) & y_{max}^2 I \end{bmatrix} \geq 0,\ j = 1, 2, ..., L, \tag{3.68}$$

where L is the number of linear models in the uncertainty description. For the structured uncertainty case, the output constraints become

$$\begin{bmatrix} y_{max}^2 Q & (c_q Q + D_{qu} Y)^T & (AQ + BY)^T C^T \\ C_q Q + D_{qu} Y & T^{-1} & 0 \\ C(AQ + BY) & 0 & I - C B_p T^{-1} B_p^T C^T \end{bmatrix} \geq 0, \tag{3.69}$$

with

$$T = \begin{vmatrix} t_1 I_{n_1} & & & & \\ & t_2 I_{n_2} & & & \\ & & . & & \\ & & & . & \\ & & & & . \\ & & & & t_r I_{n_r} \end{vmatrix} > 0. \tag{3.70}$$

The case for components of the output vector is exactly the same, except for $C = C_i$ and $T = T_i$, where i is the output component in question, in (3.68) and (3.69).

3.5.1.7 Synthesis of the controller

The controller is synthesised by applying the linear models of section 2.4.5 in (3.61) and choosing the weighting for the state deviation Q and the penalty of the control action R as in table 2.1. The input constraints are specified through (3.64) or (3.66) and the output or state constraints through (3.69) and (3.70).

3.5.1.8 Controller operation

At each time interval k, the semidefinite optimization (3.59) is performed subject to the linear matrix inequality constraints (3.60,3.61,3.62,3.66,3.69,3.70). The feedback law for time step k is $K = -F$, where $F = YQ^{-1}$.

3.5.2 Dual-mode robust model predictive controller

The controller proposed by Pluymers *et al.* (2005*b*) uses an optimized control sequence over the prediction horizon N after which a global stabilizing state feedback gain K is used.

3.5.2.1 Augmented system description

The system $\tilde{x}(k+1) = \Phi(k)\tilde{x}(k)$ uses an augmented description with vertices of the uncertainty polytope given by:

$$\Phi_i = \begin{bmatrix} A_i - B_i K & B_i & 0 \\ 0 & 0 & I_{((N-1).n_u,(N-1).n_u)} \\ 0 & 0 & 0 \end{bmatrix}, \quad i = 1, .., L, \tag{3.71}$$

where L is the number of models.

3.5.2.2 Constraints of the augmented system

The constraints of the augmented system are given by $A_{\tilde{x}}\tilde{x}(k) \leq b_{\tilde{x}}, k = 0, ..., \infty$ with $A_{\tilde{x}}$ and $b_{\tilde{x}}$ defined as:

$$A_{\tilde{x}} = \begin{bmatrix} A_x & 0 & 0 \\ -A_u K & A_u & 0 \end{bmatrix} \qquad B_{\tilde{x}} = \begin{bmatrix} b_x \\ b_u \end{bmatrix}, \tag{3.72}$$

where the state constraints are $A_x x \leq b_x$ and the input constraints are $A_u u \leq b_u$.

To calculate the robust invariant set from $A_{\tilde{x}}$ and $b_{\tilde{x}}$ the algorithm from Pluymers *et al.* (2005*a*) is used to construct $S_{aug} = \{\tilde{x} | A_S \tilde{x} \leq b_S\}$.

3.5.2.3 Quadratic problem weighting matrix

The quadratic program weighting matrix forms part of the value function (3.78) that is optimized on-line. The weighting matrix P should satisfy:

$$P - \Phi_i^T P \Phi_i \;\; > \;\; \Gamma_x^T Q \Gamma_x + \Gamma_u^T R \Gamma_u, \; i = 1, ..., L, \tag{3.73}$$

where $\Gamma_x = \begin{bmatrix} I_{(n_x,n_x)} & 0 \end{bmatrix}$, $\Gamma_u = \begin{bmatrix} -K & I_{(n_u,n_u)} & 0 \end{bmatrix}$ and $\Phi_i, i=1,...,L$. The R matrix is the weighting on the inputs and Q the weighting on the states. The P matrix can be obtained by doing convex optimization

$$\min_{P=P^T>0} \quad tr(P), \quad \text{subject to (3.73)}. \tag{3.74}$$

3.5.2.4 On-line control problem

The implemented input vector $u(k)$ is the combination of the state feedback gain and the first block of the optimized sequence of free control moves,

$$u(k) = -Kx(k) + c^o(k|k). \tag{3.75}$$

The optimized sequence of free control moves $c_N^o(k)$ is determined from a quadratic program subject to the polyhedral set constraints $A_S\tilde{x} \leq b_S$ that form S_{aug} as follows

$$\min_{c_N(k)} \quad J\left(x(k), c_N(k)\right), \tag{3.76}$$

subject to

$$\begin{bmatrix} x(k)^T & c_N(k)^T \end{bmatrix}^T \in S_{aug}, \tag{3.77}$$

where the objective function is

$$J\left(x(k), c_N(k)\right) = \begin{bmatrix} x(k)^T & c_N(k)^T \end{bmatrix} P \begin{bmatrix} x(k)^T & c_N(k)^T \end{bmatrix}^T, \tag{3.78}$$

with $P = P^T \in \Re^{(n_x+N.n_u)\times(n_x+N.n_u)}$ satisfying (3.73).

3.5.2.5 Synthesis of controller

The controller is synthesised by first constructing all the augmented linear systems as in (3.71). This controller uses the polytopic uncertainty description $\Omega = \begin{bmatrix} A_i & B_i \end{bmatrix}$, $i = 1, 2, ..., L$, where L is the number of models. The polytopic uncertainty description can be

calculated from the structured uncertainty description by applying all the combinations of the Δ operator to the structured uncertainty description. Each entry on the diagonal of Δ can be either -1 or 1 and all other entries are 0. Each combination of diagonal entries gives $\Delta_i,\ i = 1, 2, ..., L$, where $L = 2^n$ and $\Delta \in \mathbb{R}^{n \times n}$, gives a vertex of the polytopic uncertainty description by producing $\begin{bmatrix} A_i & B_i \end{bmatrix}$. The simplified model of section 2.4.5 has a Δ with dimension 4. This gives a total of $L = 2^4 = 16$ models.

The globally stabilizing unconstrained feedback gain K is then synthesised, such that all the models $\begin{bmatrix} A_i & B_i \end{bmatrix}$, $i = 1, 2, ..., L$ are stabilized by K. The augmented system is synthesised as described in section 3.5.2.1 by using the globally stabilizing unconstrained feedback gain K and the polytopic uncertain models $\Omega = \begin{bmatrix} A_i & B_i \end{bmatrix}$, $i = 1, 2, ..., L$.

The polyhedral set that describes the constraints of the system is then calculated from the augmented system description and K as in section 3.5.2.2. The weighting matrix P of the quadratic program is then calculated offline using the augmented system, K, the weighting on the state deviation Q, and weighting on the control action R as described in section 3.5.2.3. The values for Q and R are shown in table 2.1.

3.5.2.6 Controller operation

The controller components of the augmented system, globally stabilizing feedback gain K, quadratic program weighting matrix P, and the polyhedral constraint set S_{aug}, as synthesised in section 3.5.2.5, are then used as part of the quadratic program (3.76,3.77 and 3.78) at each time step k. The input vector is obtained by (3.75).

3.6 Conclusion

This chapter briefly describes the development of stability theory for model predictive control and the subsequent robust stability and robust performance theory for model predictive control. The chapter further highlights two robust model predictive controller methods, namely feedback robust model predictive control and dual-mode robust model predictive control. The synthesis and operation of both these controllers are described, as they will be compared to nominal model predictive control, in terms of performance

and stability in the presence of model uncertainty, in chapter 4.

Chapter 4

Simulation Study

In this chapter, a comparative simulation study is conducted between nominal MPC and two robust MPC schemes as applied to a model of an EAF. In the first instance, the ability of the controllers to remain stable under model mismatches that occur due to the uncertainty of the model is studied. The performance of the controllers based on a suitable value function is used to compare the controllers. Secondly, more practical scenarios are investigated, where a predictor is employed for feedback to the controllers and only limited measurements are available from the plant for feedback. This provides an opportunity to investigate the effect that a lack of measurements has on the performance of the system.

4.1 Introduction

The purpose of the refining process in an electric arc furnace is to produce a certain grade of steel. The properties that define the grade of the steel are all the impurities within the steel, of which carbon is the most important. The downstream processing of the steel requires a certain temperature at tapping.

The reduced model of Bekker *et al.* (1999) only models carbon content, temperature, FeO, Si and SiO_2. The carbon content is only marginally controllable as shown in section 2.4.4 and section 2.4.5, therefore the secondary objective, that is to control the temperature to the desired value required for downstream processing, is pursued. In section 2.4.5 it is shown that Si and SiO_2 cannot be controlled, and are as such left out

of the control objectives.

High levels of FeO in the slag are undesirable, because each time deslagging takes place, iron is lost in the form of FeO. One of the objectives would be to limit the amount of FeO in the slag in order to maximize yield. There are two methods to accomplish this:

1. The state deviation from the desired amount of FeO can be penalized. This will force the controller to apply control actions that will minimize the increase of FeO in the slag.

2. Excessive oxygen injection could be penalized, because oxygen injection increases the FeO in the slag due to the oxidation of iron.

The use of oxygen injection is governed by the trade-off between FeO production and its use as an additional source of energy. Oxygen injection is also a mechanism by which decarburization takes place. The trade-off can be made by placing a state constraint on the increase of FeO; usually it is desirable to limit FeO to less than 40% of the total slag mass. If yield is paramount, a state weighting on FeO is preferable. The controller can be tuned to minimize the energy cost by setting the weights of the inputs according to the cost of each energy source. This may result in oxygen injection being preferred as energy source because it might be less expensive than electricity.

For these simulations, the bath temperature and FeO content in the slag are shown as outputs and oxygen and graphite injection as well as electric power are shown as inputs. The carbon content in the bath is not shown because in all instances it will mirror that of figure 2.6 in section 2.4.4.

4.1.1 Controller weighting matrices

The state weighting is such that only the deviation of temperature from the setpoint or reference trajectory is penalized as shown in table 4.1. If FeO is penalized as an undesirable product, the optimization would try to minimize its production. The weighting on oxygen can be determined by energy pricing considerations.

Table 4.1: MPC weighting matrix for states.

Variable	Weighting value
FeO content in slag	0
Temperature	1
Weighting matrix Q	$\begin{bmatrix} 0 & 0 \\ 0 & 1 \end{bmatrix}$

Table 4.2: MPC weighting matrix for inputs.

Variable	Even weighting	Oxygen heavy weighting
Oxygen injection weighting	0.01	0.1
Electric power weighting	0.01	0.01
Graphite injection weighting	0.01	0.01
Input weighting matrix R	$\begin{bmatrix} 0.01 & 0 & 0 \\ 0 & 0.01 & 0 \\ 0 & 0 & 0.01 \end{bmatrix}$	$\begin{bmatrix} 0.1 & 0 & 0 \\ 0 & 0.01 & 0 \\ 0 & 0 & 0.01 \end{bmatrix}$

There are two input weighting scenarios, the first where all the inputs have an equal weighting, to encourage the controller to make use of all the inputs equally. In the second scenario, oxygen has a greater weighting to force the controller to make less use of oxygen injection to manipulate the temperature in order to reduce the amount of FeO that forms. The weighting of the inputs are summarized in table 4.2. The weighting of the inputs is less than the weighting of temperature, for two reasons: Firstly, it reduces the steady state offset if the steady state values are not at the origin, and secondly, it encourages greater control action that leads to reduced response times.

4.1.2 Closed-loop architectures

There are two control architectures for the simulation study. The first controller architecture (figure 4.1) uses full state feedback, assuming continuous feedback for all states. The setpoint or reference for the model predictive controller contains a value for the temperature and FeO content, but the controller will ignore this setting for FeO, because the weighting on the states (table 4.1) will cause no penalty in the objective function for

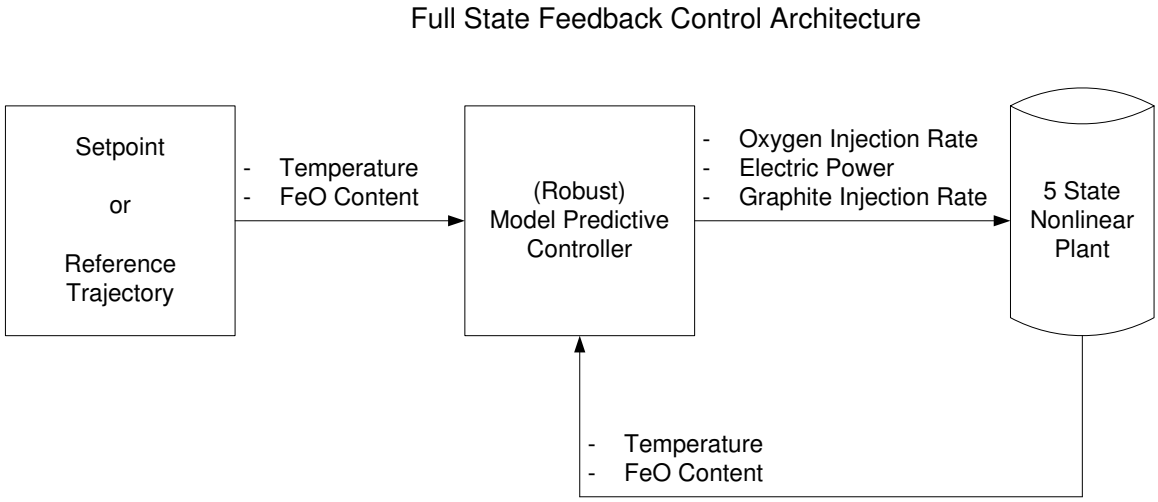

Figure 4.1: Full state feedback control architecture.

the deviation of FeO from its setpoint or reference. The controller *manipulates* oxygen injection, electric power and graphite injection. The temperature and FeO content from the plant are measured continuously and fed back to the model predictive controller.

The second control architecture (figure 4.2) is a limited measurement, predictor feedback architecture. The controller provides control action to both the plant and predictor, the five state nonlinear model of section 2.2. The predictor provides continuous estimates of the plant states, temperature and FeO, to the model predictive controller. Each time a measurement is available from the plant, it is fed to the predictor in order to correct the state values, and predictor parameter values are updated as necessary.

4.1.3 Controller objectives

In order to determine whether the controllers attained the required level of performance, the objectives against which the performance can be measured have to be clearly defined. The objectives usually stem from the process that imposes the constraints on the inputs (because of actuator limitations) and states as well as the setpoints that the controller should reach and maintain.

The minimum and maximum oxygen and carbon injection rates are determined by the injectors. The minimum oxygen and graphite injection rate is 0 kg/s, because neither

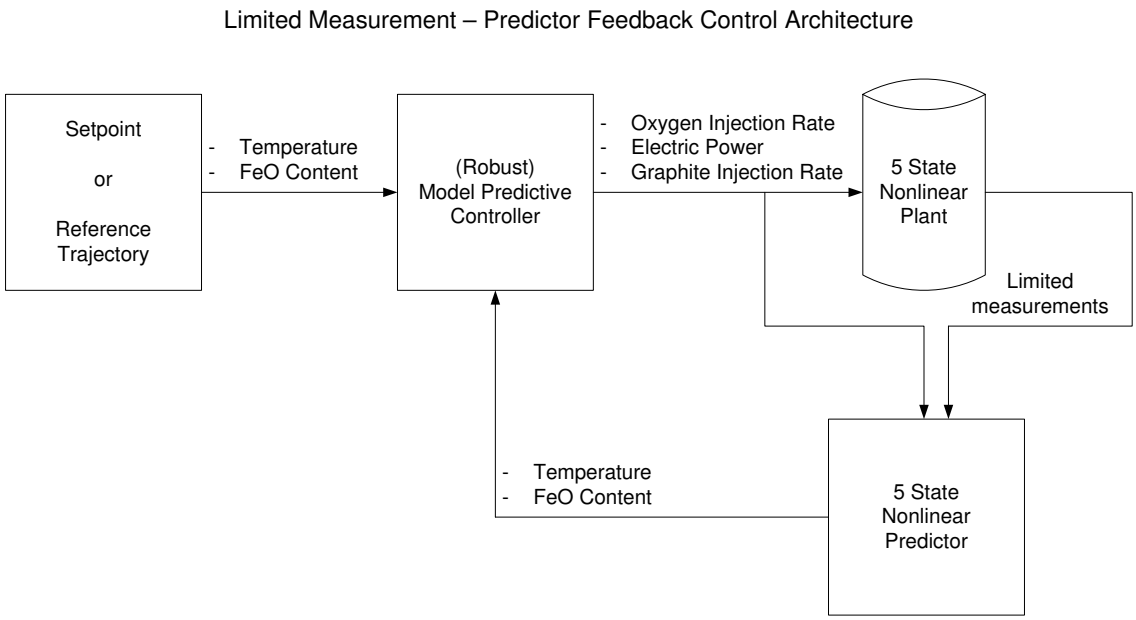

Figure 4.2: Limited measurement with predictor feedback control architecture.

oxygen nor graphite can be extracted by the injectors. The maximum oxygen injection rate is 1 kg/s and the maximum graphite injection rate is 0.5 kg/s as specified by the manufacturer.

The minimum power that the electric arc can produce is 0 Watt and the maximum power it can produce is 40 MW.

The state constraint on FeO is 40% of the total slag mass. This will prevent too much iron being lost during deslagging.

The initial conditions for the refining stage for temperature, carbon, FeO, Si and SiO_2 are calculated from the average values of measurements taken over multiple taps (Rathaba, 2004). The measurements are shown in appendix C.

The initial value for temperature is chosen to be 1600^0C, which is close to the average value, while the tap temperature should be 1650^0C as required by the industry partner (Bellingan, 2005) for downstream processing.

The initial values of the refining stage for carbon varies greatly, between 0.2% to 0.06% of the bath mass. The initial value for carbon is chosen to be 0.2% of total bath mass. The desired carbon content at tapping is 0.05% of the total bath mass as specified by the industry partner (Bellingan, 2005) for the desired grade of steel. The difference between

Table 4.3: Initial conditions for simulations

State		Initial Condition
x_3	Dissolved Carbon	160 kg
x_4	Dissolved Silicon	24 kg
x_7	FeO in bath	4250.6 kg
x_8	SiO_2 in bath	1405 kg
x_{12}	Bath temperature	1600 ^0C

Table 4.4: States and inputs constraints

State / Input	Minimum constraint	Maximum constraint
x_7 - FeO in bath	0% of total slag mass	40% of total slag mass
d_1 - Oxygen injection rate	0 kg/s	1 kg/s
d_4 - Electric power	0 kW	40 000 kW
d_5 - Graphite injection rate	0 kg/s	0.5 kg/s

the initial and desired carbon content values determines the duration of the refining stage. The time of 600s is derived from the time it takes the carbon content to reduce from 0.2% to 0.05% of the total bath mass.

The initial conditions used for the simulations are summarized in table 4.3 and the constraints on the states and inputs are summarized in table 4.4.

4.1.4 Typical operation

This section gives a quick overview of a typical tap and how control would be implemented. The tap starts with the charging of scrap. The scrap is melted down and a second bucket is added. When the second bucket is melted down, the slag layer is removed and a temperature measurement and a sample of the molten metal are taken. The temperature measurements are costly as the probes are burnt away. The temperature measurement registers within seconds on the SCADA system, while the metal sample takes a few minutes to analyze. The desired steel grade is decided before the tap commences and as soon as the sample is analyzed, the melter knows how much time is needed to bring the carbon content down to the desired level and what setting to put the burners on. Approximately halfway though the refining stage, the slag layer is again removed and another temperature measurement is taken. When the melter thinks that the composition and temperature are at the desired values, the steel is tapped into a ladle for further

processing.

If the refining stage is automated, the controller is engaged as soon as the sample analysis is available. The predictor estimates the states of the furnace from the time that the temperature measurement is taken with the sample and temperature data as initial conditions. The controller takes over the oxygen and graphite injectors as well as the power control for the furnace. The controller will give an indication to the melter when it is time to take a temperature measurement and give an indication when the steel is ready for tapping. The estimated temperature and carbon values for the furnace, as calculated by the predictor, can be displayed for the melter. The melter can use the estimates to track the progress of the process or use it to control the process manually for special scenarios.

4.2 Nominal Scenario

The nominal scenario is where there is no model mismatch between the internal model of the controllers, the predictor and the model of the plant. The nominal case is used as a benchmark for further simulation studies. In this scenario the following assumptions are made:

- Full state-feedback is available.
- There is no mismatch between the predictor and actual plant.
- There are no disturbances.

In this scenario, the effect of different weightings on the inputs as well as the use of a reference trajectory are examined. Three controllers are compared: nominal MPC, feedback robust MPC and the dual-mode robust MPC. In the nominal case there should (theoretically) be no difference between the performance of the controllers, except that the robust controllers might be more conservative than the nominal MPC. The first set of results was obtained with even weighting (table 4.2) on the inputs and a setpoint of 1650^oC for temperature.

From figures 4.3, 4.4 and 4.5, it is clear that, as expected, the nominal MPC and dual-mode robust MPC have almost the same results. The feedback robust MPC is not able to deal with the nominal case, because of limitations inherent in the theory. Feedback robust MPC can only deal with symmetric constraints, and in order to apply it where the constraints are asymmetric, a constant disturbance is added to the inputs. The conservatism of the theory shows its influence, because the inputs must be driven to the constraints in order to successfully control the system. The feedback robust MPC becomes more conservative further away from the steady state value for both the states and inputs, the origin for the states and the disturbance level for the inputs. To successfully control the system, the inputs must be driven to the constraints. Feedback robust MPC constructs the feedback policy in such a manner that the inputs do not reach the constraints and the closed-loop system can therefore not follow the setpoint successfully. The controller does this to ensure that the feedback gain can be applied to the whole trajectory of the states from the current condition until it reaches the origin without the resulting inputs violating the constraints. This method is therefore excluded from the rest of the study.

The second set of results was obtained with a higher weighting on the oxygen injection rate (table 4.2) in order to limit FeO formation, and the temperature is driven to a setpoint of 1650^oC.

Figures 4.6 and 4.7 show that the increased weighting on oxygen leads to reduced formation of FeO. The robust MPC controller made use of more oxygen, which is evident from the higher FeO content with the same weighting on the oxygen in comparison with the nominal MPC controller.

The third set of results was obtained with an even weighting on the inputs (table 4.2) and with a linear reference trajectory for the temperature over the duration of the refining stage.

Figures 4.8 and 4.9 show that the use of a reference trajectory reduces the amount of oxygen and electric power used, and that the reduced levels of electric power and oxygen injection are maintained for the entire duration of the refining stage.

The fourth set of results was obtained with a higher weighting on the oxygen injection rate (table 4.2) in order to reduce the formation of FeO, and a linear reference trajectory for temperature is employed over the duration of the refining stage.

Figures 4.10 and 4.11 show that the use of a higher weighting on oxygen injection reduces the formation of FeO and it is clear that more electricity and less oxygen is used. Again the nominal MPC controller uses less oxygen than the robust controller, resulting in significantly less FeO being produced.

From the nominal case, it is difficult to distinguish between the nominal MPC and dual-mode robust MPC, because there are no model mismatches.

Robust MPC is more conservative in using oxygen than the nominal MPC controller using the same weighting matrices, which can be attributed to the globally stabilizing feedback gain of the dual-mode robust MPC introducing extra dynamics into the QP. The reduced usage of oxygen will slightly reduce the decarburization rate as well as the amount of FeO in the slag.

With both controllers, there is a slight offset between the setpoint and outputs, which can be attributed to the steady-state inputs not reaching zero, and the offset is a result of the optimization of the objective function being a trade-off between making the state error zero and the inputs zero.

The scenarios where limited feedback is available are not investigated as it will produce the same results as above. This is because there is no model mismatch between the internal controller model and actual plant or between the predictor and actual plant.

4.3 Worst-case scenario: Efficiencies at their minimum

These worst-case scenario investigates the effect of a model mismatch between the internal model of the model predictive controllers and the actual plant when full state feedback is employed to gauge the robust stability and performance of the controllers. In the scenarios where limited plant measurements are available, the effect of model mismatches between the predictor and the actual plant is investigated in order to gauge the sensitivity of the system to the performance of the predictor. This scenario focuses on the effect that lower

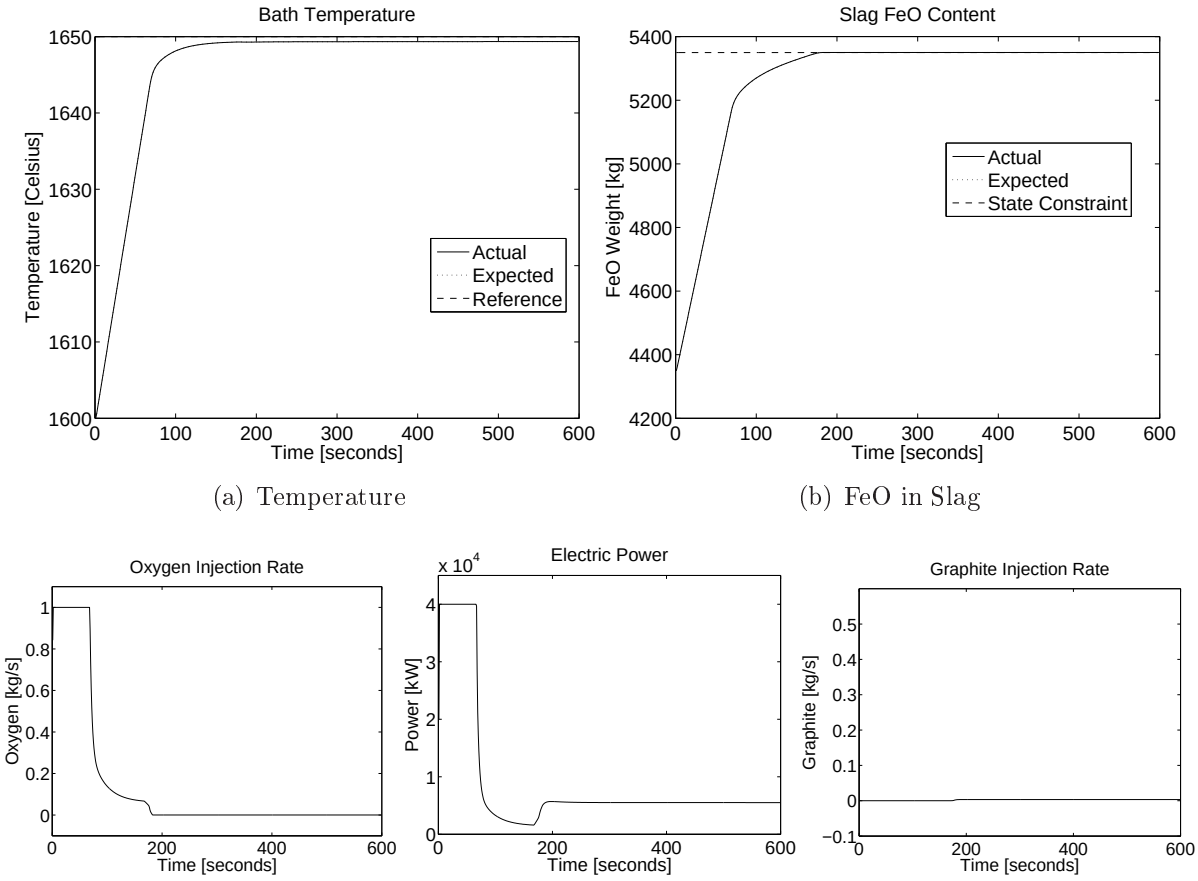

(a) Temperature (b) FeO in Slag

(c) Oxygen Injection (d) Electric Power (e) Graphite Injection

Figure 4.3: Nominal MPC - Nominal Case with full state feedback.

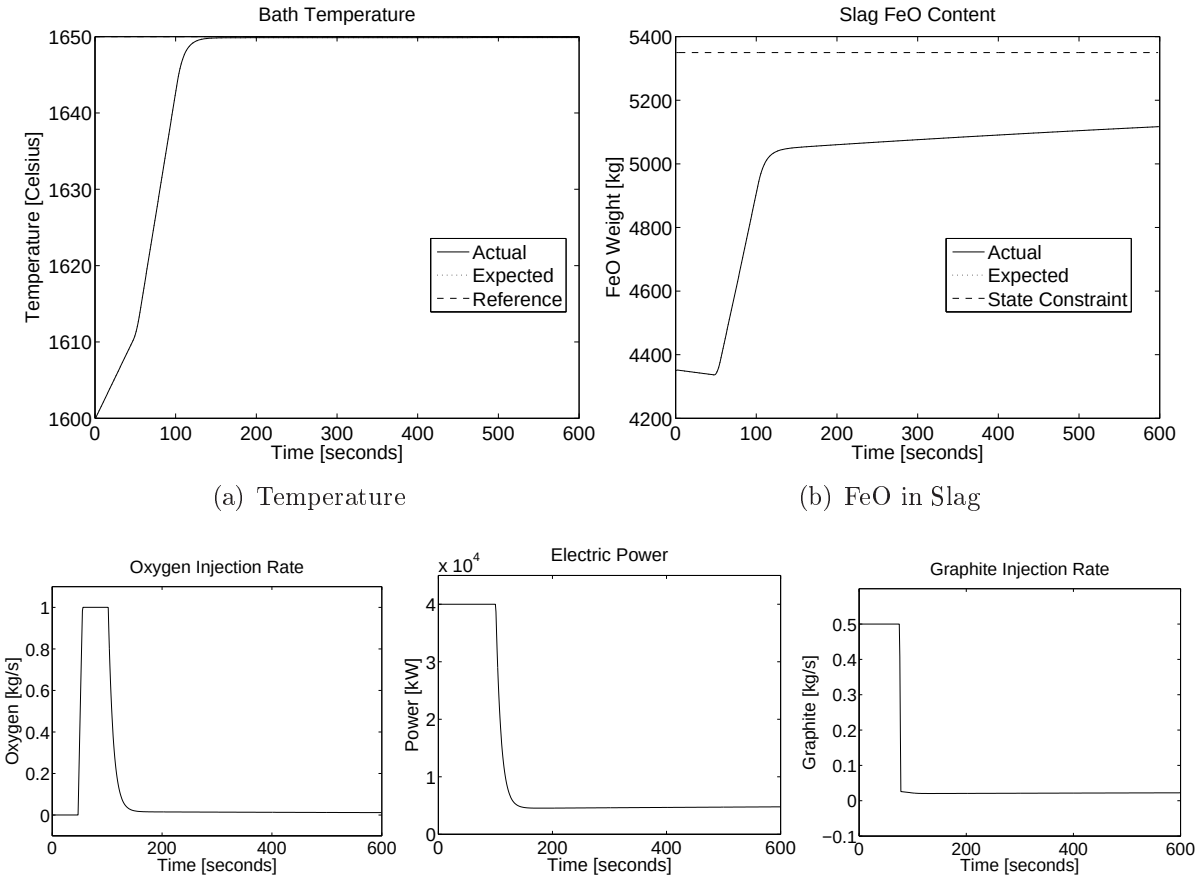

(a) Temperature (b) FeO in Slag

(c) Oxygen Injection (d) Electric Power (e) Graphite Injection

Figure 4.4: Dual Mode Robust MPC - Nominal Case with full state feedback.

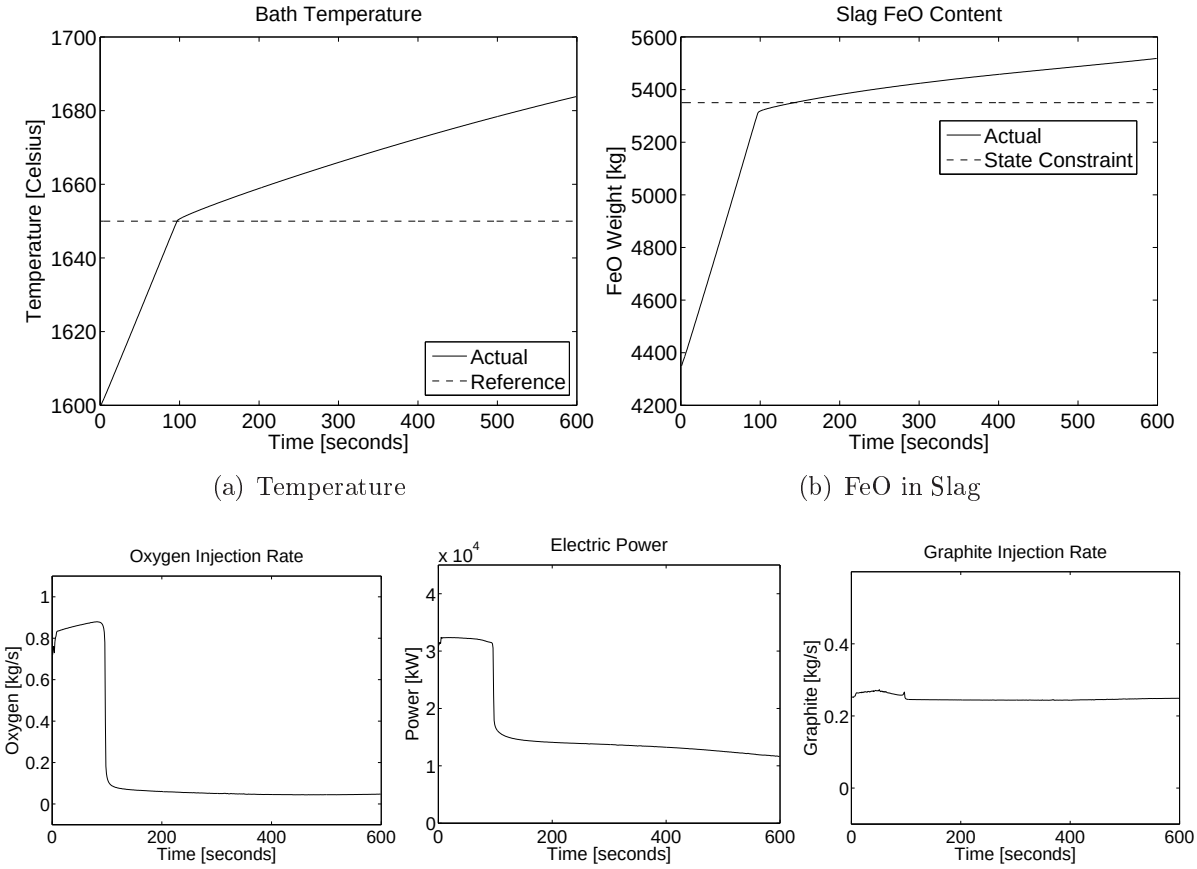

(a) Temperature (b) FeO in Slag

(c) Oxygen Injection (d) Electric Power (e) Graphite Injection

Figure 4.5: Feedback Robust MPC - Nominal Case with full state feedback.

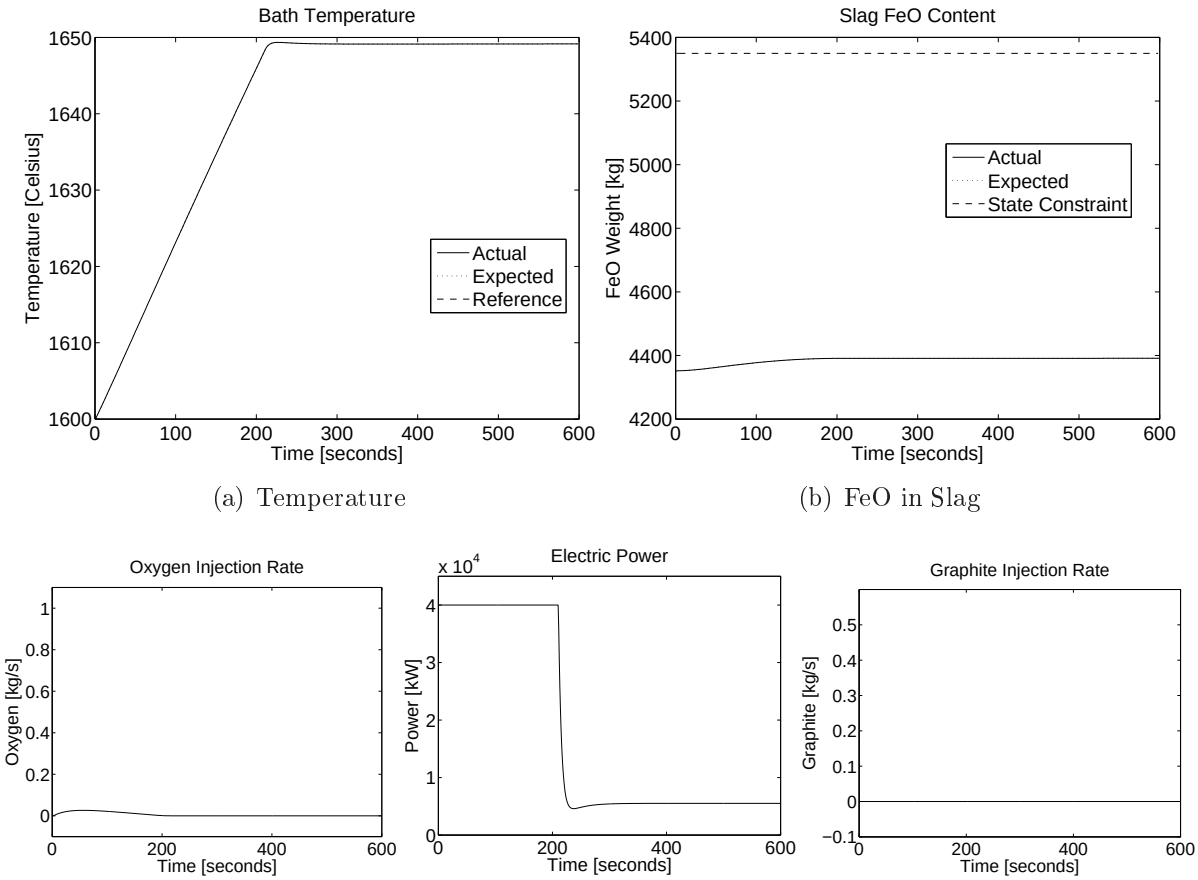

(a) Temperature (b) FeO in Slag

(c) Oxygen Injection (d) Electric Power (e) Graphite Injection

Figure 4.6: Nominal MPC - Nominal Case with full state feedback and reduced oxygen usage.

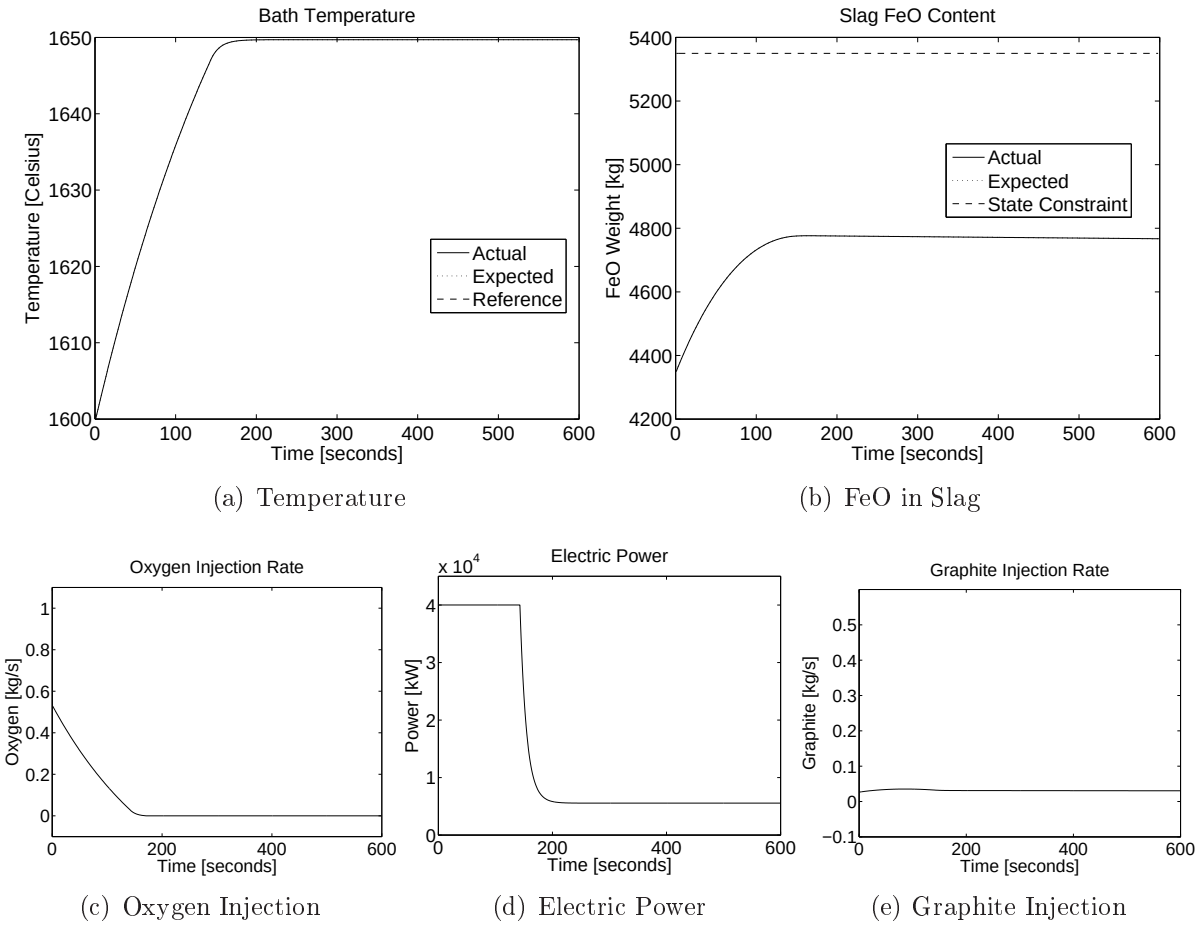

(a) Temperature (b) FeO in Slag

(c) Oxygen Injection (d) Electric Power (e) Graphite Injection

Figure 4.7: Dual Mode Robust MPC - Nominal Case with full state feedback and reduced oxygen usage.

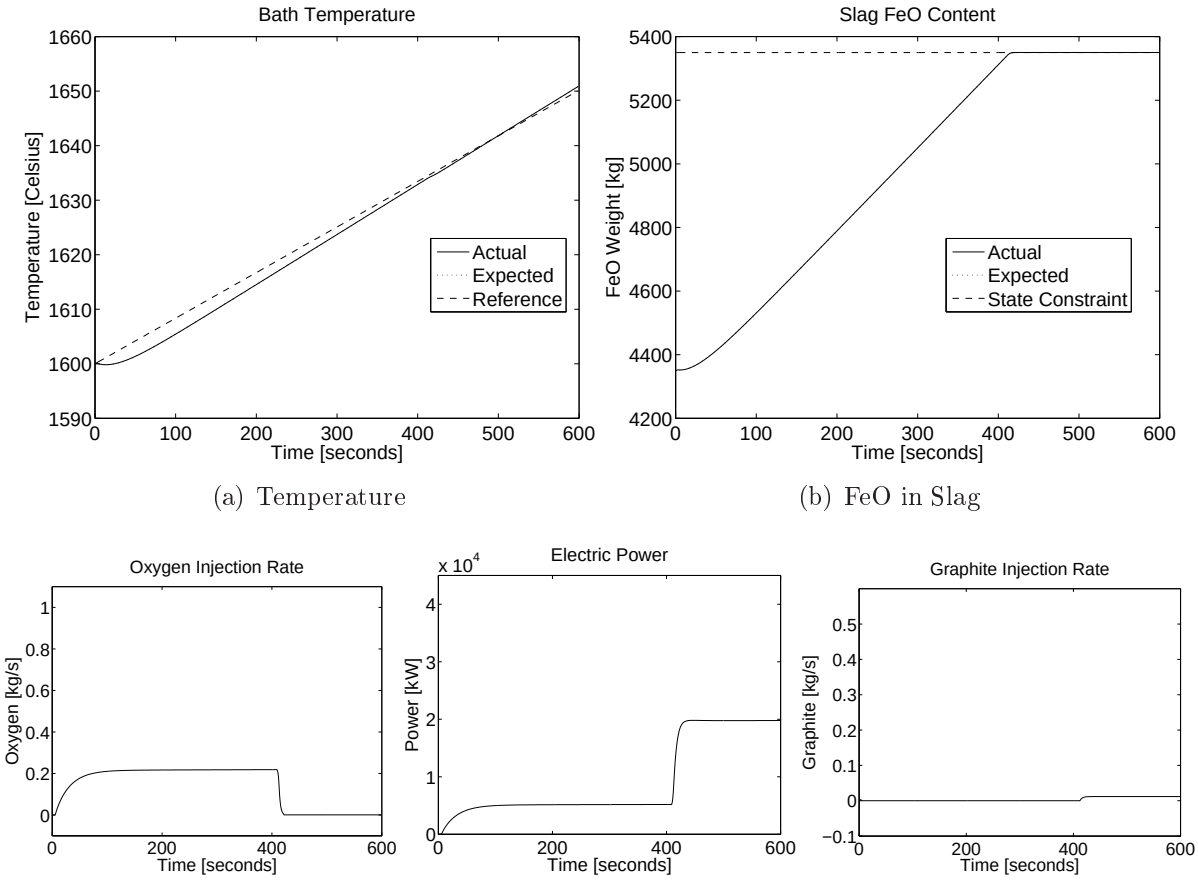

(a) Temperature (b) FeO in Slag

(c) Oxygen Injection (d) Electric Power (e) Graphite Injection

Figure 4.8: Nominal MPC - Nominal Case, full state feedback and reference trajectory.

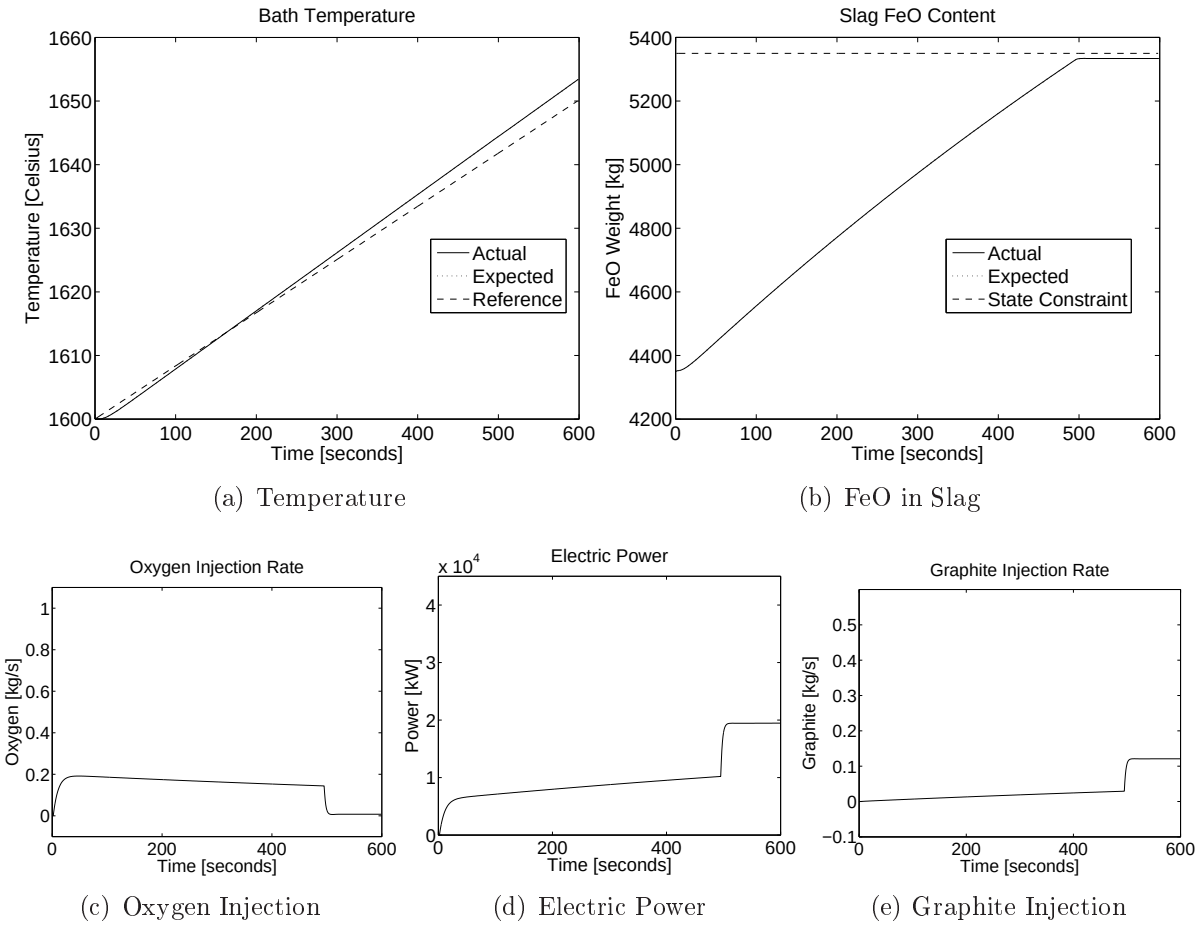

(a) Temperature (b) FeO in Slag

(c) Oxygen Injection (d) Electric Power (e) Graphite Injection

Figure 4.9: Dual Mode Robust MPC - Nominal Case, full state feedback and reference trajectory.

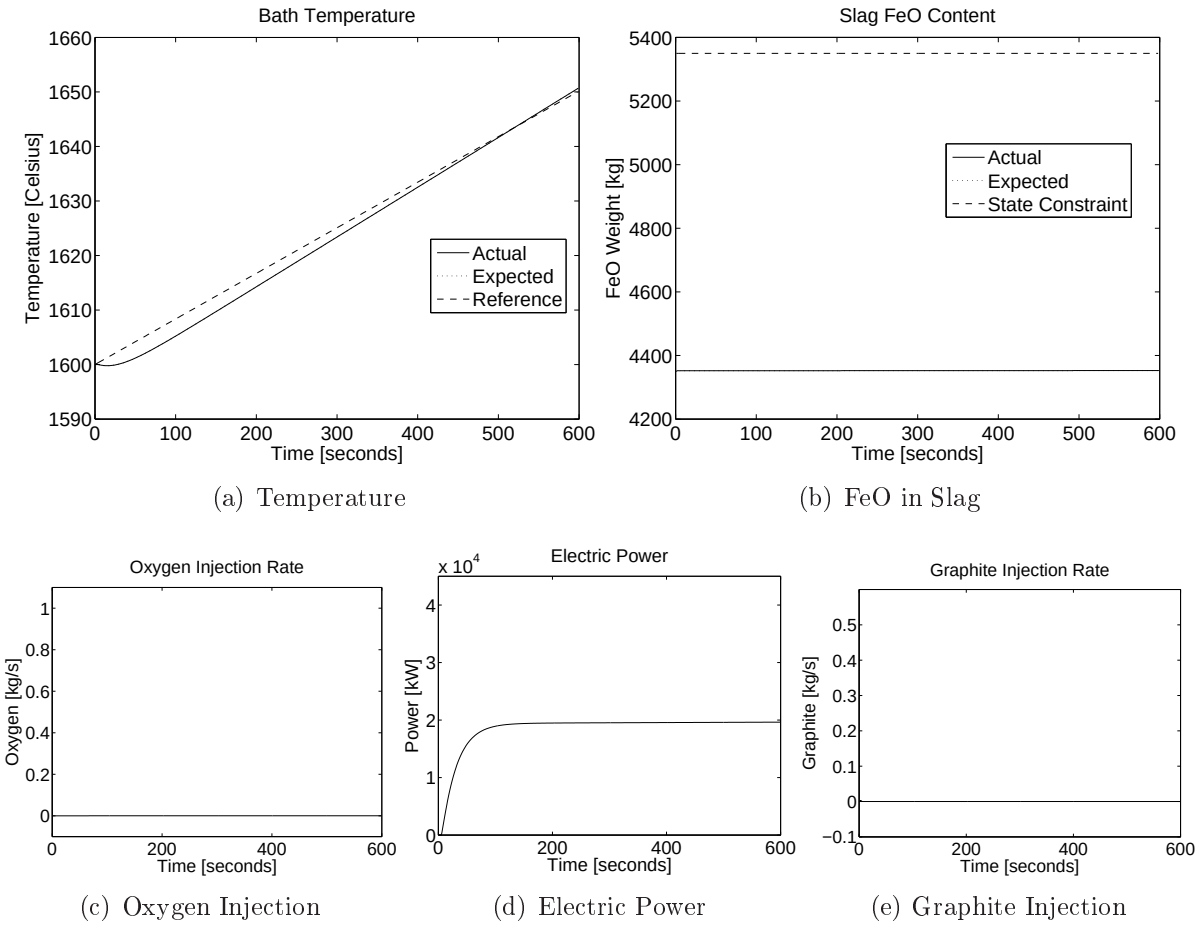

(a) Temperature (b) FeO in Slag

(c) Oxygen Injection (d) Electric Power (e) Graphite Injection

Figure 4.10: Nominal MPC - Nominal Case, full state feedback, reference trajectory and reduced oxygen usage.

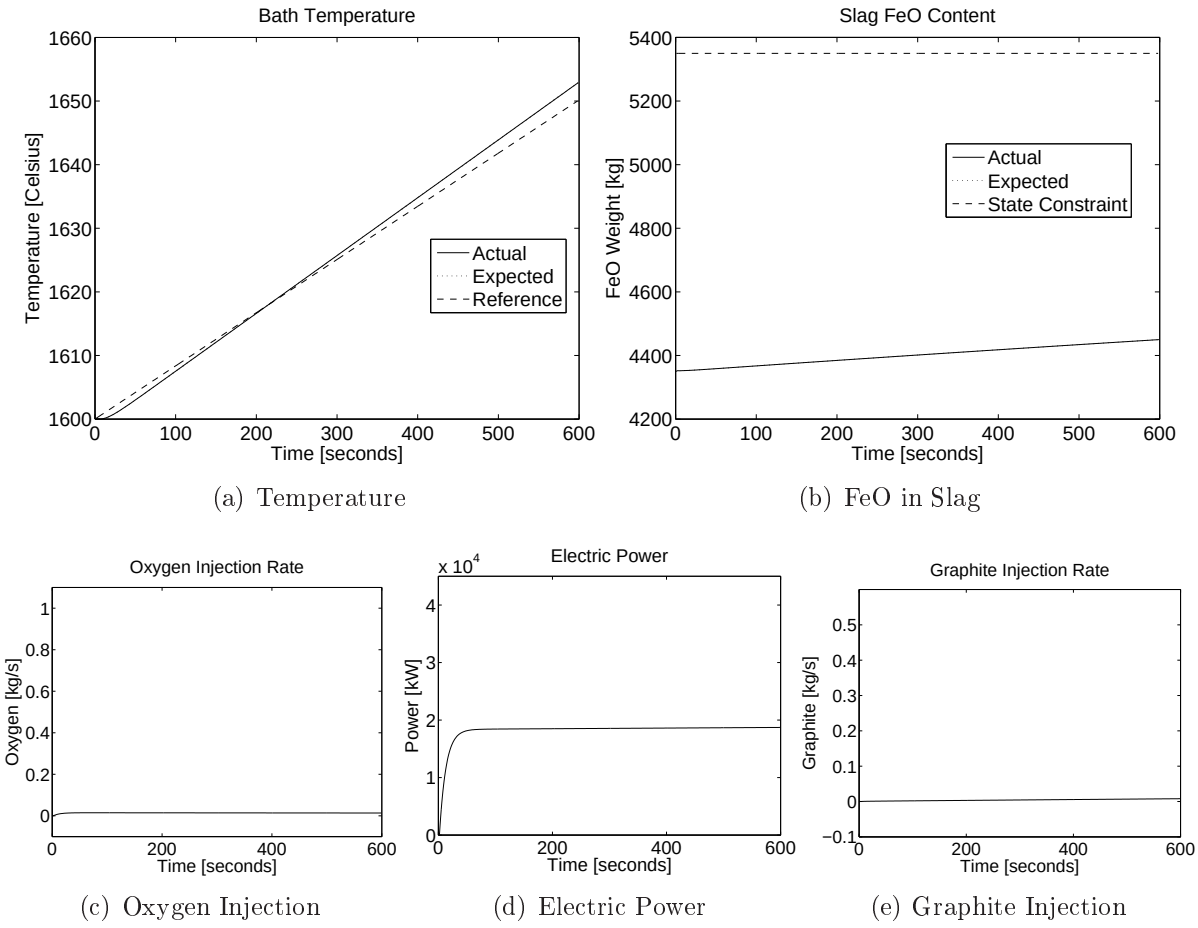

(a) Temperature (b) FeO in Slag

(c) Oxygen Injection (d) Electric Power (e) Graphite Injection

Figure 4.11: Dual Mode Robust MPC - Nominal Case, full state feedback, reference trajectory and reduced oxygen usage.

than nominal efficiencies (η_{FeO} and η_{ARC}) have on the controller and system as a whole. In these scenarios the following assumptions are made:

- There are three feedback scenarios:
  - Full state-feedback is available.
  - One temperature measurement is available.
  - One temperature measurement and an update of the efficiencies (η_{FeO} and η_{ARC}) of the predictor are available.
- The predictor and actual plant have a mismatch in their efficiencies (η_{FeO} and η_{ARC}) where the efficiencies are lower in the real plant than in the predictor.
- There are no disturbances.

The three feedback scenarios help to investigate the performance of the system with regards to the different modules in the system, especially the performance of the predictor and controller. One of the objectives of the controllers is to limit the amount of FeO that forms. Only the scenarios with a higher penalty on oxygen are evaluated here, with the other scenarios evaluated in appendix B.1.1.

4.3.1 Worst-case scenario: Efficiencies at their minimum with full state feedback

In this first instance, full-state feedback is employed to evaluate the closed-loop performance without a predictor in the loop in the extreme case where the efficiencies (η_{FeO} and η_{ARC}) are at the minimum of the model parameter confidence intervals. Robust MPC and nominal MPC are compared to determine whether robust MPC provides better performance in the presence of model mismatch compared to nominal MPC.

A setpoint of 1650^oC for temperature as well as higher weighting on oxygen injection (table 4.2) is used for the first set of simulations.

From these results (figures 4.12 and 4.13) it is clear that the robust MPC performs better than the nominal MPC. The robust controller produced a smaller steady-state

temperature offset. It is interesting to note that the nominal controller is stable for this simulation even in this extreme model mismatch situation. The heavier weighting on oxygen injection is not enough to limit the FeO production to below the constraint limit.

The second set of simulations uses a reference trajectory for temperature and a higher weighting on the oxygen injection (table 4.2).

These results (figures 4.14 and 4.15) show the superior performance of the robust MPC compared to the nominal MPC, with almost perfect tracking of the reference trajectory by the robust MPC. The higher weighting on the oxygen causes the FeO constraint to be reached much later and it forces the robust controller to use more electricity. The robust MPC used more oxygen, but this resulted in better trajectory following when compared to results obtained with the nominal MPC.

This scenario showed that both controllers are stable for the respective simulations with extreme model mismatch, but the robust controller showed better performance in terms of setpoint and reference trajectory following than the nominal controller.

4.3.2 Worst-case scenario: Efficiencies at their minimum with one plant measurement

A more realistic feedback scenario is investigated, because typically only one measurement of temperature is taken in the middle of the refining stage. The rest of the data is produced by the predictor. The predictor uses the nominal plant parameters, while the real plant uses the worst-case scenario where the efficiencies (η_{FeO} and η_{ARC}) are at their minimum. This scenario should shed light on the effect of model mismatch between the predictor and real plant when compared to the results of the previous subsection.

A setpoint of 1650^oC for temperature as well as higher weighting on oxygen injection (table 4.2) is used for the first set of simulations.

Figures 4.16 and 4.17 show that both controllers perform equally poorly as a result of the inaccurate feedback from the predictor. An acceptable margin on the tap temperature is $\pm 10^0 C$, which both the controllers were unable to attain.

A reference trajectory for temperature as well as higher weighting on oxygen injection

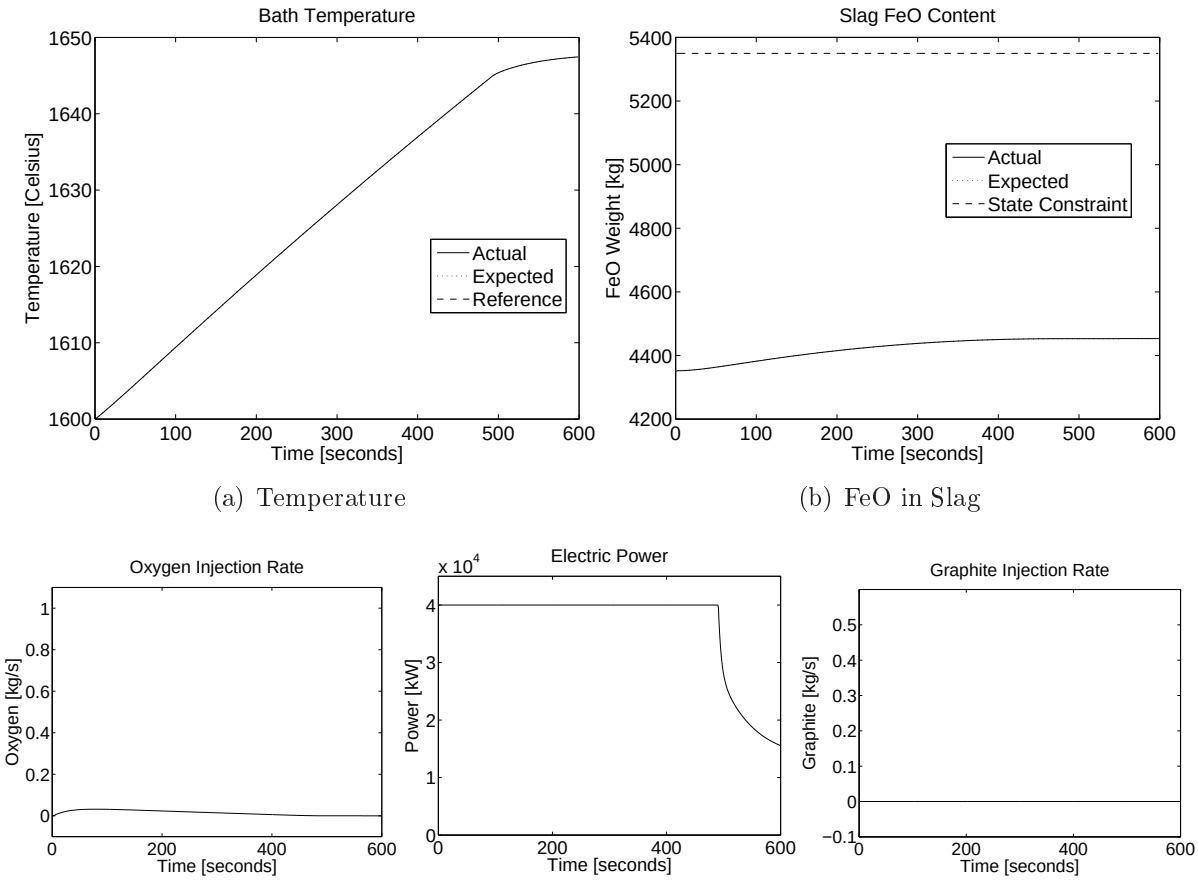

(a) Temperature (b) FeO in Slag

(c) Oxygen Injection (d) Electric Power (e) Graphite Injection

Figure 4.12: Nominal MPC - Efficiencies at a minimum, full-state feedback and reduced oxygen usage.

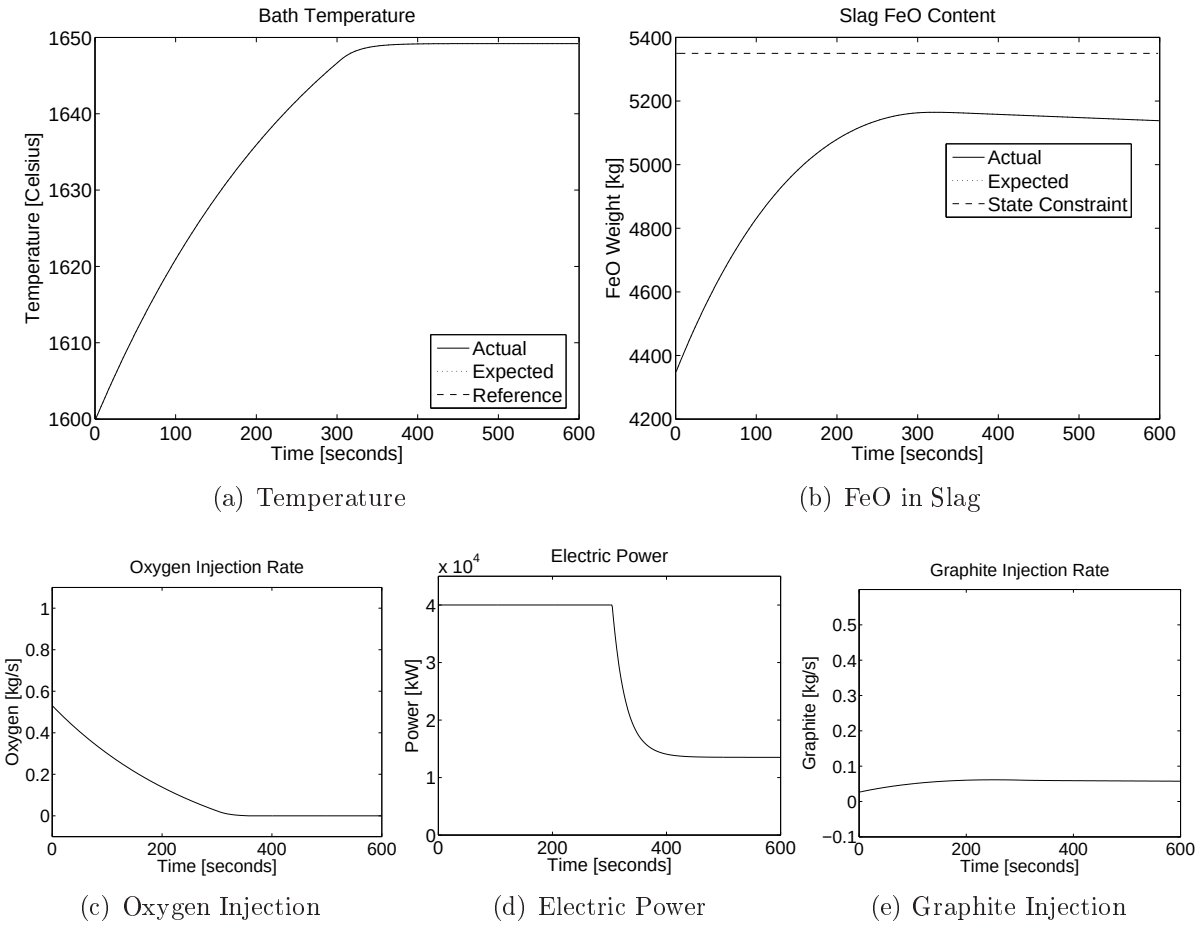

(a) Temperature (b) FeO in Slag

(c) Oxygen Injection (d) Electric Power (e) Graphite Injection

Figure 4.13: Dual-mode robust MPC - Efficiencies at a minimum, full-state feedback and reduced oxygen usage.

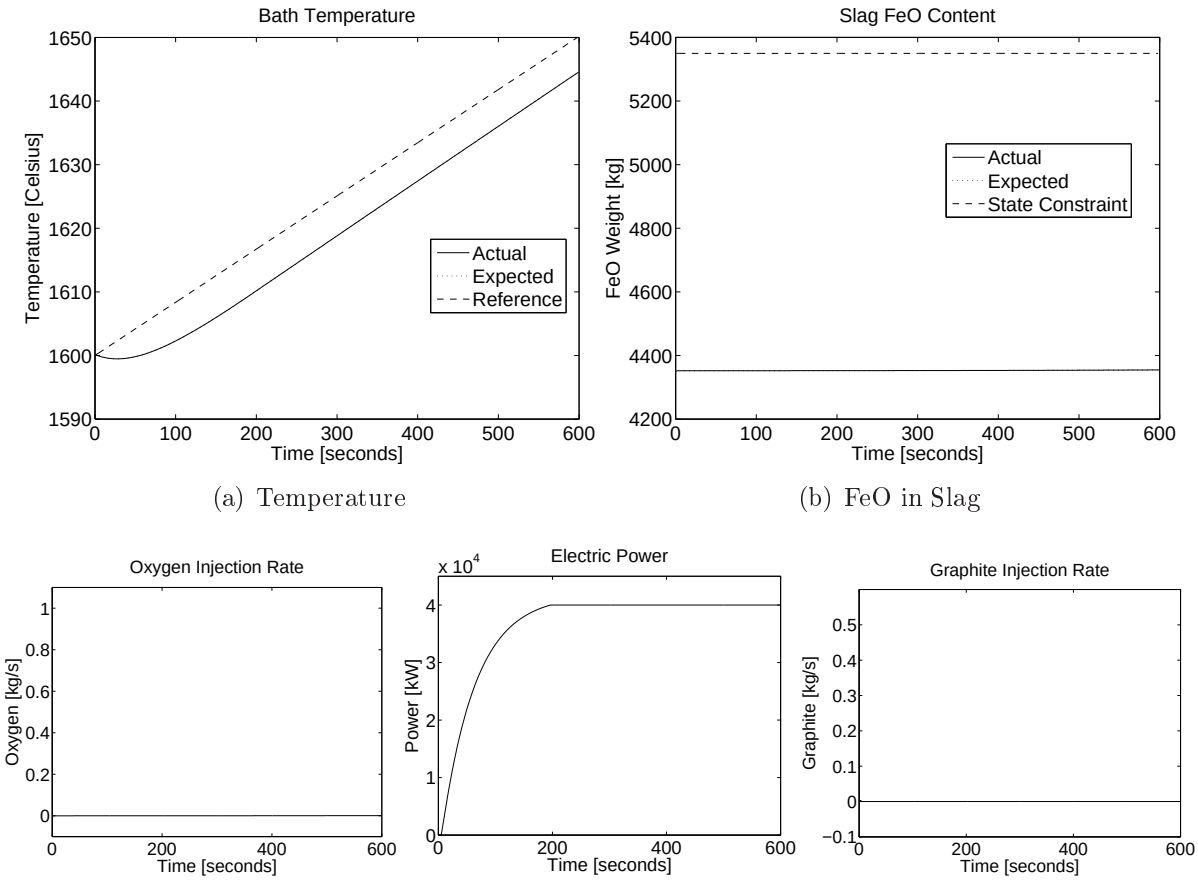

(a) Temperature (b) FeO in Slag

(c) Oxygen Injection (d) Electric Power (e) Graphite Injection

Figure 4.14: Nominal MPC - Efficiencies at a minimum, full-state feedback, reduced oxygen usage and reference trajectory.

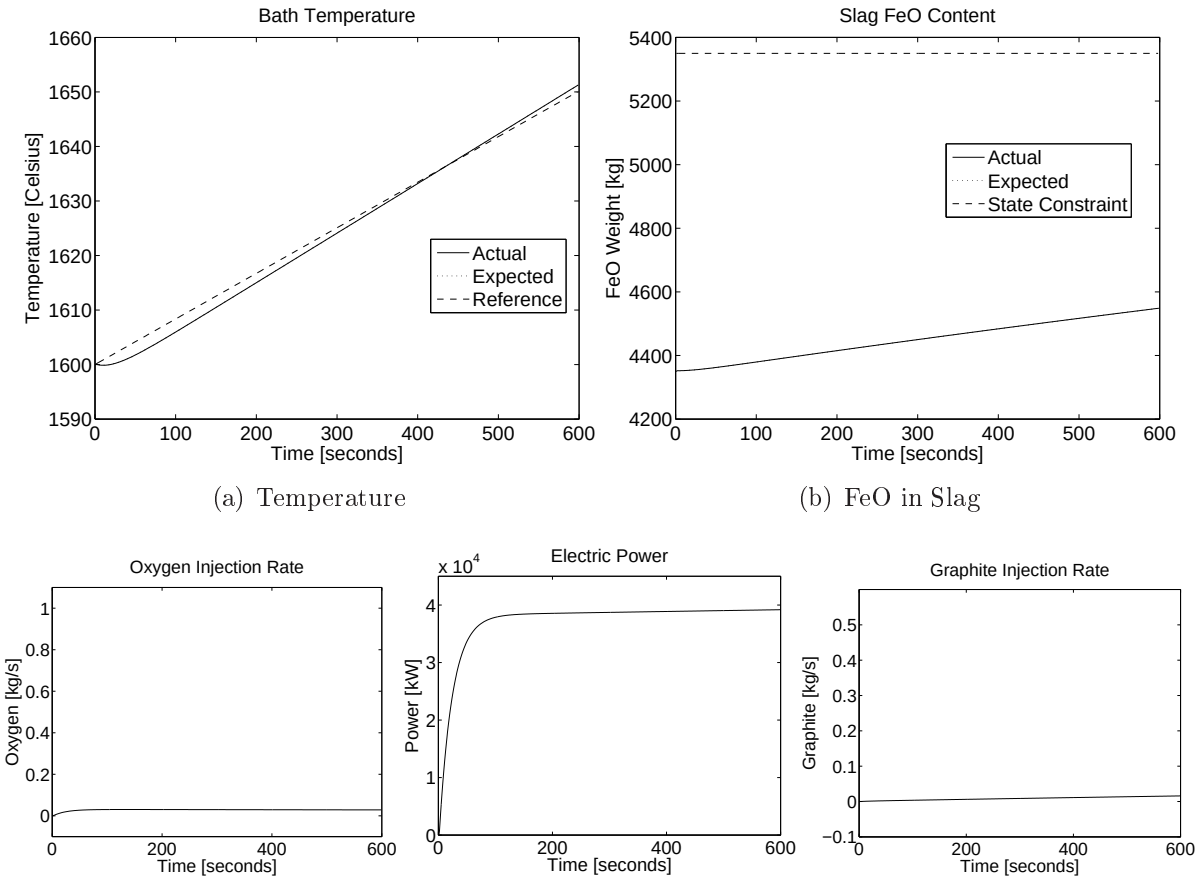

(a) Temperature (b) FeO in Slag

(c) Oxygen Injection (d) Electric Power (e) Graphite Injection

Figure 4.15: Dual-mode robust MPC - Efficiencies at a minimum, full-state feedback, reduced oxygen usage and reference trajectory.

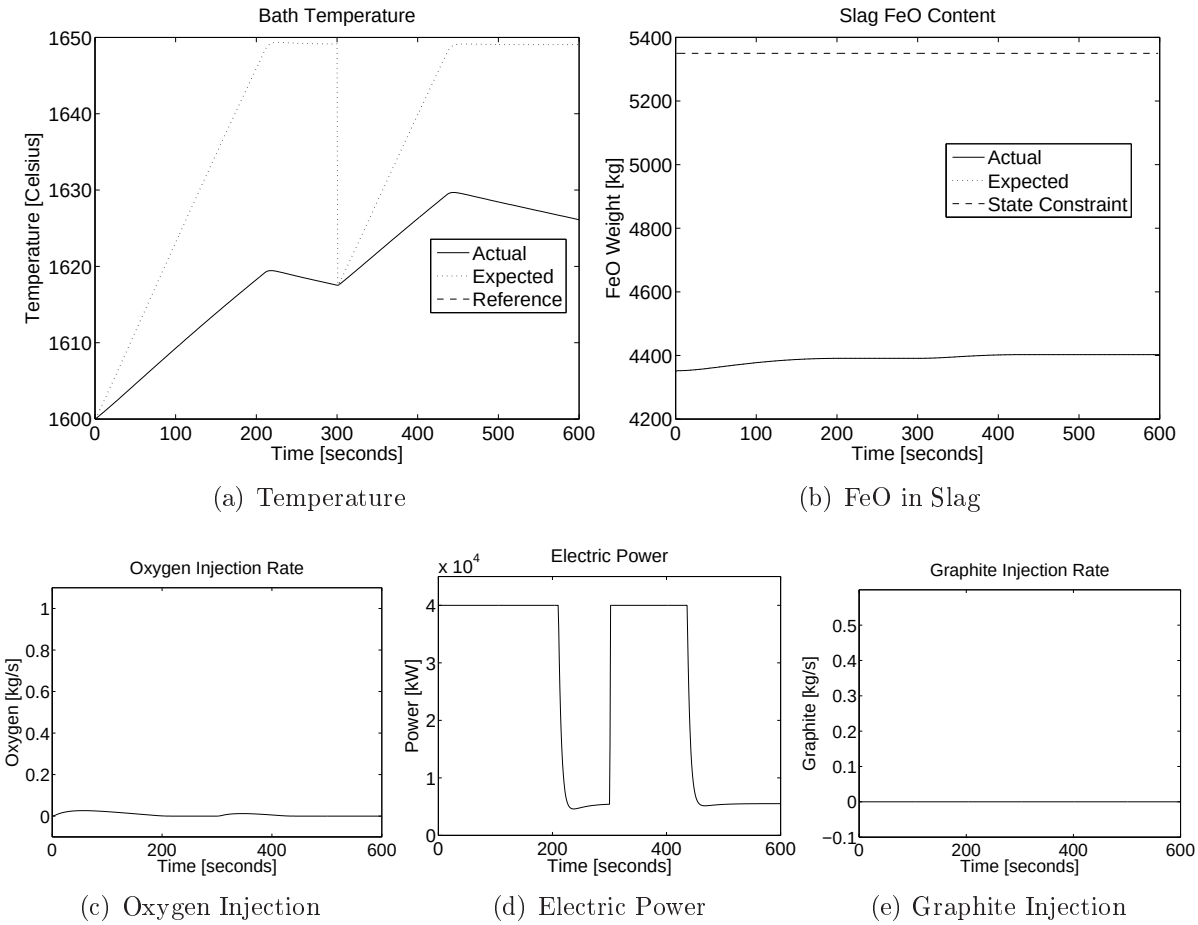

(a) Temperature (b) FeO in Slag

(c) Oxygen Injection (d) Electric Power (e) Graphite Injection

Figure 4.16: Nominal MPC - Efficiencies at a minimum, one measurement and reduced oxygen usage.

(table 4.2) is used for the second set of simulations.

These simulations (figures 4.18 and 4.19) show that the robust controller manages to trace the reference better when compared to the nominal controller, but that it is still outside the acceptable interval of $\pm 10^0 C$. Both controllers using a reference trajectory on average steer the temperature five degrees further from the desired final value compared to when a setpoint is employed. The higher weighting on the oxygen causes less FeO to be produced by both controllers and limits the FeO content to within the constraint limit.

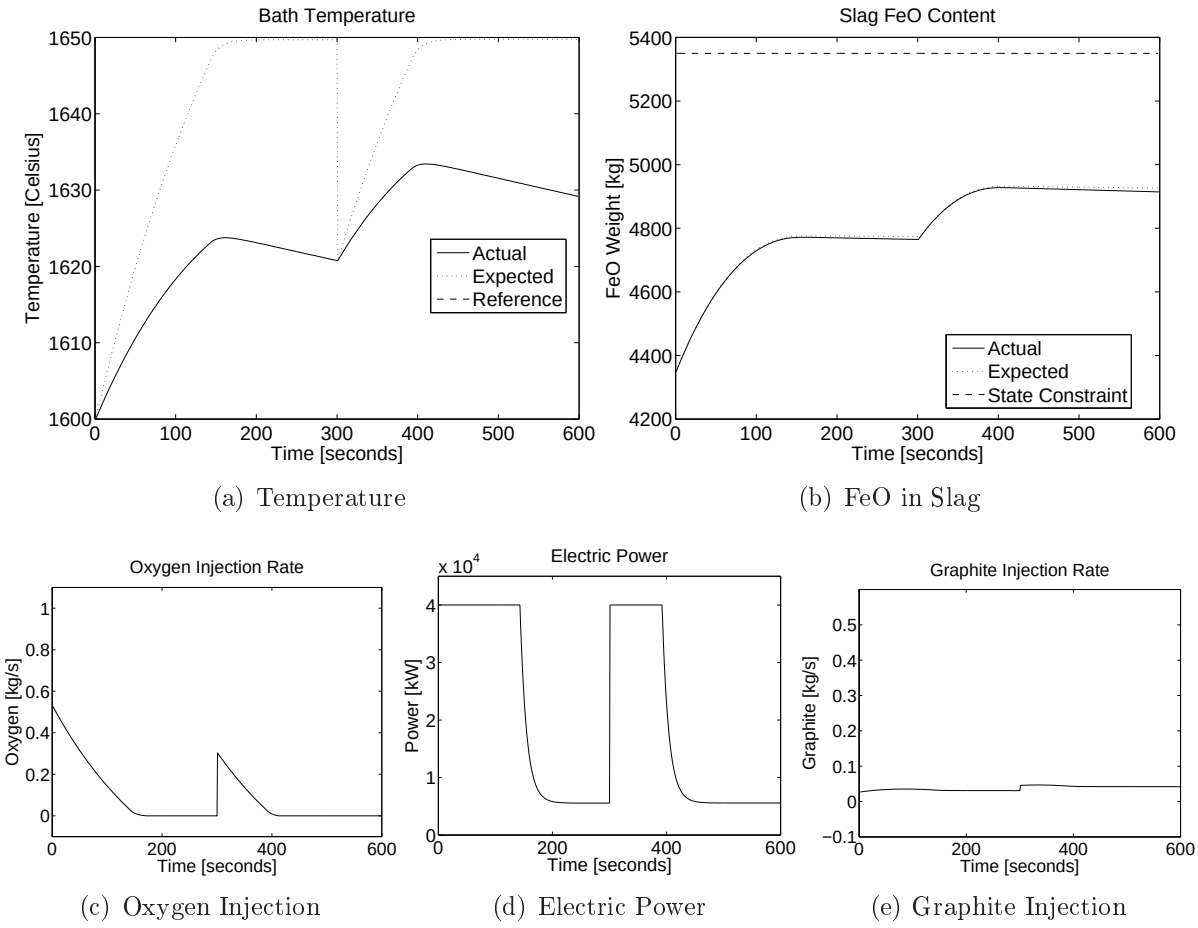

(a) Temperature (b) FeO in Slag

(c) Oxygen Injection (d) Electric Power (e) Graphite Injection

Figure 4.17: Dual-mode robust MPC - Efficiencies at a minimum, one measurement and reduced oxygen usage.

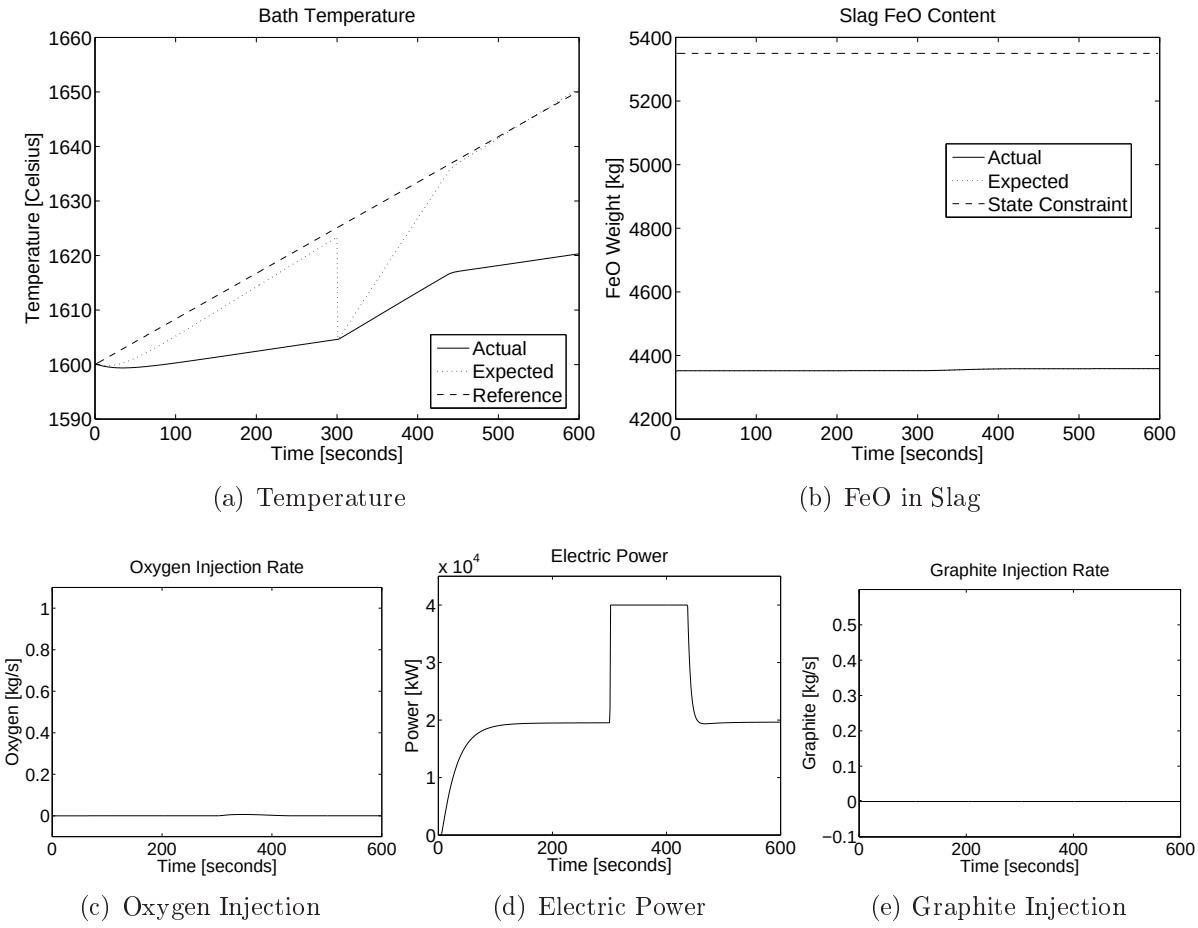

(a) Temperature (b) FeO in Slag

(c) Oxygen Injection (d) Electric Power (e) Graphite Injection

Figure 4.18: Nominal MPC - Efficiencies at a minimum, one measurement, reference trajectory and reduced oxygen usage.

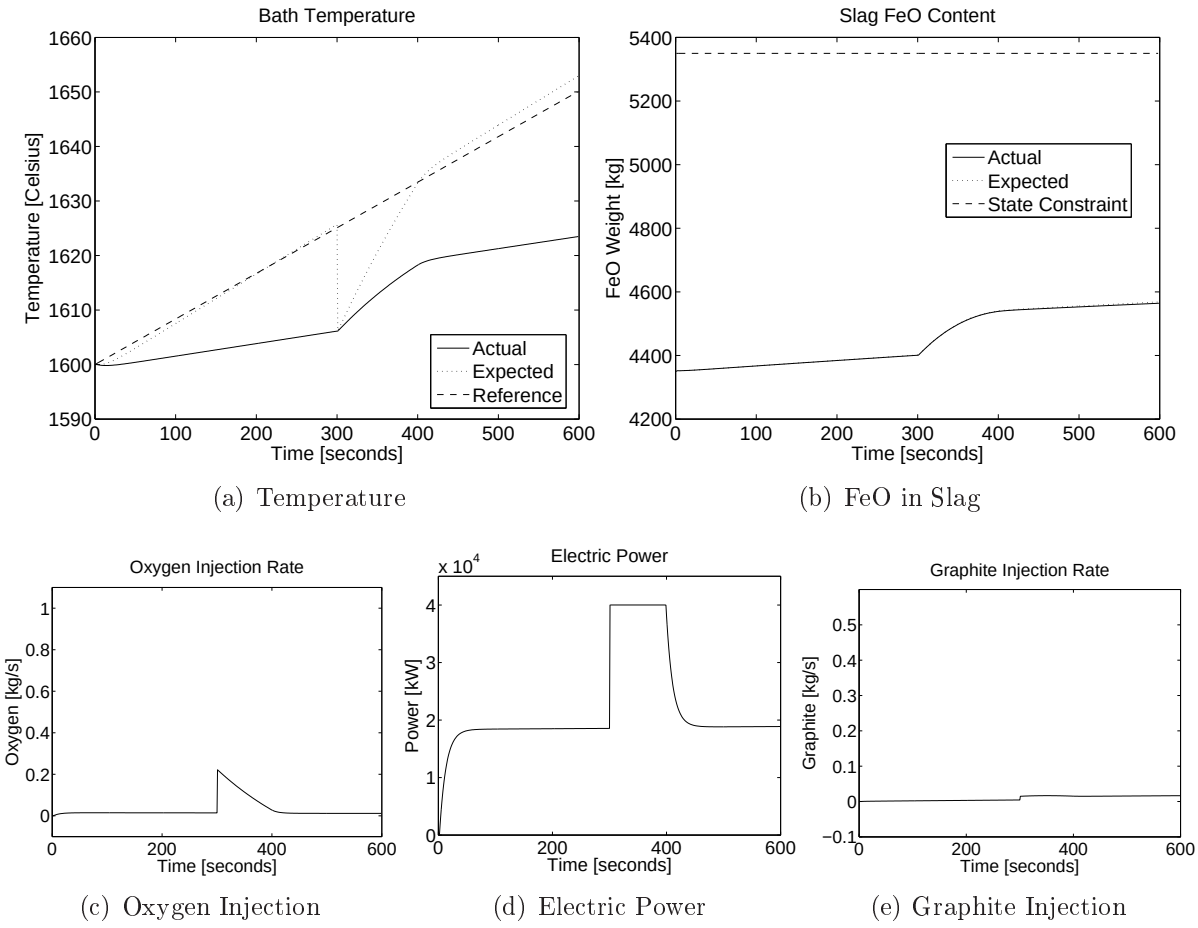

(a) Temperature (b) FeO in Slag

(c) Oxygen Injection (d) Electric Power (e) Graphite Injection

Figure 4.19: Dual-mode robust MPC - Efficiencies at a minimum, one measurement, reference trajectory and reduced oxygen usage.

4.3.3 Worst-case scenario: Efficiencies at their minimum with one plant measurement and predictor parameter update

In the previous section, the effect of model mismatch between the predictor and the actual plant on the performance of the closed-loop system is made clear. To combat this, the parameters of the predictor are updated each time a measurement is taken, in an attempt to improve performance. In this scenario only one temperature measurement is taken in the middle of the refining stage, with the rest of the state data produced by the predictor. The predictor uses the nominal plant parameters until the first measurement is taken, after which the corrected parameters are employed. The real plant uses the worst-case scenario where the efficiencies (η_{FeO} and η_{ARC}) are at their minimum.

A setpoint of 1650^oC for temperature as well as higher weighting on oxygen injection (table 4.2) is used for the first set of simulations.

Figures 4.20 and 4.21 show that both controllers are able to steer the temperature to within the desired margin of $\pm 10^0 C$. The robust controller overshoots the setpoint, which can be attributed to an overcorrection made in the predictor, as seen from the expected trajectory compared to the actual trajectory. The expected trajectory of the robust MPC ends at the desired setpoint, while the expected trajectory of the nominal MPC ends well outside the accepted margin of $\pm 10^0 C$. The nominal MPC steers the temperature to within the accepted margin of $\pm 10^0 C$, but only because of an overcorrection of the predictor. Both controllers use less oxygen, but the nominal controller less than the robust controller.

A reference trajectory for temperature as well as higher weighting on oxygen injection (table 4.2) is used for the fourth set of simulations.

These simulations (figures 4.22 and 4.23) show that the nominal controller misses the $\pm 10^0 C$ margin, while the robust controller does reach the $\pm 10^0 C$ margin. The expected trajectory of the robust controller reaches the desired value exactly, but the actual value is somewhat lower, due to an undercorrection in the parameters of the predictor. The expected trajectory of the nominal MPC barely reaches the accepted margin, but the actual trajectory misses the interval completely, due to the undercorrection in the parameters of

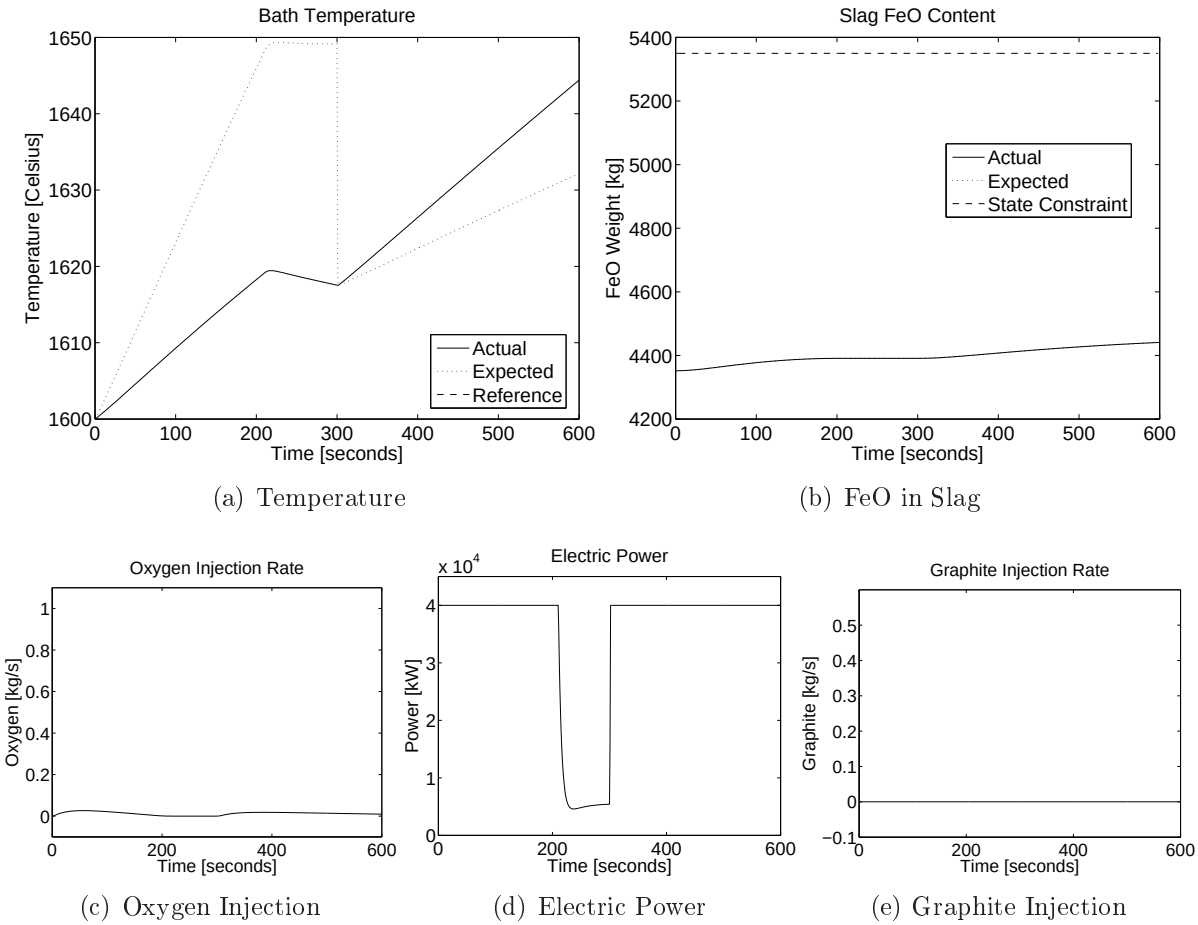

(a) Temperature (b) FeO in Slag

(c) Oxygen Injection (d) Electric Power (e) Graphite Injection

Figure 4.20: Nominal MPC - Efficiencies at a minimum, one measurement and predictor parameter update and reduced oxygen usage.

the predictor. The performance of the nominal MPC is hindered by its conservative use of oxygen.

The inability of the controllers to follow the reference is due to an undercorrection of the parameters of the predictor. The first sets of results show that the parameters of the predictor are sufficiently corrected at the measurement point to enable satisfactory results. In the reference trajectory simulations, the corrections to the parameters of the predictor are insufficient, which would require the updater to be tuned differently for the setpoint case and the reference trajectory case. The updater is sensitive to the timing of the measurement, the initial conditions that vary for each tap, and other disturbances such as late cave-ins.

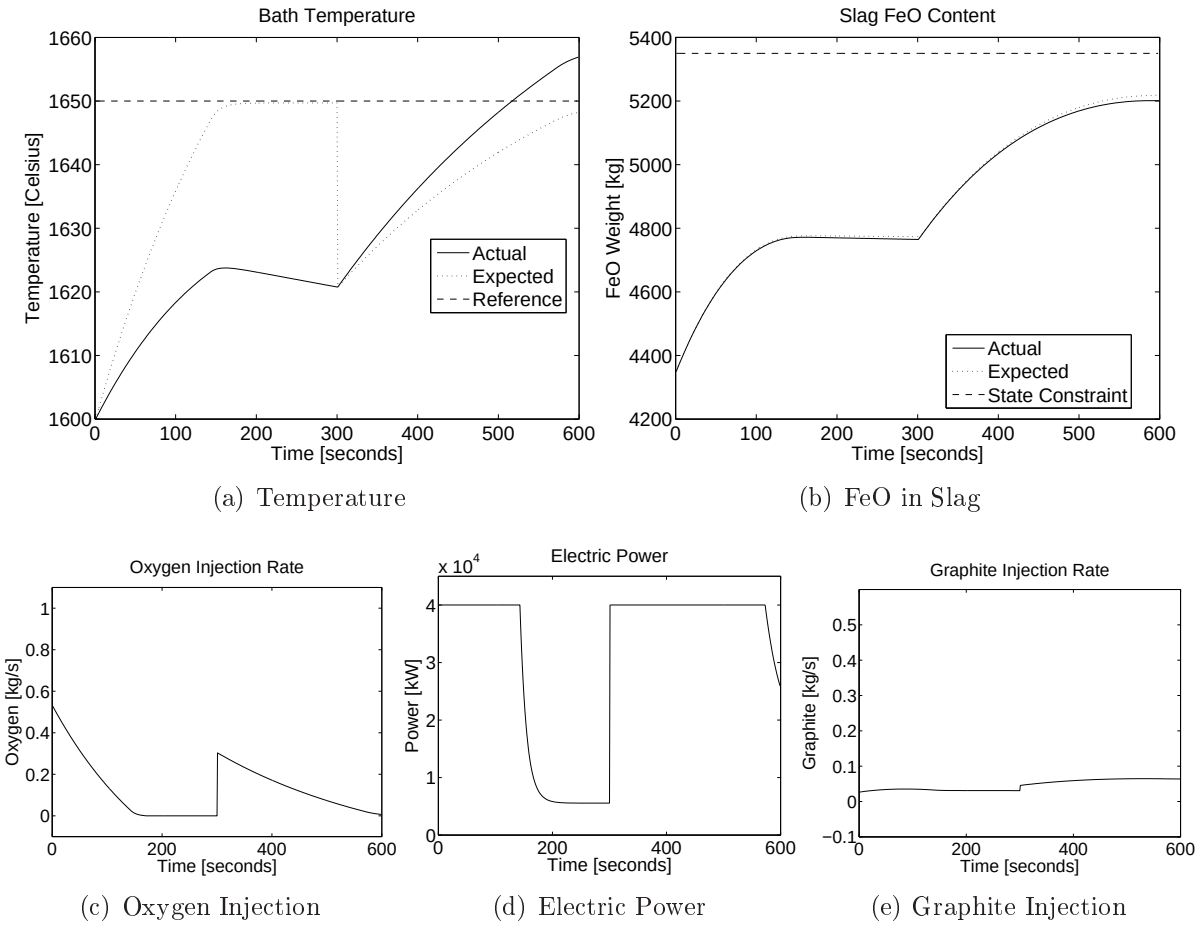

(a) Temperature (b) FeO in Slag

(c) Oxygen Injection (d) Electric Power (e) Graphite Injection

Figure 4.21: Dual-mode robust MPC - Efficiencies at a minimum, one measurement and predictor parameter update and reduced oxygen usage.

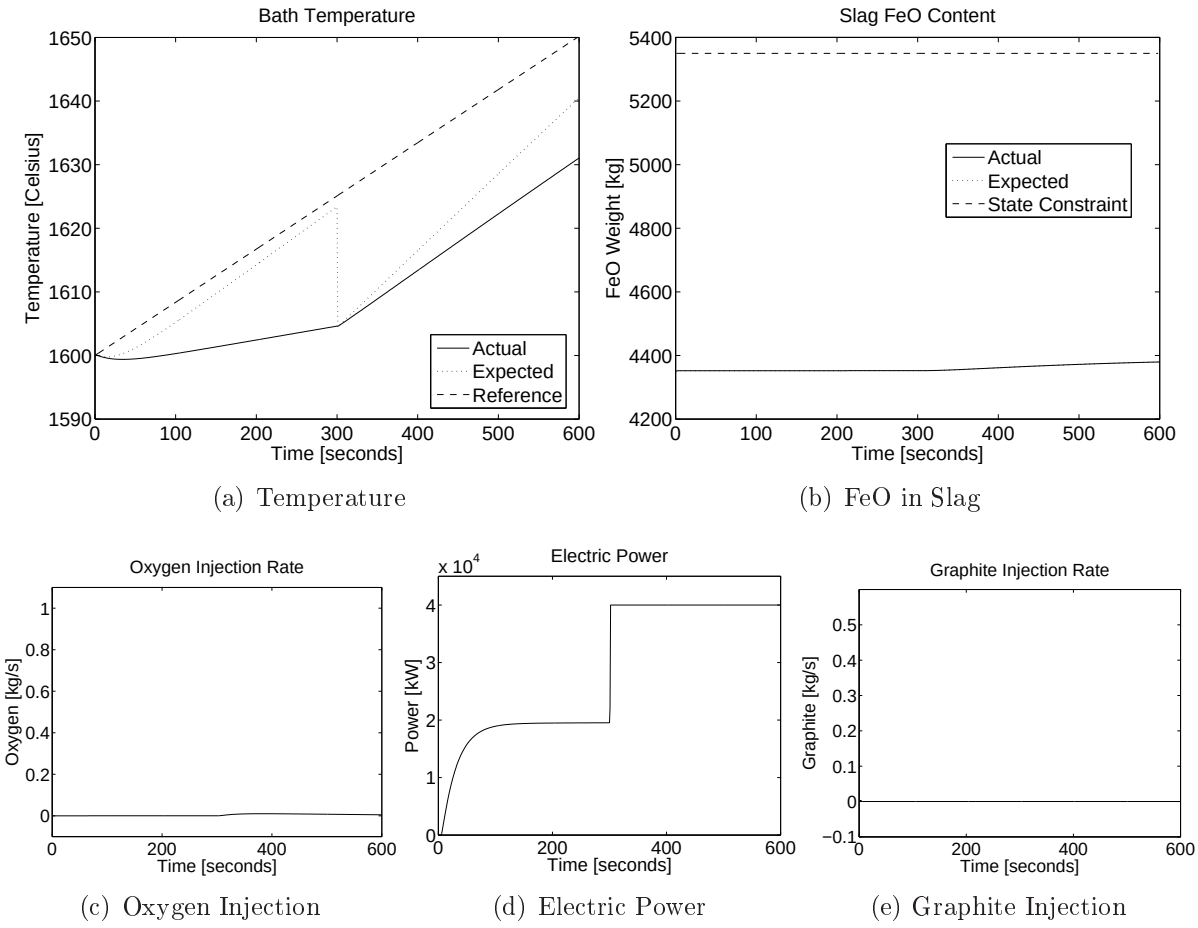

(a) Temperature (b) FeO in Slag

(c) Oxygen Injection (d) Electric Power (e) Graphite Injection

Figure 4.22: Nominal MPC - Efficiencies at a minimum, one measurement and predictor parameter update, reference trajectory and reduced oxygen usage.

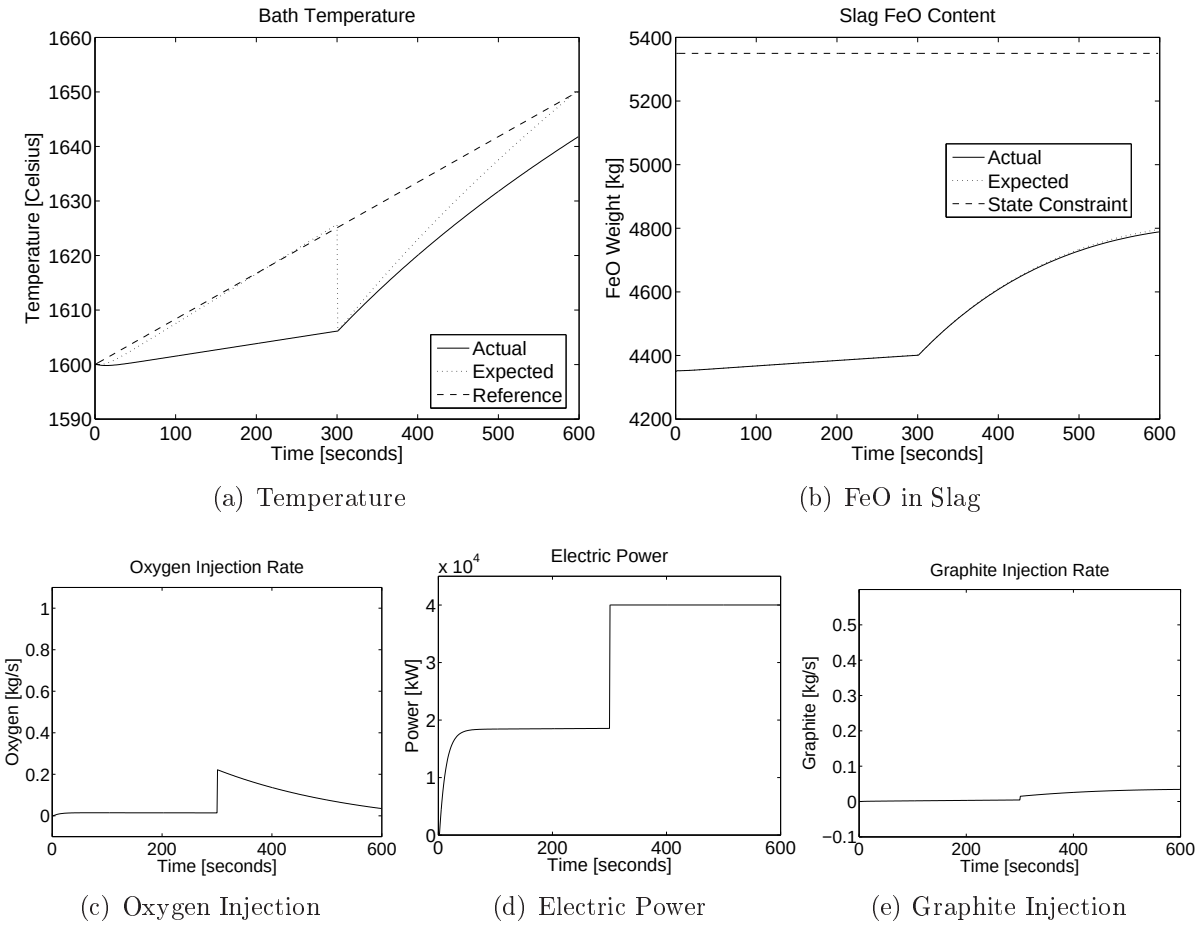

(a) Temperature (b) FeO in Slag

(c) Oxygen Injection (d) Electric Power (e) Graphite Injection

Figure 4.23: Dual-mode robust MPC - Efficiencies at a minimum, one measurement and predictor parameter update, reference trajectory and reduced oxygen usage.

4.4 Worst-case scenario: Efficiencies at their maximum

These worst-case scenarios investigate the effect of model mismatch between the internal model of the controllers and the actual plant as well as the predictor and the actual plant. This scenario focuses on the effect created if the efficiencies (η_{FeO} and η_{ARC}) are higher than nominal. This is a more theoretical scenario, because efficiencies do not tend to be higher than expected, but are necessary to determine whether the controller would be able to cope with such a situation. In these scenarios the following assumptions are made:

- There are three feedback scenarios:
  - Full state-feedback is available.
  - One temperature measurement is available.
  - One temperature measurement and an update of predictor parameters are available.
- The predictor and actual plant have a mismatch in their efficiencies (η_{FeO} and η_{ARC}) where the efficiencies are higher in the real plant than in the predictor.
- There are no disturbances.

The three feedback scenarios help to investigate the performance of the system with regards to the different modules in the system, especially the performance of the predictor and controller.

4.4.1 Worst-case scenario: Efficiencies at their maximum with full state feedback

In this first instance, full-state feedback is employed to evaluate the closed-loop performance without a predictor present, in the extreme case where the efficiencies (η_{FeO} and η_{ARC}) are at the maximum of the confidence interval for the plant model. Robust MPC and nominal MPC are compared to determine which provides better performance in the presence of model mismatch.

The first set of simulations uses a setpoint of 1650^oC for temperature as well as higher weighting on oxygen injection (table 4.2).

Figures 4.24 and 4.25 show that both controllers are capable of following the setpoint, and the increased weighting on oxygen reduces the amount of FeO that forms. The nominal MPC overshoots the temperature setpoint, while the robust MPC does not. The nominal MPC uses less oxygen than the robust MPC, which result in less FeO forming in the slag.

The second set of simulations uses a reference trajectory for temperature as well as a higher weighting on oxygen injection (table 4.2).

The last simulations (figures 4.22 and 4.23) show that both controllers have good reference following, with the robust controller overshooting slightly. The oxygen usage of the nominal controller is slightly lower than the previous run, but significantly lower than that of the robust controller.

Both controllers perform very well in this scenario where the efficiencies are higher than expected, and do not show any difficulty with the model mismatch between the internal model and the actual plant.

4.4.2 Worst-case scenario: Efficiencies at their maximum with one plant measurement

A more realistic feedback scenario is investigated, where only one measurement of temperature is taken in the middle of the refining stage, the rest of the data is produced by a predictor. The predictor uses the nominal plant parameters, while the real plant uses the worst-case scenario where the efficiencies (η_{FeO} and η_{ARC}) are at their maximum. This scenario should shed light on the effect of model mismatch between the predictor and real plant when compared to the results of the previous section.

The first set of simulations uses a setpoint of 1650^oC for temperature as well as higher weighting on oxygen injection (table 4.2).

Figures 4.28 and 4.29 show that both controllers fail to steer the temperature to within the $\pm 10^0C$ margin. The controllers overshoot the setpoint, because the efficiencies (η_{FeO}

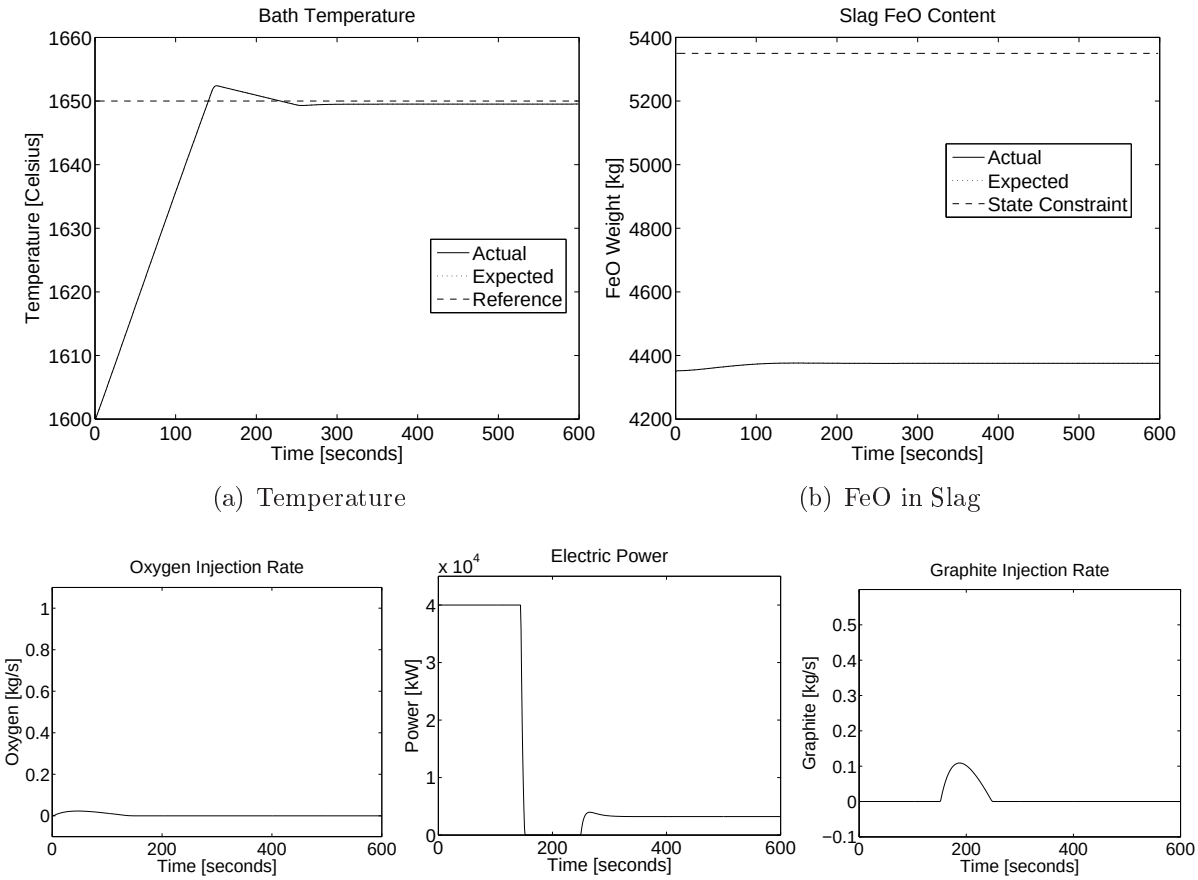

(a) Temperature (b) FeO in Slag

(c) Oxygen Injection (d) Electric Power (e) Graphite Injection

Figure 4.24: Nominal MPC - Efficiencies at maximum with full state feedback and reduced oxygen usage.

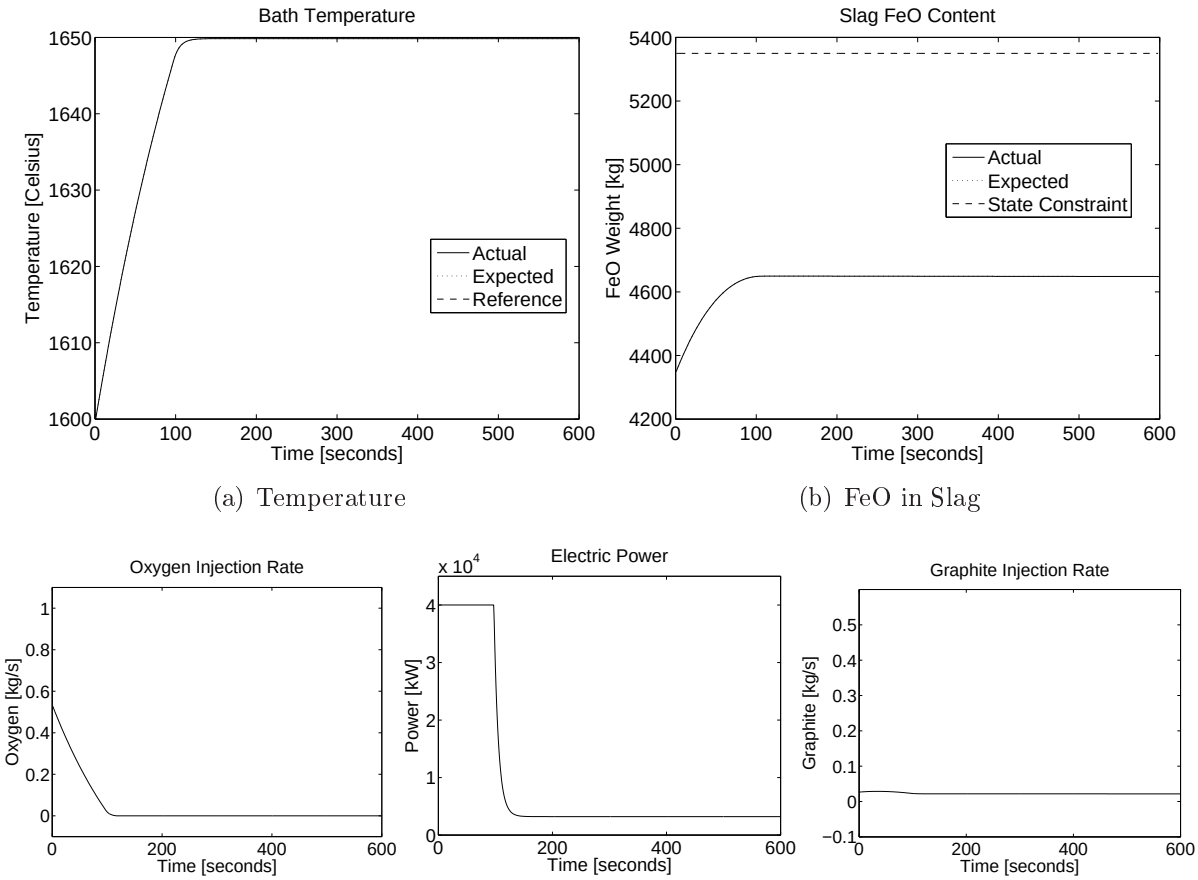

(a) Temperature (b) FeO in Slag

(c) Oxygen Injection (d) Electric Power (e) Graphite Injection

Figure 4.25: Dual-mode robust MPC - Efficiencies at maximum with full state feedback and reduced oxygen usage.

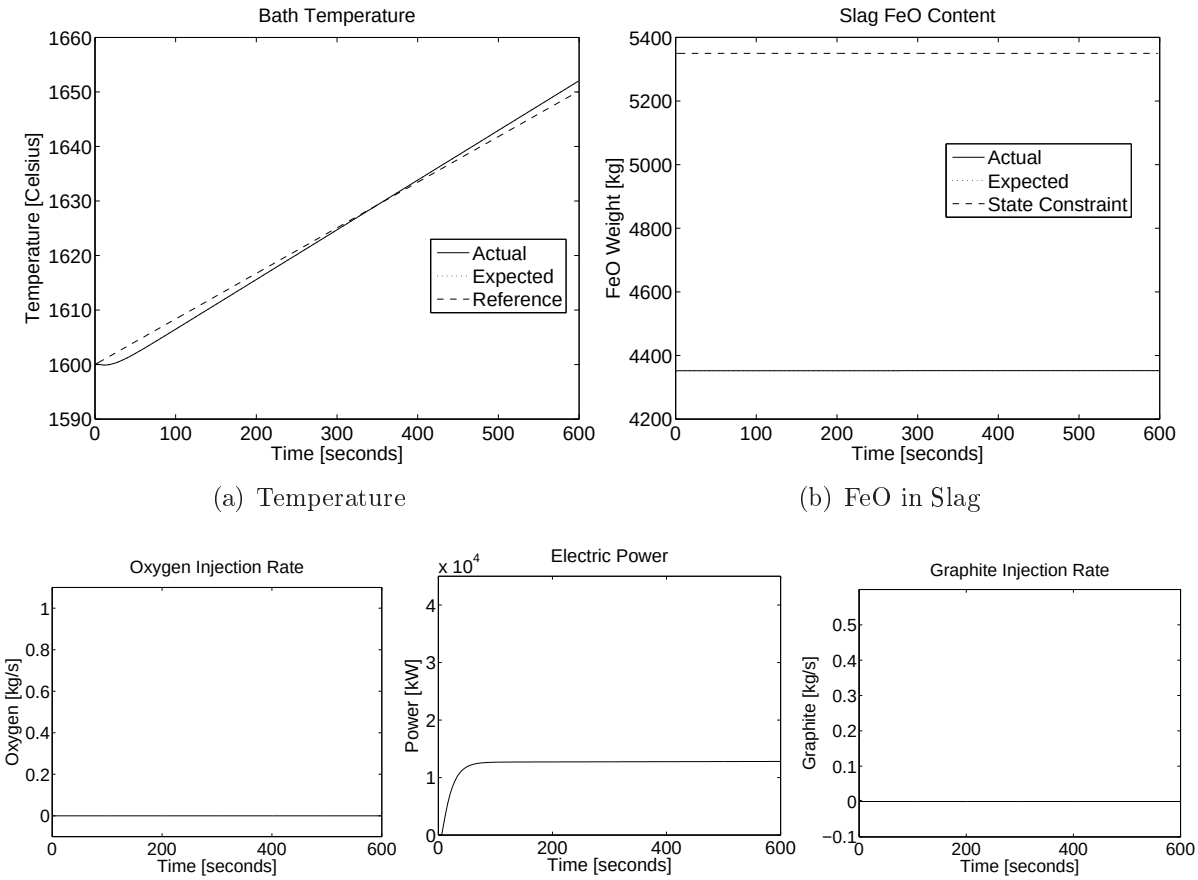

(a) Temperature (b) FeO in Slag

(c) Oxygen Injection (d) Electric Power (e) Graphite Injection

Figure 4.26: Nominal MPC - Efficiencies at maximum with full state feedback, reference trajectory and reduced oxygen usage.

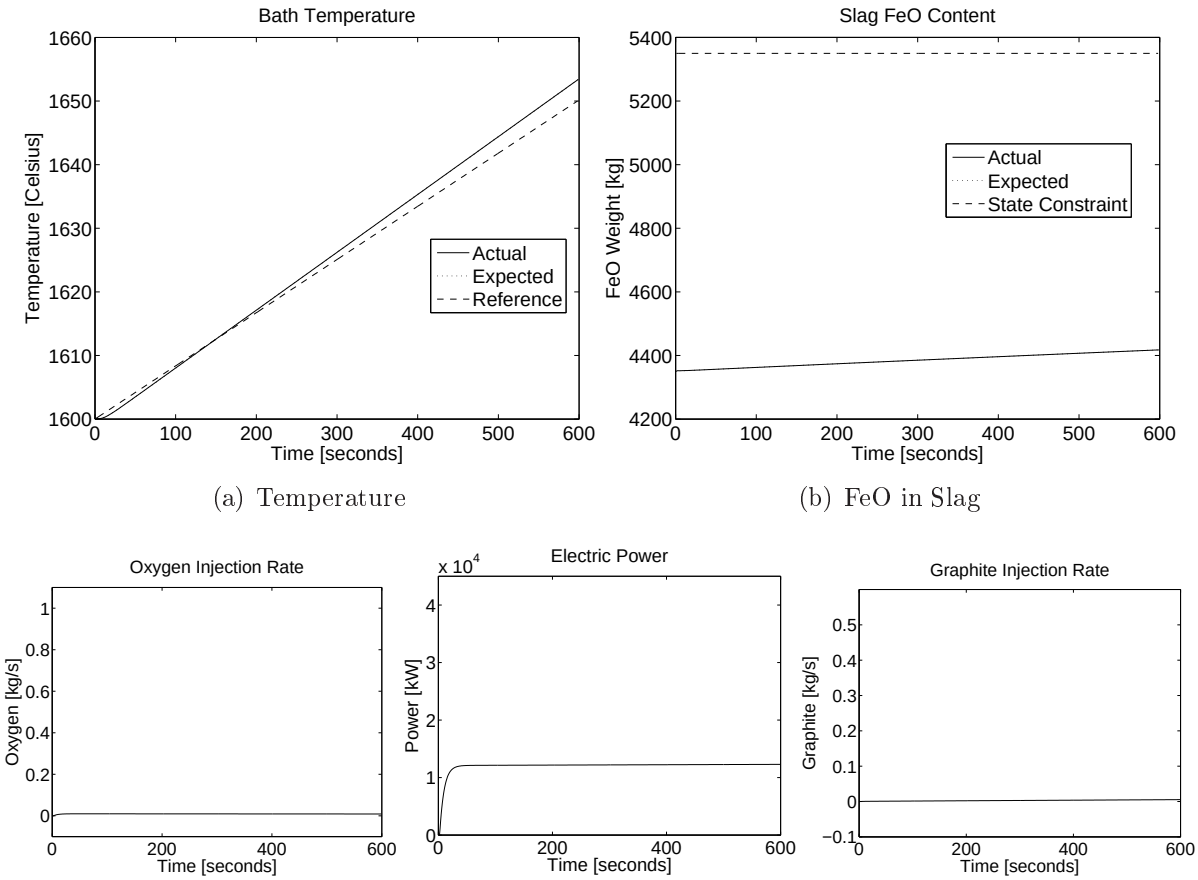

(a) Temperature (b) FeO in Slag

(c) Oxygen Injection (d) Electric Power (e) Graphite Injection

Figure 4.27: Dual-mode robust MPC - Efficiencies at maximum with full state feedback, reference trajectory and reduced oxygen usage.

and η_{ARC}) are higher than expected and the controllers drive the temperature too high. The measurement shows the controllers that the temperature is too high, and they respond by turning off all energy sources. The temperature is lowered, but is limited by the tempo of natural heat loss, which is too slow to reach the target by the end of the refining stage. The process could be accelerated by opening the furnace roof, which would aid heat loss. This situation can be prevented by taking a measurement earlier in the refining stage to identify the problem sooner.

The second set of simulations uses a reference trajectory for temperature as well as higher weighting on oxygen injection (table 4.2) and updates the parameters (η_{FeO} and η_{ARC}) of the predictor from the plant measurement.

These simulations (figures 4.30 and 4.31) show that both controllers steer the temperature to within the $\pm 10^0 C$ margin. The reference trajectory causes the temperature to increase much slower than with the setpoint, so that by the time a measurement is taken, the temperature has not yet passed the desired final value of $1650^0 C$. The temperature does increase above the reference, and after the measurement, the controller corrects the problem and once it has reached the reference, it follows it more closely. There is still an undercorrection, which causes the temperature to increase faster than expected. The final value ends within the accepted $\pm 10^0 C$ margin. The heavier weighting on oxygen injection usage results in lower FeO production without affecting the temperature response.

4.5 Temperature disturbance

A temperature disturbance can occur due to a late cave-in. This happens when there is solid scrap that falls into the bath, which is unexpected, because it is assumed that all scrap has melted when refining commences. As a result, the bath temperature drops quickly, and can be modelled by a step disturbance on the temperature. The following assumptions are used for this simulation:

- One measurement from the plant.
- No predictor parameters update.

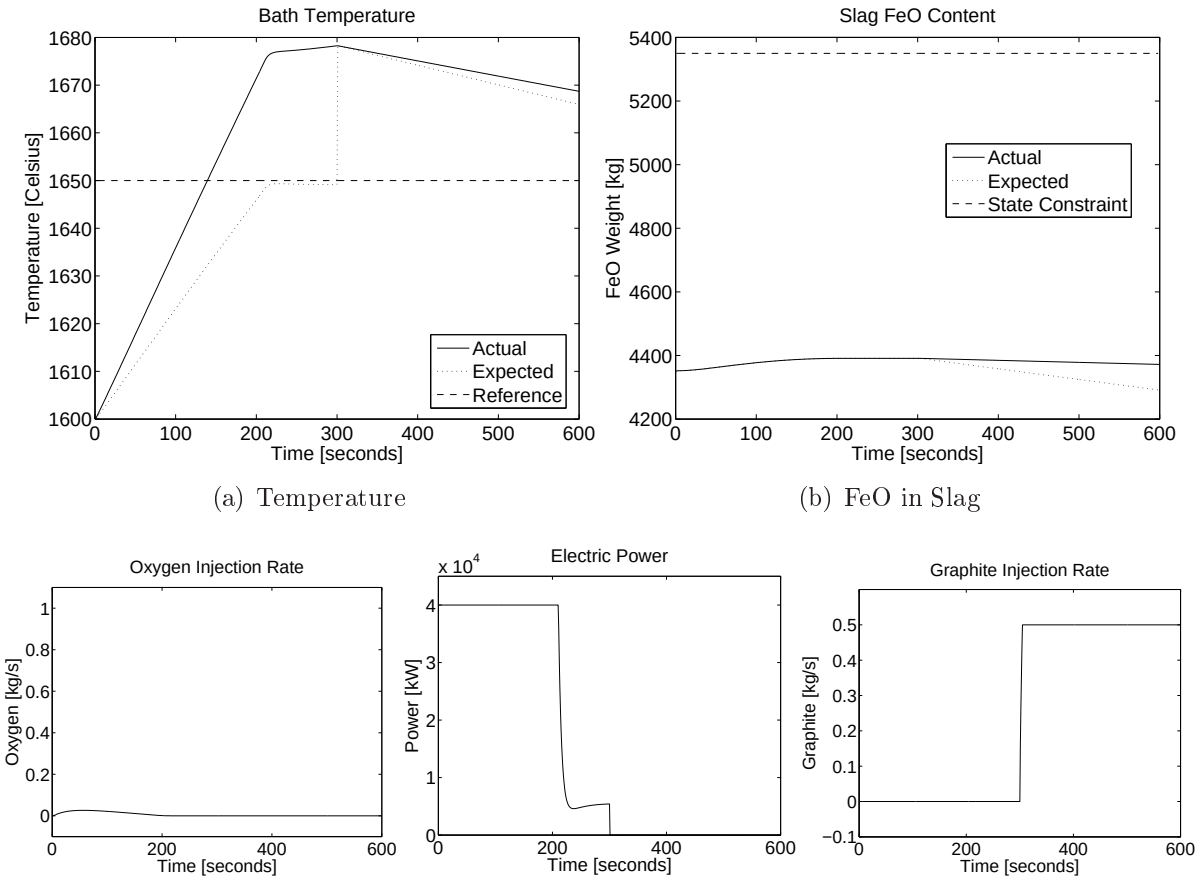

(a) Temperature (b) FeO in Slag

(c) Oxygen Injection (d) Electric Power (e) Graphite Injection

Figure 4.28: Nominal MPC - Efficiencies at maximum, one measurement and reduced oxygen usage.

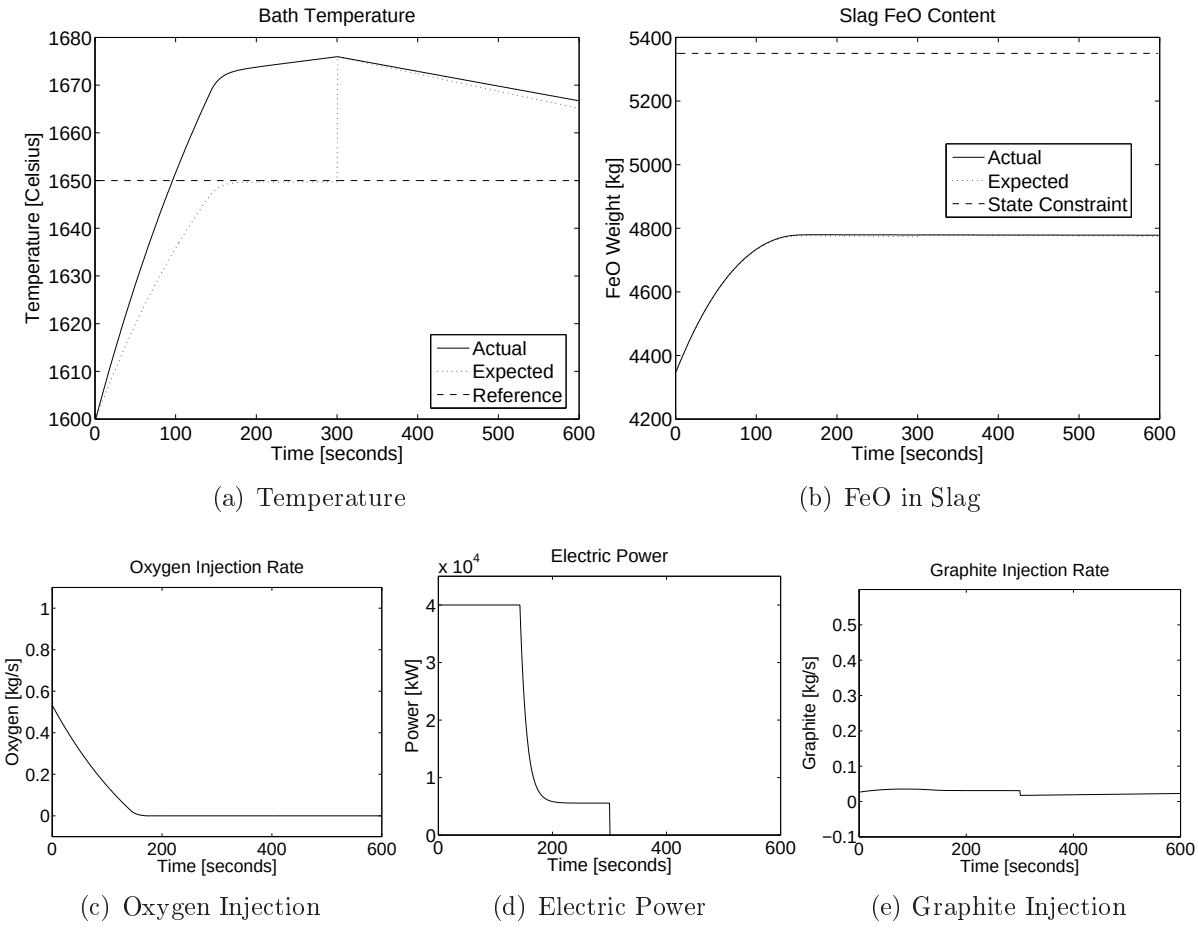

(a) Temperature (b) FeO in Slag

(c) Oxygen Injection (d) Electric Power (e) Graphite Injection

Figure 4.29: Dual-mode robust MPC - Efficiencies at maximum, one measurement and reduced oxygen usage.

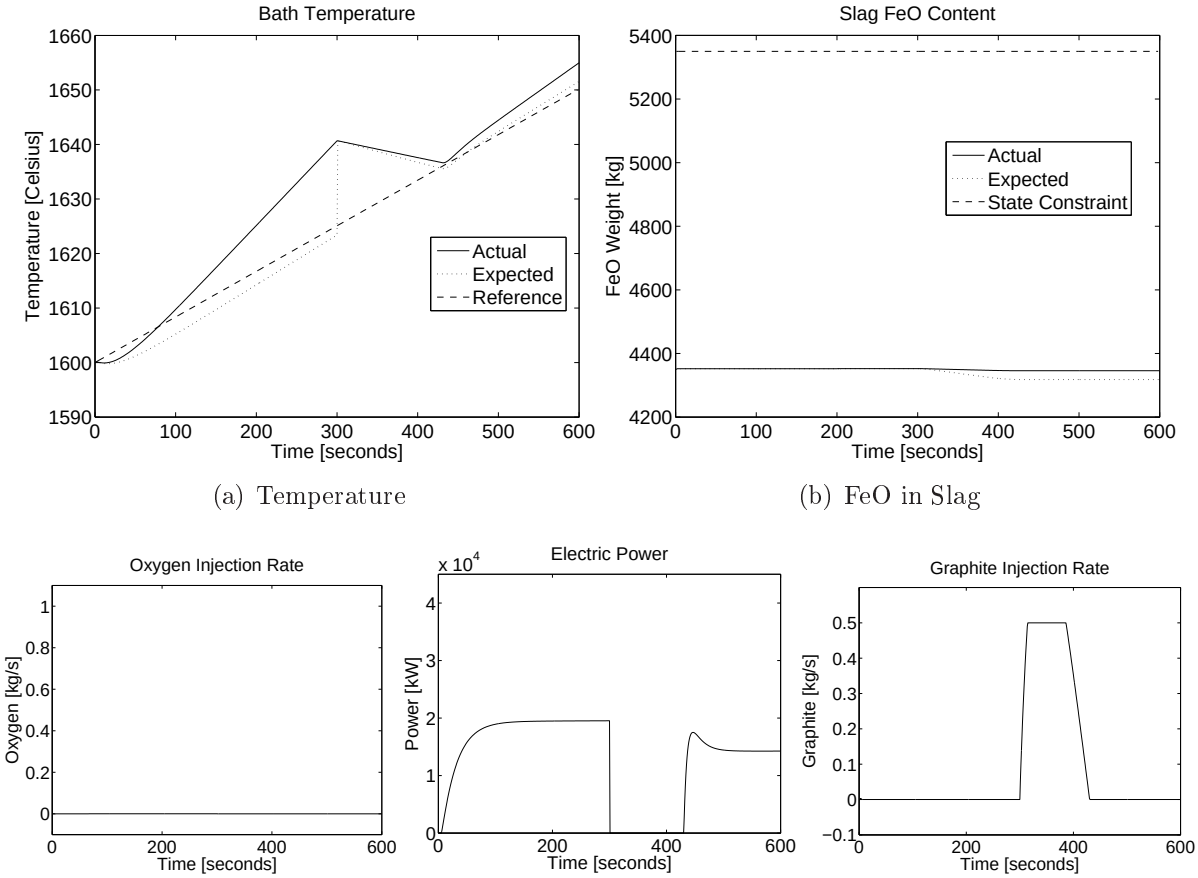

(a) Temperature (b) FeO in Slag

(c) Oxygen Injection (d) Electric Power (e) Graphite Injection

Figure 4.30: Nominal MPC - Efficiencies at maximum, one measurement and predictor update, reference trajectory and reduced oxygen usage.

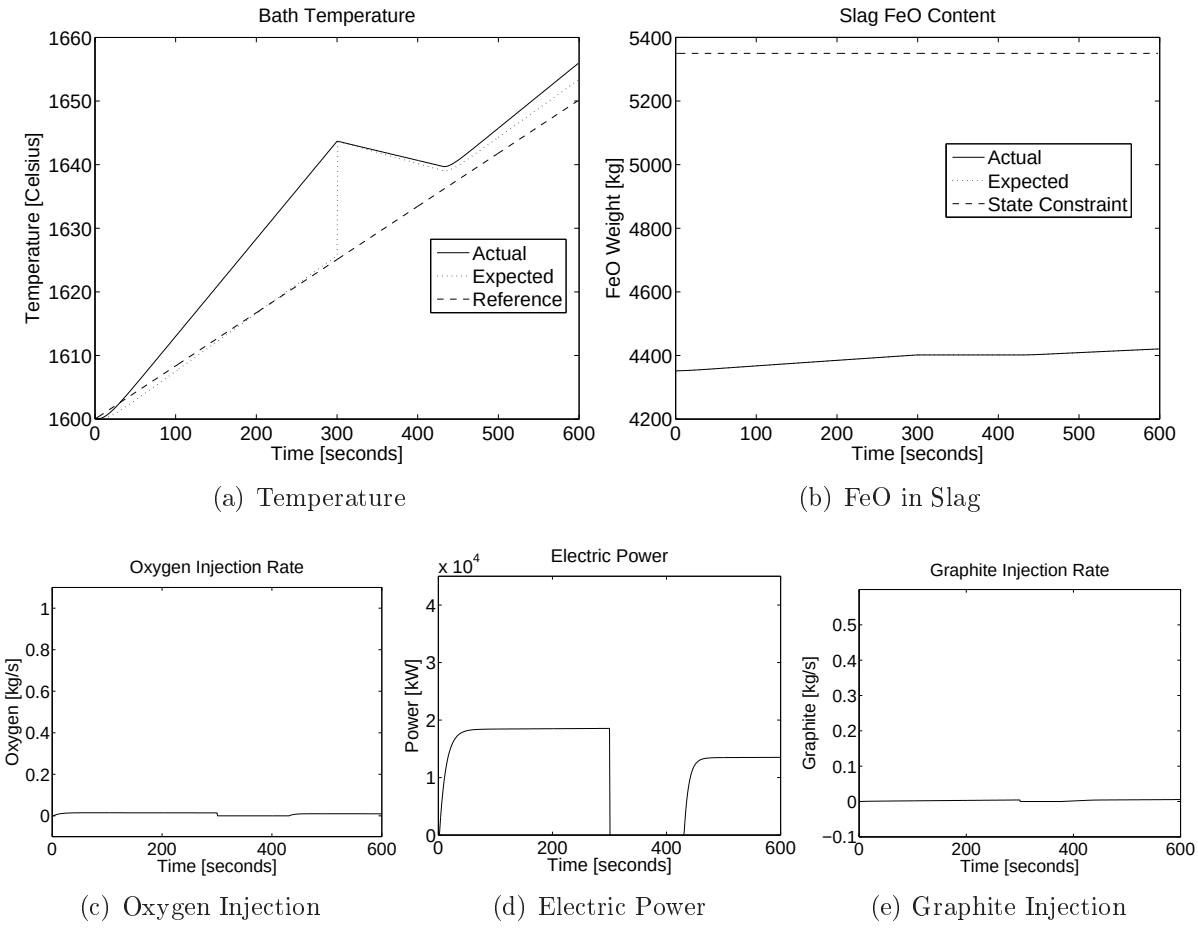

(a) Temperature (b) FeO in Slag

(c) Oxygen Injection (d) Electric Power (e) Graphite Injection

Figure 4.31: Dual-mode robust MPC - Efficiencies at maximum, one measurement and predictor update, reference trajectory and reduced oxygen usage.

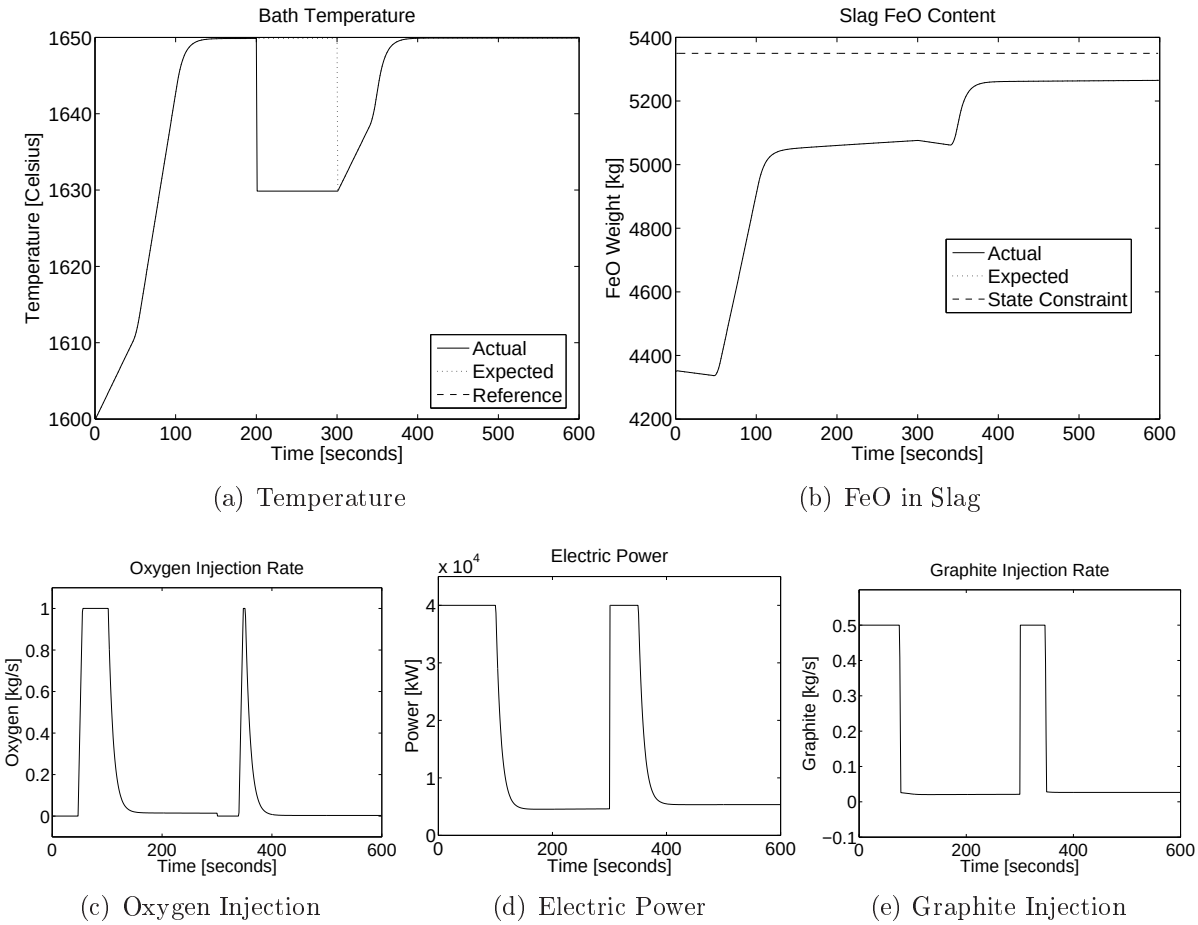

(a) Temperature (b) FeO in Slag

(c) Oxygen Injection (d) Electric Power (e) Graphite Injection

Figure 4.32: Dual-mode robust MPC - Temperature disturbance of -20^0C at time 200s with setpoint of 1650^0C.

- Actual plant and predictor use nominal plant parameters.
- Disturbance of -20^0C on temperature at time 200s.

The first simulation uses a setpoint of 1650^0C for temperature and even weighting on the inputs (table 4.2) with a temperature disturbance of -20^0C at time 200s.

Figure 4.32 shows that the robust controller is capable of handling a quite severe temperature drop of 20^0C and recover from it.

The second simulation uses a reference trajectory for temperature with even weighting on the inputs (table 4.2) with a temperature disturbance of -20^0C at time 200s.

Figure 4.33 shows that the robust controller is capable of handling a quite severe temperature drop of 20^0C and recover from it even when employing a reference trajectory. The controller makes full use of the energy sources when the disturbance is detected.

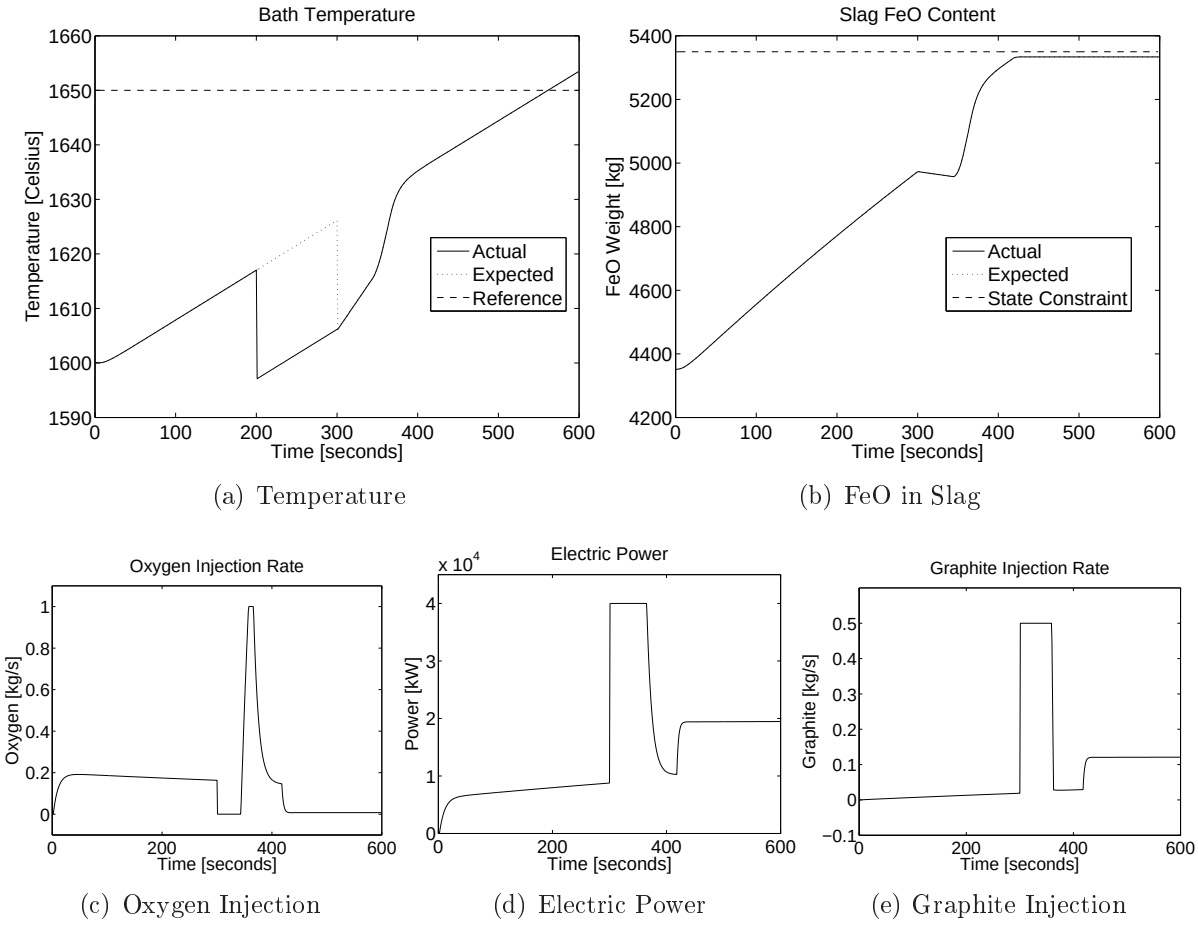

(a) Temperature (b) FeO in Slag

(c) Oxygen Injection (d) Electric Power (e) Graphite Injection

Figure 4.33: Dual-mode robust MPC - Temperature disturbance of -20^0C at time 200s with a reference trajectory for temperature.

In the limited feedback scenarios, the disturbance will only be detected when it occurs before a measurement, of which there is usually only one during the refining stage. In this case, predictor parameter update will have a detrimental effect on the performance, because the difference would be attributed to model mismatch where the efficiencies are lower than nominal, and an overcorrection would be made to the predictor. This will result in the temperature ending up much higher than desired.

4.6 Summary

This section provides a summary of the results obtained in the previous sections. The results are summarized in tables 4.5, 4.6, 4.7, 4.8 and4.9. The notation used in the tables is as follows:

- Feedback:
  - FSF - Full state feedback.
  - OM - One temperature measurement is taken in the middle of the refining stage with the rest of the data produced by a predictor.
  - OMPU - One temperature measurement is taken in the middle of the refining stage with which the parameters of the predictor are updated.
- Setpoint or Reference:
  - Setpoint - A constant setpoint for temperature of 1650^0C is employed.
  - Reference - A linearly increasing reference is employed for temperature that reaches 1650^0C at the end of the refining stage period.
- Input weighting:
  - Even - All inputs are penalized equally in the objective function (table 4.2).
  - Oxygen Heavy (OH) - Oxygen usage is penalized more than the other inputs in the objective function (table 4.2).

- ΔT - Temperature difference - The amount that the final temperature value differs from 1650^0C.
- Acceptable - If the final temperature value is within a $\pm 10^0C$ margin of 1650^0C.
- Energy usage - The value of a linear penalty function that uses the same weightings of the inputs as the controllers.

The energy usage is a function that sums up all the inputs together over the whole duration of the refining stage. All the inputs are scaled so that the maximum value of each contributes equally to the energy usage metric. This metric gives an indication of how much energy is applied throughout the refining stage for each simulation scenario. The metric is calculated as follows

$$EU = \sqrt{u * R_1 * u^T} \tag{4.1}$$

where R_1 is the scaling matrix and $u \in \mathbb{R}^{600\times 3}$, where there is a sample every second over 10 minutes and three inputs. The scaling matrix is

$$R_1 = \begin{bmatrix} 10 & 0 & 0 \\ 0 & 0.00025 & 0 \\ 0 & 0 & 20 \end{bmatrix}. \tag{4.2}$$

This gives an indication of overall controller action employed by the controller, because the same metric was included in the controller. The metric can be changed to include energy cost that will lead to the most energy efficient solution.

4.7 Conclusion

This comprehensive simulation study looked at some theoretical as well as more practical scenarios in order to investigate the performance of the robust and nominal controllers in the presence of model mismatch. The performance of the closed-loop system where there is model mismatch between the predictor and actual plant was also studied.

Table 4.5: Summary of simulation results with nominal efficiencies.

Controller	Feedback	Setpoint or Reference	Input weighting	Temperature difference	Energy usage	Fig
Nominal MPC	FSF	Setpoint	Even	$< 1^0C$	8.5e+004	4.3
Robust MPC	FSF	Setpoint	Even	$< 1^0C$	1.0e+005	4.4
Nominal MPC	FSF	Setpoint	Oxygen Heavy	$< 1^0C$	1.7e+005	4.6
Robust MPC	FSF	Setpoint	Oxygen Heavy	$< 1^0C$	1.4e+005	4.7
Nominal MPC	FSF	Reference	Even	$< 1^0C$	8.9e+004	4.8
Robust MPC	FSF	Reference	Even	3^0C	9.6e+004	4.9
Nominal MPC	FSF	Reference	Oxygen Heavy	$< 1^0C$	1.8e+005	4.10
Robust MPC	FSF	Reference	Oxygen Heavy	3^0C	1.7e+005	4.11

Table 4.6: Summary of simulation results with efficiencies at their minimum.

Controller	Feedback	Setpoint or Reference	Input weighting	ΔT	Acceptable	Energy usage	Fig
Nominal MPC	FSF	Setpoint	Even	-2^0C	Yes	2.3e+005	B.1
Robust MPC	FSF	Setpoint	Even	$< 1^0C$	Yes	2.3e+005	B.2
Nominal MPC	FSF	Setpoint	Oxygen Heavy	-2^0C	Yes	3.5e+005	4.12
Robust MPC	FSF	Setpoint	Oxygen Heavy	$< 1^0C$	Yes	2.7e+005	4.13
Nominal MPC	FSF	Reference	Even	-4^0C	Yes	2.2e+005	B.3
Robust MPC	FSF	Reference	Even	$< 1^0C$	Yes	2.5e+005	B.4
Nominal MPC	FSF	Reference	Oxygen Heavy	-5^0C	Yes	3.4e+005	4.14
Robust MPC	FSF	Reference	Oxygen Heavy	$< 1^0C$	Yes	3.5e+005	4.15
Nominal MPC	OM	Setpoint	Even	-20^0C	No	1.4e+005	B.5
Robust MPC	OM	Setpoint	Even	-20^0C	No	1.1e+005	B.6
Nominal MPC	OM	Setpoint	Oxygen Heavy	-23^0C	No	2.4e+005	4.16
Robust MPC	OM	Setpoint	Oxygen Heavy	-21^0C	No	1.9e+005	4.17
Nominal MPC	OM	Reference	Even	-24^0C	No	1.2e+005	B.7
Robust MPC	OM	Reference	Even	-22^0C	No	1.3e+005	B.8
Nominal MPC	OM	Reference	Oxygen Heavy	-30^0C	No	2.2e+005	4.18
Robust MPC	OM	Reference	Oxygen Heavy	-27^0C	No	2.1e+005	4.19
Nominal MPC	OMPU	Setpoint	Even	-5^0C	Yes	2.2e+005	B.9
Robust MPC	OMPU	Setpoint	Even	$+2^0C$	Yes	2.6e+005	B.10
Nominal MPC	OMPU	Setpoint	Oxygen Heavy	-6^0C	Yes	3.3e+005	4.20
Robust MPC	OMPU	Setpoint	Oxygen Heavy	$+6^0C$	Yes	3.0e+005	4.21
Nominal MPC	OMPU	Reference	Even	-17^0C	No	1.6e+005	B.11
Robust MPC	OMPU	Reference	Even	-12^0C	No	1.9e+005	B.12
Nominal MPC	OMPU	Reference	Oxygen Heavy	-19^0C	No	2.7e+005	4.22
Robust MPC	OMPU	Reference	Oxygen Heavy	-9^0C	Yes	2.7e+005	4.23

Table 4.7: Summary of simulation results with efficiencies at their maximum.

Controller	Feedback	Setpoint or Reference	Input weighting	ΔT	Acceptable	Energy usage	Fig
Nominal MPC	FSF	Setpoint	Even	$< 1^0C$	Yes	4.3e+004	B.13
Robust MPC	FSF	Setpoint	Even	$< 1^0C$	Yes	7.4e+004	B.14
Nominal MPC	FSF	Setpoint	Oxygen Heavy	$< 1^0C$	Yes	1.1e+005	4.24
Robust MPC	FSF	Setpoint	Oxygen Heavy	$< 1^0C$	Yes	9.1e+004	4.25
Nominal MPC	FSF	Reference	Even	$< 1^0C$	Yes	4.3e+004	B.15
Robust MPC	FSF	Reference	Even	$+4^0C$	Yes	5.8e+004	B.16
Nominal MPC	FSF	Reference	Oxygen Heavy	$< 1^0C$	Yes	1.2e+005	4.26
Robust MPC	FSF	Reference	Oxygen Heavy	$+3^0C$	Yes	1.1e+005	4.27
Nominal MPC	OM	Setpoint	Even	$+11^0C$	No	6.0e+004	B.17
Robust MPC	OM	Setpoint	Even	$+14^0C$	No	8.3e+004	B.18
Nominal MPC	OM	Setpoint	Oxygen Heavy	$+19^0C$	No	1.4e+005	4.28
Robust MPC	OM	Setpoint	Oxygen Heavy	$+18^0C$	No	1.1e+005	4.29
Nominal MPC	OM	Reference	Even	$+11^0C$	No	5.8e+004	B.19
Robust MPC	OM	Reference	Even	$+13^0C$	No	6.4e+004	B.20
Nominal MPC	OM	Reference	Oxygen Heavy	$+11^0C$	No	1.3e+005	B.21
Robust MPC	OM	Reference	Oxygen Heavy	$+13^0C$	No	1.3e+005	B.22
Nominal MPC	OMPU	Setpoint	Even	$+11^0C$	No	6.0e+004	B.23
Robust MPC	OMPU	Setpoint	Even	$+14^0C$	No	8.3e+004	B.24
Nominal MPC	OMPU	Setpoint	Oxygen Heavy	$+19^0C$	No	1.4e+005	B.25
Robust MPC	OMPU	Setpoint	Oxygen Heavy	$+18^0C$	No	1.1e+005	B.26
Nominal MPC	OMPU	Reference	Even	$+7^0C$	Yes	4.9e+004	B.27
Robust MPC	OMPU	Reference	Even	$+8^0C$	Yes	6.0e+004	B.28
Nominal MPC	OMPU	Reference	Oxygen Heavy	$+5^0C$	Yes	1.2e+005	4.30
Robust MPC	OMPU	Reference	Oxygen Heavy	$+7^0C$	Yes	1.2e+005	4.31

Table 4.8: Summary of simulation results with efficiencies at nominal and temperature disturbance.

Controller	Feedback	Setpoint or Reference	Input weighting	ΔT	Acceptable	Energy usage	Fig
Robust MPC	OM	Setpoint	Even	$< 1^0C$	Yes	1.4e+005	4.32
Robust MPC	OM	Reference	Even	$+2^0C$	Yes	1.4e+005	4.33

Table 4.9: Summary of simulation results that produced acceptable results excluding nominal and full state feedback scenarios.

Controller	Feedback	Setpoint or Reference	Input weighting	ΔT	Efficiencies	Energy usage	Fig
Nominal MPC	OMPU	Reference	Even	$+7^0C$	Max	4.9e+004	B.27
Robust MPC	OMPU	Reference	Even	$+8^0C$	Max	6.0e+004	B.28
Nominal MPC	OMPU	Reference	Oxygen Heavy	$+5^0C$	Max	1.2e+005	4.30
Robust MPC	OMPU	Reference	Oxygen Heavy	$+7^0C$	Max	1.2e+005	4.31
Nominal MPC	OMPU	Setpoint	Even	-5^0C	Min	2.2e+005	B.9
Robust MPC	OMPU	Setpoint	Even	$+2^0C$	Min	2.6e+005	B.10
Nominal MPC	OMPU	Setpoint	Oxygen Heavy	-6^0C	Min	3.3e+005	4.20
Robust MPC	OMPU	Setpoint	Oxygen Heavy	$+6^0C$	Min	3.0e+005	4.21
Robust MPC	OMPU	Reference	Oxygen Heavy	-9^0C	Min	2.7e+005	4.23
Robust MPC	OM	Setpoint	Even	$< 1^0C$	Dist	1.4e+005	4.32
Robust MPC	OM	Reference	Even	$+2^0C$	Dist	1.4e+005	4.33

In the scenarios where full state feedback is available, both the dual-mode robust model predictive controller and the nominal model predictive controller perform equally well. The model uncertainty is such that the nominal controller is capable of handling it satisfactorily. The feedback robust MPC cannot handle asymmetric constraints such as those present in the EAF refining process. An ad-hoc solution to compensate for this limitation is to add a constant disturbance to the inputs. This was not a successful strategy, because the inputs have to be driven to their constraints, which the feedback robust MPC avoids. This prevents the feedback robust MPC method from successfully following the temperature setpoint or reference.

A bigger problem with automating the process is the lack of feedback from the plant. A predictor is used to estimate the plant states in order for the controller to generate control actions for the plant. With the limited number of measurements, the effect of model mismatch between the predictor and actual plant has a much bigger impact on the performance of the closed-loop system than the effects of model uncertainty. The effects of model mismatch can be reduced by using the plant measurement to update the predictor parameters, but this will meet with varying success, because there is usually only one measurement available during the refining stage from which to update the parameters of the predictor. If a late cave-in occurs, the predictor will be incorrectly updated, which will hinder further performance. The updating of the parameters of the predictor was done using an ad-hoc method to determine if it will produce better results than a predictor without parameter update. The predictor utilizing this ad-hoc method shows an improvement over the predictor without parameter updates. A more in-depth study is necessary to design a proper predictor for the EAF refining process, one that utilizes better updating methods and takes all other aspects into consideration through a more systematic design. This was not done here, because it falls outside the scope of this dissertation.

Chapter 5

Conclusions and recommendations

5.1 Summary of dissertation

The main aim of the dissertation was to synthesise a robust and nominal model predictive controller for the electric arc furnace refining process and to evaluate the feasibility of such a controller through a simulation study. This work is based on a five state nonlinear model that was derived by Rathaba (2004) for the electric arc furnace refining stage from previous work by Bekker *et al.* (1999) and Oosthuizen *et al.* (2001) who created a full twenty-two state nonlinear model of the electric arc furnace process.

In Chapter 2 the five state nonlinear model was linearized for use in the model predictive controllers. A structured uncertainty description was used to describe all the linear models that resulted from the uncertain nonlinear model. The linear models were reduced to simplify the controllers by eliminating states that are practically uncontrollable.

In Chapter 3 a brief overview was given of the development of stability theory for robust model predictive controllers. Two control methods, feedback robust model predictive control and dual-mode robust model predictive control, were examined in more detail with regards to synthesis and use.

In Chapter 4 an extensive simulation study was done on the refining stage of the electric arc furnace refining process. Simulations were done where full state feedback was assumed in order to evaluate the baseline performance and stability of the robust and nominal controllers. Both the nominal and robust controllers were stable during all the

simulations and performed well under model mismatch. More practical scenarios were also investigated where there was only a limited number of measurements and a predictor was employed to estimate the furnace states. Each time a measurement was available, the predictor was corrected. In an extension, each time a measurement was available, the predictor was corrected and its internal model parameters updated to better approximate the real plant. The simulations show that the lack of feedback has a far greater effect on performance than model mismatch.

5.2 Conclusion

A robust model predictive controller seemed appropriate at the onset of this study in order to explicitly take the model uncertainty into consideration as part of the controller synthesis. For comparison, a nominal model predictive controller was used to quantify the advantage of using a robust controller. In the academic problem it was clear that the robust controllers were the only ones to successfully control the uncertain system. The electric arc furnace process does not become unstable for all the simulations when nominal model predictive control is used, even under extreme model mismatch. The nominal model predictive controller is therefore more than adequate for controlling the process.

The lack of feedback is a much bigger obstacle in automating the electric arc furnace refining process. The predictor needs to be very accurate, but with the uncertainty and lack of measurements, it is very difficult to ensure accuracy. More frequent measurements would need to be taken and improvements need to be made to the updating of the internal model of the predictor to ensure satisfactory results.

The electric arc furnace refining process has states that are manipulated by more than one input. The inputs and certain states have constraints. A simple single-input-single-output controller will be difficult to tune in order to control the process and the constraints will be handled in an ad-hoc fashion. A better strategy is to use a multi-variable control system that can explicitly take constraints into account, e.g. model predictive control. This study has shown that it is not necessary to use robust model predictive control,

because the parameter variation does not pose a problem for nominal model predictive control.

Operators are using the electric arc furnace daily without control and are able to reach the targets more often than not. This study shows that robust model predictive control have difficulty to steer the temperature to the desired setpoint with the limited number of measurements available. All simulation, except for the nominal cases, assumed worst-case scenarios. It is therefore likely that the worst-case scenarios do not occur frequently in practice and that the performance of the closed-loop system might be better in reality. The uncertainties in the model might also be overstated and therefore lead to overly conservative results in the simulations.

5.3 Further work

There are certain areas where further work needs to be done in order to make automatic control of the furnace practical:

- A better predictor needs to be developed in order to handle the model uncertainty and take late cave-ins into account, by using a more systematic design method and verifying it on real plant data.
- Methods should be devised to increase measurements during the refining stage. This is quite a challenge due to the harsh environment that the furnace operates in. A possible solution is to develop soft sensors that estimate bath temperature from the off-gas temperature and coolant temperature.

Improvements can be made to the control strategy in the following areas:

- Add economic objectives to the control by examining:
  - Energy cost of electricity and chemical sources as in Oosthuizen *et al.* (2004).
  - Optimizing yield.
  - Different reference trajectories for temperature and other variables.

- Safety and environmental impact.

References

Bekker, J.G., I.K. Craig and P.C. Pistorius (1999). Modelling and simulation of an electric arc furnace process. *ISIJ International* **39**(1), 23–32.

Bellingan, F. (2005). *Private Communication*. Cape Gate. Vanderbijlpark.

Billings, S.A. and H. Nicholson (1977). Modelling a three-phase electric arc furnace: comparative control strategies. *Applied Mathematical Modelling* **1**, 355–361.

Billings, S.A., F.M. Boland and H. Nicholson (1979). Electric arc furnace modeling and control. *Automatica* **15**, 137–148.

Bitmead, R. R., M. Gevers and V. Wertz (1990). *Adaptive optimal control - The thinking man's GPC*. Prentice-Hall. Englewood Cliffs, NJ.

Boyd, S., L. El Ghaoui, E. Feron and V. Balakrishnan (1994). *Linear Matrix Inequalities in System and Control Theory*. SAIM. Philadelphia.

Camacho, E.F. and C. Bordons (2003). *Model Predictive Control*. Vol. Second Edition. Springer-Verlag. London, UK.

Cameron, A., N. Saxena and K. Broome (1998). Optimizing EAF operations by dynamic process simulation. In: 56^{th} *Electric Furnace Conference Proceedings*. ISS Publishers. Warrendale, Pennsylvania. pp. 689–696.

Casavolaa, A., D. Famularob and G. Franzéa (2004). Robust constrained predictive control of uncertain norm-bounded linear systems. *Automatica* **40**, 1865—1876.

Chen-Wen, L., H. Shyh-Jier and H. Ching-Lien (2000). Flicker characteristics estimation of an AC electric arc furnace. *Electric Power Systems Research* **54**(2), 121–130.

Clarke, D.W., C. Mohtadi and P.S. Tuffs (1987*a*). Generalized predictive control: Part I: The basic algorithm. *Automatica* **23**(2), 137–148.

Clarke, D.W., C. Mohtadi and P.S. Tuffs (1987*b*). Generalized predictive control: Part II: Extensions and interpretations. *Automatica* **23**(2), 149–160.

Collantes-Bellido, R. and T. Gomez (1997). Identification and modeling of a three phase arc furnace for voltage disturbance simulation. *IEEE Transactions on Power Delivery* **12**(4), 1812–1817.

Cutler, C.R. and B.L. Ramaker (1980). Dynamic matrix control - A computer control algorithm. In: *Proceedings of the Joint Automatic Control Conference*. Vol. 1. San Francisco, CA.

Cuzzola, F. A., J. C. Geromel and M. Morari (2002). An improved approach for constrained robust model predictive control. *Automatica* **38**, 1183–1189.

De la Pena, D. Munoz, A. Bemporad and C. Filippi (2004). Robust Explicit MPC Based on Approximate Multi-parametric Convex Programming. In: 43^{th} *IEEE Conference on Decision and Control*. Atlantis, Paradise Island, Bahamas. pp. 2491–2496.

De Nicolao, G., L. Magni and R. Scattolini (1996). On the robustness of receding horizon control with terminal constraints. *IEEE Transactions on Automatic Control* **41**(3), 451–453.

De Vos, B.J. (1993). Optimization of raw material additions for an oxygen-blowing arc furnace. Master's thesis. University of Pretoria. Pretoria, South Africa.

Deo, B. and Boom, R., Eds. (1993). *Fundamentals of Steelmaking Metallurgy*. Prentice Hall International.

Ding, B., Y. Xi and S. Li (2004). A synthesis approach of on-line constrained robust model predictive control. *Automatica* **40**, 163–167.

Fruehan, R.F., Ed. (1998). *The Making, Shaping and Treating of Steel: Steelmaking and Refining*. 11 ed.. Association of Iron and Steel Engineers.

Fukushima, H. and R. R. Bitmead (2005). Robust constrained predictive control using comparison model. *Automatica* **41**, 97–106.

Galgali, R.K., P. Datta, A.K. Ray, Prasad K.K. and H.S. Ray (2001). Reduction and foaming of FeO containing slag. *Ironmaking and Steelmaking* **28**, 321–327.

Ge, M., M. Chiu and Q. Wang (2002). Robust PID controller design via LMI approach. *Journal of Process Control* **12**, 3–13.

Gilbert, E. G. and K. T. Tan (1991). Linear systems with state and control constraints: The theory and application of maximal output admissible sets. *IEEE Transactions on Automatic Control* **36**(9), 1008–1020.

Goodwin, G.C., S.F. Graebe and M.E. Salgado (2001). *Control system design*. Prentice Hall. New Jersey.

Gou, H., G. Irons and W.K. Lu (1996). A multiphase fluid mechanics approach to gas holdup in bath smelting processes. *Metallurgical and Materials Transactions B* **27B**(2), 195–201.

Guo, D. and G. Irons (2003). Modeling of Radiation intensity in an EAF. In: *Third International Conference on CFD in the Minerals Process Industries*. Melbourne, Australia. pp. 651–659.

Holmes, G. and F. Memoli (2001). Operational improvements achieved in davsteel, utilizing the new techint kt injection system and tdr digital regulation: case study. In: *Electric Furnace Conference Proceedings*. Iron and Steel Society. pp. 527–537.

How, J. (2001). *OCW - Feedback Control 16.31 - Topic 12 - State-space model features*. Massachusetts Institute of Technology. Cambridge, Massachusetts, USA.

IISI (2003). World steel in figures 2003. Technical report. International Iron and Steel Institute.

Jiang, R. and R.J. Fruehan (1991). Slag foaming in bath smelting. *Metallurgical Transactions B* **22**(4), 481–489.

Khan, M.H., E.J. Evenson and O.I. Negru (2003). Results of the Goodfellow EFSOP^{TM} at Birmingham Steel Corp., Seattle, WA, USA. In: *Electric Furnace Conference Proceedings*. Iron and Steel Society. pp. 415–428.

Kimihisa, I. and R.J. Fruehan (1987). Slag foaming in electric furnace steelmaking. In: *Electric Furnace Proceedings*. Iron and Steel Society. pp. 345–351.

Kimihisa, I. and R.J. Fruehan (1989*a*). Study on the foaming of CaO-SiO_2-FeO slags: Part 1. Foaming parameters and experimental results. *Metallurgical and Materials Transactions B* **20B**, 509–514.

Kimihisa, I. and R.J. Fruehan (1989*b*). Study on the foaming of CaO-SiO_2-FeO slags: Part 2. Dimensional analysis and foaming in iron and steelmaking processes. *Metallurgical and Materials Transactions B* **20B**, 515–521.

King, P.E. and M.D. Nyman (1996). Modeling and control of an electric arc furnace using a feedforward artificial neural network. *Journal of Applied Physics* pp. 1872–1877.

Kleimt, B. and S. Kohle (1997). Power consumption of electric arc furnaces with post-combustion. *MPT Metallurgical Plant and Technology International* **20**(3), 56–57.

Kleinman, B. L. (1970). An easy way to stabilize a linear constant system. *IEEE Transactions on Automatic Control* **15**(12), 693.

Kothare, M. V., V. Balakrishnan and M. Morari (1996). Robust constrained model predictive control using linear matrix inequalities. *Automatica* **32**, 1361–1379.

Kouvaritakis, B., J. A. Rossiter and J. Schuurmans (2000). Efficient robust predictive control. *IEEE Transactions on Automatic Control* **45**(8), 145–159.

Langson, W., I. Chryssochoos, S. V. Rakovic and D. Q. Mayne (2004). Robust model predictive control using tubes. *Automatica* **40**, 125–133.

Lee, E. B. and L. Markus (1967). *Foundations of optimal control theory*. Wiley. New York.

Lee, J. H. and Z. Yu (1997). Worst-case formulations of model predictive control for systems with bounded parameters. *Automatica* **33**(5), 763–781.

Lee, Y. I. and B. Kouvaritakis (2000). Robust receding horizon control for systems with uncertain dynamics and input saturation. *Automatica* **36**(10), 1497–1504.

Lee, Y. I. and B. Kouvaritakis (2002). Superposition in efficient robust constrained predictive control. *Automatica* **38**, 875–878.

MacRosty, R. (2005). Modelling, Optimization and Control of an Electric Arc Furnace. PhD thesis. McMaster University. Hamilton, Ontario, Canada.

Magni, L. and R. Sepulchre (1997). Stability margins of nonlinear receding-horizon control via inverse optimality. *Systems & Control Letters* **32**(4), 241–245.

Magni, L., H. Nijmeijer and A. van der Schaft (2001). A receding horizon approach to the nonlinear H_∞ problem. *Automatica* **37**(3), 429–435.

Marique, C., P. Nyssen and P. Salamone (1999). On-line control of the foamy slag in EAF. In: *Proceedings of the* 6^{th} *European Electric Steelmaking Conference*. Düsseldorf. pp. 154–161.

Matson, S. and W.F. Ramirez (1999). Optimal Operation of an Electric Arc Furnace. In: 57^{th} *Electric Furnace Conference Proceedings*. ISS Publishers. Warrendale, Pennsylvania. pp. 719–728.

Mayne, D. Q., J. B. Rawlings, C. V. Rao and P. O. M. Scokaert (2000). Constrained model predictive control: Stability and optimality. *Automatica* **36**, 789–814.

Mayne, D.Q., M.M. Seron and S.V. Rakovi (2005). Robust model predictive control of constrained linear systems with bounded disturbances. *Automatica* **41**, 219–224.

Meng, M. and G. Irons (2000). Comparison of Electric Arc Models with Industrial Data. In: 58^{th} *Electric Furnace Conference and* 17^{th} *Technology Conference Proceedings*. ISS Publishers. Warrendale, Pennsylvania.

Michalska, H. and D.Q. Mayne (1993). Robust receding horizon control of constrained nonlinear systems. *IEEE Transactions on Automatic Control* **38**(11), 1623–1633.

Modigell, M., A. Traebert and P. Monheim (2001*a*). A modeling technique for metallurgical processes and its application. *AISE Steel Technology* **28**, 45–47.

Modigell, M., A. Traebert, P. Monheim, S. Peterson and U. Pickartz (2001*b*). A new tool for process modeling of metallurgical processes. *Computers & Chemical Engineering* **25**, 723–727.

Morales, R.D., A.N. Conejo and H.H. Rodriguez (2002). Process dynamics of electric arc furnace during Direct Reduced Iron melting. *Metallurgical and Materials Transactions B* **33B**, 187–199.

Morales, R.D., H. Rodriguez-Hernández and A.N. Conejo (2001*a*). A mathematical simulator for the EAF steelmaking process using Direct Reduced Iron. *ISIJ International* **41**(5), 426–435.

Morales, R.D., R. Lule, F. López, J. Camacho and J.A. Romero (2001*b*). The slag foaming practice in EAF and its influence on the steelmaking shop productivity. *ISIJ International* **35**(9), 1054–1062.

Nyssen, P., C. Marique, C. Prüm, P. Bintner and L. Sivini (1999). A new metallurgical model for the control of EAF operations. In: *Proceedings of the* 6^{th} *European Electric Steelmaking Conference*. Düsseldorf. pp. 43–50.

Nyssen, P., R. Colin, S. Knoops and J.L. Junque (2002). On-line EAF control with a dynamic metallurgical model. In: *Proceedings of the* 7^{th} *European Electric Steelmaking Conference*. Venice. pp. 293–304.

Oosthuizen, D.J., I.K. Craig and P.C. Pistorius (2004). Economic evaluation and design of an electric arc furnace controller based on economic objectives. *Control Engineering Practice* **12**, 253–265.

Oosthuizen, D.J., J.H. Viljoen, I.K. Craig and P.C. Pistorius (2001). Modeling of the offgas exit temperature and slag foam depth of an electric arc furnace process. *ISIJ International* **41**(4), 399–401.

Pannocchia, G. (2004). Robust model predictive control with guaranteed setpoint tracking. *Journal of Process Control* **14**, 927–937.

Park, M. and H. Rhee (2001). LMI-based robust model predictive control for a continuous MMA polymerization reactor. *Computers & Chemical Engineering* **25**, 1513–1520.

Peterka, V. (1984). Predictor-based self tuning control. *Automatica* **20**(1), 39–50.

Pluymers, B., J.A. Rossiter, J. Suykens and B. De Moor (2005*a*). The efficient computation of polyhedral invariant sets for linear systems with polytopic uncertainty. In: *Proceedings of the American Control Conference 2005,*. Portland, USA. pp. 804–809.

Pluymers, B., J.A. Rossiter, J.A.K. Suykens and B. De Moor (2005*b*). A simple algorithm for robust MPC. In: *Procedings of the 16th IFAC World Congress*. Prague, Czech Republic.

Pujadas, A., J. McCauley and M. Iacuzzi (2003). EAF energy optimization at Nucor Yamato Steel. In: *ISSTech 2003 Conference Proceedings*. Iron and Steel Society. pp. 391–402.

Qin, S. J. and T. A. Badgwell (2003). A survey of industrial model predictive control technology. *Control Engineering Practice* **11**, 733–764.

Raisz, D., M. Sakulin, H. Renner and Y. Tehlivets (2000). Recognition of operational states in electric arc furnaces. In: *Proceedings of the Ninth International Conference on Harmonics and Quality of Power*. Vol. 2. IEEE. pp. 475–480.

Rathaba, P.L. (2004). Model fitting for an electric arc furnace refining. Master's thesis. University of Pretoria. Pretoria, South Africa.

Rawlings, J. B. and K. R. Muske (1993). Stability of constrained receding horizon control. *Transactions on Automatic Control* **38**(10), 1512–1516.

Richalet, J., A. Rault, J.L. Testud and J. Papon (1978). Model predictive heuristic control: Applications to industrial processes. *Automatica* **14**(5), 413–428.

Rodríguez, P. and D. Dumur (2005). Generalized predictive control robustification under frequency and time-domain constraints. *IEEE Transactions on Control Systems Technology* **13**(4), 577–587.

Rossiter, J. A., B. Kouvaritakis and M. J. Rice (1998). A numerically robust state-space approach to stable-predictive control strategies. *Automatica* **34**(1), 65–73.

Schuurmans, J. and J. A. Rossiter (2000). Robust model predictive control using tight sets of predicted states. In: *IEE Proceedings - Control Theory and Applications*. Vol. 147. pp. 13–18.

Scokaert, P. O. M. and D. Q. Mayne (1998). Min-max feedback model predictive control for constrained linear systems. *IEEE Transactions on Automatic Control* **43**(8), 1136–1142.

Scokaert, P. O. M., D. Q. Mayne and J. B. Rawlings (1999). Suboptimal model predictive control (feasibility implies stability). *IEEE Transactions on Automatic Control* **44**(3), 648–654.

Tang, X., M. Kirschen and H.P. Abel (2003). Modelling of EAF Offgas Post Combustion in Dedusting Systems using CFD Methods. *Steel Research* **74**(4), 201–210.

Taylor, C.R., Ed. (1985). *Electric Furnace Steelmaking*. Iron and Steel Society.

Thomson, M.J., N.G. Kournetas, E. Evenson, I.D. Sommerville, McLean A. and Guerard J. (2001). Effect of Oxyfuel burner ratio changes on energy efficiency in electric arc furnace at Co-Steel Lasco. *Ironmaking and Steelmaking* **28**, 267–272.

Traebert, A., M. Modigell, P. Monheim and K. Hack (1999). Development of a modelling technique for non-equilibrium metallurgical processes. *Scandanavian Journal of Metallurgy* **28**, 285–290.

Tsai, P., J. Chu, S. Jang and S. Shieh (2002). Developing a robust model predictive control architecture through regional knowledge analysis of artificial neural networks. *Journal of Process Control* **13**(5), 423–435.

Turkdogan, E.T. (1989). *Fundamentals of Steelmaking*. Institute of Materials. London.

Wan, Z. and M. V. Kothare (2003). An efficient off-line formulation of robust model predictive control using linear matrix inequalities. *Automatica* **39**, 837–846.

Wang, D. and J. A. Romagnoli (2003). Robust model predictive control design using a generalized objective function. *Computers & Chemical Engineering* **27**(7), 965–982.

Wang, Y. J. and J. B. Rawlings (2004*a*). A new robust model predictive control method I: Theory and computation. *Journal of Process Control* **14**, 231–247.

Wang, Y. J. and J. B. Rawlings (2004*b*). A new robust model predictive control method II: Examples. *Journal of Process Control* **14**(3), 249–262.

Wu, F. (2001). LMI-based robust model predictive control and its application to an industrial CSTR problem. *Journal of Process Control* **11**, 649–659.

Appendix A

Academic Problem

In this chapter, an academic problem is used to compare the two robust MPC together with nominal MPC, with respect to robust stability and performance. The academic problem consists of a system with greatly varying dynamic behaviour, which provides an excellent test of the stability and robustness of the different controllers.

A.1 Academic problem model

This academic problem was taken from Kothare *et al.* (1996). The problem is a two-mass-spring system (figure A.1). The system was discretized using Euler's first order approximation for the derivative with a sampling time of 0.1s. The discretized system is

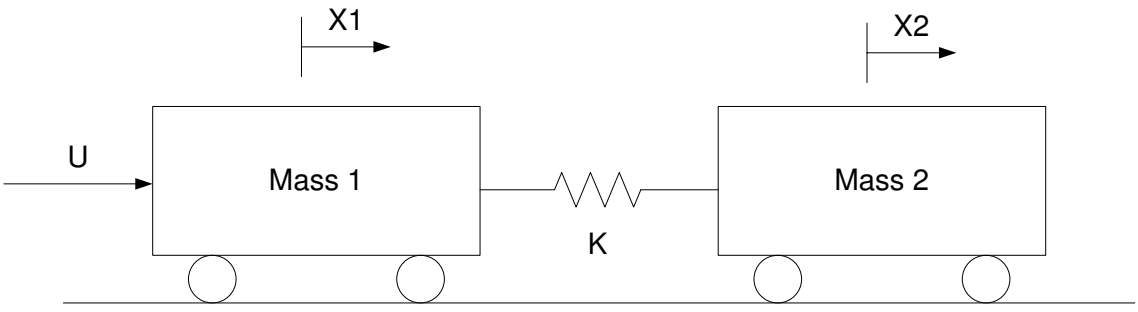

Figure A.1: Coupled mass-spring system.

given by

$$\begin{bmatrix} x_1(k+1) \\ x_2(k+1) \\ x_3(k+1) \\ x_4(k+1) \end{bmatrix} = \begin{bmatrix} 1 & 0 & 0.1 & 0 \\ 0 & 1 & 0 & 0.1 \\ -0.1K/m_1 & 0.1K/m_1 & 1 & 0 \\ 0.1K/m_2 & -0.1K/m_2 & 0 & 1 \end{bmatrix} \begin{bmatrix} x_1(k) \\ x_2(k) \\ x_3(k) \\ x_4(k) \end{bmatrix} + \tag{A.1}$$

$$\begin{bmatrix} 0 \\ 0 \\ 0.1/m_1 \\ 0 \end{bmatrix} u(k) \tag{A.2}$$

$$y(k) = x_2(k) \tag{A.3}$$

where x_1 and x_2 are the positions of body 1 and body 2 respectively and x_3 and x_4 are the respective velocities of body 1 and body 2. The mass of body 1 is m_1 and the mass of body 2 is m_2, while K is the spring constant. The input of the system u is the force that is applied to the first body. The performance specifications can be summarized as follows

- Use constant mass for body 1 and body 2 of 1 kg: $m_1 = m_2 = 1$.
- Use an uncertain spring constant that varies between 0.5 and 10: $0.5 \leq K \leq 10$.
- An input constraint of $|u| \leq 1$ should be maintained.
- A output unit step should be followed.
- Assume full state feedback is available.

To describe the effect of the uncertain spring constant K, a *structured uncertainty* description is used. The structured uncertainty description has the form

$$\Omega = \begin{bmatrix} A + B_p \delta C_q & B + B_p \delta D_{qu} \end{bmatrix} \tag{A.4}$$

where Ω is the system space, δ is an operator that varies between -1 and 1, $B_p C_q$ describes the deviation from the nominal for A, and $B_p D_{qu}$ describes the deviation from nominal

for B.

The system in (A.1) can be rewritten as a *structured uncertainty* description with the constant values substituted as:

$$\delta = \frac{K - K_{nom}}{K_{dev}} \tag{A.5}$$

$$A = \begin{bmatrix} 1 & 0 & 0.1 & 0 \\ 0 & 1 & 0 & 0.1 \\ -0.1K_{nom} & 0.1K_{nom} & 1 & 0 \\ 0.1K_{nom} & -0.1K_{nom} & 0 & 1 \end{bmatrix} \tag{A.6}$$

$$B = \begin{bmatrix} 0 \\ 0 \\ 0.1 \\ 0 \end{bmatrix} \tag{A.7}$$

$$B_p = \begin{bmatrix} 0 \\ 0 \\ -0.1 \\ 0.1 \end{bmatrix} \tag{A.8}$$

$$C_q = \begin{bmatrix} K_{dev} & -K_{dev} & 0 & 0 \end{bmatrix} \tag{A.9}$$

$$D_{qu} = 0 \tag{A.10}$$

A.2 Simulation Results

Three controllers were used in the simulation study. The controller closed-loop system structure is shown in figure A.2. The feedback robust model predictive controller is shown first, the dual-mode robust model predictive controller second, and the nominal model predictive control as a benchmark last. Three simulation scenarios were considered:

1. The nominal case where $\delta = 0$.

2. Extreme deviation from nominal δ =-1.

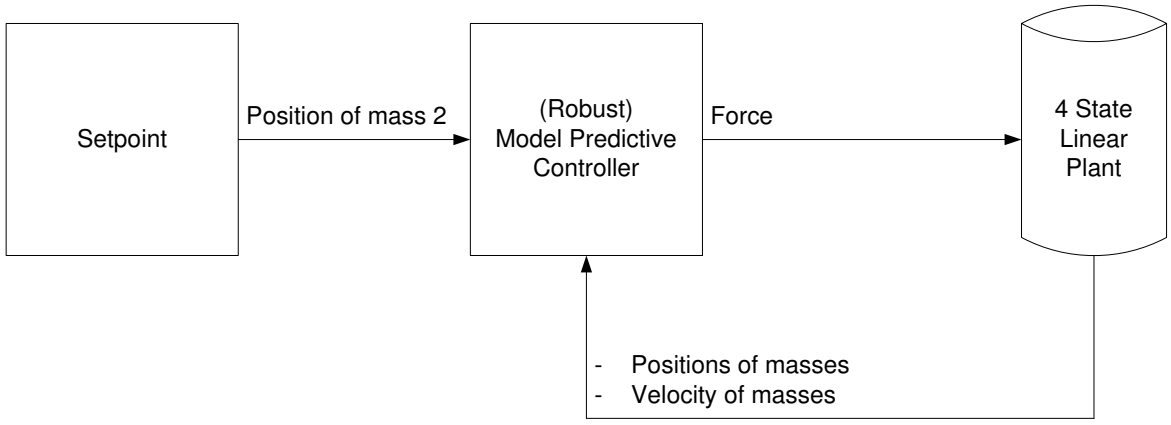

Figure A.2: Academic problem closed-loop system.

Table A.1: Academic problem MPC state and input weighting.

Variable	Description	Value
Q	State weighting	$\begin{bmatrix} 1 & 0 & 0 & 0 \\ 0 & 1 & 0 & 0 \\ 0 & 0 & 1 & 0 \\ 0 & 0 & 0 & 1 \end{bmatrix}$
R	Input weighting	0.00001

3. Extreme deviation from nominal δ =1.

The nominal scenario gives an indication of the conservatism that is introduced in order to robustify the closed loop. The nominal MPC will be the benchmark with which to compare the two robust controllers. The two extreme cases provide a measure of the performance of the two robust controllers.

A.2.1 Nominal scenario

The nominal scenario uses the nominal model ($\delta = 0$). All the controllers use the same state and input weighting (shown in table A.1) in order to gauge their relative performance, and to get a feel for the amount of conservatism that is introduced in order to robustify the controllers.

These results (figures A.3 and A.4) show that the nominal MPC gives the best performance when $\delta = 0$. This is to be expected, because the robust controllers are more

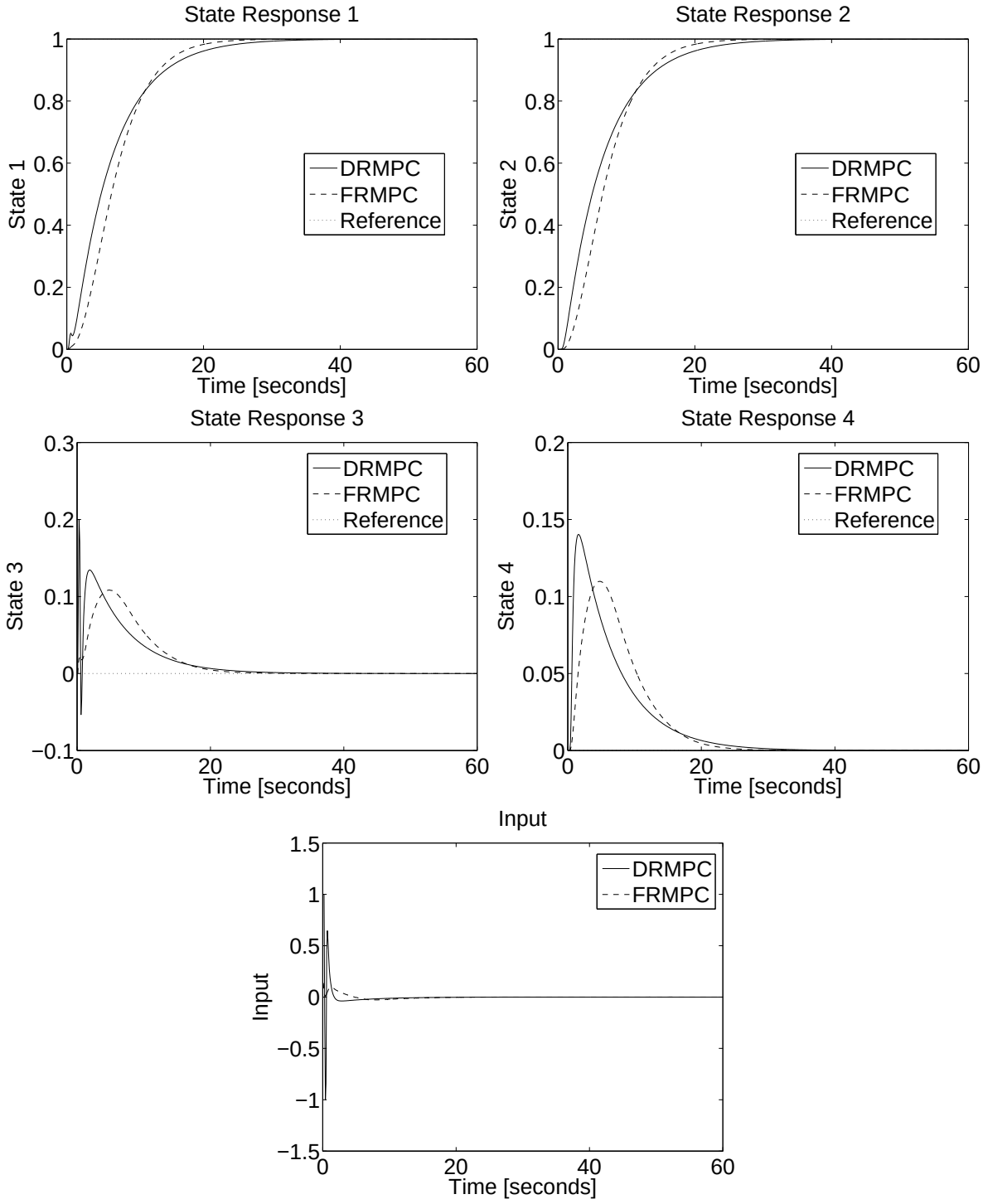

Figure A.3: Feedback and Dual-mode Robust MPC - Nominal Scenario

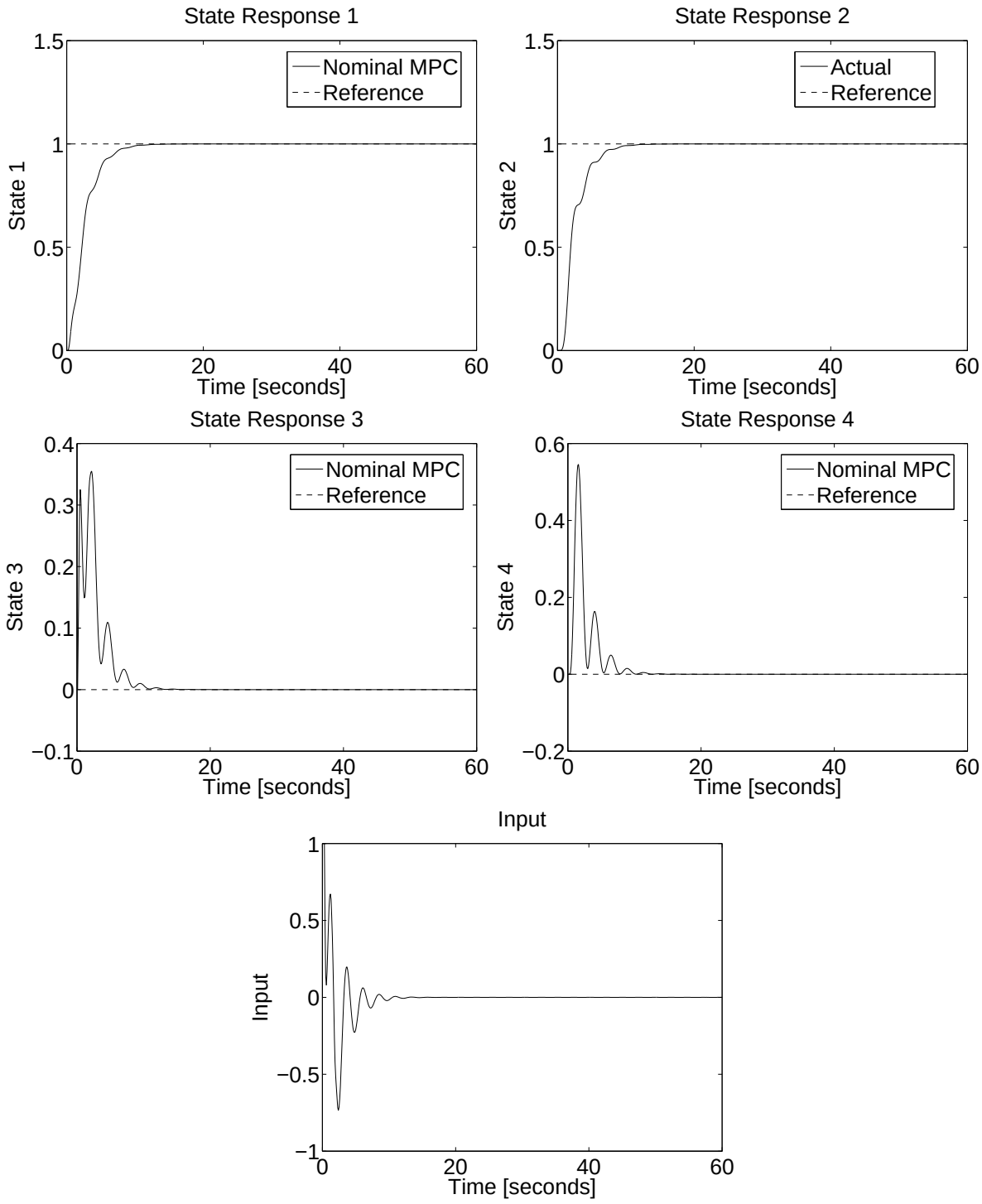

Figure A.4: Nominal MPC - Nominal Scenario

conservative in order to ensure stability for all the system realizations. The results also show that the feedback robust model predictive controller gives better performance than the dual-mode robust model predictive controller. The internal, globally stabilizing feedback control employed by the dual-mode controller is generated by the feedback robust control algorithm for the initial state. The feedback gain was generated without taking the input constraint into account in order to reduce conservatism for the dual-mode controller.

A.2.2 Extreme deviation $\delta = -1$ and $\delta = 1$

The extreme deviation scenarios help gauge the performance of the robust controllers. Both controllers use the same weighting on state and input deviation as shown in table A.1.

The results in figure A.5 show that both robust controllers are stable in this simulation, because the closed-loop system converges to the setpoints, but the feedback robust model predictive controller delivers better performance in terms of settling time.

The results in figure A.6 mirror the previous conclusion, because both robust controllers are stable in this simulation, but the feedback robust model predictive controller delivers better performance in terms of reaching the desired setpoint as well as overshoot. Figure A.7 shows the performance of the closed-loop system with nominal MPC. Here it is clear that the closed-loop is unstable for this simulation, because the closed-loop system oscillates with increasing amplitude, and the same result is obtained in the case where $\delta = 1$.

A.3 Conclusion

The academic problem shows the advantage of using robust model predictive control, where uncertainty causes large variations in dynamic behaviour. Both the robust controllers were stable for all the simulations over the whole variation in system dynamics, whereas the nominal MPC was unstable in both extreme scenario simulations. The feed-

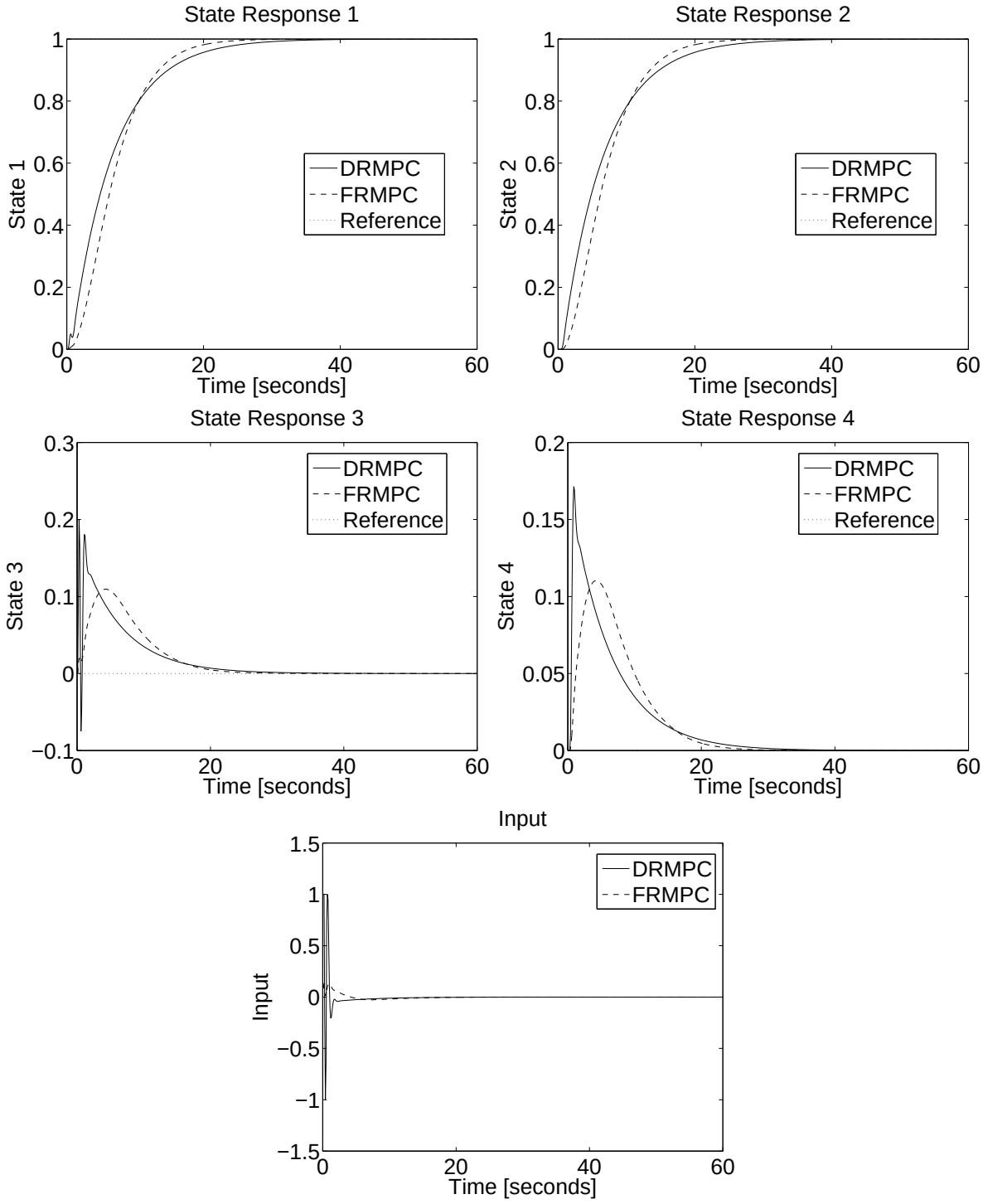

Figure A.5: Feedback and Dual-mode Robust MPC - Extreme scenario $\delta = 1$

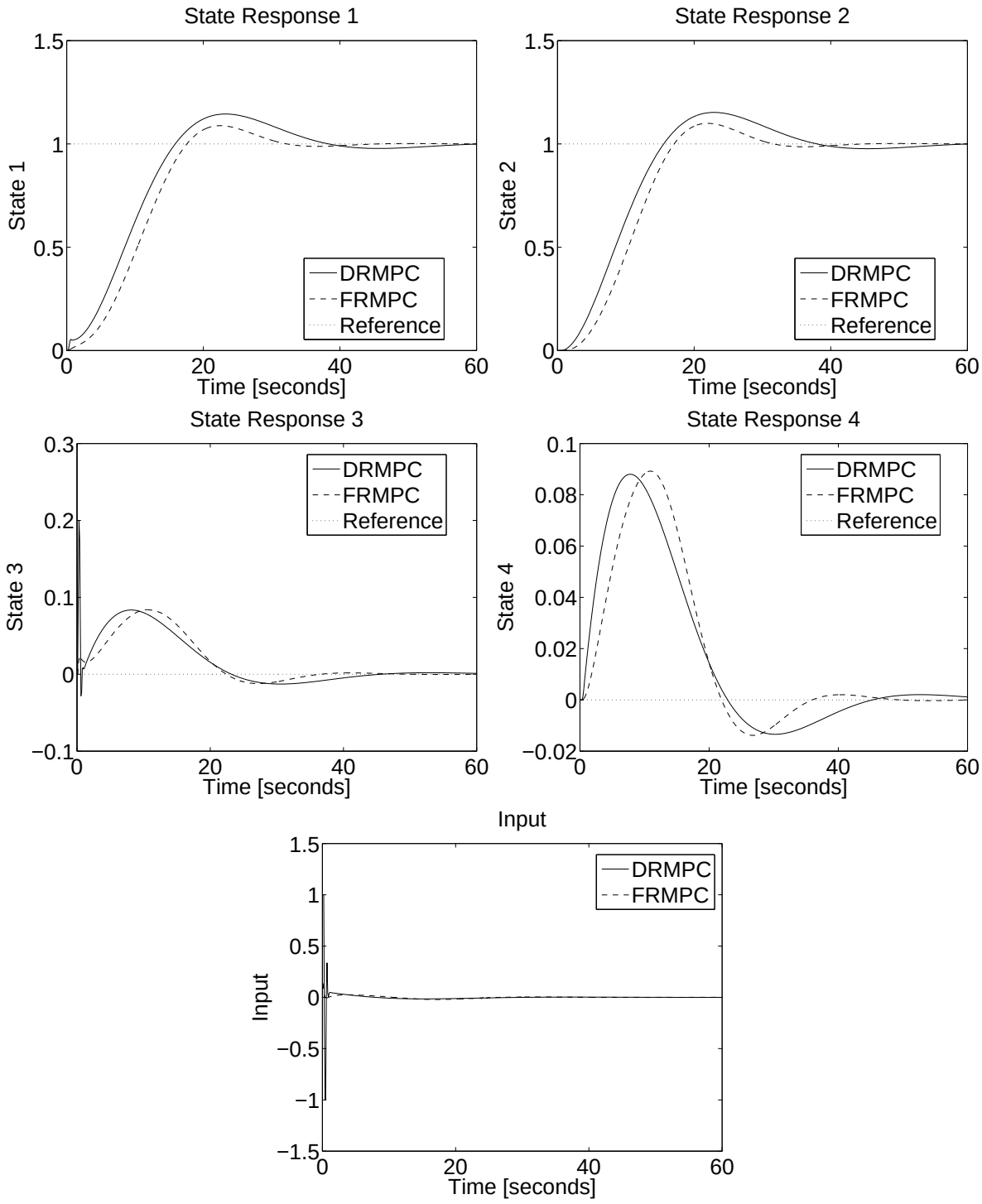

Figure A.6: Feedback and Dual-mode Robust MPC - Extreme scenario $\delta = -1$

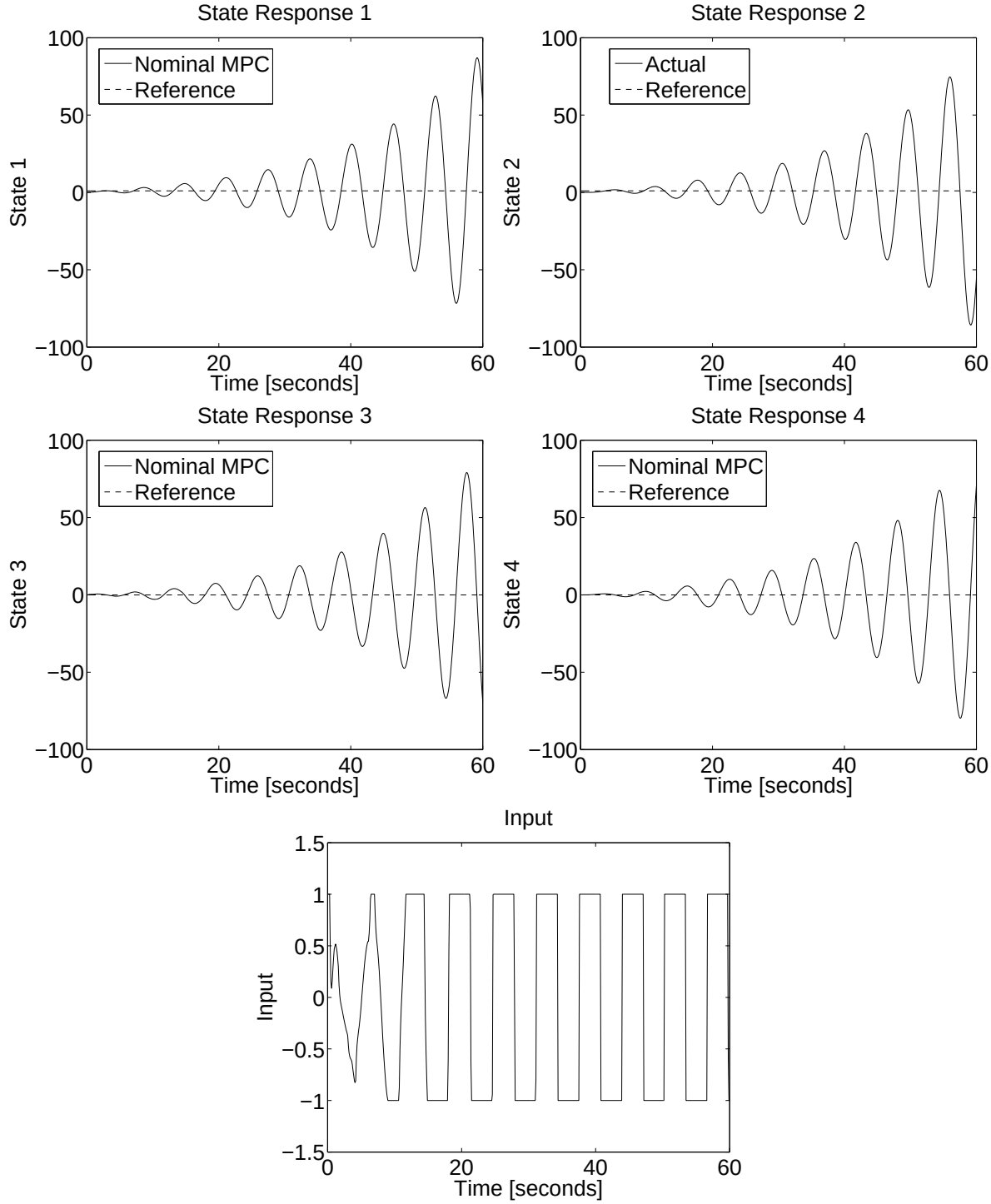

Figure A.7: Nominal MPC - Extreme scenario $\delta = -1$

back robust controller delivered better performance than the dual-mode robust controller, because as the state and inputs approach 0, the controller makes the feedback gain less conservative. The feedback controller has a problem with non-symmetric input constraints when there is a steady-state other than the origin, because the feedback gain of the controller stays conservative and might also lead to large steady-state offsets in the states. The behaviour of the dual mode controller is greatly influenced by the globally stabilizing feedback gain K, more so than by the weighting matrices Q and R.

Appendix B

Auxiliary simulation results

In this appendix, all the auxiliary simulation results of chapter 4 are shown with a short description of the simulation parameters and a short discussion of the results. In this appendix, only the scenarios where there are even weightings on the inputs are evaluated. This gives an indication how it will affect the temperature response if more oxygen is available as an energy source when compared to the reduced oxygen usage scenarios shown in chapter 4.

B.1 Worst-case scenario: Efficiencies at their minimum

This scenario focuses on the effect that lower than nominal efficiencies (η_{FeO} and η_{ARC}) have on the controller and system as a whole. In this scenario the following assumptions are made:

- There are three feedback scenarios:
  - Full state-feedback is available.
  - One measurement is available.
  - One measurement and update of the efficiencies (η_{FeO} and η_{ARC}) of the predictor are available.
- The predictor and actual plant have a mismatch in their efficiencies (η_{FeO} and η_{ARC}) where the efficiencies are lower in the real plant than in the predictor.

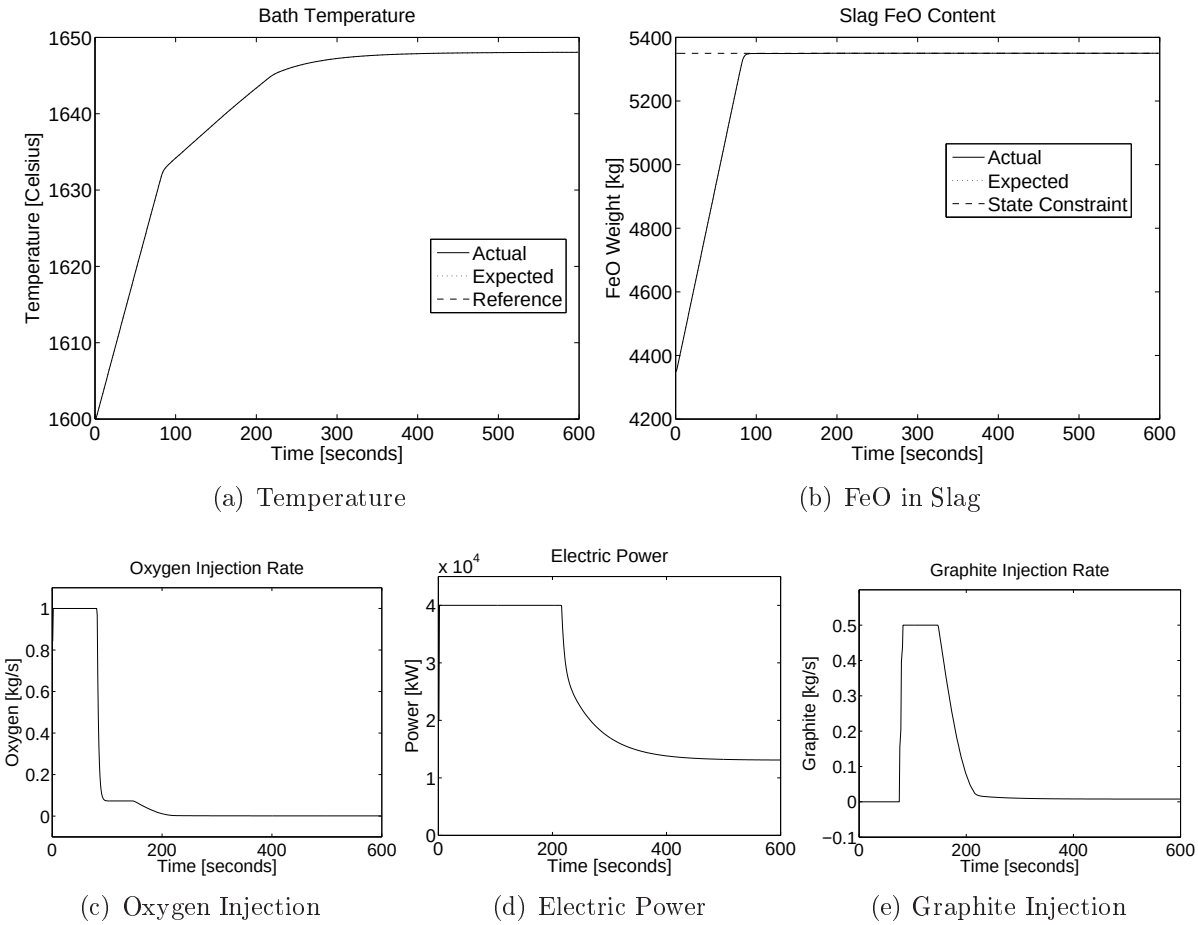

(a) Temperature (b) FeO in Slag

(c) Oxygen Injection (d) Electric Power (e) Graphite Injection

Figure B.1: Nominal MPC - Efficiencies at a minimum with full-state feedback.

- There are no disturbances.

B.1.1 Worst-case scenario: Minimum efficiencies with full state feedback

In this first instance, full-state feedback is employed to evaluate the closed-loop performance without a predictor in the loop, in the extreme case where the efficiencies (η_{FeO} and η_{ARC}) are at the minimum of the confidence interval for the plant model. Robust MPC and nominal MPC are compared to determine whether robust MPC provides better performance in the presence of model mismatch compared to nominal MPC.

A temperature setpoint of 1650^oC as well as even weighting (table 4.2) is used for the first set of simulations.

From these result (figures B.1 and B.2), it is clear that the robust MPC performs

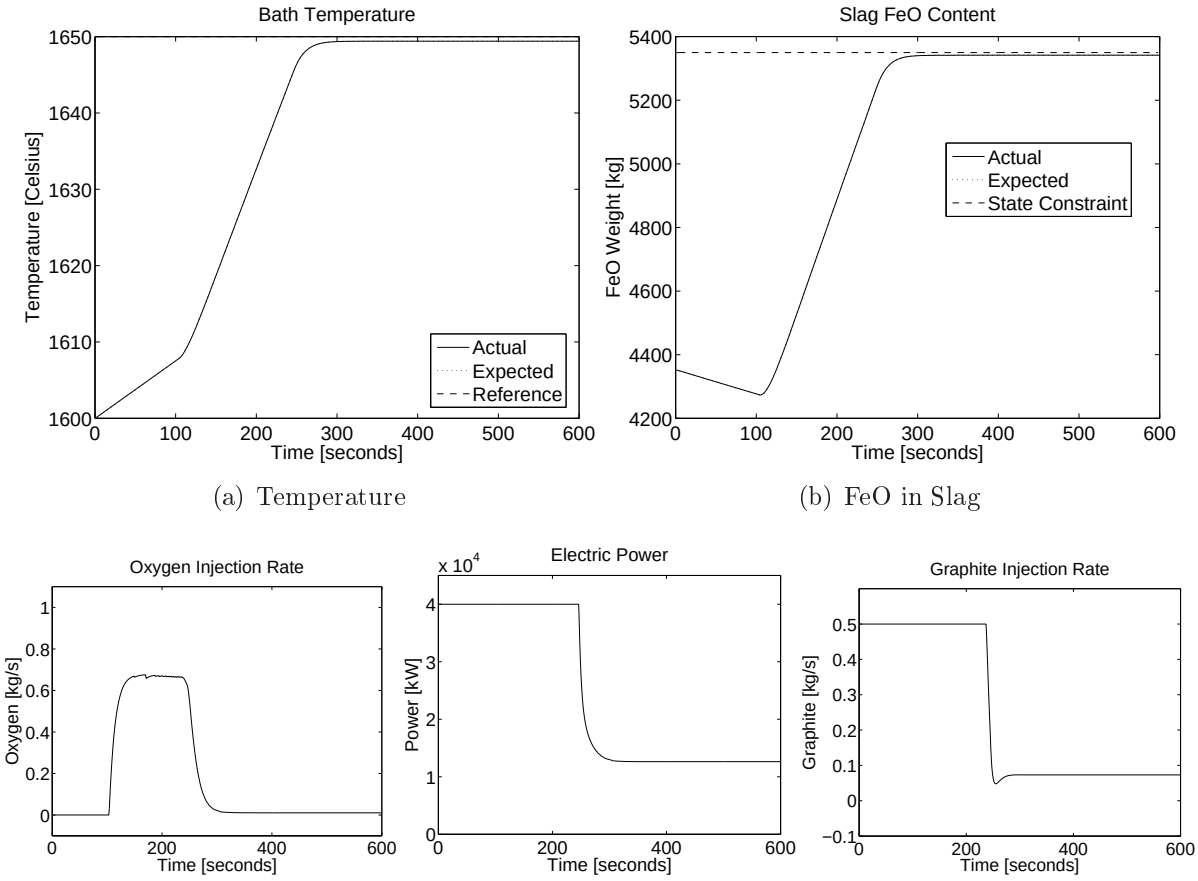

(a) Temperature (b) FeO in Slag

(c) Oxygen Injection (d) Electric Power (e) Graphite Injection

Figure B.2: Dual-mode robust MPC - Efficiencies at a minimum with full-state feedback.

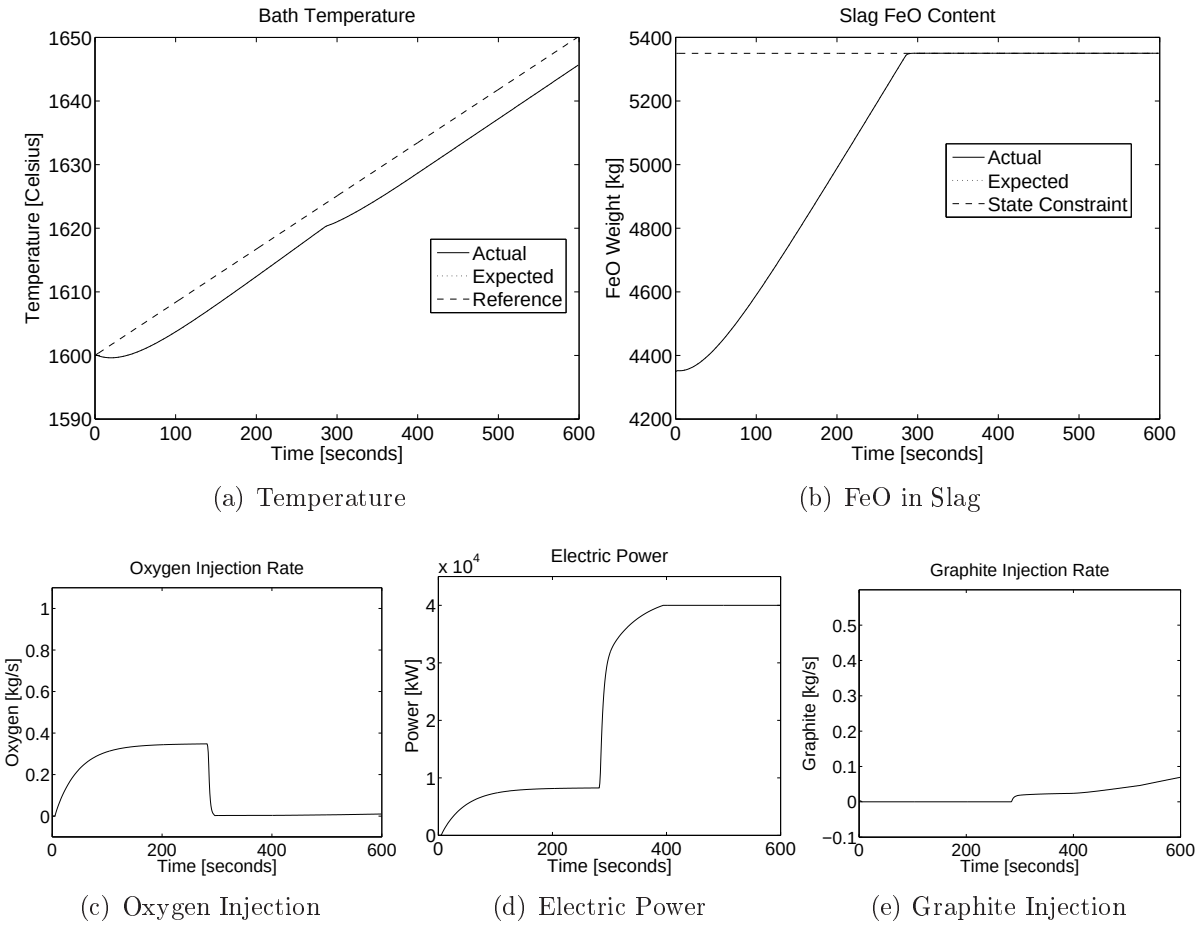

(a) Temperature (b) FeO in Slag

(c) Oxygen Injection (d) Electric Power (e) Graphite Injection

Figure B.3: Nominal MPC - Efficiencies at a minimum, full-state feedback and reference trajectory.

better than the nominal MPC. The robust controller produced a smaller steady-state offset for the temperature. It is interesting to note that the nominal controller is stable for this simulation with extreme model mismatch.

A reference trajectory is used for temperature over the duration of the refining stage as well as even weighting (table 4.2) on the inputs for the second set of simulations.

These results (figures B.3 and B.4) show that the robust controller performs much better with almost perfect reference following compared to the nominal controller. The nominal controller uses much less oxygen than the robust controller, which can account for the difficulty in following the reference trajectory.

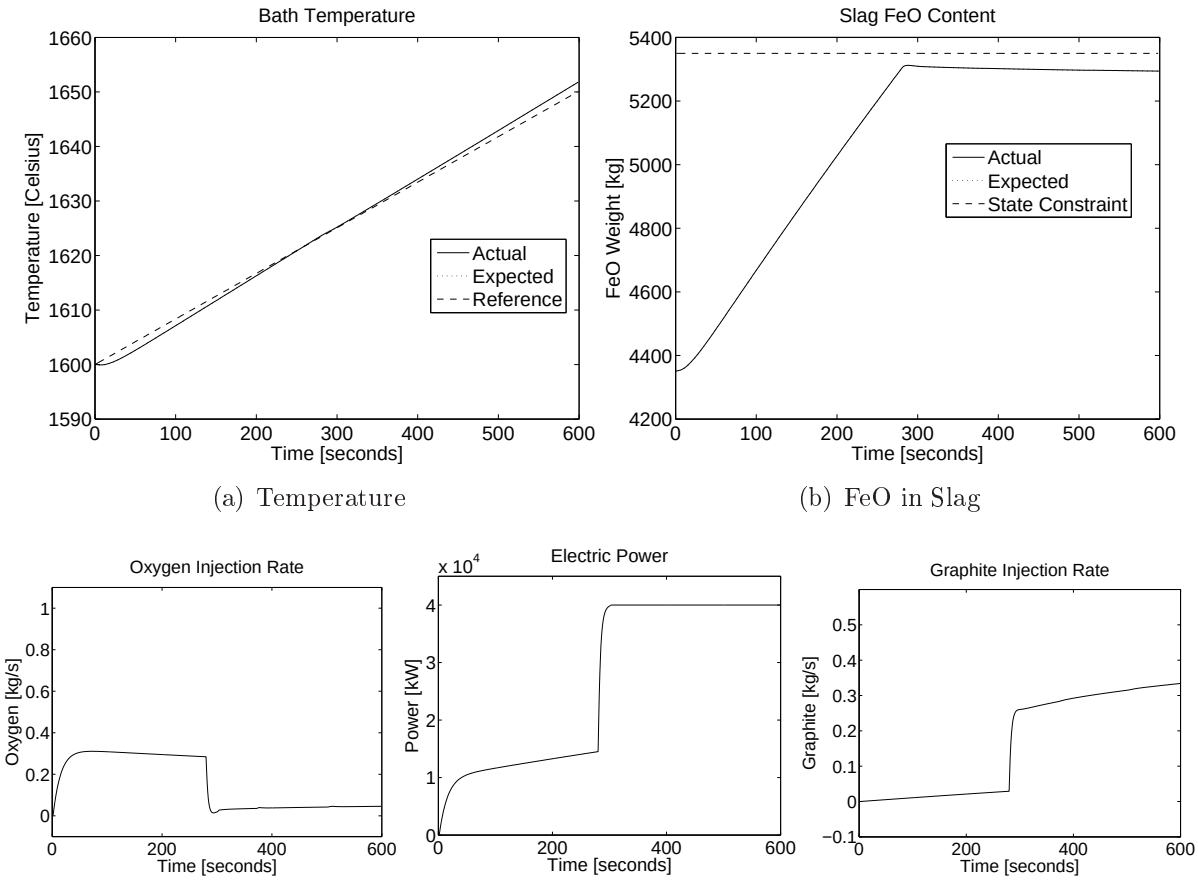

(a) Temperature (b) FeO in Slag

(c) Oxygen Injection (d) Electric Power (e) Graphite Injection

Figure B.4: Dual-mode robust MPC - Efficiencies at a minimum, full-state feedback and reference trajectory.

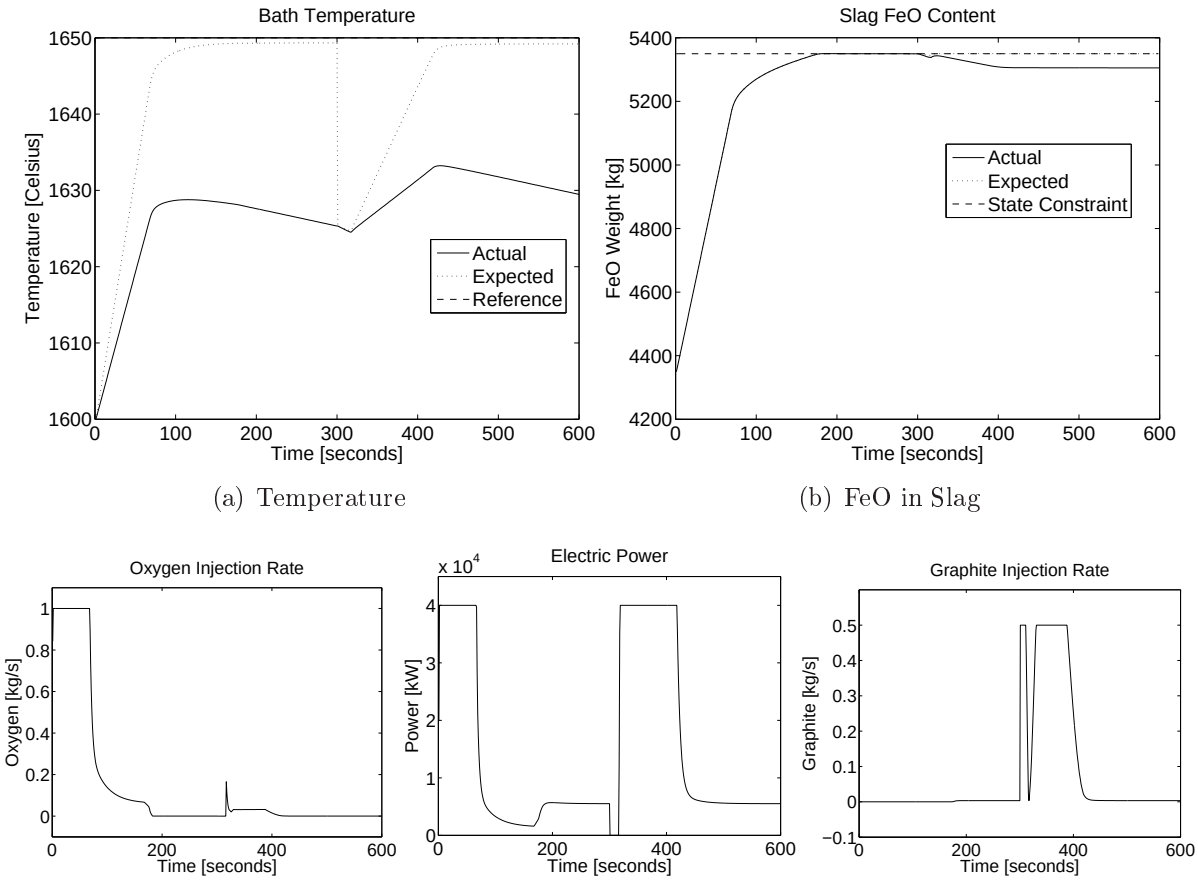

(a) Temperature (b) FeO in Slag

(c) Oxygen Injection (d) Electric Power (e) Graphite Injection

Figure B.5: Nominal MPC - Efficiencies at a minimum with one measurement.

B.1.2 Worst-case scenario: Minimum efficiencies with one plant measurement

In this scenario only one measurement of temperature is taken in the middle of the refining stage, the rest of the data is produced by the predictor. The predictor uses the nominal plant parameters, while the real plant uses the worst-case scenario where the efficiencies (η_{FeO} and η_{ARC}) are at their minimum. This scenario should shed light on the effect of model mismatch between the predictor and real plant model.

A setpoint of 1650^oC for temperature as well as even weightings on the inputs (table 4.2) are used for the first set of simulations.

These results (figures B.5 and B.6) show that both controllers perform equally poorly. The controllers are under the impression that they have reached the desired setpoint as indicated by the expected line, but in reality the temperature is lower. At the measurement

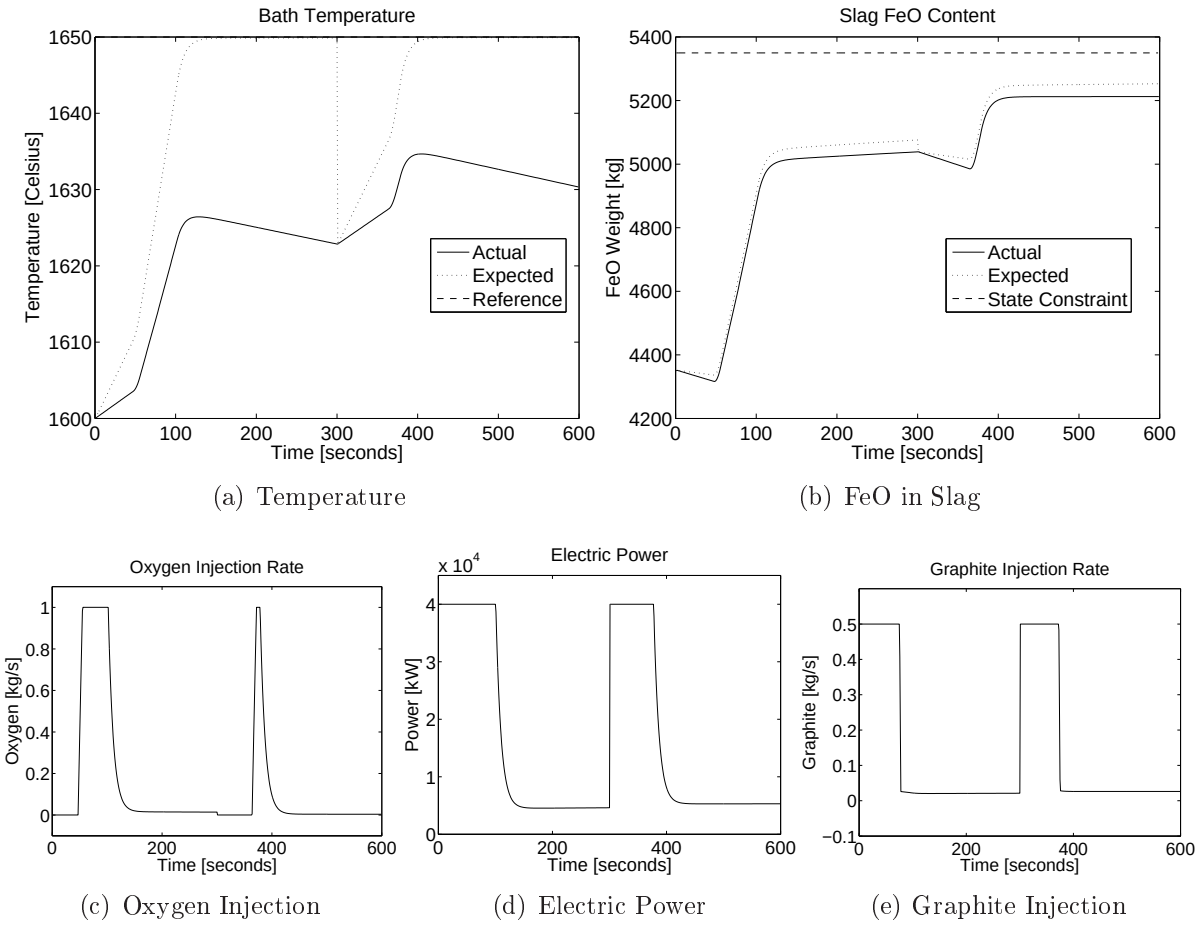

(a) Temperature (b) FeO in Slag

(c) Oxygen Injection (d) Electric Power (e) Graphite Injection

Figure B.6: Dual-mode robust MPC - Efficiencies at a minimum with one measurement.

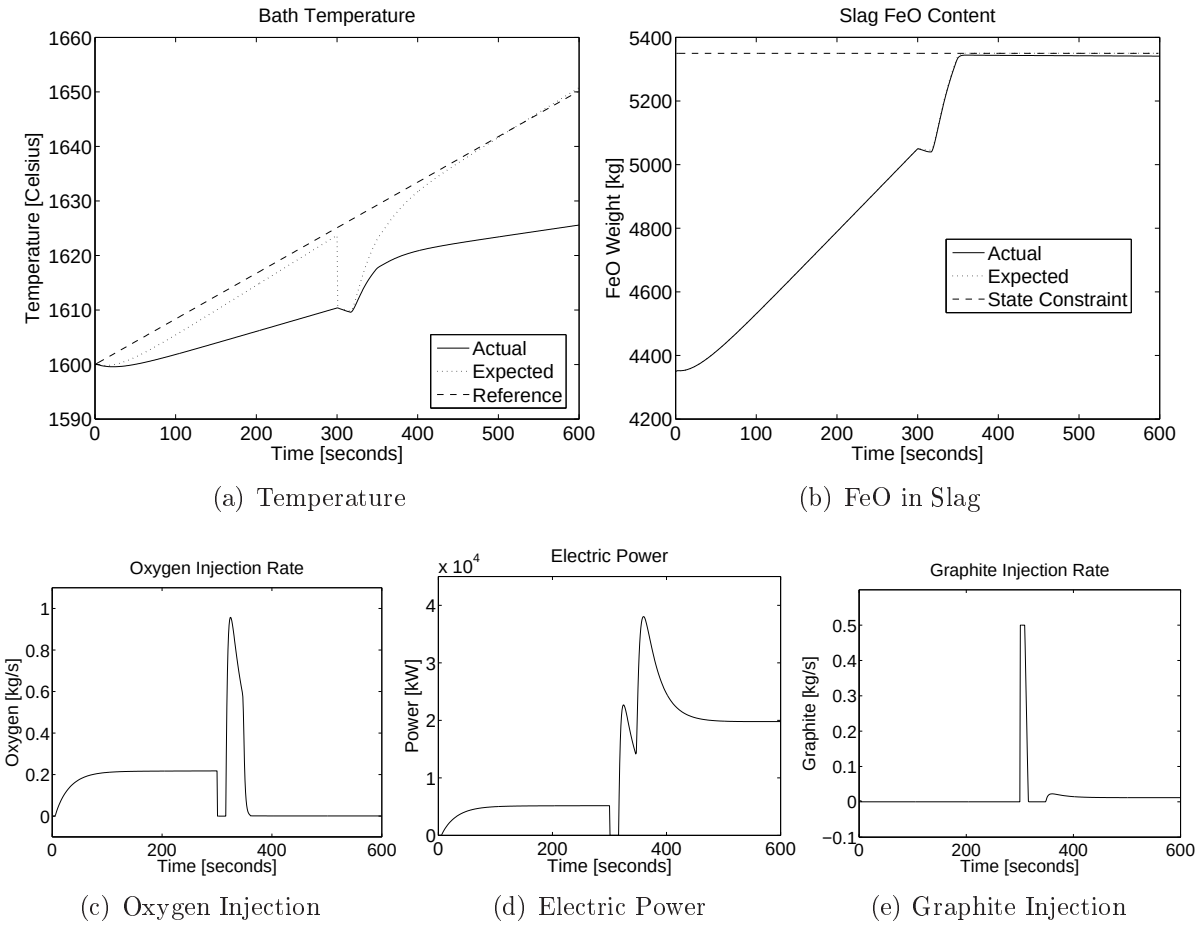

(a) Temperature (b) FeO in Slag

(c) Oxygen Injection (d) Electric Power (e) Graphite Injection

Figure B.7: Nominal MPC - Efficiencies at a minimum, one measurement and reference trajectory.

point, the value of the predictor is corrected, and the controllers respond accordingly. The final value is still below the desired value, because of the mismatch in the predictor. An accepted margin of error is 10^0C each way, which the controllers are not capable of attaining.

A reference trajectory for temperature as well as even weighting on the inputs (table 4.2) is used for the second set of simulations.

Figures B.7 and B.8 show poor reference following by both controllers due to the inaccuracy of the predictor. The expected line shows what the controller expects the values to be. The robust controller follows the reference slightly better than the nominal controller but still ends below the 10^0C accepted interval.

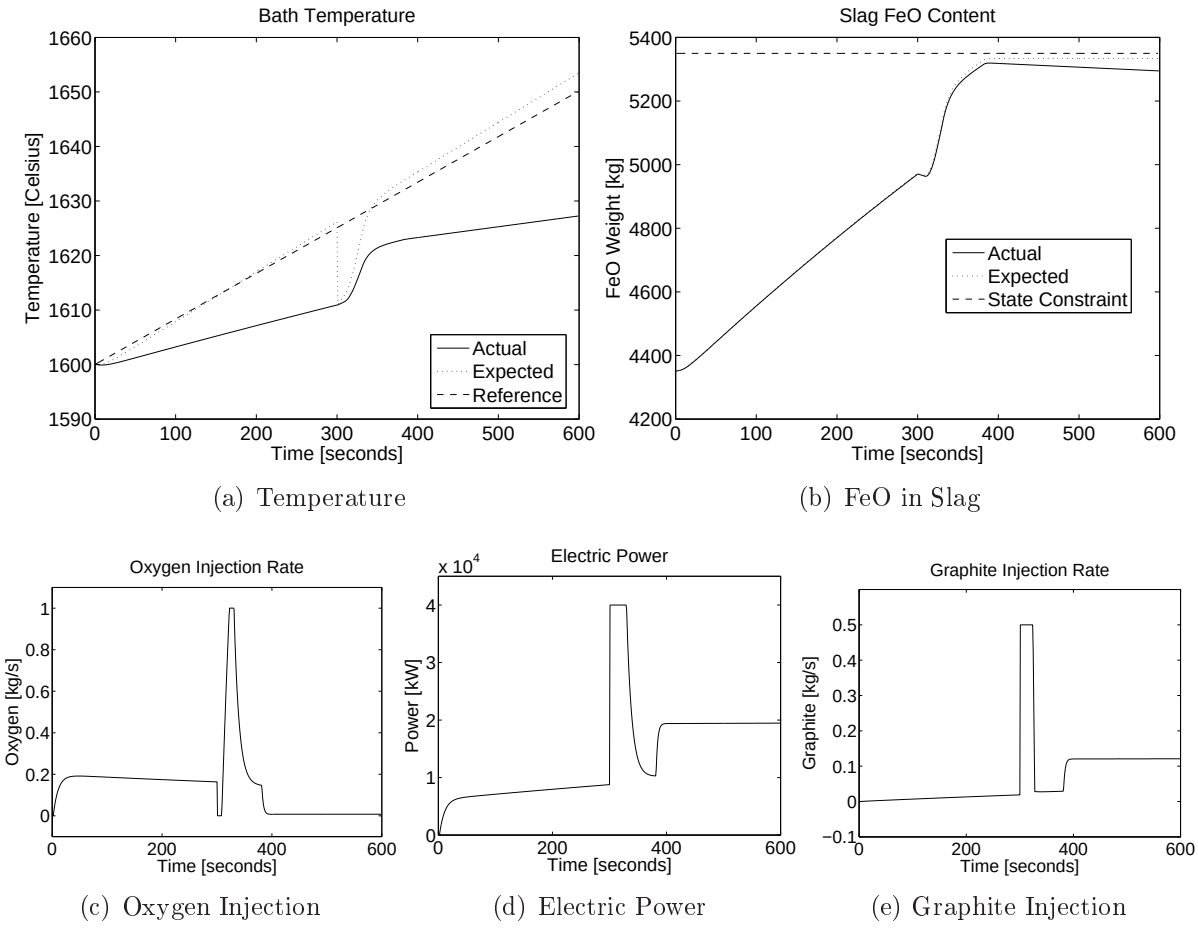

(a) Temperature (b) FeO in Slag

(c) Oxygen Injection (d) Electric Power (e) Graphite Injection

Figure B.8: Dual-mode robust MPC - Efficiencies at a minimum, one measurement and reference trajectory.

B.1.3 Worst-case scenario: Minimum efficiencies with one plant measurement and predictor parameter update

In the previous section, the effect of model mismatch between the predictor and the actual plant on the performance of the closed-loop system is clear. To combat this, the parameters of the predictor are updated each time a measurement is taken, in an attempt to improve performance. In this scenario only one measurement is taken in the middle of the refining stage, the rest of the state data is produced by the predictor. The predictor uses the nominal plant parameters until the first measurement is taken, after which the updated parameters are employed. The real plant uses the worst-case scenario where the efficiencies (η_{FeO} and η_{ARC}) are at their minimum.

A setpoint of 1650^oC for temperature as well as even weighting on the inputs (table 4.2) is used for the first set of simulations.

Figures B.9 and B.10 show that both controllers are now able to steer the process to within the desired $\pm 10^0 C$ margin. The robust controller is able to reach the desired set-point by the end of the refining stage, which is slightly better than the nominal controller.

A reference trajectory for temperature as well as even weighting for the inputs (table 4.2) is used for the second set of simulations.

Figures B.11 and B.12 show that neither of the controllers can steer the temperature to within $\pm 10^0 C$. This is due to an undercorrection made in the predictor. In both cases, the expected state propagation follows the reference trajectory, but the actual performance of the robust controller is better than that of the nominal controller. The nominal controller uses significantly less oxygen than the robust controller which can explain why the robust MPC performs slightly better than the nominal MPC.

B.2 Worst-case scenario: Efficiencies at their maximum

This worst-case scenario investigates the effect of model mismatch between the internal model of the controllers and the actual plant, as well as the predictor and the actual plant. This scenario focuses on the effect created if the efficiencies (η_{FeO} and η_{ARC}) are higher

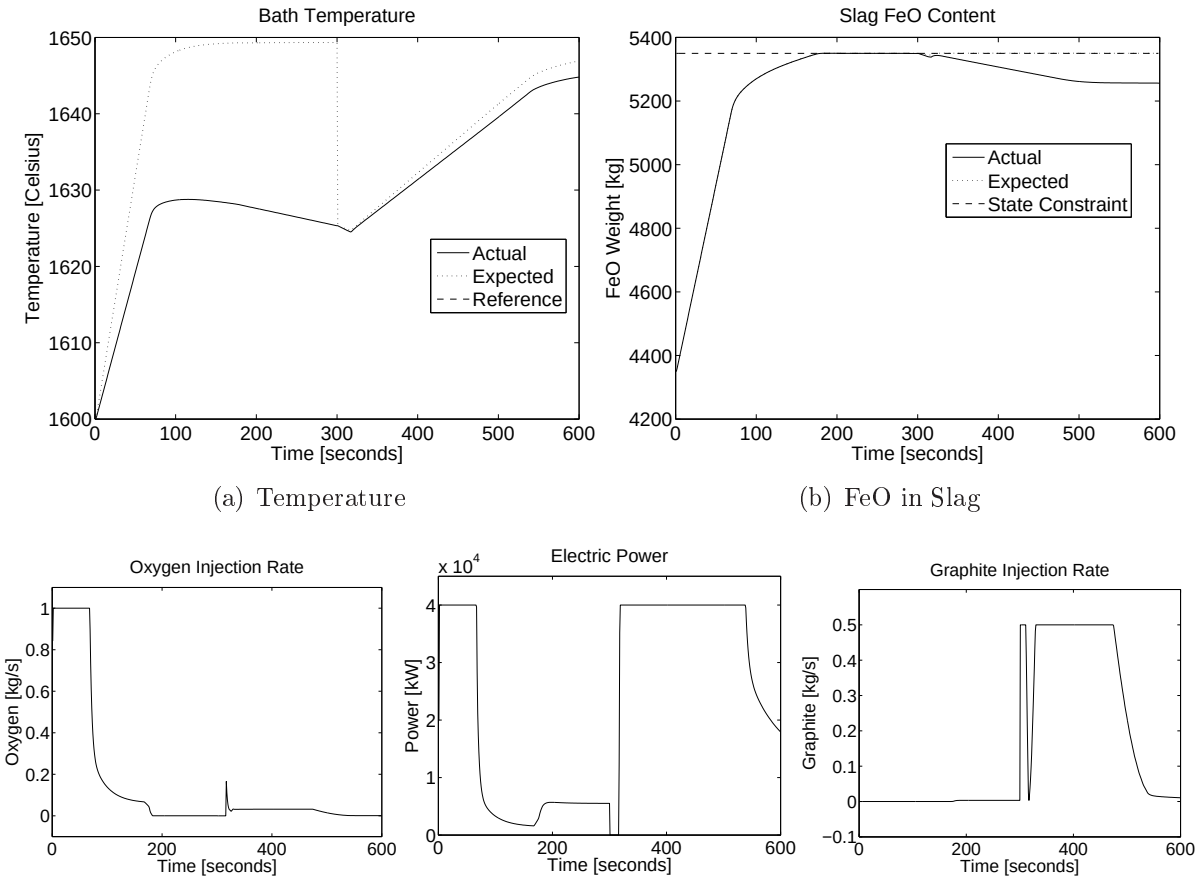

(a) Temperature (b) FeO in Slag

(c) Oxygen Injection (d) Electric Power (e) Graphite Injection

Figure B.9: Nominal MPC - Efficiencies at a minimum with one measurement and predictor parameter update.

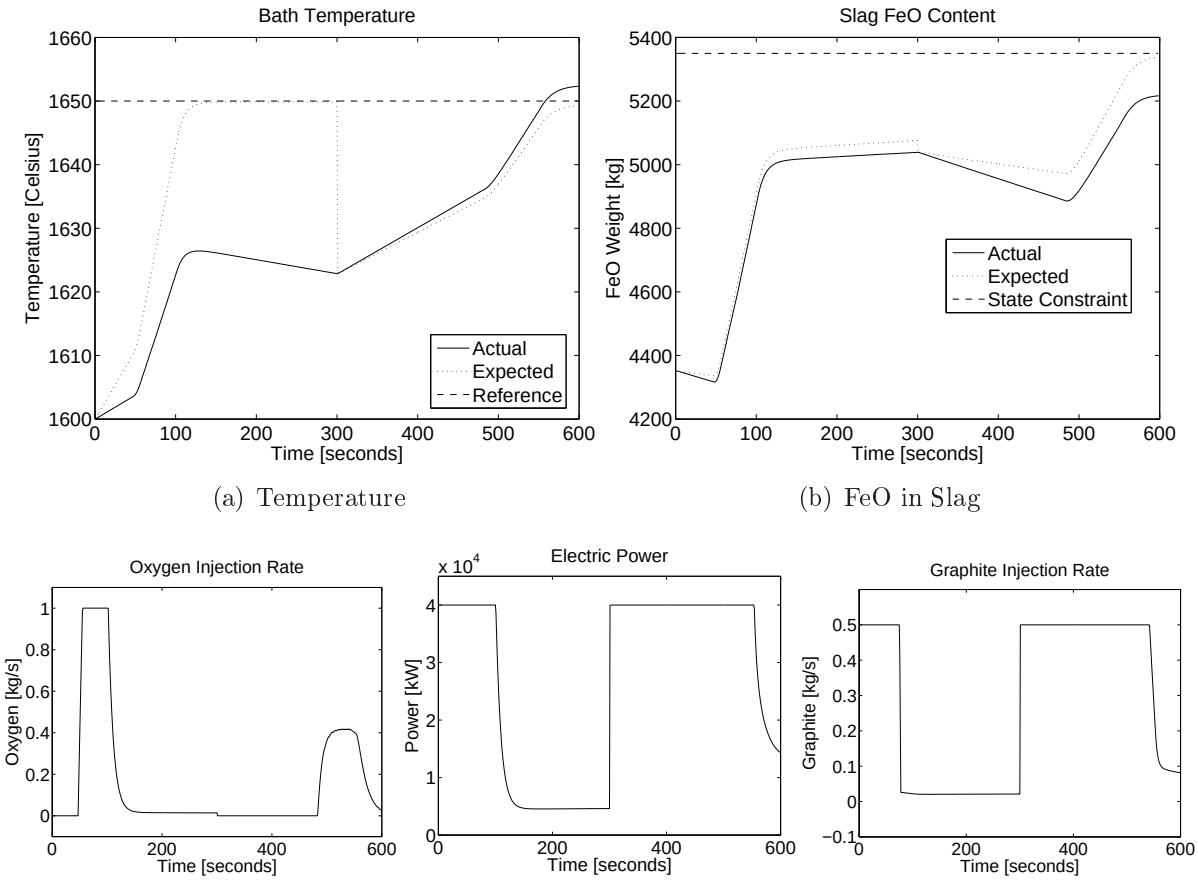

(a) Temperature (b) FeO in Slag

(c) Oxygen Injection (d) Electric Power (e) Graphite Injection

Figure B.10: Dual-mode robust MPC - Efficiencies at a minimum with one measurement and predictor parameter update.

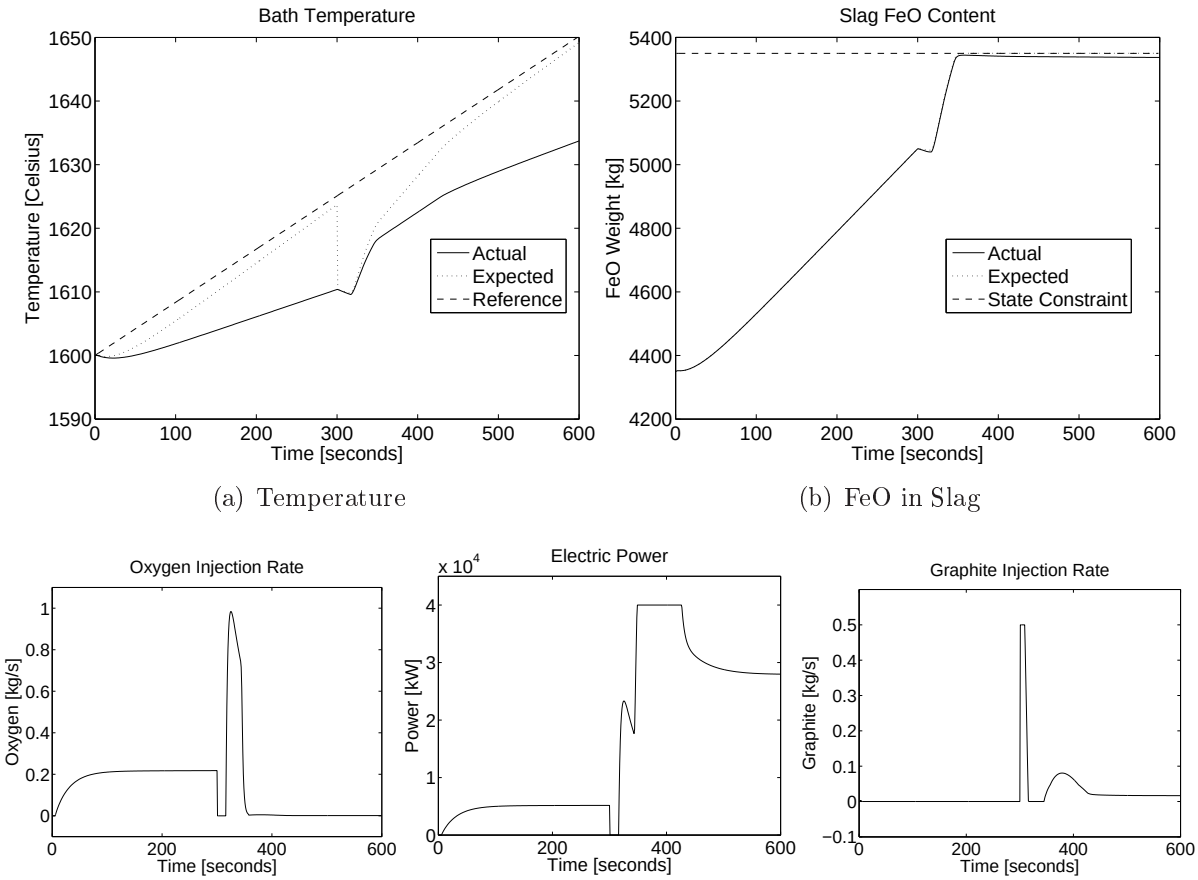

(a) Temperature (b) FeO in Slag

(c) Oxygen Injection (d) Electric Power (e) Graphite Injection

Figure B.11: Nominal MPC - Efficiencies at a minimum, one measurement and predictor parameter update and reference trajectory.

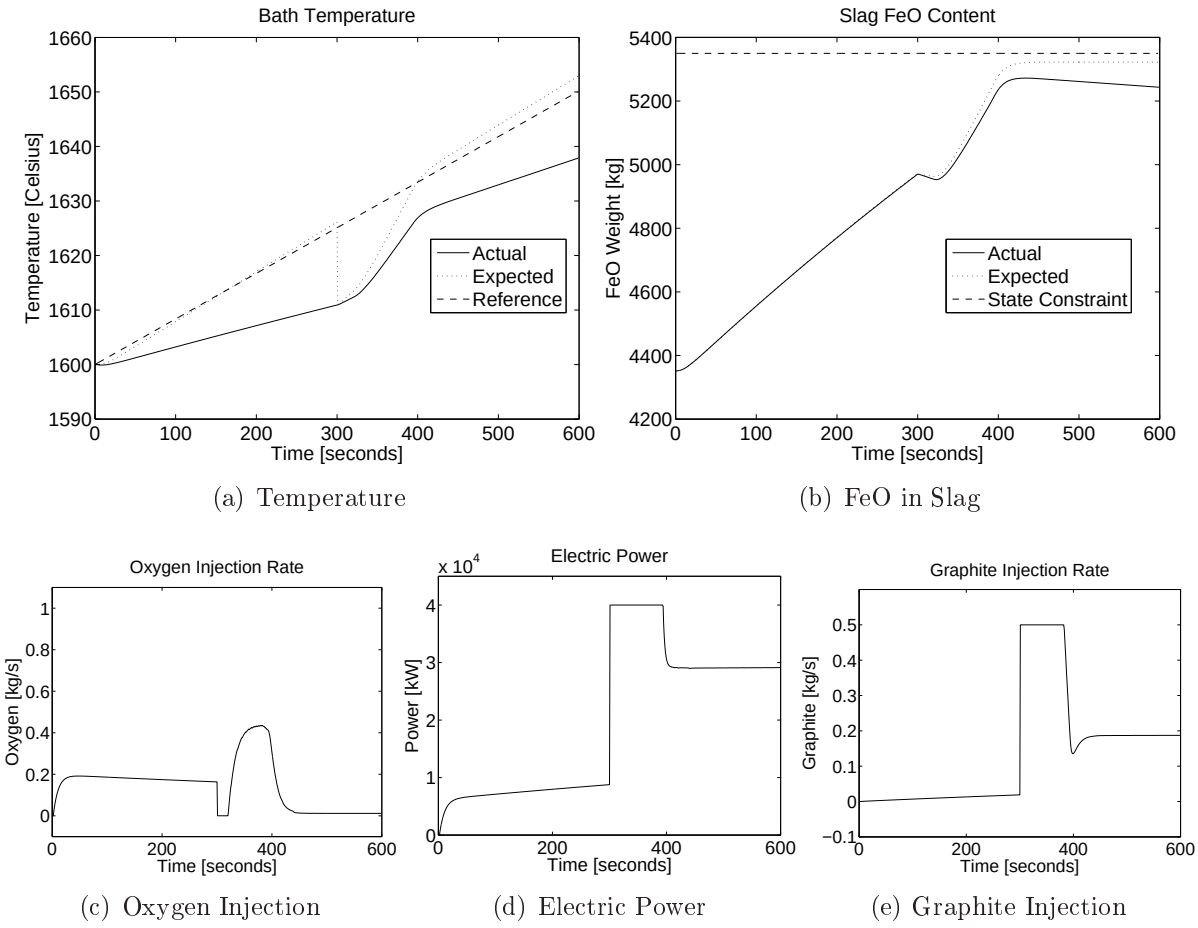

(a) Temperature (b) FeO in Slag

(c) Oxygen Injection (d) Electric Power (e) Graphite Injection

Figure B.12: Dual-mode robust MPC - Efficiencies at a minimum, one measurement and predictor parameter update and reference trajectory.

than nominal. This is a more theoretical scenario, because efficiencies do not tend to be higher than expected, but it is necessary to determine whether the controller would be able to cope with such a situation. In this scenario the following assumptions are made:

- There are three feedback scenarios:
  - Full state-feedback is available.
  - One measurement is available.
  - One measurement and update of predictor parameters are available.
- The predictor and actual plant have a mismatch in their efficiencies (η_{FeO} and η_{ARC}) where the efficiencies are higher in the real plant than in the predictor.
- There are no disturbances.

B.2.1 Worst-case scenario: Maximum efficiencies with full state feedback

In this first instance, full-state feedback is employed to evaluate the closed-loop performance without a predictor present in the extreme case where the efficiencies (η_{FeO} and η_{ARC}) are at the maximum of the confidence interval for the plant model. Robust MPC and nominal MPC are compared to determine which provides better performance in the presence of model mismatch.

The first set of simulations uses a setpoint of 1650^oC for temperature as well as even weighting on the inputs (table 4.2).

Figures B.13 and B.14 show that both controllers are able to follow the setpoint, and because of the increased efficiency of the oxygen and electric power, less energy is needed, which results in both controllers keeping the FeO content below the constraint level.

The second set of simulations uses a reference trajectory for temperature as well as even weighting on the inputs (table 4.2).

Figures B.15 and B.16 show that both controllers have good reference following. The nominal controller uses much less oxygen than the robust controller, which is evident in

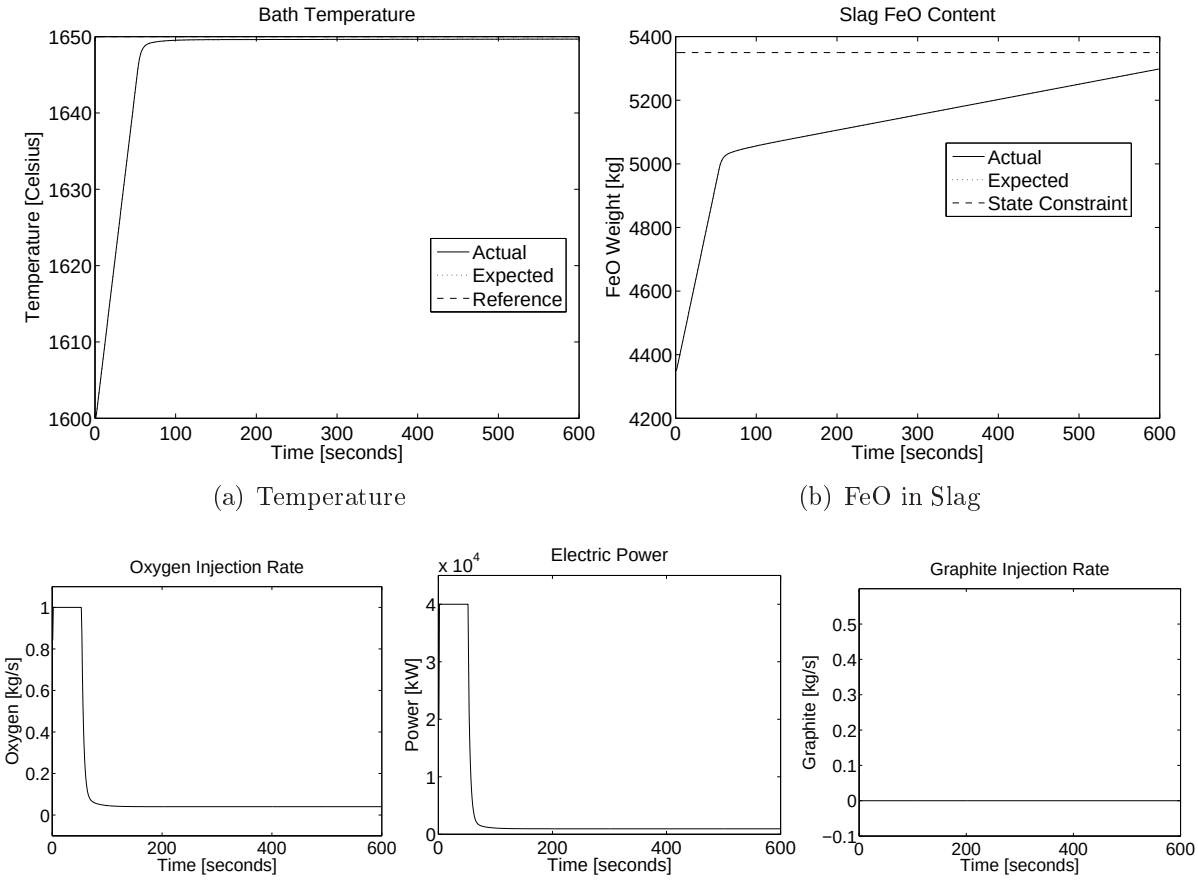

(a) Temperature (b) FeO in Slag

(c) Oxygen Injection (d) Electric Power (e) Graphite Injection

Figure B.13: Nominal MPC - Efficiencies at maximum with full state feedback.

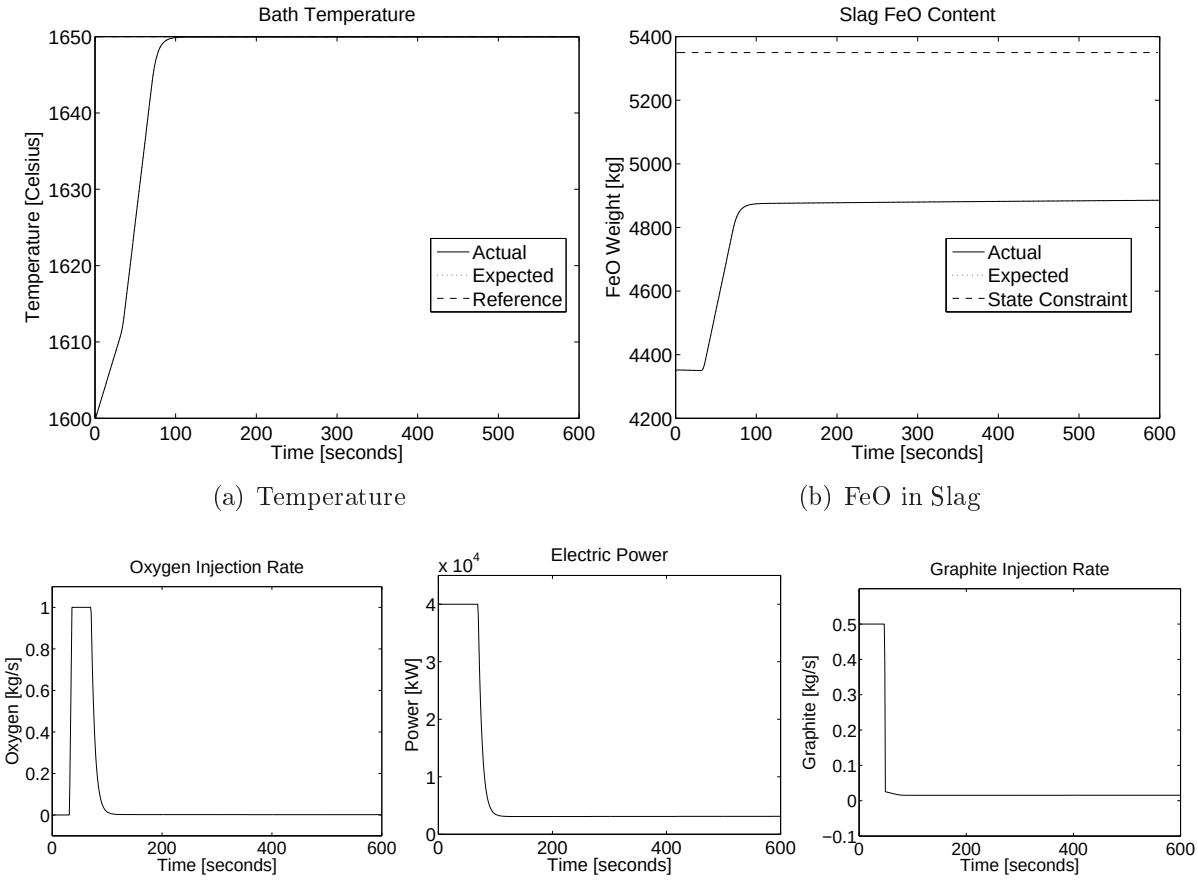

(a) Temperature (b) FeO in Slag

(c) Oxygen Injection (d) Electric Power (e) Graphite Injection

Figure B.14: Dual-mode robust MPC - Efficiencies at maximum with full state feedback.

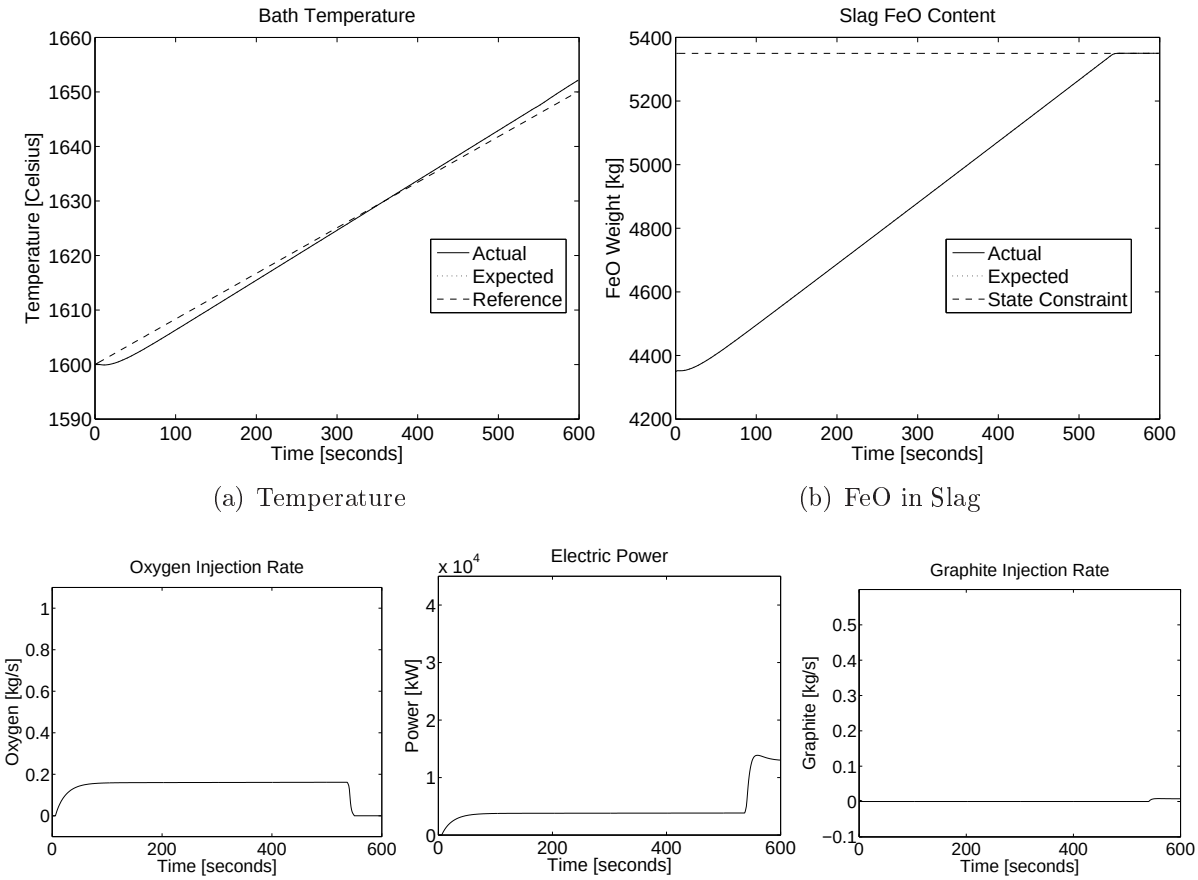

(a) Temperature (b) FeO in Slag

(c) Oxygen Injection (d) Electric Power (e) Graphite Injection

Figure B.15: Nominal MPC - Efficiencies at maximum with full state feedback and reference trajectory.

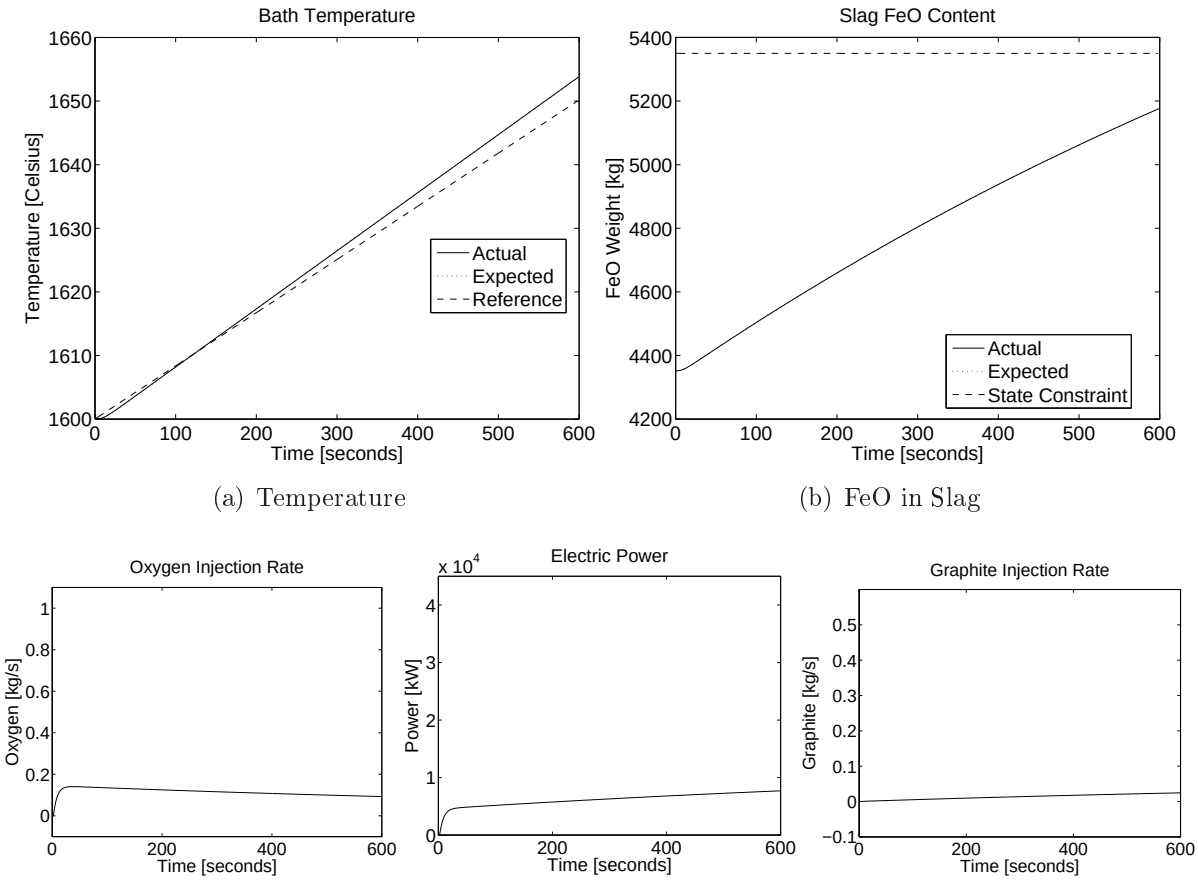

(a) Temperature (b) FeO in Slag

(c) Oxygen Injection (d) Electric Power (e) Graphite Injection

Figure B.16: Dual-mode robust MPC - Efficiencies at maximum with full state feedback and reference trajectory.

the final values of the FeO content. The robust controller slightly overshoots the final value for the temperature but is still well within the desired $\pm 10^0 C$ interval.

B.2.2 Worst-case scenario: Efficiencies at their maximum with one plant measurement

A more realistic feedback scenario is investigated, where only one temperature measurement is taken in the middle of the refining stage, the rest of the state data is produced by a predictor. The predictor uses the nominal plant parameters, while the real plant uses the worst-case scenario where the efficiencies (η_{FeO} and η_{ARC}) are at their maximum. This scenario should shed light on the effect of model mismatch between the predictor and real plant when compared to the results of the previous section.

The first set of simulations uses a setpoint of $1650^o C$ for temperature as well as even weighting on the inputs (table 4.2).

Figures B.17 and B.18 show that both controllers fail to steer the temperature to within the $\pm 10^0 C$ margin. The controllers overshoot the setpoint, because the efficiencies (η_{FeO} and η_{ARC}) are higher than expected and the controllers drive the temperature too high. The measurement shows the controllers that the temperature is too high, and they respond by turning off all energy sources. The temperature is lowered, but is limited by the tempo of natural heat loss, which is too slow to reach the target by the end of the refining stage. The process could be accelerated by opening the furnace roof, which would aid heat loss. This situation can be prevented by taking a measurement earlier in the refining stage to identify the problem sooner.

The second set of simulations uses a reference trajectory for temperature as well as even weighting on the inputs (table 4.2).

Figures B.19 and B.20 show that both controllers overshoot the final temperature with more than the accepted margin of $\pm 10^0 C$. By the time that the measurement is taken, the temperature is still below the desired value, but already higher than the reference. The controllers correct the problem by steering the temperature back to the reference, but as soon as the error is corrected, the temperature is again steered faster than the

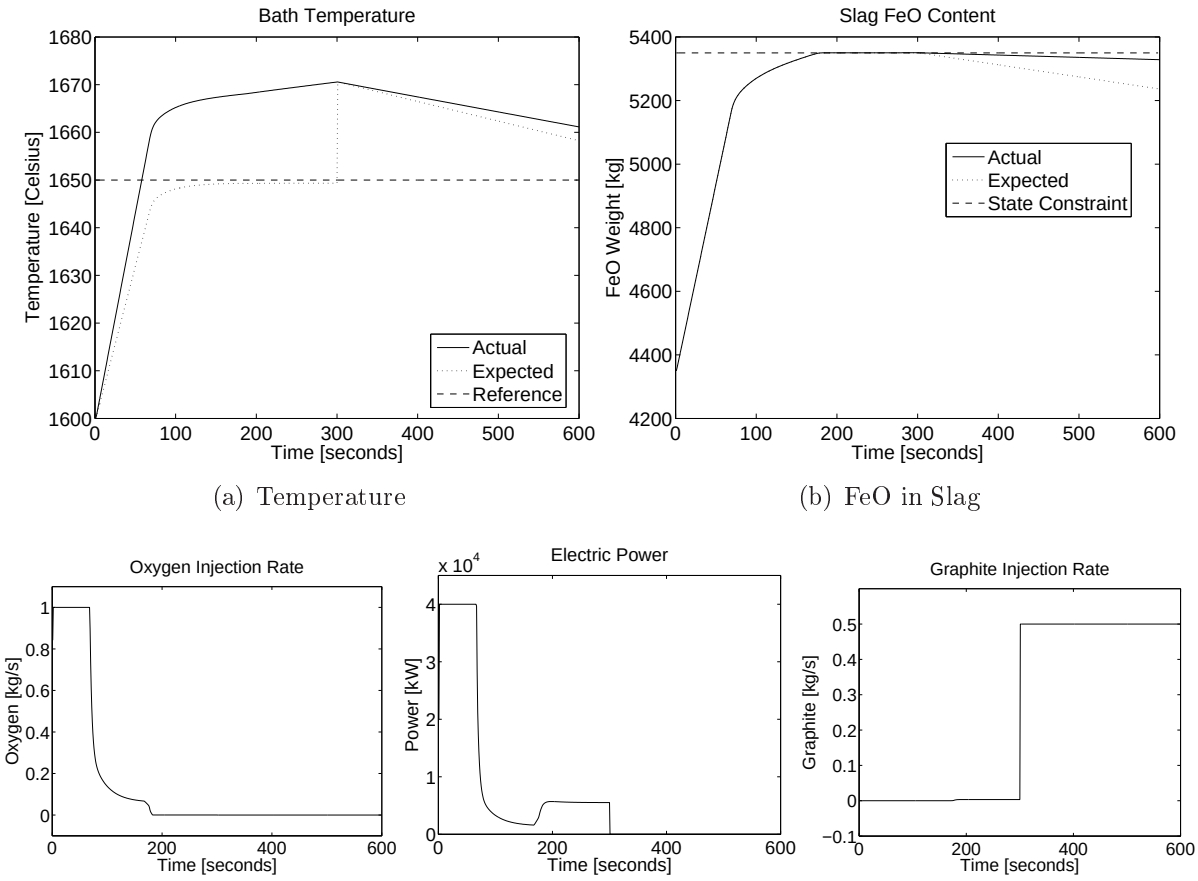

(a) Temperature (b) FeO in Slag

(c) Oxygen Injection (d) Electric Power (e) Graphite Injection

Figure B.17: Nominal MPC - Efficiencies at maximum with one measurement.

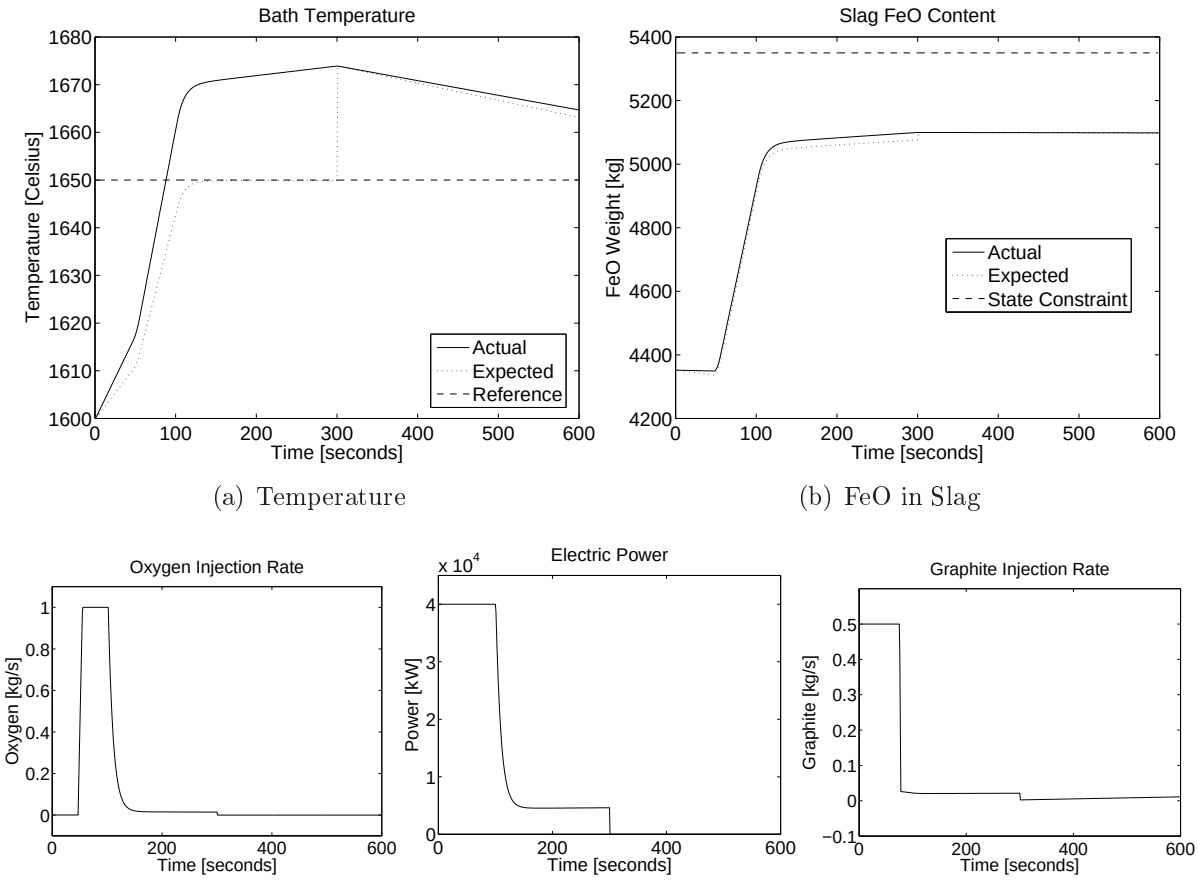

(a) Temperature (b) FeO in Slag

(c) Oxygen Injection (d) Electric Power (e) Graphite Injection

Figure B.18: Dual-mode robust MPC - Efficiencies at maximum with one measurement.

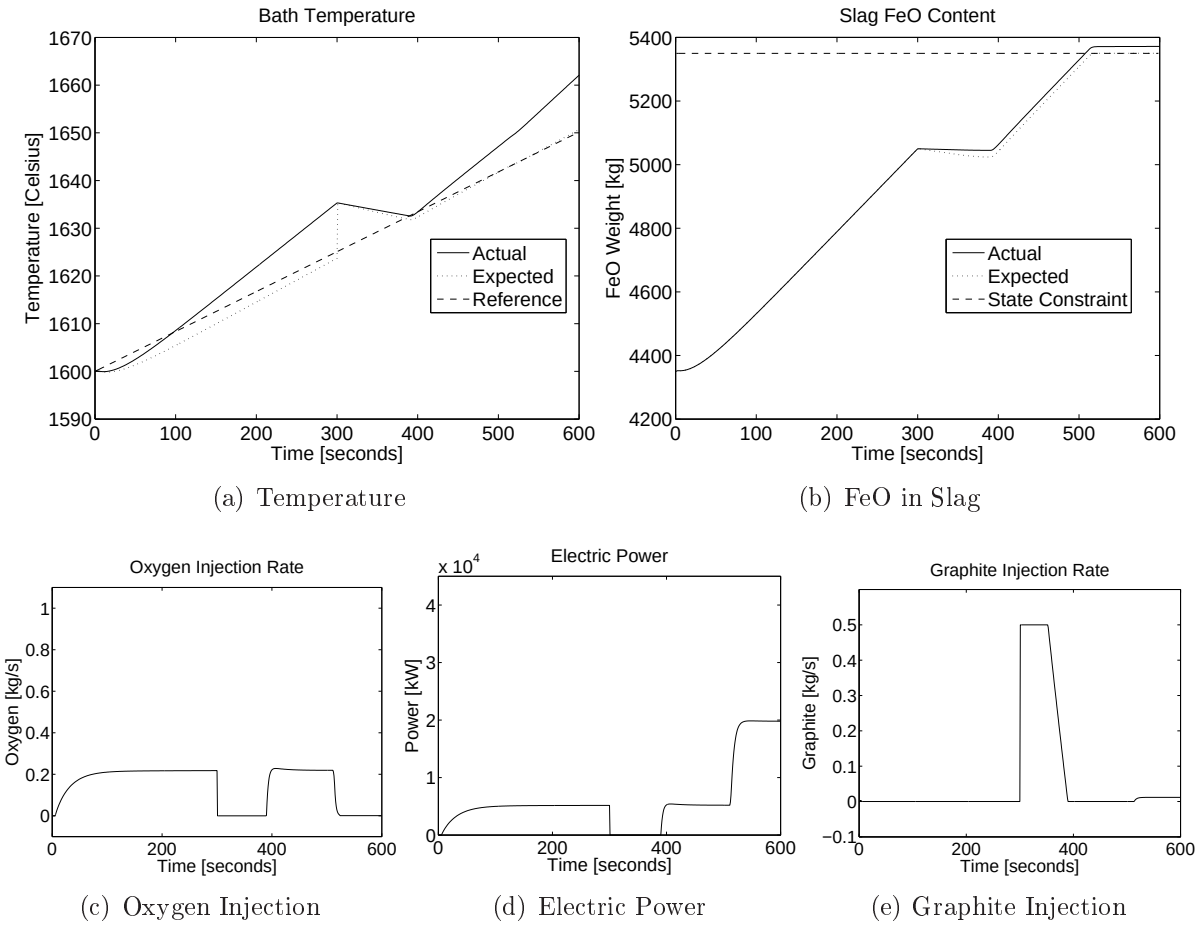

(a) Temperature (b) FeO in Slag

(c) Oxygen Injection (d) Electric Power (e) Graphite Injection

Figure B.19: Nominal MPC - Efficiencies at maximum, one measurement and reference trajectory.

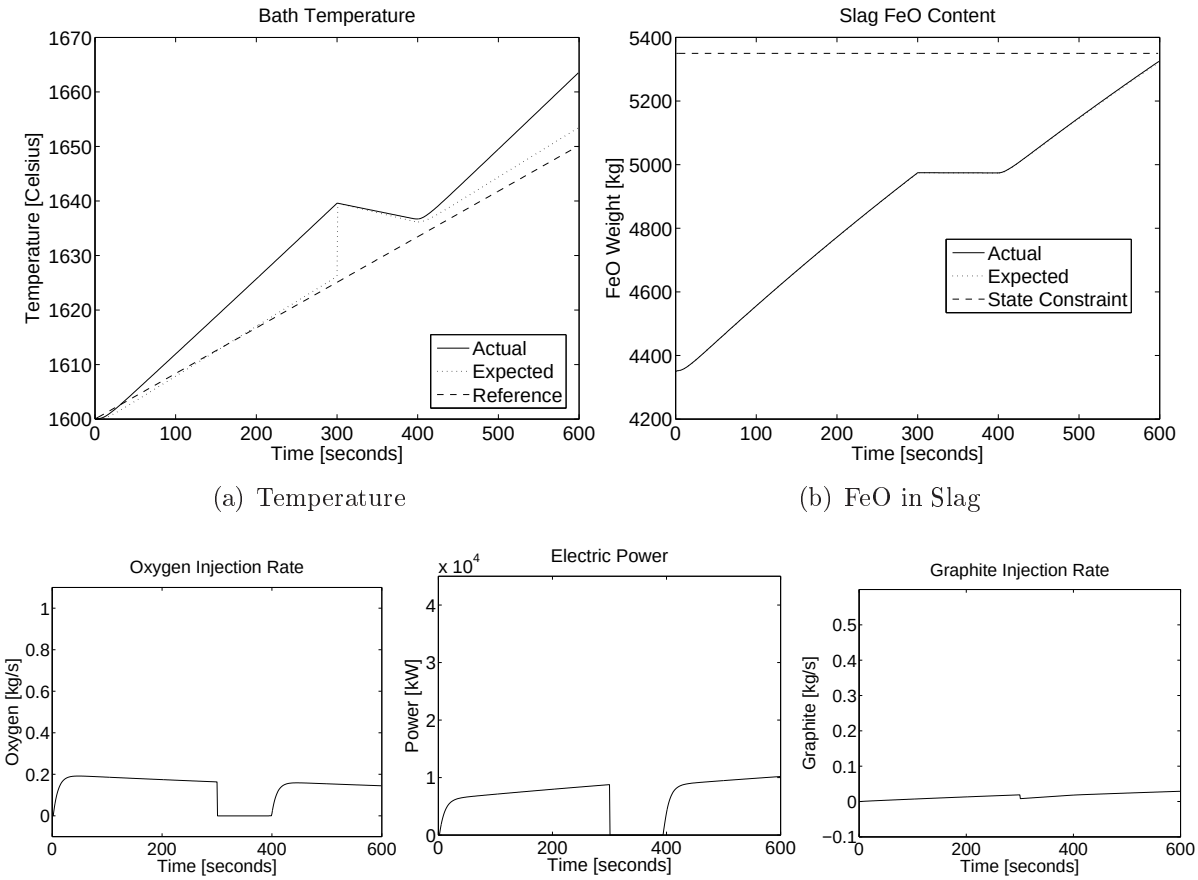

(a) Temperature (b) FeO in Slag

(c) Oxygen Injection (d) Electric Power (e) Graphite Injection

Figure B.20: Dual-mode robust MPC - Efficiencies at maximum, one measurement and reference trajectory.

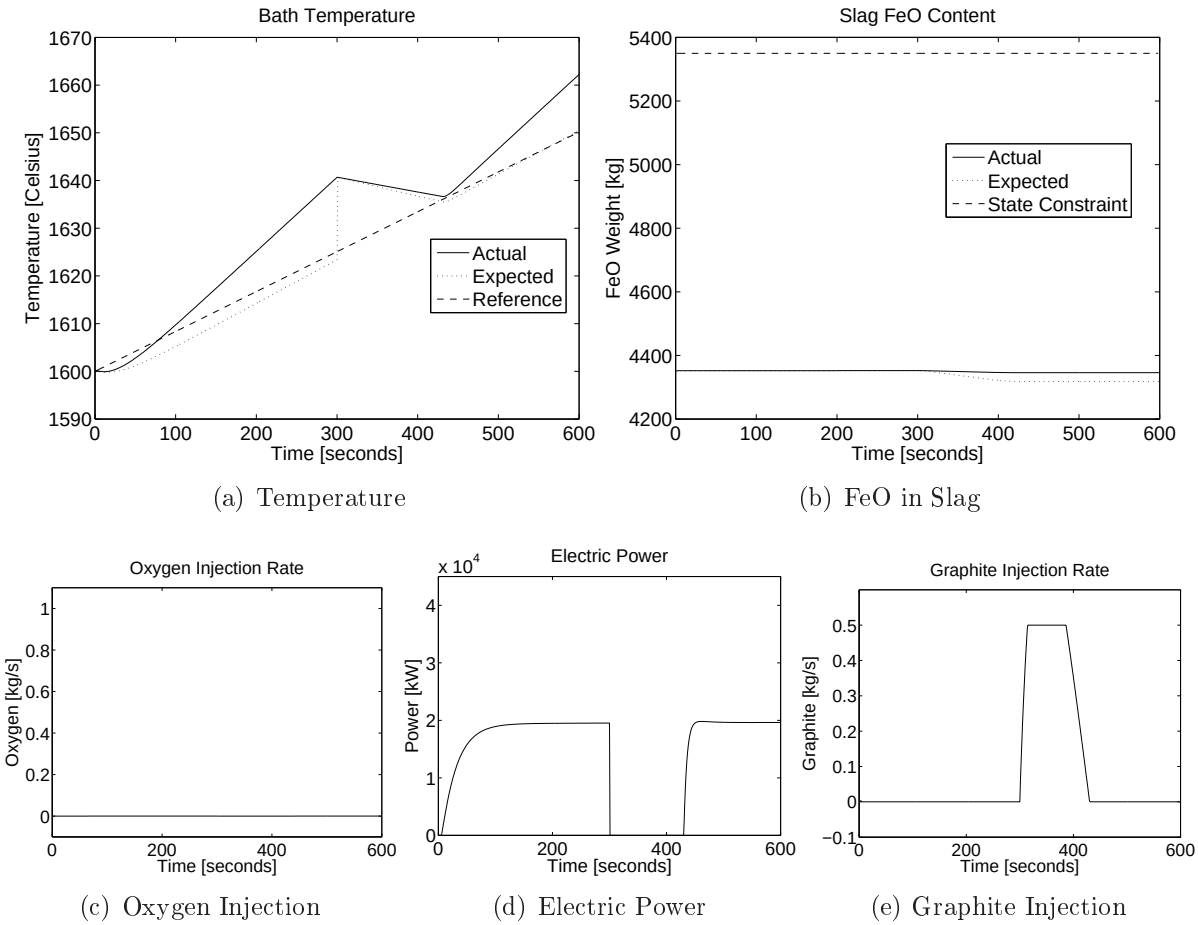

(a) Temperature (b) FeO in Slag

(c) Oxygen Injection (d) Electric Power (e) Graphite Injection

Figure B.21: Nominal MPC - Efficiencies at maximum, one measurement, reference trajectory and reduced oxygen usage.

reference.

The third set of simulations uses a reference trajectory for temperature as well as higher weighting on oxygen injection (table 4.2).

These simulations (figures B.21 and B.22) show much the same trend as the previous set, with the exception that both controllers use less oxygen, which in turn produces less FeO, but the robust controller uses significantly less oxygen compared with the previous simulation in figure B.20.

The model mismatch between the predictor and the actual plant in this scenario, causes the temperature to overshoot the desired value of 1650^0C. The effect can be reduced by taking a sample earlier in the refining stage, which will minimize the overshoot and give more time for the bath to cool off. The second solution is to use the reference trajectory, but from the last two simulations it is clear that the predictor parameters should be

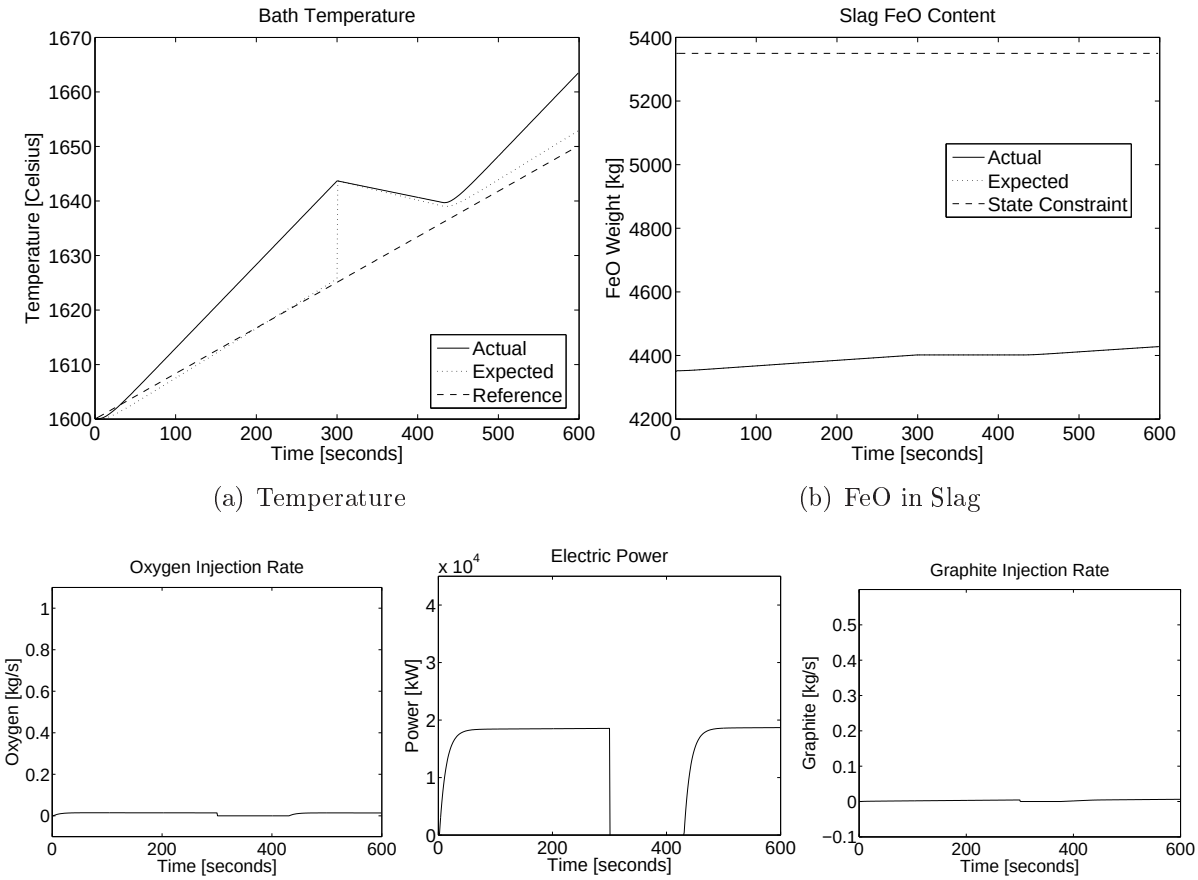

(a) Temperature (b) FeO in Slag

(c) Oxygen Injection (d) Electric Power (e) Graphite Injection

Figure B.22: Dual-mode robust MPC - Efficiencies at maximum, one measurement, reference trajectory and reduced oxygen usage.

updated to prevent overshoot from occurring after the measurement.

B.2.3 Worst-case scenario: Efficiencies at their maximum with one plant measurement and predictor parameters update

In the previous section, the effect that model mismatch has on the performance of the system is apparent. To combat the effect, the parameters of the predictor are updated each time a measurement is taken, in an attempt to improve performance. In this scenario only one measurement of temperature is taken in the middle of the refining stage, the rest of the data is produced by the predictor. The predictor uses the nominal plant parameters for the efficiencies (η_{FeO} and η_{ARC}) until a measurement is taken, after which the corrected parameters are employed. The "real plant" uses the worst-case where the efficiencies (η_{FeO} and η_{ARC}) are at their maximum.

The first set of simulations uses a setpoint of 1650^oC for temperature as well as even weighting on the inputs (table 4.2).

Figures B.23 and B.24 show much the same results as in section 4.4.2. The update in the predictor does not aid in accelerating the cooling of the bath. The only solution here would be to take a measurement earlier in the process.

The second set of simulations uses a setpoint of 1650^oC for temperature as well as higher weighting on oxygen injection (table 4.2).

Figures B.25 and B.26 show much the same result as the previous simulation where the predictor update does not solve the cooling limitation. The only difference is that, where energy is applied, less oxygen is used because of the heavier weighting on the oxygen injection rate.

A reference trajectory for temperature as well as even weighting on the inputs (table 4.2) is used for the third set of simulations.

Figures B.27 and B.28 show encouraging results. The reference trajectory causes the temperature to increase much slower than with the setpoint, so that by the time a measurement is taken, the temperature has not yet passed the desired final value of 1650^0C. The temperature does increase above the reference, and after the measurement,

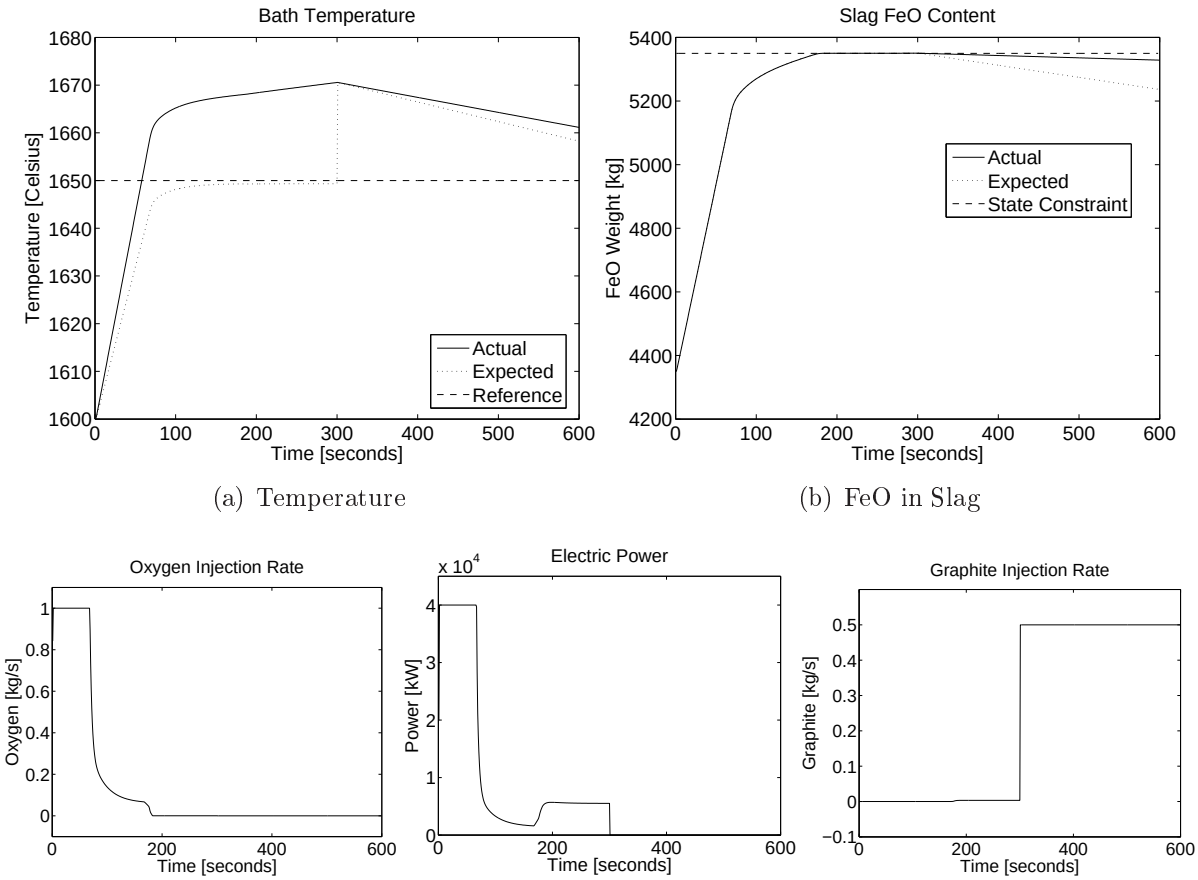

(a) Temperature (b) FeO in Slag

(c) Oxygen Injection (d) Electric Power (e) Graphite Injection

Figure B.23: Nominal MPC - Efficiencies at maximum with one measurement and predictor update.

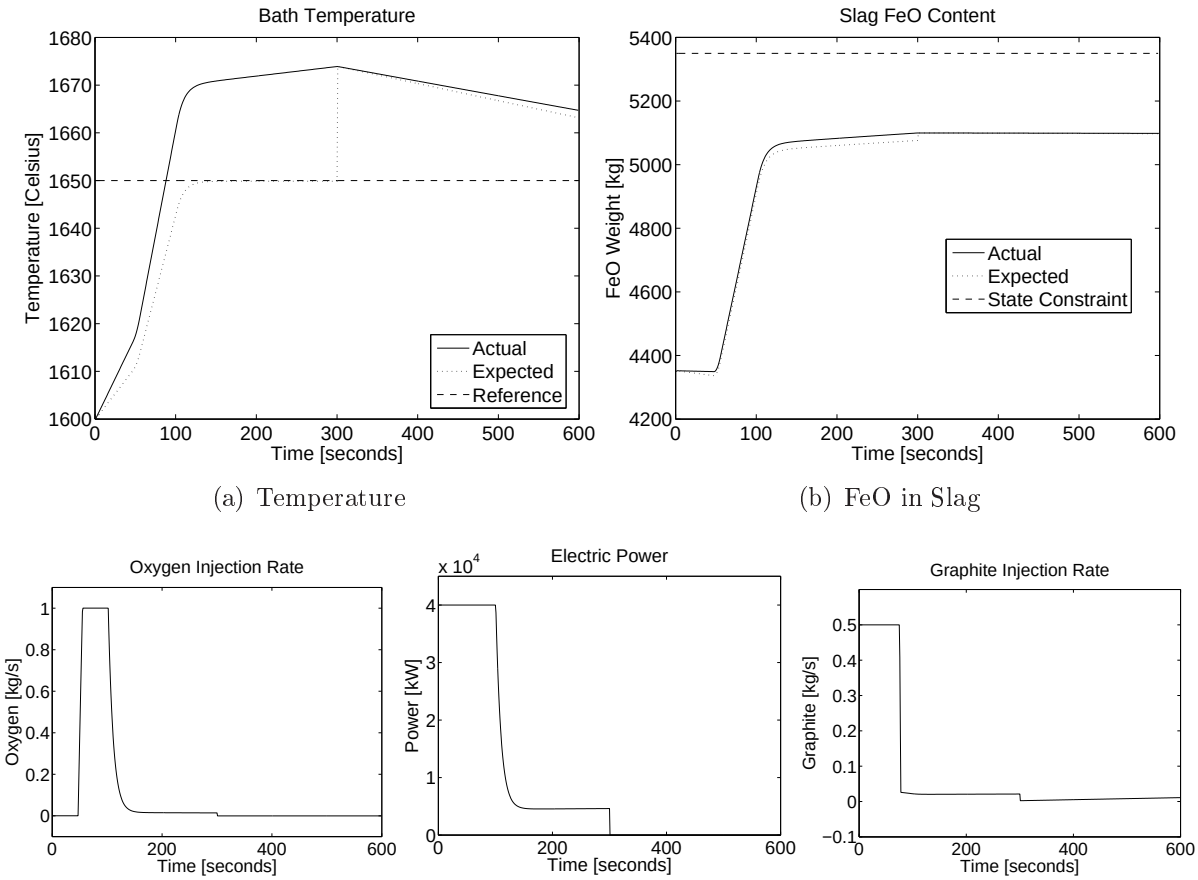

(a) Temperature (b) FeO in Slag

(c) Oxygen Injection (d) Electric Power (e) Graphite Injection

Figure B.24: Dual-mode robust MPC - Efficiencies at maximum with one measurement and predictor update.

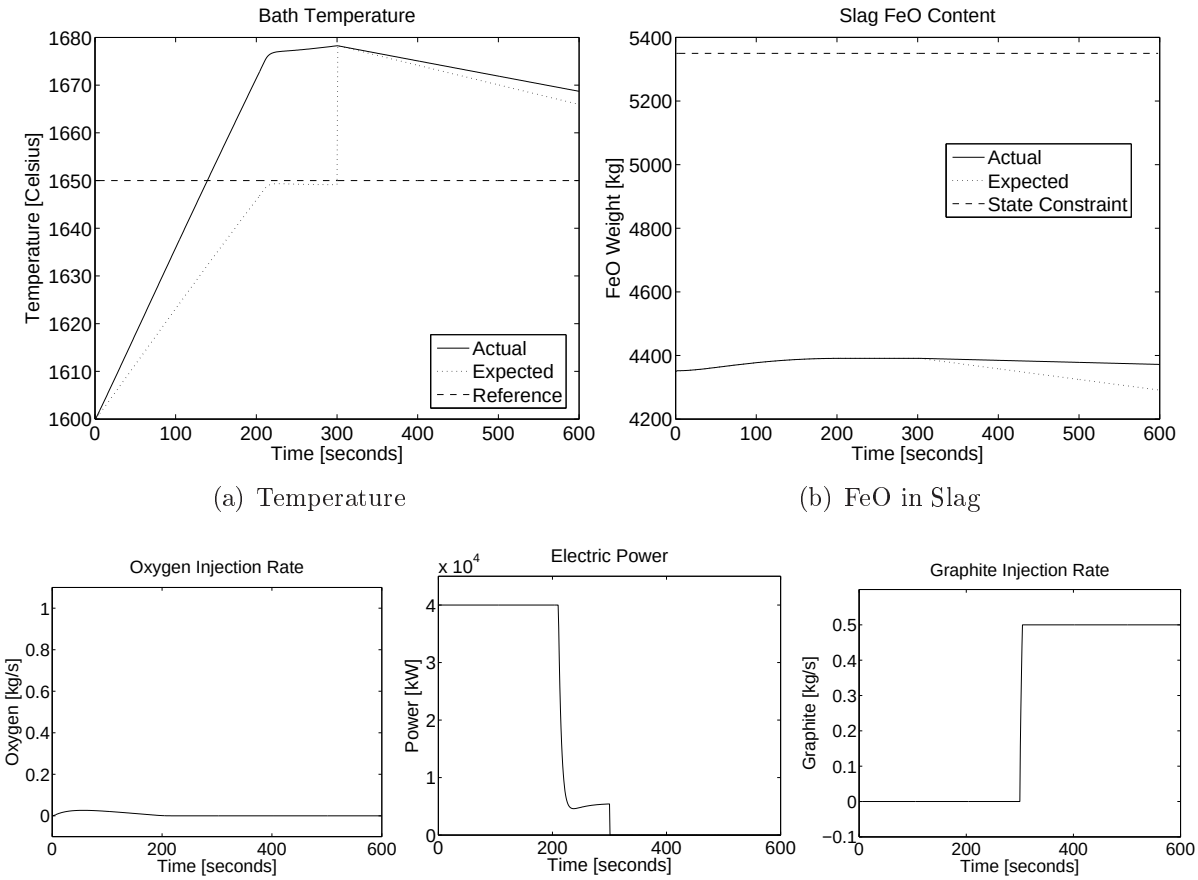

(a) Temperature (b) FeO in Slag

(c) Oxygen Injection (d) Electric Power (e) Graphite Injection

Figure B.25: Nominal MPC - Efficiencies at maximum, one measurement and predictor update and reduced oxygen usage.

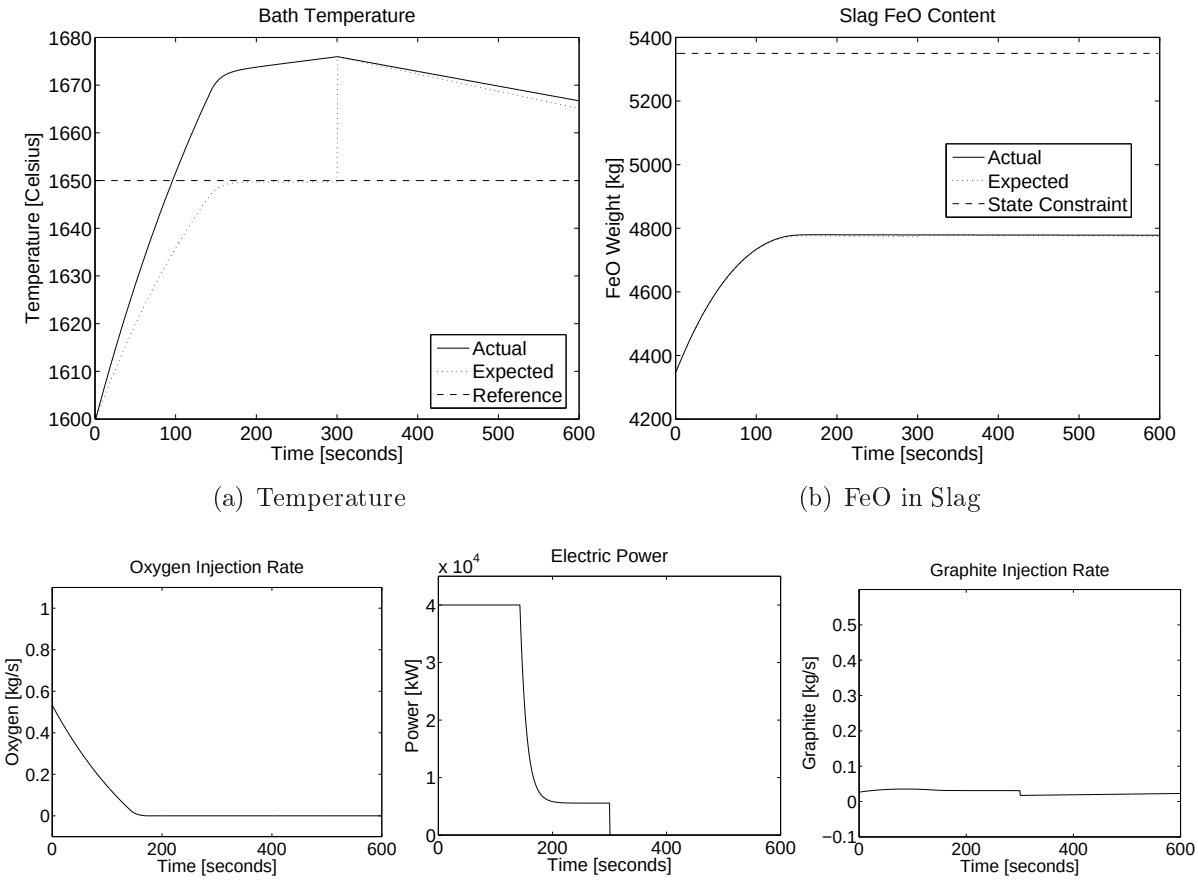

(a) Temperature (b) FeO in Slag

(c) Oxygen Injection (d) Electric Power (e) Graphite Injection

Figure B.26: Dual-mode robust MPC - Efficiencies at maximum, one measurement and predictor update and reduced oxygen usage.

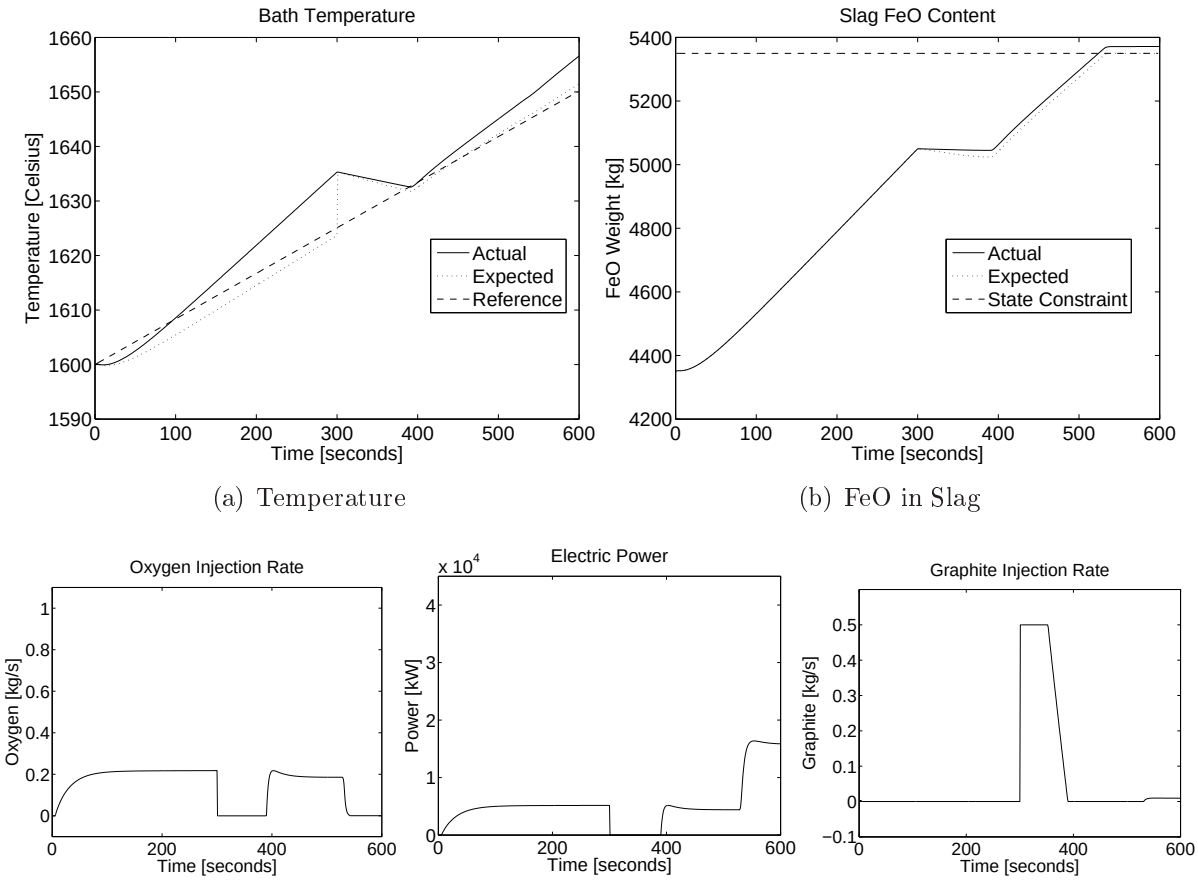

(a) Temperature (b) FeO in Slag

(c) Oxygen Injection (d) Electric Power (e) Graphite Injection

Figure B.27: Nominal MPC - Efficiencies at maximum, one measurement and predictor update and reference trajectory.

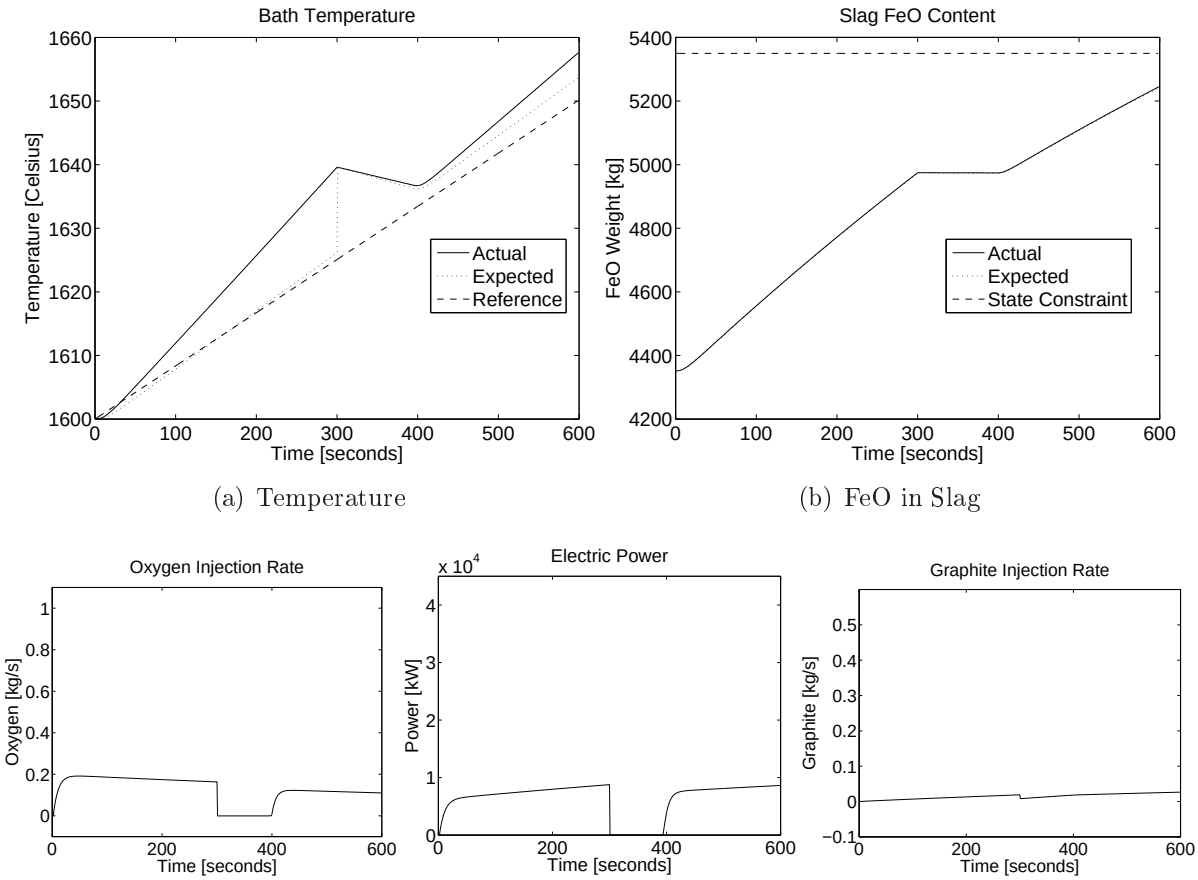

(a) Temperature (b) FeO in Slag

(c) Oxygen Injection (d) Electric Power (e) Graphite Injection

Figure B.28: Dual-mode robust MPC - Efficiencies at maximum, one measurement and predictor update and reference trajectory.

the controller corrects the problem and once it has reached the reference, it follows it more closely. There is still an undercorrection, that causes the temperature to increase faster than expected. The final value ends within the accepted $\pm 10^0 C$ margin. The nominal controller uses less oxygen than the robust controller as evident from the final FeO values.

Appendix C

Measured bath and slag data

Tables C.1 and C.2 show measured bath and slag data for 18 taps. This data were collected by Rathaba (2004).

Table C.1: Measured bath and slag data (Rathaba, 2004) part 1.

Tap #	Time	% C	% Si	O_2 [ppm]	Time	Temp^{0}C	Time	% FeO	% SiO_2	% CaO	% MgO	% Al_2O_3
1	7.05	0.199	0.03	-	7.15	1619	7.04	17.70	18.2	50.53	3.53	5.10
	7.15	0.125	-	219	7.16	1630	7.16	31.55	10.5	43.45	3.33	3.07
	7.16	0.119	-	229	7.20	1678	7.20	36.53	9.08	37.57	3.47	2.73
	7.20	0.043	-	658								
2	8.14	0.082	0.01	-	8.14	1598	8.11	27.04	13.7	43.74	5.08	3.69
	8.16	0.060	-	448	8.16	1618	8.16	30.25	12.5	43.09	5.42	3.51
	8.18	0.054	-	504	8.18	1638	8.18	39.20	10.3	34.41	5.43	3.01
	8.21	0.039	-	704	8.21	1640						
3	9.10	0.111	0.03	-	9.13	1597	9.10	31.50	13.4	40.13	5.04	4.13
	9.14	0.053	-	514	9.15	1636	9.14	26.21	12.6	46.07	6.38	3.90
	9.17	0.043	-	623	9.18	1631	9.17	31.82	11.4	40.48	6.14	3.48
4	10.14	0.078	0.02	-	10.14	1594	10.13	32.13	11.6	41.14	5.46	4.32
	10.20	0.043	-	648	10.20	1610	10.18	29.80	10.7	43.12	5.77	4.13
					10.21	1658	10.20	31.65	10.1	41.13	5.77	3.78
5	11.36	0.060	0.02	-	11.37	1586	11.33	37.80	9.85	36.39	5.14	3.48
	11.42	0.056	-	466	11.42	1602	11.43	38.25	7.58	36.15	5.11	2.72
	11.44	0.040	-	699	11.44	1658	11.45	38.12	8.10	39.83	5.69	2.91
6	12.51	0.060	0.03	-	12.53	1615	12.50	43.95	10.8	29.38	5.25	4.14
	12.55	0.048	0.03	-	12.55	1647	12.53	43.65	10.1	30.32	5.43	3.84
	12.55	0.026	-	1048			12.56	45.29	9.61	30.21	5.38	3.68
7	13.43	0.088	0.03	-	13.43	1571	13.40	34.52	11.7	37.95	5.41	5.00
	13.45	0.071	0.03	-	13.47	1546	13.44	34.81	11.6	37.65	5.49	5.03
	13.47	0.065	-	376	13.49	1601	13.48	36.35	9.41	32.00	5.71	3.96
	13.49	0.054	-	481	13.51	1615						
	13.55	0.046	-	572								
8	15.05	0.056	0.03	-	15.07	1630	15.04	37.33	8.96	38.27	8.07	3.81
	15.07	0.051	0.03	-	15.08	1643	15.06	35.64	9.24	37.74	7.81	3.92
	15.08	0.037	-	738			15.08	35.06	8.57	34.60	7.30	3.62
9	16.02	0.157	0.03	-	16.05	1540	15.56	26.96	11.7	40.20	7.23	4.58
	16.06	0.106	0.03	-	16.08	1615	16.06	26.57	10.6	43.41	7.05	4.22
	16.08	0.062	-	481	16.10	1636	16.09	27.05	10.2	39.16	6.34	4.00
	16.09	0.072	0.03	-	16.13	1660						
	16.10	0.093	-	293								
	16.13	0.033	-	845								

Table C.2: Measured bath and slag data (Rathaba, 2004) part 2.

Tap #	Time	% C	% Si	O_2 [ppm]	Time	Temp^{0}C	Time	% FeO	% SiO_2	% CaO	% MgO	% Al_2O_3
10	17.03	0.078	0.03	-	17.05	1579	17.02	24.57	14.8	42.47	5.31	4.36
	17.05	0.085	0.03	-	17.07	1614	17.05	23.91	15.0	44.46	5.98	4.57
	17.09	0.044	-	624	17.09	1647	17.09	25.08	15.2	43.29	6.50	4.64
	17.09	0.059	0.03	-								
11	10.37	0.112	0.02	-	10.36	1570	10.43	35.69	11.1	36.17	5.59	3.83
	10.39	0.034	-	760	10.39	1600						
	10.42	0.030	-	894	10.42	1638						
	10.44	0.045	-	604	10.44	1631						
12	11.34	0.057	0.02	-	11.41	1566	11.47	36.34	11.6	34.72	6.96	3.89
	11.45	0.034	-	804	11.45	1631						
	11.47	0.031	-	920	11.47	1673						
13	12.43	0.081	0.02	-	12.45	1585	12.50	34.91	10.2	37.55	5.68	3.59
	12.48	0.042	-	642	12.48	1623						
	12.50	0.039	-	678	12.50	1621						
14	13.42	0.115	0.04	-	13.47	1594	14.10	36.18	10.8	34.39	5.48	3.78
	13.50	0.050	-	531	13.50	1610						
	14.08	0.033	-	823	14.05	1658						
	14.10	0.030	-	930	14.08	1621						
					14.10	1652						
15	14.56	0.068	0.03	-	15.02	1589	15.09	41.95	10.2	34.43	6.04	3.57
	15.06	0.036	-	861	15.05	1626						
	15.09	0.035	-	757	15.06	1641						
	15.11	0.030	-	907	15.08	1626						
					15.10	1650						
16	16.03	0.075	0.03	-	16.04	1624	16.05	37.33	10.2	37.51	5.83	3.47
	16.06	0.034	-	861	16.06	1645						
17	16.54	0.080	0.03	-	17.00	1564	17.10	31.93	12.4	39.96	4.31	4.53
	17.06	0.036	-	356	17.04	1566						
	17.08	0.035	-	592	17.06	1588						
					17.08	1639						
18	17.56	0.169	0.03	-	18.05	1582	17.10	31.93	11.2	39.96	6.76	4.20
	18.01	0.093	0.02	-	18.08	1618						
	18.09	0.060	-	592	18.09	1661						